Transactions of the ASME

TRANSACTIONS OF THE AMERICAN SOCIETY OF MECHANICAL ENGINEERS

VOLUME 80 AUGUST 1958 NUMBER 6

Transactions

of The American Society of Mechanical Engineers

Published on the tenth of every month, except March, June, September, and December

Published monthly by The American Society of Mechanical Engineers. Publication office at 20th and Northampton Streets, Easton, Pa. The editorial department is located at the headquarters of the Society, 29 West Thirty-Ninth Street, New York 18, N. Y. Cable address, "Mechaneer," New York. Price $1.50 a copy, $12.00 annually for Transactions and the *Journal of Applied Mechanics* to members, $1.00 a copy, $6.00 annually. Add $1.50 for postage to all countries outside the United States, Canada, and Pan American Union. Changes of address must be received at Society headquarters seven weeks before they are to be effective on the mailing list. Please send old as well as new address. . . . By-Law: The Society shall not be responsible for statements or opinions advanced in papers or . . . printed in its publications (B13, Par. 4). . . . Entered as second-class matter March 2, 1928, at the Post Office at Easton, Pa., under the Act of August 24, 1912. .

Controlled Starting and Loading of Modern Central Power Stations

By F. W. KUEHN,[1] HAZLETON, PA.

The paper outlines experiences in starting major central-station equipment of all vintages under controlled conditions, with emphasis on a new 160-mw, 1250-lb, 950-F, single-shell tandem-compound turbine. The influence of steam leads between turbine and boiler on turbine end steam temperatures; quenching of valve bowls; and relation between horizontal turbine-flange temperature differentials and permissible loading rates are explained in detail. Use of steam from the first turbine stage for heating massive horizontal flange sections in the first to seventh-stage region of the high-pressure turbine as an operating routine, over a two-year period, to reduce loading time for starts from cold and after weekend shutdown, and to minimize flange distortion, is discussed. Boiler-drum circulation difficulties and remedies, and some innovations in furnace tube-metal temperature measurements are covered.

Pennsylvania Power & Light Company, since 1948, has added almost 900,000 kw of capability to the system in new modern equipment. During this same period, about 160,000 kw of small, thin-cylinder, easy-start equipment, with units ranging in size from 1000 to 15,000 kw have been taken out of service, most of it permanently.

It was realized, in advance, that the removal from service of the older equipment eventually would require the frequent shutting down and starting up of some of the new, large, single-unit, high-pressure high-temperature turbines and boilers. The last two units, which were added to the system at Martins Creek in 1954 and 1956, were designed accordingly in so far as possible to operate as peak-load units. Boiler and turbine of the first unit, for example, were provided with a thorough complement of instrumentation for measuring boiler-drum and turbine-metal temperatures during starts; special provisions were made for boiler-drum end circulation; combination radiant-convection superheating was chosen for the steam generator because of better steam-temperature characteristic for starting conditions; and somewhat larger than ordinary boiler and steam-lead drains were provided in the interest of easier starting.

Prior to placing the first of these new peak-load units into service, much valuable information was obtained from Consolidated Edison Company of New York through on-the-job study of its techniques. The material proved to be very helpful in preparing start procedures for our topping units and other new types.

The intent of this paper is to discuss the operating problems which are encountered in the starting of modern central stations and their solutions as applied specifically to the types of equipment involved, while adhering to the basic principles which have been formulated and amended by designers and operators over the past few years; to point out needed changes in design; to emphasize the importance of boiler-turbine steam leads in the starting operation; and to provide additional backup information concerning the thermal behavior of the large metal masses in modern turbines.

The basic principles of controlled starting which were used in this study have been ably set down by several writers in recently published ASME papers and discussions and are respectfully acknowledged. They are outlined briefly herewith to round out the report since they provided the framework on which the program was built.

Principles of Controlled Start-Up

1 Fire the boiler symmetrically so that distortion is kept to a minimum.

2 Bring up saturated water temperature in boiler at a rate which will produce a metal-temperature difference in any part of the drum with respect to any other part not exceeding 100 F.

3 Keep gas temperature around nondrainable superheater sections below point where damage to tubes or shortened life will result from overheating until sufficient flow of cooling steam is established.

4 Have steam temperature going to turbine at least 50 to 100 F above the front-end turbine-metal temperature before rolling.

5 On starts from cold, begin the roll of turbine with steam at the lowest temperature and pressure possible.

6 Do not exceed 150 F temperature differential across massive turbine valve chest and bowl sections. On modern high-pressure, single-shell turbines this corresponds to a uniform temperature rise (or drop) of 300 to 500 F per hr depending on the thickness of the sections involved. For thicker sections, the lower figure will apply.

7 Load at a rate which will produce a temperature differential between inner and outer horizontal turbine-flange surfaces of single-shell machines not exceeding 250 F. This figure varies between different authorities from 200 to 300 F. Experience in this study has shown that 250 F is satisfactory, while 300 F may produce distortion of flanges in single-shell machines.

8 Control condenser vacuum during roll period and amount of load applied immediately after synchronizing the generator so that exhaust-end metal will cool at a rate not in excess of 500 F per hr.

While these principles are essentially the same for all units and it is hoped that the material presented here will be of help to those who are confronted with similar problems, it should be emphasized that the only way to establish correct starting procedures for any given unit is for the owner company to conduct a thorough investigation on that unit (boiler-leads-turbine-generator) using only the best instrumentation available.

Sunbury No. 3 Unit—100 mw, 1250 psi, 950 F

Some interesting facts were uncovered in regard to cooling of steam leads during unit shutdown in the course of the controlled-start study of this unit.

Initial installation at Sunbury, consisting of four anthracite-burning boilers rated at 420,000 lb per hr each and two turbine-generators at 75 mw each, went into service in late 1949. No. 3 boiler, which burns bituminous coal, and its turbine-generator,

[1] Plant Betterment Engineer, Pennsylvania Power and Light Company, Cedar and Buttonwood Streets, Hazleton, Pa. Mem. ASME.

Contributed by the Power Division and presented at the ASME Power Conference, Allentown, Pa., October 21–23, 1957, of The American Society of Mechanical Engineers.

Note: Statements and opinions advanced in papers are to be understood as individual expressions of their authors and not those of the Society. Manuscript received at ASME Headquarters, July 31, 1957. Paper No. 57—PWR-7.

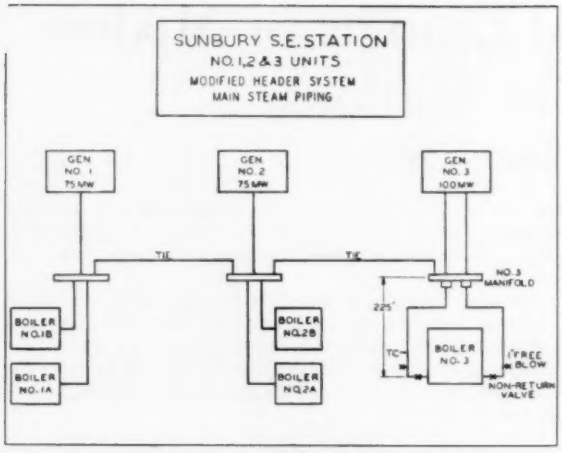

Fig. 1 Location of free blows with respect to No. 3 boiler nonreturn valves

800,000 lb per hr and 100 mw, respectively, came on-the-line early in 1951.

The three units operate at 1250 psi, 950-F throttle and are tied together on a modified header system, as shown in Fig. 1.

There is some extra steam-producing capacity left in the four anthracite boilers above the full-load requirements of Units 1 and 2. During off-peak periods, when the load for the three units is equal to or less than the capability of the four anthracite boilers, it is advantageous from a cost standpoint to take No. 3 boiler out of service while keeping No. 3 turbine-generator on-the-line.

The problem then was to get No. 3 boiler off and on-the-line with minimum shutdown and fire-up costs and, more important, with a steam delivery temperature high enough to prevent excessive shrinkage of the turbine spindle as the boiler came on-the-line.

To take the boiler off-the-line, the superheater-outlet drains are opened, the last coal burners are removed and purged in the normal manner, and air flow through the furnace is maintained for a few minutes until the drum pressure reaches a predetermined level, in this case, 250 psi under the lowest safety-valve popping pressure. The fans are then taken out of service, the outlet drains are closed, and the stem of the nonreturn valve is physically run down onto the valve piston to lock the valve in the closed position. In the case of a unit boiler-turbine system, the boiler is bottled and under pressure to the boiler-lead valves for weekend shutdowns, and to the turbine stop valves for overnight shutdowns.

After the last torches are removed from the furnace, steam pressure in the bottled boiler increases slowly to a maximum just under popping pressure in about six hours as the residual heat in furnace and boiler soaks into the water, after which there is a slow pressure decay, Fig. 2.

The pressure is not allowed to drop below 500 psi, however (40 per cent of normal throttle pressure), both in the interest of fuel economy and boiler-drum temperature differentials, if the boiler is to go on-the-line within 72 hr after shutdown. If the scheduled shutdown is to be much over three days, it becomes economical to take the pressure off the boiler and fire-up from cold. The practice of holding boiler-drum pressure above 500 psig effectively removes the limitation placed on permissible rate of increase of saturated water temperature when firing up by the 100-F criterion in drum differential, since saturation temperature at 500 psi is 470 F and at 1450 psi (drum pressure at rated load), it is 593 F, a difference of only 123 F. Because of the time interval involved in going from the lower to the higher pressure, it is practically impossible to exceed 100 F differential regardless of the furnace heat input rate.

By a series of trial fire-ups after weekend bottled shutdowns,

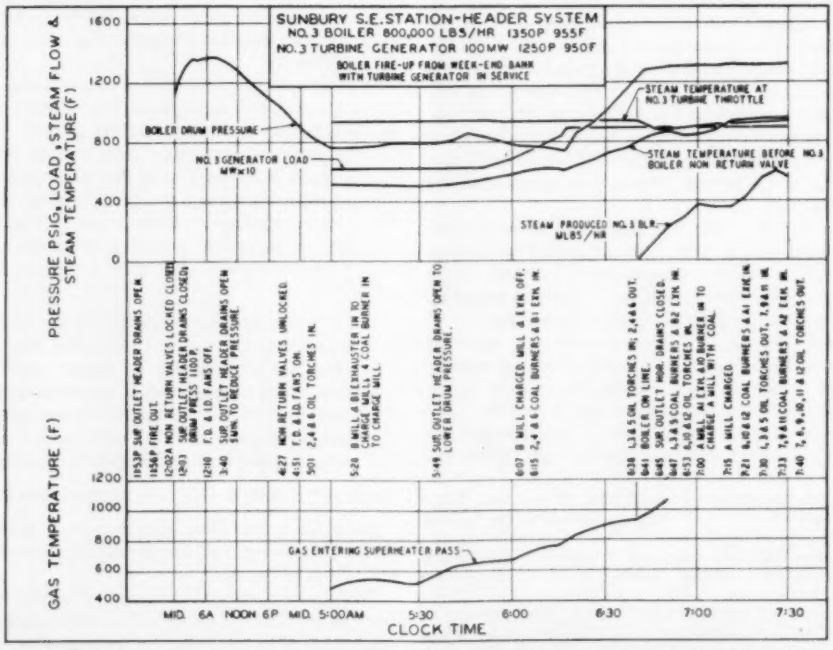

Fig. 2 Reducing temperature shock to running turbine as boiler comes on line; intermediate phase. Also shows method of conserving pressure during 30-hr bottle period without using fuel.

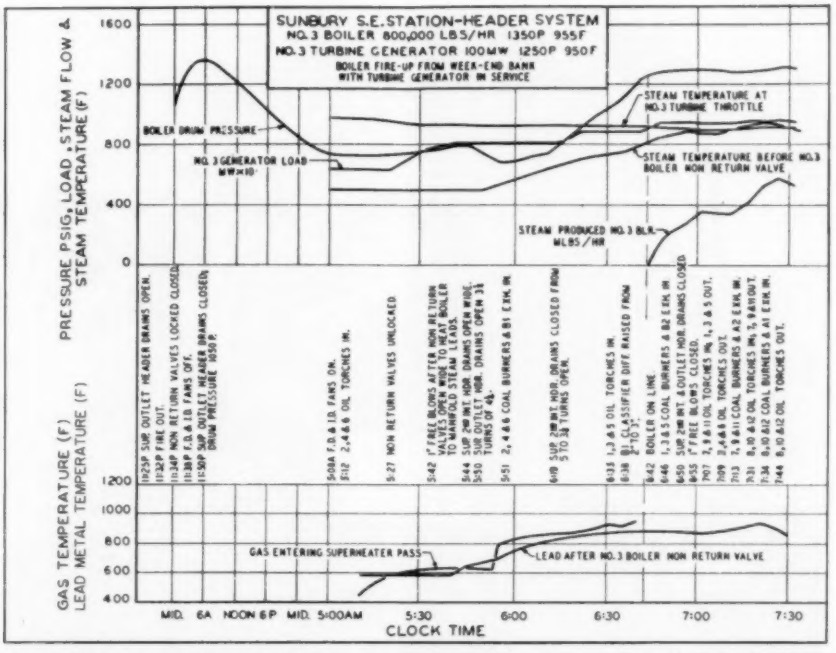

Fig. 3 Reducing temperature shock to running turbine as boiler comes on line; final phase. Steam leads heated by venting down-stream of nonreturn valves.

the steam temperature delivered by the boiler at superheater-outlet header as it came on-the-line was increased from 760 F on the first trial with a corresponding drop in steam temperature to No. 3 turbine throttle of 85 F, to 810 F with a drop in steam temperature to No. 3 turbine of only 50 F; the latter start being shown in Fig. 2. This was accomplished by reducing the drum-pressure level at which heavy firing with coal was begun on successive starts to a practical minimum of about 700 psig—the lower the drum pressure at start of accelerated firing, the higher the delivered steam temperature was found to be as the nonreturn valve opened. As much of the load as possible also was transferred from Nos. 1 and 2 units to No. 3 unit shortly prior to time that No. 3 boiler came on line, in order to reduce the proportion of cooler No. 3 boiler steam going to No. 3 turbine and thereby lessen the drop in turbine temperature.

The 50-F drop in steam temperature at the turbine still seemed to be too drastic considering the large quantity of steam coming from Nos. 1 and 2 boiler groups—620,000 lb per hr at 950 F four minutes after No. 3 boiler came on-the-line, contrasted with the small quantity coming from No. 3 boiler—120,000 lb per hr at 860 F. By simple calculation the temperature of the mixture at the turbine should have been about 935 F instead of the actual measured value of only 900 F. This seemed to indicate that the two parallel sections of steam leads between the nonreturn valves of No. 3 boiler and No. 3 unit manifold, Fig. 1, were cooling down considerably during the boiler shutdown even though they were open and under pressure from unit No. 2 system up to No. 3 boiler nonreturn valves.

A thermocouple was peened into one of No. 3 boiler steam leads just downstream of the nonreturn valve and a convenient 1-in. free-blow valve, prior to the next trial start. Some cooling was expected, to be sure, but no one was prepared to see the temperature drop down to the saturation point and lower, as it was found to be after a 30-hr shutdown of the boiler, in a lead which was open to 950 F steam. The two leads from the nonreturn valves to No. 3 turbine manifold were some 225 ft long, the nonreturn valves were considerably higher than the manifold and the leads were pitched to the manifold which should have made them self-draining. Pipe insulation was up to normally accepted standards for central-station application.

On succeeding starts, the leads were heated to equal "on-line" boiler steam temperature in the 850 F region by using steam from the manifold flowing in the reverse direction and venting through the free-blow connections near the closed boiler nonreturn valves during the boiler fire-up. This practice produced a drop of only 20 F in steam temperature at turbine throttle valves as the boiler came on line, Fig. 3, which was entirely satisfactory so far as turbine-spindle differential movement was concerned. The unit has been started up repeatedly using this procedure without any signs of distress.

Martins Creek No. 1 Unit—132.5 mw, 1250 psi, 950 F

The major portion of the paper is taken up with discussion of the controlled starting study on this unit which was begun just a few weeks after initial operation.

This plant is of the semi-outdoor design, Fig. 4.

Boiler is by Foster Wheeler, 1,200,000 lbs per hr continuous rating with divided wall, horizontally fired furnace, and combination radiant-convection superheater. Twelve intervane-type burners, arranged in two horizontal tiers of six burners each, intersect the front wall, which is occupied entirely by the radiant superheater, Fig. 5. Each row of six burners is served by one mill and two exhauster fans. The convection superheater is drainable. Flow of steam from drum is through the superheat-control condenser, to downtake tubes of radiant superheater, to radiant-superheater intermediate headers, to uptake tubes of radiant superheater, to drainable convection superheater, which is made up of two sections in series, to superheater-outlet headers, and finally to the two boiler-lead valves. Each of two radiant-superheater intermediate headers is provided with 1-in. drains

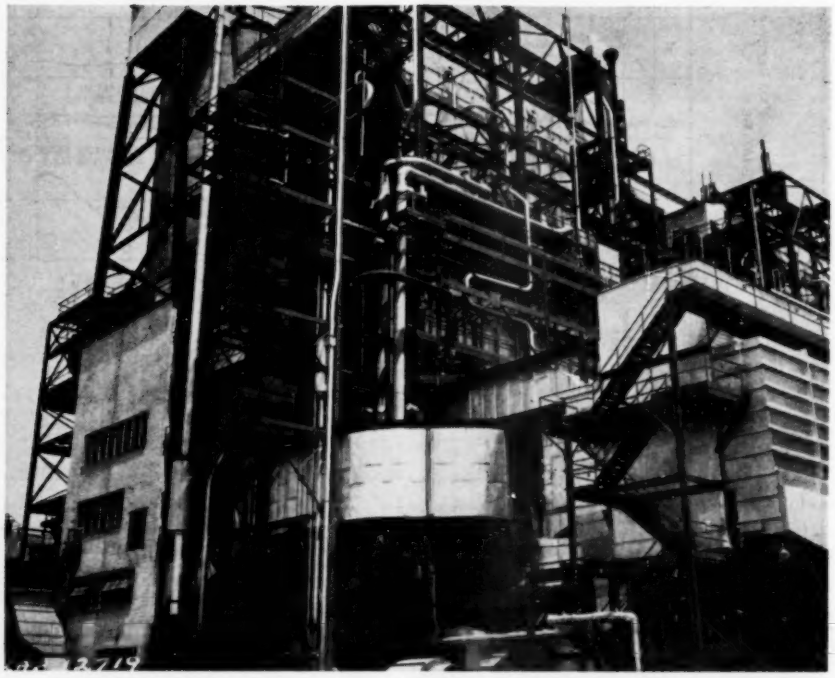

Fig. 4 Martins Creek Steam Electric Station, outdoor design showing exposed length of two main steam leads from rear of boiler to mill room

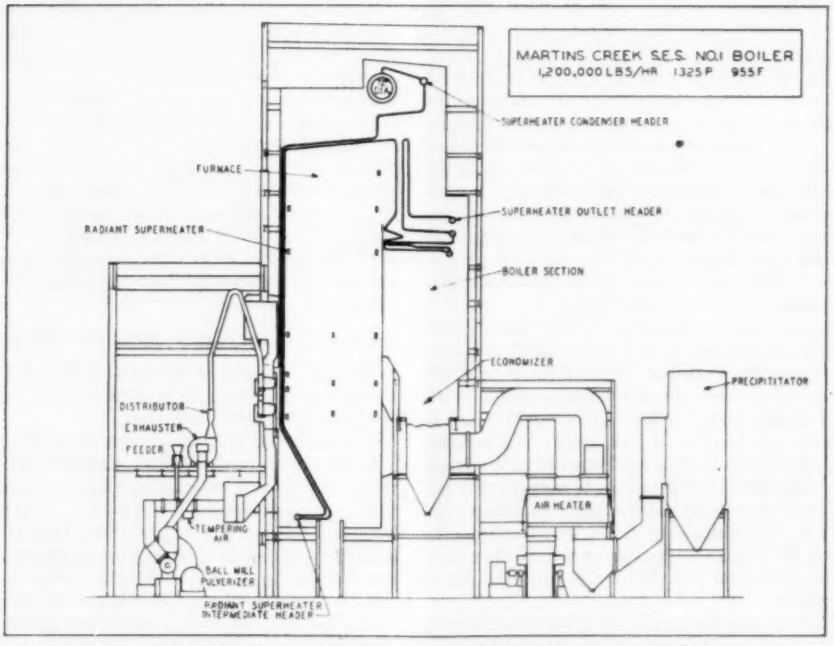

Fig. 5 Martins Creek No. 1 Boiler. Steam path from drum to outlet header.

located toward the middle of the boiler front wall in each header, and the two convection superheater-outlet headers are provided with extra large $2^1/_2$-in. drains, Fig. 6.

Steam leads originally were equipped with a 1-in. drain at the mixing-chamber section and a pair of 1-in. drains before the seats of the turbine stop valves. These drains proved to be inadequate for starts from overnight shutdown and had to be enlarged as the program developed.

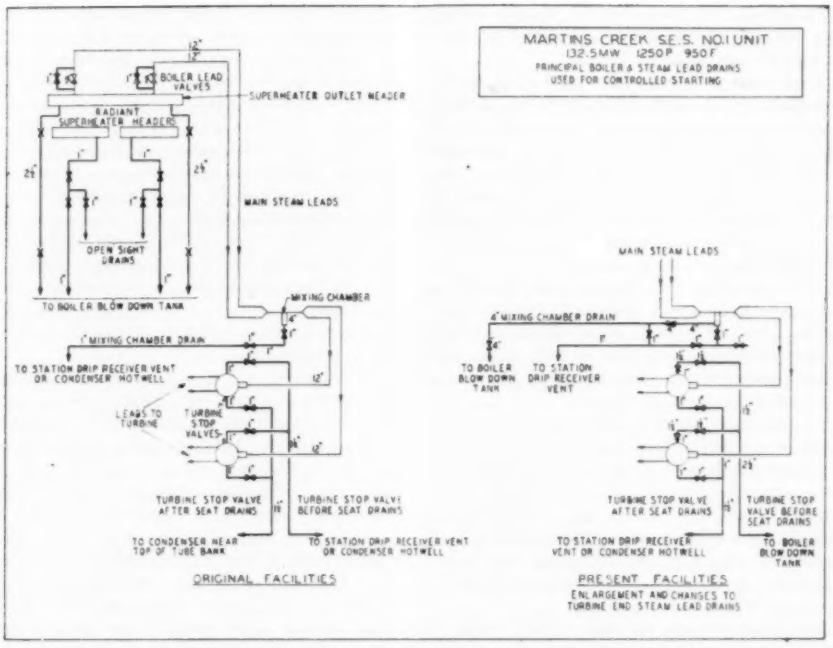

Fig. 6 Changes made to original turbine end lead drains to speed up heating of steam leads on overnight starts

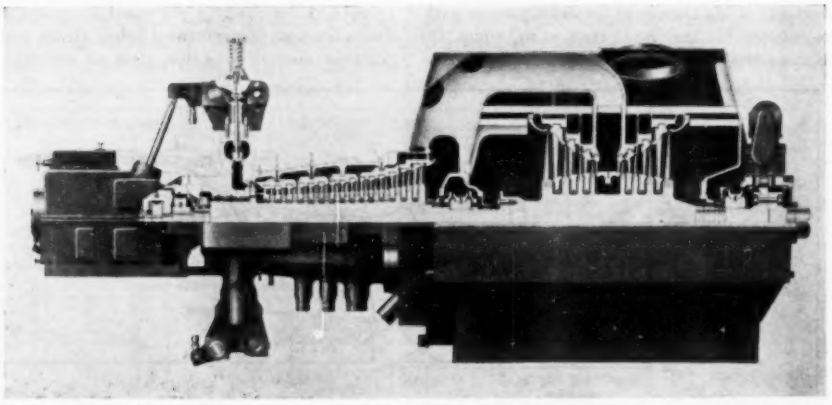

Fig. 7 Martins Creek No. 1 turbine. Sectional view showing massive valve chests, bowl, and packing-hub sections.

The high-pressure section of the turbine is of single-shell construction, equipped with top and bottom steam chests, four control or governing valves in each chest. Steam from the stop valves enters both ends of the steam chests, Fig. 7. Each turbine stop valve is equipped with a small bypass or pilot. Neither main valve nor bypass valve can be controlled or held in a part-open position for starting like the throttle valve and bypass combination on some designs. This means that the governing valves must open successively as the machine is rolled and loaded to accomplish the necessary throttling, and the walls between adjacent valve bowls in the massive front end of the turbine may be subjected to severe temperature differentials with improper operation.

Upward of 40 thermocouples were imbedded into critical turbine sections at the factory initially through co-operation of General Electric Company, and some 23 thermocouples were installed in the boiler drum, with the help of Foster Wheeler Corporation, along with many miscellaneous elements in the radiant superheater tubes adjacent to burners in the furnace and in some tubes near convection superheater headers, extended-surface headers, and so on, Figs. 22 and 23.

Development of Starting Procedures

Starts From Overnight Shutdown. Most of the early runs were taken up in trying to devise means of firing with coal prior to rolling the turbine in order to obtain a satisfactory margin of steam temperature at stop valves over turbine inner valve-chest temperatures at roll time without causing overheating of the radiant-superheater tubes in front furnace walls adjacent to the burners. Thermocouples had been peened into the two tubes

with the greatest exposure to flame on either side of each burner.

An arbitrary top metal-temperature limit of 1100 F on these tubes was used as a guide in firing.

The minimum heat input to the furnace per burner recommended by the manufacturer to avoid coking and burner damage was fairly high, for radiant superheater-metal temperature considerations during start-up, at 45 million Btu per hr. Expressed in terms of firing rate, this represented a coal flow corresponding to 1.8 in. of water-pressure drop (classifier differential) across the mill classifier in the coal-primary air mixture as it passed from one end of the mill through classifier to exhauster fan when the latter was serving its full complement of three burners.

On the first few starts, in order to maintain firing symmetry on both sides of the furnace division wall, only one burner of three per exhauster fan was used. This arrangement did not work too well because of poor control characteristic of mill primary-air damper in the almost closed position when supplying only two of possible six burners at very light coal-air flows.

The next step was to go to 2-burner operation per exhauster (rather than 3) both in the interest of symmetrical firing in the two furnaces and to reconcile the high minimum permissible firing rate (45 million Btu per burner per hr) with the small boiler and lead-venting facilities available. Using the manufacturer's recommended minimum of 1.8 in. classifier differential with two burners per exhauster during the preroll-heating period unhappily ran the radiant superheater-tube metal temperature to prohibitive levels above 1100 F.

The only practical alternative at the time seemed to be to forego the preroll steam-temperature-raising operation and to roll the turbine either coincidentally with, or before introducing coal to the fire.

The next few overnight starts then were necessarily made with steam temperature entering the turbine at start of roll some 100 F cooler than the front-end turbine metal. Roll periods were progressively reduced from one hour to 20 min and loading rates were raised from 1 mw per min to 2 mw per min. Conforming to accepted practice prevailing at the time, a substantial load was applied to the generator immediately after synchronizing.

Fig. 8 shows data from one of the early controlled starts from overnight shutdown and illustrates the disadvantages of starting with low steam temperature and high initial load followed by fast loading. Initial load application was 18 mw, after which the load was raised at about 2.7 mw per min for the next 14 min to 58 mw. The thinking in controlling rate of steam-temperature rise at the turbine on this start was that application of a large load initially and fast loading would cause a larger quantity of steam to pass through the radiant-convection superheater, which should result in less heat absorption per unit weight of saturated steam passing toward the turbine and keep the turbine steam-temperature-rise rate at a minimum.

This thinking was essentially correct for behavior of the steam at superheater outlet, but wrong for its action at the turbine end since it neglected the inertial or cushioning effect of the comparatively cool piping between boiler and turbine. Steam temperature at turbine stop valves increased at a rate of 1080 F per hour during the initial 14-min loading period and inner first valve-bowl temperature increased at 1290 F per hr during the same period, both of which were far in excess of the recommended 500 F per hr maximum metal-temperature rate of change. In addition, there was a sharp reversal of temperature differential (and stress) across the first valve-bowl section from about 200 F outer surface over inner surface shortly before synchronizing to 163 F inner surface over outer surface a short time later. It became obvious for a given difference in steam temperature between superheater outlet and turbine stop valves at the moment the generator was synchronized, and with steam leads at temperatures below steam temperature at either point—a normal condition after an overnight shutdown—that

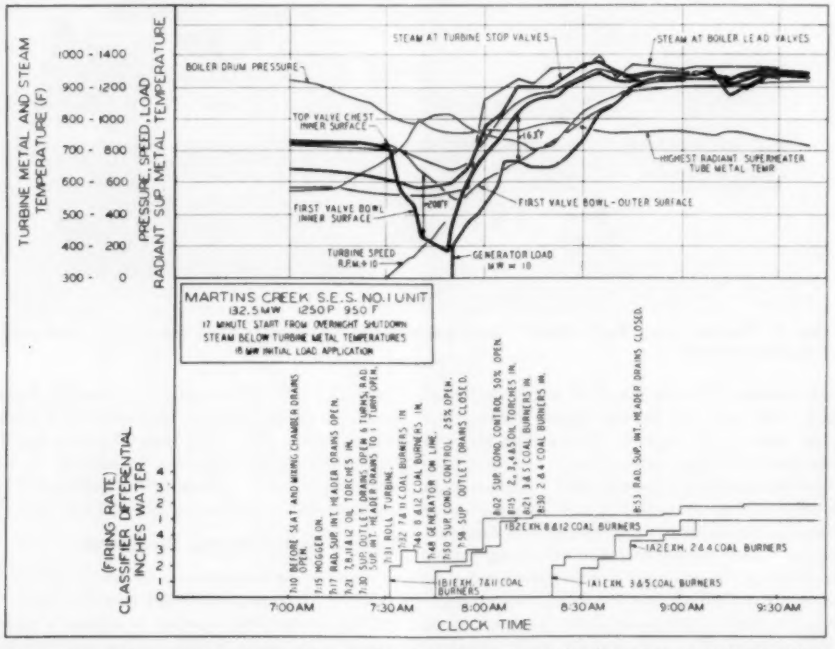

Fig. 8 Severe first valve-bowl quenching produced during roll period when steam is below turbine-metal temperature. Prohibitive metal temperature-rise rates and differentials resulting from application of too much load initially. Note small scale for steam and metal temperature when comparing with Figs. 9 and 10.

the spread between superheater-outlet and stop-valve steam temperatures decreased directly with rate of load pickup or steam flow pickup because of the higher rate at which the leads absorbed heat at the higher flow rates.

When enough information had been collected to understand the combined effects of the boiler steam-temperature characteristics and the cool-steam leads on steam temperature at turbine stop valves, it was realized that the most effective method of controlling steam and turbine metal-temperature-rise rates was (*a*) to apply as little load as possible to the generator initially, while keeping the firing rate fairly constant; (*b*) to hold this load for a short soak period while the steam leads (initially close to saturation temperature) were absorbing heat; and (*c*) to start increasing the load and firing rate parabolically with time to a maximum rate governed by behavior of later valve-bowl temperatures, as soon as the rate of temperature increase of the most critical turbine front-end area started to fall below the desired rate. In this case, the critical areas at the end of the soak period were the first and second valve bowls.

Application of the lowest practical load to the generator immediately after synchronizing and holding for a short soak period had the added advantage of reducing the cooling shock to the turbine-exhaust-end components.

Radial cracks, which recently were found in the outer last-stage diaphragm rings of one of the Sunbury 75-mw, 1250-psi, 950-F base-load units, are believed to be the result of excessively fast exhaust end cooling brought about by large initial load application during the few starts that were made over the past eight years, combined with insufficient rolling vacuum because of undersized condenser-hogging equipment.

The difficulty in excessive radiant tube-metal temperature was largely overcome when it was realized that the minimum classifier differential of 1.8 in. water recommended by the boiler manufacturer to avoid coking of burners applied only when using three coal burners per exhauster. With two burners per exhauster, it was found by calculation that the classifier differential could be lowered to 1.3 in. without reducing coal and primary-air flow through burners to a point where coal fall-out would induce burner coking. This cleared the way for effective firing with coal before rolling the turbine to bring about proper relation between steam and front-end turbine-metal temperatures. Although the threat of overheated radiant-superheater tubes was never dispelled completely, both units are being started regularly as required after weekend and overnight shutdowns and without difficulty.

The boiler manufacturer has since changed the design of front-wall radiant-superheater units by replacing the first superheater tube or two adjacent to burners with waterwall tubes.

Fig. 9 shows a start which embodies the principles just outlined and which, in general, determined the pattern for future starts. Burner problems had been quite well solved at this time because of permissible reduction of classifier differential to 1.3 in. water when using two burners per exhauster as indicated by moderate temperatures of radiant-superheater-tube metal during the preroll firing period. Drain facilities at the turbine end of the leads still consisted of only the original three 1-in. drains and obviously were inadequate for optimum heating of the steam leads at roll time.

Steam temperature at boiler lead valves at start of fire-up was only slightly above saturation, and started to increase almost immediately after light-off with before seat stop-valve and mixing-chamber drains opened wide. Steam temperature ahead of turbine stop valves at the same time, on the other hand, was much higher because of greater heat retention in the massive stop valves nearby.

As these data show, the concern which is felt in some circles regarding presence of water at closed stop-valve seats when under pressure from the boiler during normal overnight shutdown is unfounded. Saturation temperatures at stop valves are not reached until about 14 hr after the turbine is shut down on this unit.

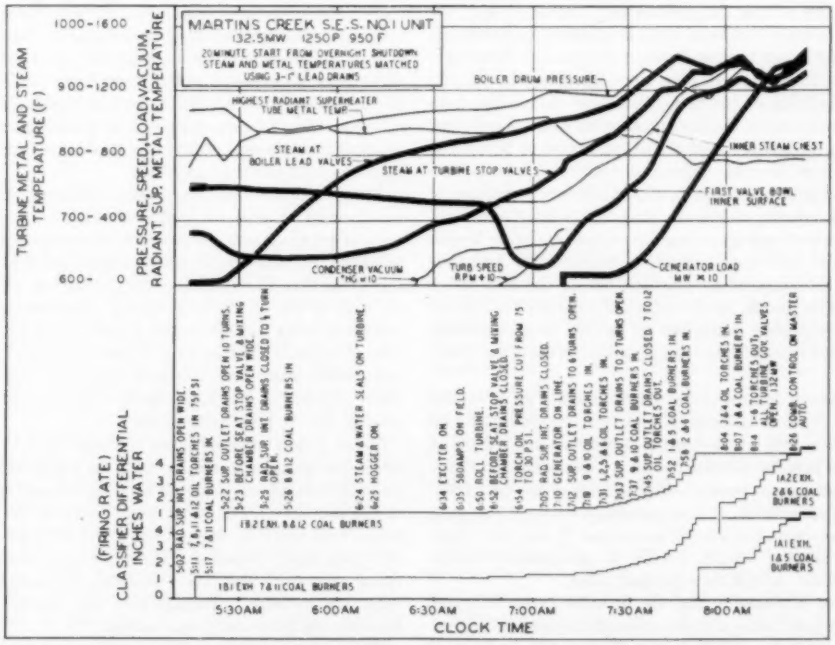

Fig. 9 Effect of short soak period at 4.5 per cent capability on steam and turbine-metal temperature rise rates

As soon as flow through the cool leads to the turbine-end drains was established, temperature of steam at the turbine stops began to drop and leveled off after a few minutes at about 100 F above saturation. A long wait followed, during which coal and igniting oil were fired to the furnace symmetrically through four burners at minimum firing rates to raise steam temperature at the boiler, but primarily to heat the leads and get steam temperature to proper levels at the turbine. Firing rates were still limited by allowable radiant superheater-tube metal temperatures for the steam flows possible through two $2^1/_2$-in. superheater-outlet drains and three 1-in. turbine-end drains.

On this run, it took about 90 min of preroll firing to barely match the steam temperature ahead of stop valves with inner surface temperature of turbine steam chest and first valve bowl.

Quenching of Valve Bowls. Still referring to Fig. 9, it will be noted that as soon as the stop valves were opened some 4 min before rolling the turbine (with the governing valves closed) the inner surface of the first valve bowl began to cool down very rapidly because of the throttling of steam through the first control or governing valve which, although closed, was actually passing steam. It must be remembered that the control valves are not shut-off valves and, therefore, do not effectively seal off bowls from chests when in closed position. This tendency is actually beneficial in the case of the later valve bowls. Cooling continued after the turbine was rolled until sufficient steam was passing through the valve bowl to bring the turbine speed to about 600 rpm. At this point, the rate slowed down perceptibly but the cooling continued until a minimum metal temperature of about 630 F was reached.

Curiously enough, for isenthalpic or complete throttling expansion at that particular moment in the roll cycle from actual steam conditions ahead of the first control valve of 1165 psi and 768 F, to 10 psia (assumed) in the valve-bowl cavity after the first control valve, final steam temperature would have had to be about 653 F or 23 F above the temperature to which the inner valve-bowl surface was actually quenched.

On weekend starts during the steam-chest heating period just prior to roll, dips in temperature of inner first valve bowl as much as 145 F below final steam temperatures to be expected from completed throttling expansion to 10 psia, were experienced, Fig. 17.

This severe quenching of the first valve bowl during the time when the first control valve is either cracked or fully closed then seems to indicate an incompleted throttling action in which the valve bowl or plenum after the valve is not surfeited with steam, and there is not enough turbulence produced to convert the kinetic energy of the high-velocity steam resulting from nearly isentropic expansion back to heat energy to regain original enthalpy levels.

The sharp dip in inner first valve-bowl temperature and subsequent reversal of temperature gradient across the first valve bowl to outer surface and to inner surface of adjacent valve bowl as load is applied imposes a limitation on loading rates, since this metal must be raised from a lower level than that of the other front-end sections.

On the start shown from overnight shutdown, Fig. 9, it was necessary to hold the load at 7 mw (4.5 per cent capability) for 15 min while the inner first valve-bowl temperature was rising at close to maximum permissible rate before it was possible to apply more load. On subsequent runs when quenching of the first valve bowl was largely eliminated, it was possible to reduce the soak period to five minutes and reach full load some 72 min after synchronizing, still staying within maximum permissible metal-temperature-rise rate, as will be explained later.

Two methods of minimizing the dip in valve-bowl temperatures of a hot machine after a short overnight shutdown suggest themselves. The first involves bringing the machine up to full speed in a very short time, possibly in five minutes or less, in order to fill up the bowl plenum quickly after the control valve, and move a greater portion of the expansion zone over to the main nozzles. Temperature and differential-expansion considerations should not present barriers to the idea so long as temperatures are matched at start of roll; but there would be a disadvantage in the shorter time allowed the operator to check the unit while it is coming up to speed and also possibly because of exhaust end heating complications. For these reasons and because of possible cries of heresy, this procedure was not tried.

The second and standard method, of course, is to have a healthy margin of steam temperature at stop valves over front-end turbine-metal temperature before rolling turbine so that the dip in steam temperature as it passes through the control valve will depress the inner valve-bowl surface temperature only a minimum amount. On this unit it was found that a margin of 130 F steam over metal temperature depressed the inner first valve-bowl surface only about 10 F and a margin of 75 F dropped it 45 F for a 20-min turbine roll in both cases.

Fig. 10 illustrates the second case, which was adopted as standard procedure for the subject units. The hold period required at 7 mw was only five minutes as compared with 15 min for the run shown in Fig. 9 where steam and metal temperatures were just matched. Moreover, for inner-bowl temperature-rise rates of about 325 F per hr in both cases and the same over-all loading rate, the temperature differential from inner to outer surface of first valve bowl for the case where temperatures at roll time were matched was 115 F as against only 100 F where the steam over metal margins were maintained. Although the difference in temperature differential between the two cases cited seems rather small, it is felt that any procedure which will reduce thermal stresses in the heavy, irregular-shaped front-end turbine sections, however small, and which will allow reasonably fast load application, is worth consideration.

Turbine-End Steam-Lead Drains. Referring to Fig. 9, it required some 90 min of preroll firing as explained previously to just match steam temperatures ahead of stop valves with that of turbine-metal temperature after an overnight shutdown when using only the three existing 1-in. drains at the turbine end of the leads. This resulted in a waste of both condensate and fuel, since the $2^1/_2$-in. superheater-outlet drain had to be kept open blowing to atmosphere throughout the period in order to produce enough additional flow for proper cooling of the radiant superheater, while the small turbine-end drains were used primarily to heat the steam leads between boiler and turbine.

It was obvious from the results obtained thus far that larger turbine-end steam-lead drains would have to be provided, not only to get the steam temperature at turbine to the right point in less time, but also to permit safer starting by allowing more cooling-steam flow through the radiant superheater. A convenient 4-in. stub in the steam-lead mixing chamber located about 40 ft upstream from the turbine stop valves was utilized to provide a 4-in. drain into the lead at this point and the before seat turbine stop-valve drains were enlarged from 1 to $1^1/_2$ in. except for the short nipples at the stop valves which could not be changed readily, Fig. 6, present facilities.

Table 1 lists metered flows through the 4-in. mixing-chamber drain line along with related data for a typical routine start from overnight shutdown, which it is thought may be of value to others in the industry. The inner drain valve or the one closer to the steam lead was fully opened and the outer valve was used to control drain flow. Opening of the outer valve is shown in number of turns open from the closed position, 11 turns being required to open it completely. Impact tube was located in the drain line between the inner and outer valves.

Turbine was rolled at 6:50 a.m. and synchronized on line at 7:10 a.m. Note how steam temperature at turbine lagged be-

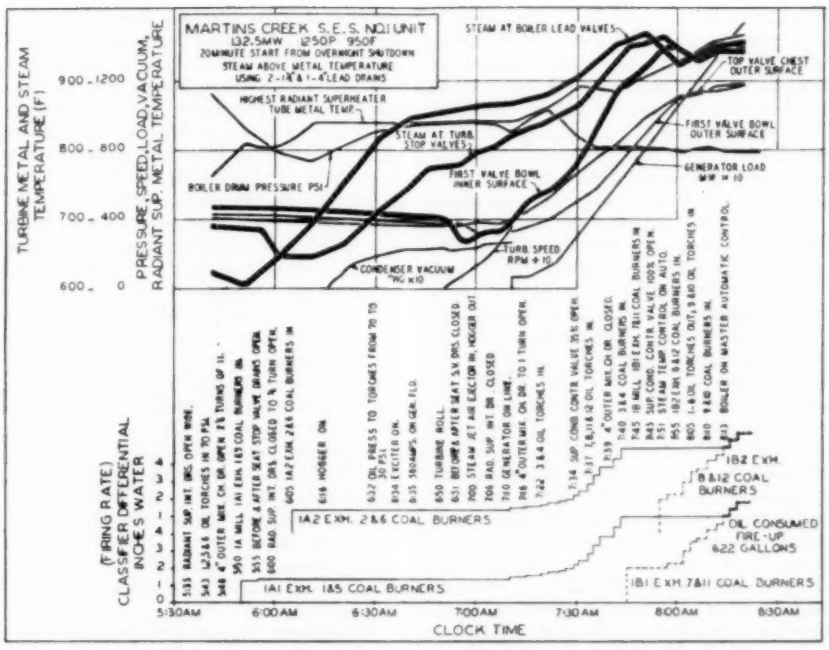

Fig. 10 Effect of large turbine end lead drains on turbine-end steam temperature and preroll firing time

Table 1 Steam flow through 4-in drain near turbine end of lead on start from overnight shutdown and related data

Time a.m.	Opening of outer 4-in. drain valve, turns	Manometer differential, in. Hg	Static plus velocity pressure at impact tube, psig	Static press. at impact tube, psig	Steam temp at impact tube, deg F	Press in boiler drum, psig	Steam temp at boiler superheater outlet, deg F	Steam temp before turbine stop valves, deg F	Steam flow at impact tube, lb/hr	Velocity in 4-in. drain line, fps
6:00	2½	15.0	738	730	581	780	624	635	56,300	130.9
6:10	2½	21.8	770	757	615	820	690	635	70,200	159.7
6:20	2½	29.1	985	968	707	1000	795	662	86,400	172.0
6:30	2½	31.2	1053	1040	748	1135	843	718	90,250	175.4
6:40	2½	33.0	1105	1090	778	1200	862	765	94,100	178.4
6:50	2½	34.3	1150	1130	816	1240	873	798	94,800	182.7
7:00	2½	35.3	1180	1160	831	1265	878	815	96,600	184.7
7:10	2½	35.3	1188	1168	837	1275	882	835	97,000	184.5
7:20	1½	2.3	1430	1420	854	1450	920	870	27,500	42.3
7:35	1½	1.7	1300	1290	888	1400	936	908	22,050	39.2

hind that in the drain line at the impact tube until after the generator was carrying load, except for short initial period when residual heat in the massive turbine stop valves affected turbine-end lead temperatures, because of heat absorption in the boiler-turbine leads. Note also the tremendous difference in flows resulting from changes in valve setting near the closed position.

In the final development stages of the overnight starts, flows through the new large drains for heating steam leads and establishing proper steam-to-turbine metal-temperature relation were regulated reasonably close to the specified 100,000 lb per hr rating of the silencer. A 60-min preroll firing period under optimum firing conditions produced a margin of steam over turbine front-end metal temperature of about 75 F at time of roll, Fig. 10. Compare longer preroll firing time necessary and slow temperature response when using the original drains, Fig. 9. A slight dip in inner first valve-bowl temperature was accepted as a compromise instead of resorting to heavier blowing and/or longer preroll firing both in the interest of good public relations and safety to personnel and equipment.

While this relatively inexpensive means of attaining proper steam-temperature conditions at start of roll as installed left much to be desired when compared with the bypass line-heat exchanger combination which returns the blown condensate to the cycle via the condenser hotwell, its chief drawback of limited capacity can be remedied by doubling the blowdown tank, vent-stack, and silencer facilities. There is no real problem in making up the blown condensate. Before putting large amounts of drain flows through blowdown tank, silencer, and vent, the capacity o the silencer and water separator or steam dome at the top of the stack should be investigated.

Overnight Starts—Miscellany

Several practices, discoveries, or modes of operation which presented themselves as the controlled-start program developed, are mentioned here as a matter of general interest.

Warming Turbine-Valve Chests. As the program developed and steam temperatures were finally brought to desired levels above turbine steam-chest temperatures, the question of actual

need for preheating steam chests for starts after overnight shutdown, prior to rolling turbine by repeated opening and tripping of the turbine stop valves presented itself. Daily pounding of these heavy valves it was felt could only lead to expensive maintenance, unnecessary heating of the turbine-exhaust components, waste of fuel, and bottling difficulties.

Accordingly, several starts were made without heating the chests, using progressively higher steam temperatures. Fig. 11 shows plotted data from one of them in which the steam temperature at stop valves, inner steam-chest surface, and outer steam-chest surface temperatures just before rolling the turbine were 768 F, 725 F, and 705 F, respectively. When the stop valves were opened to roll the turbine there was an upward jog in the inner-chest surface temperature of only 7 F followed by a slow steady rise of something under 200 F per hr. From these tests, it was evident that no worth-while gains could be realized from chest preheating on overnight starts and the practice was discontinued for temperature margins under 100 F.

Influence of Later Valve-Bowl Considerations on Permissible Loading Rate. The characteristic quenching action of steam on the first and second valve bowls as it expands through the corresponding partly opened control valves during the preheating and rolling periods has been discussed, along with related temperature and thermal-stress reversal and possible methods of ameliorating its harmful effects.

Behavior of the valve-bowl temperatures after the remaining control valves also must be taken into account in determining permissible loading rates. During the early loading stages, the expansion zone moves downstream from the first and second control valves to the main nozzles under those valves. The second valve on this unit begins to open when the first valve has attained 10 per cent of full lift.

Steam temperature at exhaust tips of main nozzles drops considerably as evidenced by a decrease of almost 100 F in the first-stage-shell inner-surface temperature, Fig. 11. If this cool steam in the first stage can gain access to the idle valve bowls under the closed valves, assuming there is no leakage past the valves, the valve bowls will be cooled rather than heated. If, on the other hand, there is leakage through the closed valves which seems more likely to be the case, in view of the preroll expansion which is known to exist through the first control valve, there also will be cooling of the idle valve bowls because of nearly isentropic expansion of the leaking steam.

Whichever is the case, the plots of both 6th and 8th valve-bowl metal temperatures indicate that a drop in inner valve-bowl surface temperature actually does take place, and that the minimum temperatures in both bowls is reached about 15 min after the generator is synchronized. As late as 35 min after synchronizing and with the generator carrying 46-mw load (132.5 mw nameplate) the 6th and 8th valve-bowl temperatures were still 4 and 19 F, respectively, under the original levels at light-off in the 700 F region. At this point, steam temperature at stop valves was over 900 F, some 200 F higher than the 6th and 8th valve-bowl temperatures.

It becomes evident then that caution must be observed in the rate of load pickup, even from load levels as high as 35 per cent of name plate. In this case, a loading rate of just under 3 mw per min produced a metal temperature-rise rate of 480 F per hour in the 6th valve bowl and 285 F per hr in the 8th valve bowl. In general then, 3 mw per min should be considered as the top loading rate on a machine of this type and size for an overnight start.

For weekend and cold starts the loading rates would have to be correspondingly lower.

One of the devices which was used to good effect in lessening the severity of the temperature shock on the later valve bowls while allowing a more rapid load pickup, was purposely to hold down the boiler steam pressures so that as many turbine control valves as possible were opened before steam temperature at stop valves reached rated levels. In practice, all of the control

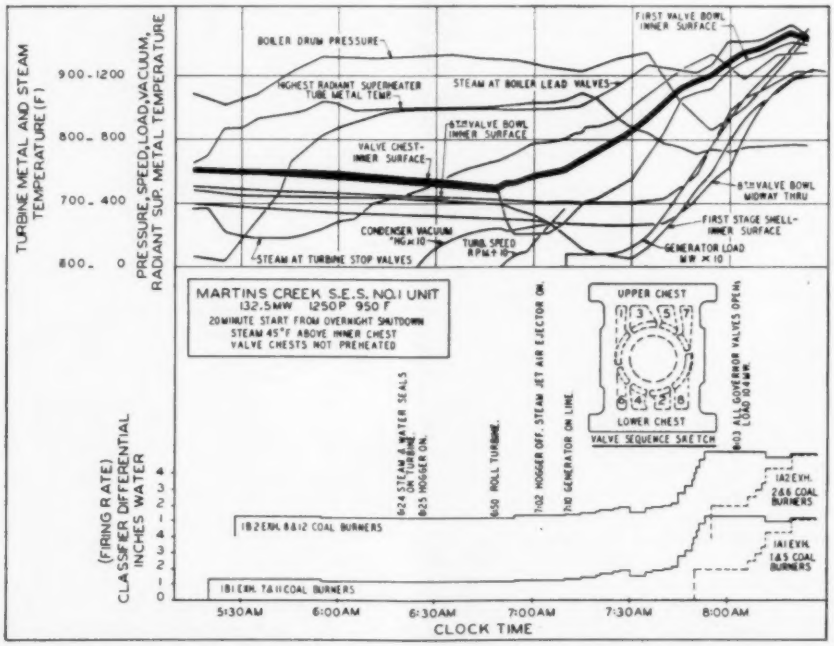

Fig. 11 Smooth rise of inner valve-chest temperatures demonstrates chest preheating unnecessary on overnight starts. Slow heating of later valve bowls poses a design problem.

valves are usually completely opened when load is in the 80 to 110-mw range on the 160-mw (rated capability) subject unit. The remainder of the load pickup is then accomplished by increasing pressure to normal values with all control valves open. With this mode of operation it is of course not possible to switch to master automatic control for systems working on steam pressure as master impulse and it becomes necessary for operators to control firing rates as well as load manually.

Valve Sequence. Arrangement of control valves with respect to opening sequence, in some cases, may make the task of averting excessive thermal stresses in the massive transition sections between the valve chest and cylinder extremely difficult, if not impossible, during starting operations. In the case of the subject unit, for example, referring to the valve-sequence sketch in Fig. 11, No. 8 valve, which is the last one on the bottom chest to open, is placed next to No. 2 valve, the first one to open. Although no thermocouple was installed in the second valve bowl, the temperature existing there at any moment in the loading period above 45-mw load may be safely assumed for purpose of discussion to have been about equal to those existing in the first valve bowl, since the first two valves are fully open at this point.

Approximately 35 min after going on line with load at 47 mw, metal temperature midway through the wall of the 8th valve bowl (about $1^1/_2$ in. from the inner surface) was 681 F and temperature of the inner surface of the second valve bowl was 862 F, or a difference of 181 F. The inner surface of the 8th valve bowl moreover may be presumed to have been cooler than the 681 F measured midway through the bowl-wall section because it was either exposed to first-stage steam which averaged less than the 629 F measured inner first-stage shell temperature for the previous half hour, or it was cooled by the steam expanding isentropically through the closed 8th control valve, as explained previously. It is safe to say then that there must have been a maximum temperature differential in excess of 185 F existing across the wall between the 2nd and 8th valve bowls under the valves where they are tangent, in the very heavy section over the packing hub, and in the nozzle bridges where much of the cracking recently experienced in the industry is taking place. The manufacturer's recommendation for maximum temperature differential it will be remembered is 150 F which is 35 F lower than the figure attained on this unit with very conservative loading rates.

This is a matter that cannot be wholly remedied in operation no matter how conservative the loading rates are made, although bringing the unit on with lower steam pressures is helpful to a degree. The real need is for a change in design which will separate hot and cold valve bowls, or better still, one which provides a throttling device upstream of the turbine that will cause all control valves to open and heat front-end turbine cavities evenly during the entire start-up process.

Starts From Cold and Weekend Shutdowns

Many problems were encountered in starting from cold in addition to the ubiquitous one of firing the boiler satisfactorily with coal before rolling the turbine. Among these were boiler-drum circulation, warming of turbine-valve chests, and turbine horizontal-flange limitations on loading.

Warming Turbine-Valve Chests. On the cold start shown in Fig. 12 the valve chests were heated in the conventional manner by opening and tripping the main stop valves, starting about 45 min before rolling the turbine after the boiler-drum pressure was up to the 300-psi level needed to actuate the condenser-hogging equipment. The inner-chest metal temperature rose almost instantly from 90 to 380 F at a rate of about 6000 F per hr.

On the next cold start, Fig. 13, in order to eliminate some of the temperature shock, the stop valves were opened and tripped at regular intervals starting as soon as a slight amount of pressure was built up in the steam leads and the steam was slightly superheated. The valves were opened for the usual second or two, then tripped and the condensed water was drained through the

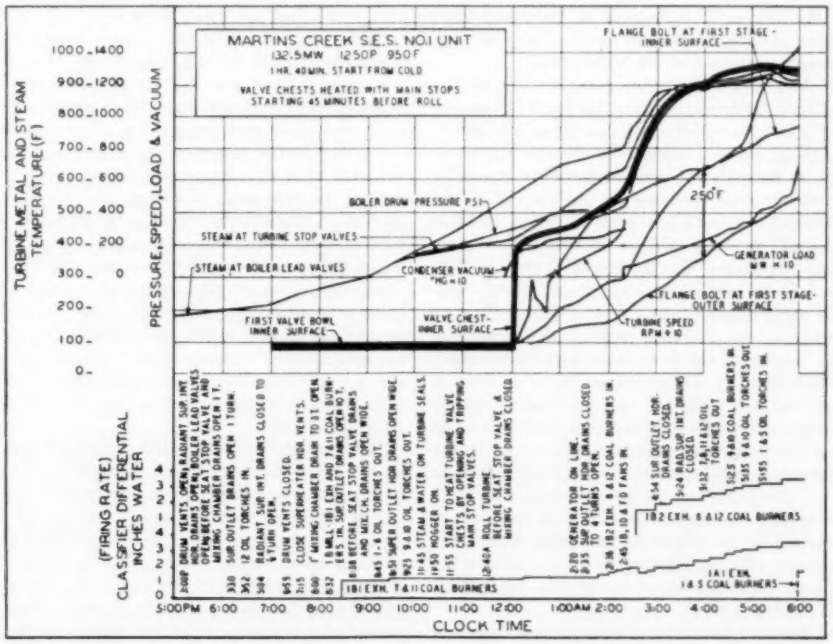

Fig. 12 Illustrates severe temperature shock imposed on valve-chest metal by conventional heating method. Cold start.

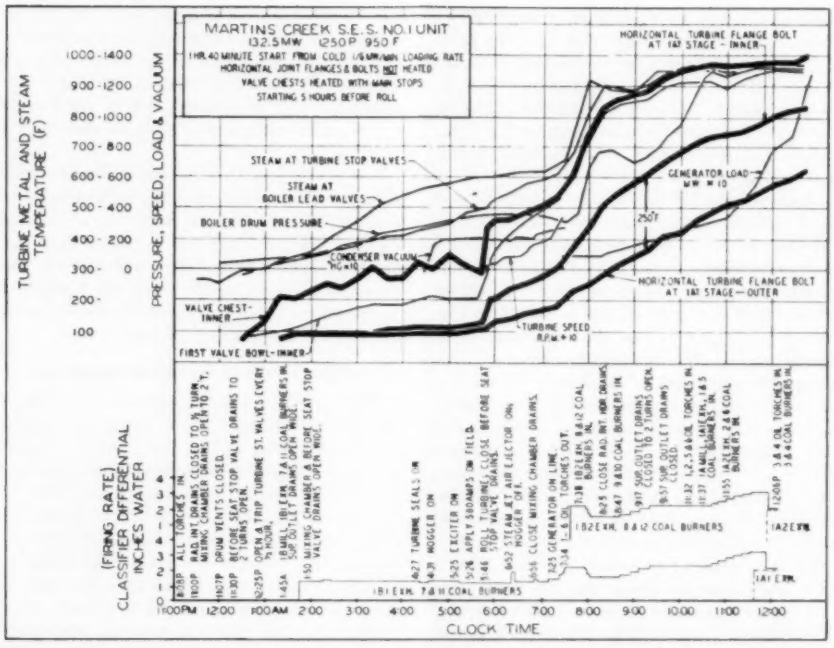

Fig. 13 Temperature shock to valve chests reduced by early heating, when steam pressure and temperature are low. Six hours required to load unit without flange heating. Cold start.

after-seat stop-valve drains every 15 min as the pressure was building up for the entire five hours before rolling the turbine.

This performed a fairly good job of valve-chest heating but still imposed a mild temperature shock at the moment the turbine was rolled. The practice also was objectionable because of certain valve maintenance and overheating of turbine-exhaust ends during shutdown periods, which was sure to follow as a result of repeated pounding imposed on the valve seats.

Some talks were had with the turbine manufacturer on the possibility of installing a drain connection at the low mid-point of each of the chests. The stop valves could then be opened at the start of the cold fire-up and the steam flow through the valve chests to chest drains through the open stop valves would be controlled by the warm-ups or bypasses around the boiler lead valves with the latter closed until just prior to rolling the turbine. This would result in slow, uniform heating of the entire heavy chest and bowl portions of the high-pressure casing. The manufacturer demurred because of the objectionable field welding required on the valve chests to get the connections made.

They suggested instead an alternate method of heating the chests to eliminate banging of the main stop-valve seats, which involved (*a*) partially opening the governing valves as soon as vacuum was established, (*b*) operating the stop-valve controls to open only the stop-valve pilots with the stop valve after seat drains open, and (*c*) tripping the stop-valve pilots just before pressure in the chests had built up to the point where the main valves would open. The procedure would be repeated as often as necessary to accomplish the heating desired. The idea did not hold much operating appeal because of the possibility of the main stops opening suddenly with an existing upstream pressure of 300 to 600 psi to send an avalanche of energy into the turbine while it was on the turning gear.

It was tried once, however, for a start after a one-day shutdown with boiler cold in a much emasculated form; i.e., with the governing valves closed. The stop-valve controls on this trial, Table 2, were put into the reset position in order to open the pilots, 29 min before rolling the turbine at 4:36 a.m. Pressure in the chests rose slowly to 250 psi (boiler-drum pressure 550 psi) in about 10 sec on the first try, with the stop valve after seat drains open and then rose so rapidly from that point owing to downstream pressure assist that the main stops lifted before the valve control could be tripped. The stop valves were tripped by hand immediately. After investigating to see that there were no obstructions, such as closed valves, to impede the free flow of steam from the after seat drains to the condenser, the stop-valve controls were again reset to open the pilots at 4:51 a.m.

Pressure in the steam chests rose slowly to 250 psi as before with the after seat stop-valve drains open. At the instant its rate of rise changed, the control was tripped. This closed the stop-valve pilots. Absence of panel-light indication and characteristic heavy bang, which takes place when the main stops trip, were sufficient evidence that the main stop valves had not opened on this try. The procedure was then successfully repeated several times without opening the main stops. As Table 2 shows, however, it was not only ineffective in heating the chests, but there is a suspicion that it actually tended to cool them because of the steam expansion through the pilots since the drop in chest temperature during the operation was greater than that due to natural cooling.

When it became evident that the chests were not being heated by use of the stop-valve pilots alone, the main stops were opened and tripped twice shortly before rolling the turbine.

The record is extended beyond the time of rolling the turbine to show by the very gradual rise in inner-chest temperature during roll and early loading periods that it was really unnecessary to preheat the valve chests in this case where, without preheating, the temperature would have been some 130 F above the chest-metal temperature at roll time. At the time the run was made, however, the action was not too well understood and standard starting procedures were used in this respect.

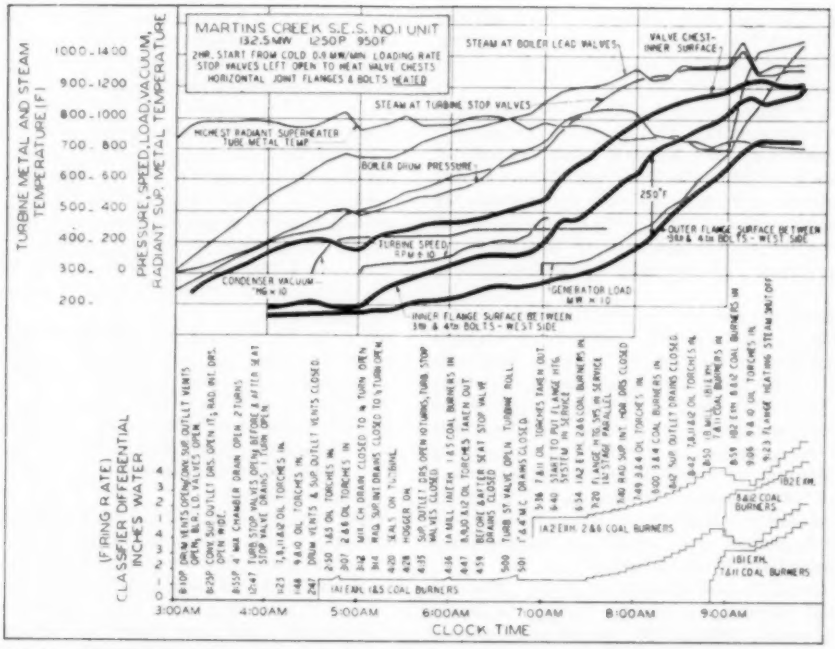

Fig. 14 Temperature shock to valve chests eliminated. Main stop valves are tripped only once, reducing seat wear. Three hours required to load unit with flange heating. Cold start.

Finally, after giving the problem more thought, the idea of opening the main stops early in the start procedure and leaving them open through the entire start was hit upon—to allow free flow of steam from the boiler drum right up to the turbine governing valves. Actually on cold starts, the stop valves and boiler lead valves were opened before lighting off the boiler—with the before and after seat stop-valve drains open a turn or two to drain off the condensed water as it formed, Fig. 14. This represents the finished cold start as now used in operation, except in cases where the generator field must be preheated. On weekend starts, the boiler lead valves were left closed until pressure was equalized around the lead valves by means of the lead-valve warm-ups and some superheat was showing at the stop valves.

This scheme worked fine for heating turbine valve chests but produced some unwelcome heating of the low-pressure turbine shell as the turbine approached full speed. Curiously enough, the overheating was corrected to the point where exhaust metal temperatures just before synchronizing generator on-the-line were reduced to around 100 F by the simple device of closing the main stop valves about 35 min before rolling for the cold start, and 7 min before rolling on the weekend start. This one closing operation of the main stops per weekend or cold start was not considered excessive in view of the benefits gained in the form of reduced cooling-temperature shock to exhaust-end components as load was applied, and was, therefore, adopted as standard practice.

There does not seem to be any plausible explanation for the influence which the operation of the stop valves prior to roll had on turbine-exhaust metal temperature when at governor speed, unless it would be in the small amount of heat that is carried to the condenser through the stop-valve after-seat drains which on this unit are piped to the condenser hot well. The facts are simply (*a*) that the practice of opening the turbine stop valves a long while before rolling the turbine raised the exhaust metal temperatures when at full speed from the customary 175 to 200 F and over, (*b*) that because of this, as a trial measure, the stop valves were closed a few minutes before rolling the turbine after having been opened for an extended period to heat the valve

Table 2 Attempt to warm valve chests with stop-valve pilots

Time, a.m.	Temp of steam in leads ahead of turbine stop valves, deg F	Temp inner surface upper valve chest, deg F	Operating log remarks
4:36.0	548	462	Open stop-valve pilots with after seat drains open wide at 4:36 a.m. Stop valves also opened. Tripped immediately by hand.
4:49.6	558	460	Open and trip stop-valve pilots with after seat drains open wide at 4:51 a.m. Stop valves did not open.
4:52.2	572	458	Ditto at 4:52 a.m.
			Ditto at 4:53 a.m.
4:54.8	576	458	Ditto at 4:54 a.m.
			Ditto at 4:55 a.m.
4:57.4	579	460	Open and trip main stop valves at 4:57 a.m. and at 4:59 a.m.
5:02.6	587	486	
5:05.2	591	490	Roll turbine at 5:05 a.m.
5:10.0	600	490	
5:20	610	490	
5:30	620	520	
5:40	630	548	
5:45	640	570	Generator on line at 5:45 a.m. Load 7 mw
5:50	660	600	Load 7 mw
6:00	697	637	
6:10	740	680	Load 9 mw
6:20	795	725	Load 13 mw

chests, and (*c*) that the exhaust metal temperature when this was done was down around 100 F a few minutes before synchronizing. Vacuum conditions at time of roll, at sealing speed, and at full speed were substantially the same in all cases.

Evolution of valve-chest heating techniques on cold starts may be studied by comparing Figs. 12, 13, and 14. The last one which represents present practice indicates maximum rates of temperature change well within the 500 F per hr limit recommended by the turbine manufacturer, at 315 F per hr during the first hour of load application and 120 F per hr during the preroll and roll periods. These changes are in sharp contrast to the 6000 F per hr experienced with commonly accepted methods of cold starting.

It should be pointed out that the temperature shock to valve chests shown in Fig. 12 could have been reduced appreciably if the installation had been provided with dry-vacuum pumps instead of steam-actuated air-scavenging equipment. Vacuum could then have been established at will, irrespective of the boiler steam pressure, and the turbine possibly could have been rolled with 275-F steam instead of the 430-F steam actually used, because of air-extractor requirements. Steam ties from a second "in-service" unit to supply the steam-actuated hogging equipment of the oncoming unit also would accomplish the same thing. Ties for this purpose were installed at Martins Creek shortly after the second unit went into service.

Heating of Horizontal Turbine Flanges and Bolts. This is a highly controversial subject. The case for heating the flanges and bolts of large modern turbines with the use of an external heat source has been ably presented by others, most recent and comprehensive among which was the Consolidated Edison Company of New York paper on "Accelerated Loading of Large High Pressure-High Temperature Turbine Generators."

The Martins Creek study substantiates what has been said for the case of flange heating. Large temperature differences between inner and outer-flange elements produce (*a*) prohibitive crushing stresses at the inner joint faces, which eventually will lead to flange distortion and steam leakage along the flange from valve bowls to first stage; (*b*) excessive tensile stresses in the already stretched flange bolts, which also will contribute to the leakage; (*c*) distorting radial and axial forces between the comparatively limber cylinder and stiff restraining belt of flange metal—the inner and outer-cylinder surface temperatures actually run about 75 and 50 F higher, respectively, than the inner-flange temperatures in the first-stage region during a typical weekend start without flange heating, Fig. 17; and (*d*) large differential expansion of spindle with respect to cylinder, which, in extreme cases, may result in axial rubbing of blades. The only way to avoid these harmful effects on cold and weekend starts without resorting to external heating of flanges is to apply the load very slowly.

At about the time the Consolidated Edison paper was being presented in 1955, the controlled-start study at Martins Creek was running into confining restrictions in loading rates far beyond expectations during starts from cool-turbine states because of excessive temperature differentials experienced between the inner horizontal-flange surfaces on the one hand, and flange-bolt and outer-flange surfaces on the other in the packing-hub and first-stage regions.

On the first cool start that was made after a $2^1/_2$-day shutdown, for example, with outer-flange temperature at 290 F a loading rate of 0.25 mw per min was used in the belief that the temperature differential across horizontal flanges in the hottest zone would round off at something under the classic 200 F; and on succeeding starts the 200-F figure could then be approached from the underside by stepping up loading rates.

Actually, this mild loading procedure produced a flange temperature differential of inner to outer surface of 323 F in the plane of the main nozzle block between the 3rd and 4th flange bolts counting from the front end, Fig. 15. The flange cross section at this point is about $12^1/_4$ in. across the joint face by $12^3/_4$ in. vertically and the cylinder is about $3^3/_8$ in. thick. The turbine manufacturer indicated at the time and in later statements

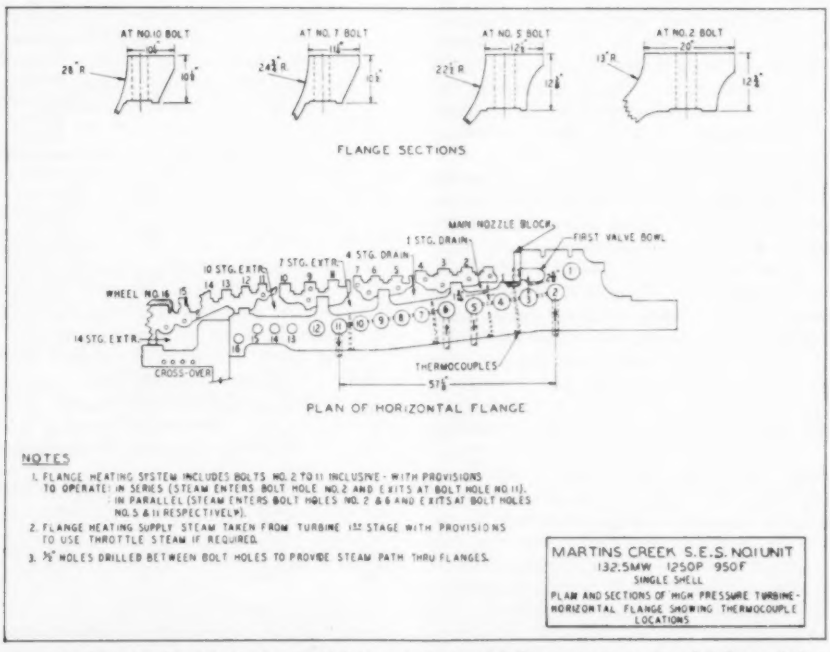

Fig. 15 Showing how first valve bowl intersects horizontal flange near nos. 2 and 3 flange bolts

that a temperature differential across flanges in the neighborhood of 300 F would not be excessive for a machine of this general design. However, in view of the lower figure of 200 F generally accepted elsewhere, a compromise 250 F was adopted as standard for all succeeding test and operational starts on this unit.

The discussion on flange-heating limitations applies only to starts from cool turbine states; i.e., when flanges prior to starting turbine are below 500 F. Maximum loading rates on typical overnight starts as governed by factors other than flange considerations produce flange-temperature differentials of about 170 F which, of course, are not considered to be serious.

There is a school of thought which maintains that, if the steam temperature to the turbine is held constant, the loading rate will have very little bearing on the flange-temperature differential, which is to say that it also will have little or no effect on the inner-flange temperature, since this temperature, for a given flange section and rate of temperature change, determines the temperature differential across the section.

First of all, the steam temperature to the turbine on start-up cannot be held constant even if the boiler temperature-load characteristic were perfectly flat; it would approach the fixed boiler steam temperature asymptotically as the flow increased because of the effect of cool-steam leads, as discussed previously. However, if the turbine-end steam temperature actually could be held constant, the increase in first-stage pressure with load would cause the steam temperature and the inner-flange temperature in that stage to go up with it.

That this is true is shown graphically in Fig. 14 and Fig. 20 from 8:30 a.m. to 9:00 a.m., when turbine steam temperature had stabilized temporarily near rated value at about 960 F, while the load was still going up. The inner-flange temperature in the first-stage region increased from 730 to 810 F; the first-stage steam temperature (flange-heating supply steam) increased from 725 to 880 F, and the first-stage pressure rose from 310 psi to

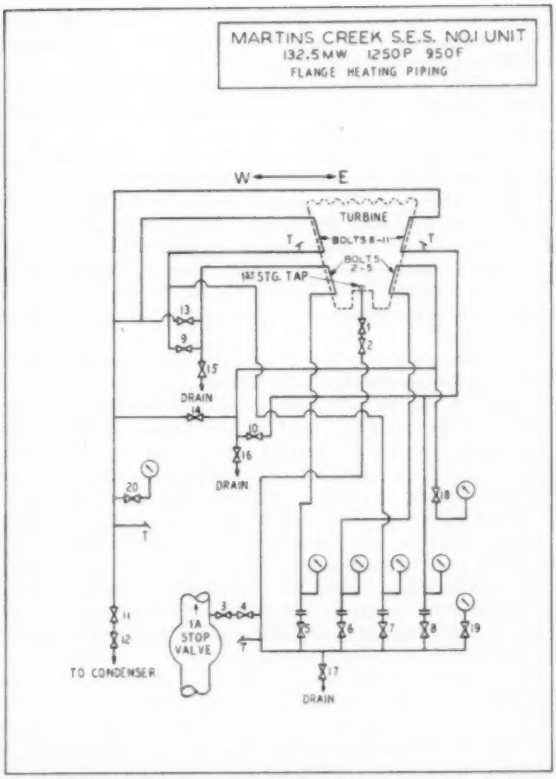

Fig. 16 Arrangement allows heating of bolt groups in series or parallel from steam lead or first turbine stage

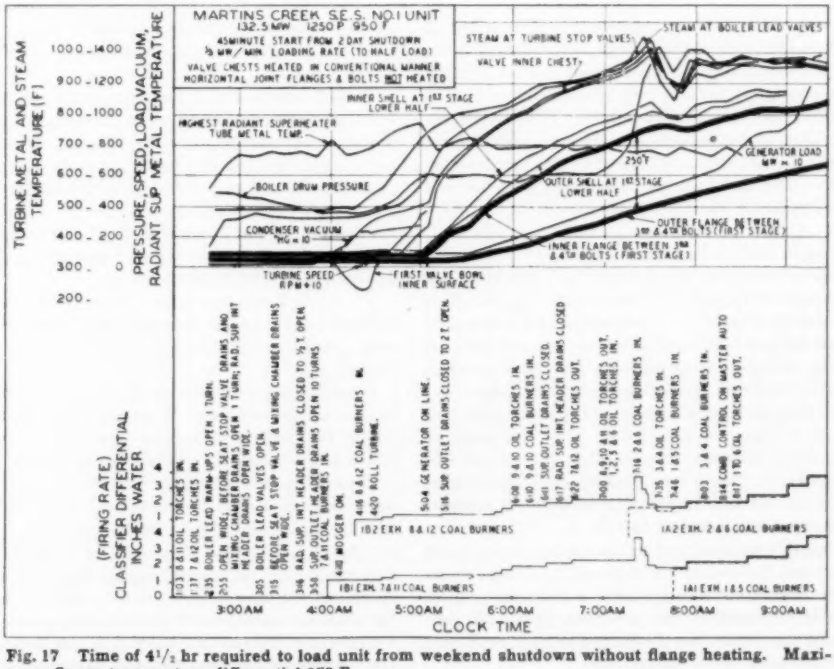

Fig. 17 Time of 4½ hr required to load unit from weekend shutdown without flange heating. Maximum flange temperature differential 250 F.

545 psi while the generator load went from 47 to 76 mw. The same relationships would hold down through the high-pressure turbine as well as in the first stage.

It must be recognized then that the only way to limit flange-temperature differentials without resorting to flange heating is by control of the generator loading rate alone.

After making the first trial run described in the foregoing when the flange-temperature differential reached 323 F, it was found on succeeding starts that flange considerations took over as limiting conditions early in the post-soak loading period, and that loading rates on cold starts had to be limited to 1/4 mw per min, Fig. 13, for the first 3 1/2 hr while those on weekend starts had to be held to 1/2 mw per min, Fig. 17, for the first 3 hr in order to keep the flange-temperature differential in the desired 250-F region.

Since the unit was to be shut down and started regularly every weekend, the prospect of loading a 160-mw machine to half load at only 1/2 mw per min was especially undesirable, not only because of the time factor involved both in bringing the unit up and having only part of its capacity available for long periods, but also because of the additional condensate and fuel that had to be expended during an extended and hazardous venting period.

Therefore the decision was taken to install flange-heating facilities after the unit had been in service about a year. Considerable study was given to five Consolidated Edison Company of New York flange-heating installations which were either completed or under construction at the time. Valuable information was obtained regarding proportioning of system components, layout, and method of drilling flanges.

Two sources of steam supply to the flange-heating system were provided—the first from one of the main steam leads after the main stop valve, and the second from the first turbine stage through the turbine shell (which was 3 3/8 in. thick at point of drilling) by means of a custom-designed welded connection by the turbine manufacturer. The latter connection was made into the bottom half of the shell some 18 in. below the horizontal flange-joint face.

It was agreed with the turbine manufacturer that 10 of the 16 large flange bolts on each side of the high-pressure section of the turbine up to the 4-way joint would be steam heated. Subsequent test runs showed this to have been a happy choice. The heated zone included 2nd to 5th bolts and 6th to 11th bolts, inclusive, in the sections of flanges opposite the intersecting valve bowls, and opposite the 1st, 4th, and 7th stage drain or extraction chambers, Fig. 15. The first bolt opposite the packing hub and the last five bolts opposite the 10th-stage extraction belt were not heated.

Piping was arranged to allow heating of bolts 2 to 11, inclusive, and adjacent flanges in series, or bolt groups 2 to 5, inclusive, and adjacent flanges, and 6 to 11, inclusive, in parallel, Fig. 16. This was done, along with the provision of two sources of steam supply to permit a certain amount of flexibility because of a definite lack of design knowledge in regard to pressure drops, heat absorption in the flange metal, moisture formation, and so on, especially when it came to using the cooler first-stage steam as a heating medium. Internal diameter of supply lead from first stage to flange-heating manifold measured 1 1/8 in., that of feed and discharge piping to and from flanges measured 19/32 in.; 1/2-in. holes were drilled diagonally through the flange metal between adjacent bolt holes to carry the steam from bolt to bolt.

Some anxiety was felt in regard to possible leakage between the flange nut washers and the spot-face surfaces of the flanges under the high-pressure conditions anticipated. Fortunately, these joints held perfectly in operation with pressures up to 1250 psi.

Spent steam from the system was discharged to main condenser via one of the low-pressure heater-dump lines.

The use of first-stage steam as a heat source was chosen primarily because it eliminated the need for close regulation of flow through the flanges to prevent overheating of flanges and negative differential expansion; i.e., fast stretch-out of casing with respect to spindle. While there certainly was no danger of overheating the bolts and outer flange surfaces when using first-stage steam for heating, since this steam was also contacting the inner flange surfaces in the first-stage zone, there was some question as to whether the scheme would provide enough heating in the hottest flange region to allow appreciably faster loading.

On the first cold start that was made after installing the flange-heating facilities, the front and rear-bolt groups were connected in series and supplied from the first-stage source. Maximum flange-temperature differentials reached 230 F between 10th and 11th bolts at 7th-stage extraction belt, while the differentials in the first-stage and valve-bowl region went only to 185 F. This was partly because of a relief valve on the flange-heating piping system which made it necessary to throttle the supply as first-stage turbine pressure increased with load to keep the system pressure under 300 psi. Pressure at the discharge end of the system reached subatmospheric levels which probably had a tendency to cool the bolts and outer flange surfaces at the tail end rather than heat them. The relief valve was later removed, but it was also apparent that the pressure drop through the system would be too great to heat the later bolts with all ten of them connected in series, even though the supply steam went unthrottled.

On the next try, the system was valved to supply the two bolt groups in parallel with steam from the first stage. Loading on this start was controlled as expected by flange-temperature relations in the first-stage zone rather than by those farther down the turbine as before. There also was no overheating in the downstream-flange areas in the 7th-stage regions, although the discharge pressures were well on the positive side throughout the heating cycle, Figs. 20 and 21.

In operation, the system does not actually pass steam until about 20 min after the generator is on-the-line, because of the necessary job of draining some of the water-leg sections in the piping, which cannot be started before the unit is synchronized, after the first-stage pressure has passed over from negative to positive levels.

Table 3 lists inner and outer-flange temperatures for the weekend start shown in Fig. 18 when the flanges were heated with the bolt groups in parallel, from first-stage source. The time intervals are irregular because of a faulty stepping switch on the scanning-type instrument used. Scanners definitely are not recommended for test work of this nature.

Figs. 19, 20, and 21 show plots of differential and cylinder expansion for cold starts with and without flange heating, and a weekend start with flange heating.

No marked differences in relative movement of spindle and cylinder are evident as between cases where flanges are unheated and heated, primarily because of the compensation produced by loading rate.

Of particular interest is the behavior of steam-supply temperature to flanges with load. Except for the sensible heat loss in the piping this represents turbine first-stage temperature, a figure which is not ordinarily available to operators.

Since the source of supply from the steam lead after the stop valve was never used, it was left out of the design of the second Martins Creek unit along with the provision for series heating of the flange bolts which proved to be unsatisfactory.

Summing up on flange heating then, for cold starts, it has shortened the time required to load the unit from 6 to 3 hr, and for weekend starts from 4 1/2 to 2 1/2 hr, with the same maximum temperature differentials holding across flanges of 250 F. It is our considered opinion that the flange-heating investment has

Table 3 Flange temperatures during start from 2-day shutdown

	Flange between 3rd and 4th bolts—East			Flange between 3rd and 4th bolts—West			Flange between 4th and 5th bolts—East			Flange between 4th and 5th bolts—West		
Time a.m.	Inner	Outer	Diff.	Inner	Outer	Diff.	Middle	Outer	Diff.	Middle	Outer	Diff.
7:30	313	277	36	432	300	132	292	292	0	321	310	11
7:42	367	292	75	502	318	184	302	298	4	351	350	1
7:54	445	315	130	577	353	224	372	325	47	418	400	18
8:06	517	352	165	643	400	243	425	363	52	477	460	17
8:16	590	405	185	698	458	240	485	417	68	537	525	12
8:31	677	487	190	767	540	227	571	500	71	617	605	12
8:44	722	552	170	780	600	180	625	567	58	666	665	1
8:55	724	588	136	761	630	131	642	603	39	673	655	18
9:07	722	620	102	787	652	135	675	631	44	701	682	19
9:18	790	640	150	830	667	163	691	648	43	713	693	20
9:33	825	647	178	855	671	184	715	660	55	737	717	20
9:40	845	652	193	865	679	186	726	668	58	747	727	20

	Flange between 6th and 7th bolts—East			Flange between 6th and 7th bolts—West			Flange between 10th and 11th bolts—East			Flange between 10th and 11th bolts—West		
Time a.m.	Inner	Outer	Diff.	Inner	Outer	Diff.	Inner	Outer	Diff.	Inner	Outer	Diff.
7:30	285	292	−7	287	293	−7	285	287	−2	290	290	0
7:42	325	308	17	330	312	18	340	285	55	343	287	56
7:54	393	330	63	398	333	65	397	303	94	403	303	100
8:06	470	373	97	480	375	105	458	335	123	465	335	130
8:16	545	428	117	557	437	120	518	380	138	522	378	144
8:31	635	518	117	650	528	122	578	455	123	580	455	125
8:44	671	577	94	680	595	105	585	520	65	585	523	62
8:55	670	607	63	678	623	55	598	557	41	600	560	40
9:07	707	639	68	713	655	58	637	590	47	641	595	46
9:18	725	644	81	727	661	66	648	591	57	648	595	53
9:33	750	647	103	761	663	98	678	587	91	673	592	81
9:40	762	652	110	772	669	103	682	591	91	680	596	84

NOTE: Flange heating steam—turned on at 7:25 a.m.—shut off at 9:08 a.m.

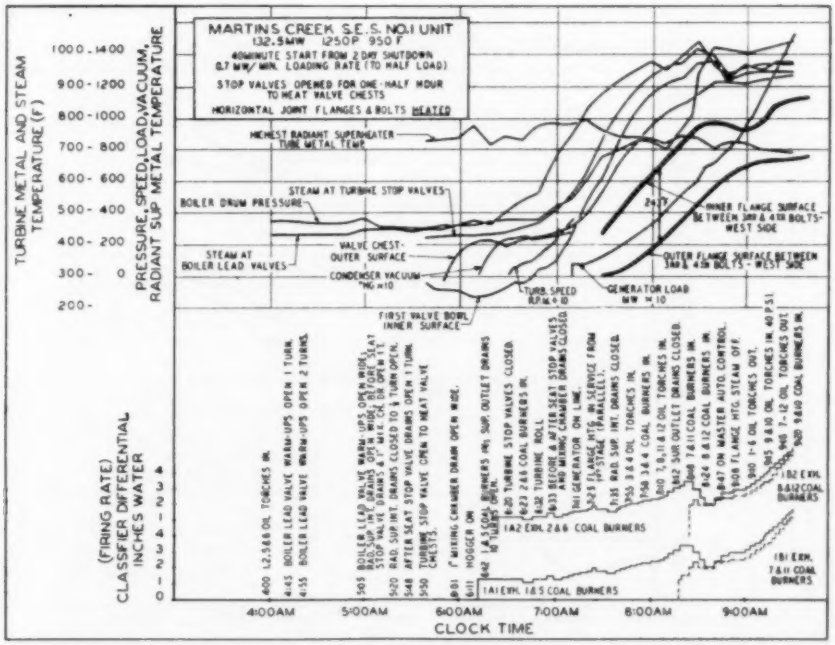

Fig. 18 Time of 2½ hr required to load unit from weekend shutdown when using flange heating. Maximum flange-temperature differential 243 F.

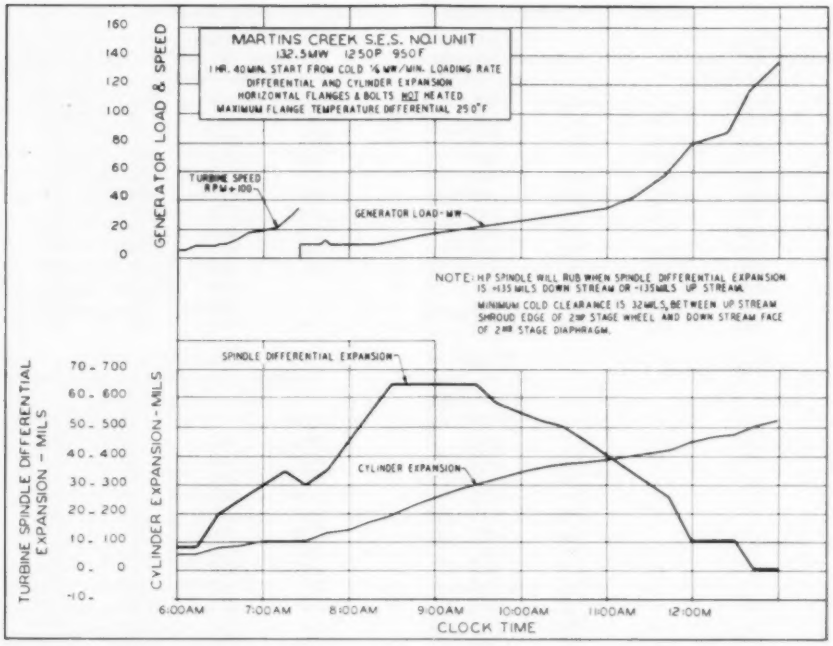

Fig. 19 Differential and cylinder expansion on cold start without flange heating. See Fig. 13 for additional material on this start.

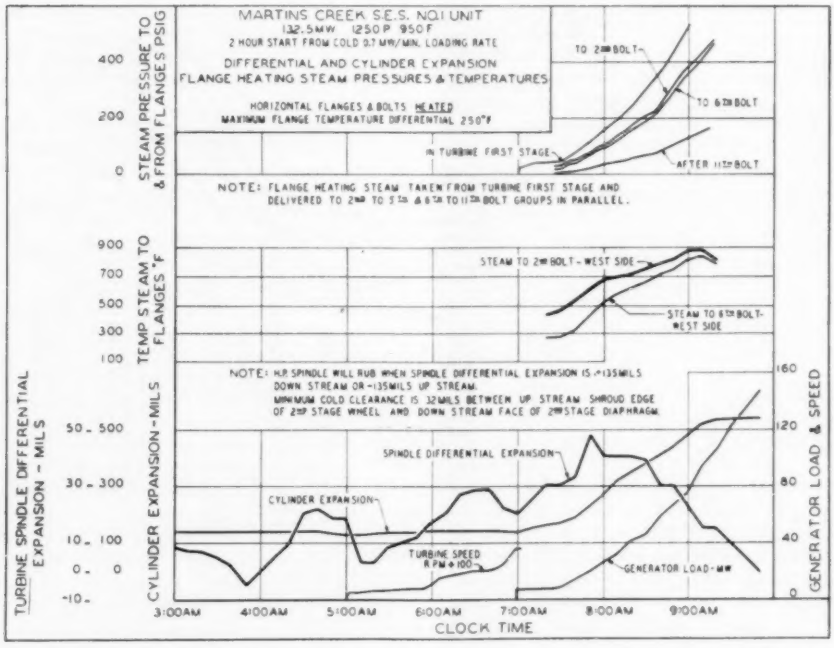

Fig. 20 Differential and cylinder expansion on cold start. Flanges heated. See Fig. 14 for additional material on this start.

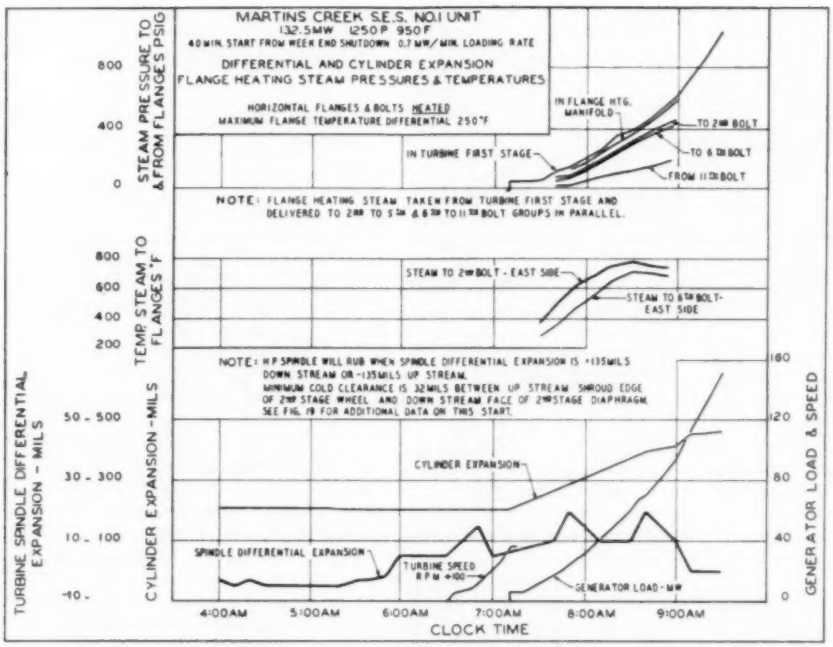

Fig. 21 Differential and cylinder expansion on start from weekend shutdown. Flanges heated. See Fig. 18 for additional material on this start.

Table 4 Portion of a typical schedule Martins Creek Steam Electric Station skeleton procedure and time table for controlled start from overnight shutdown—boiler bottled

SCHEDULE B

Firing Rate and Load Regulated Manually Until After Second Mill is in Service.

Light-Off Conditions. Drum pressure 1000–1250 psi; Mills charged to 1 in., boiler-drum water level about 11 in. in gage glass; 8 divisions on Yarway; boiler lead valves open; turbine stop valves closed; unit on turning gear; steam-metal temperature at turbine stop valves 600–725 F; turbine chest temperature 650–750 F; 1, 2, 5, and 6 windbox dampers open; 1, 2, 5, and 6 coal shut-off valves open; 1, 2, 5, 6, 7, 8, 11, and 12 vent plugs inserted; 1, 2, 5, and 6 burner registers at 45 per cent; 3, 4, 7, 8, 9, 10, 11, and 12 registers at 10 per cent; exhauster auxiliary air dampers zero spaces open; 5 million Btu per hr tips in all torches.

Have all oil-torch tips cleaned on night shift just prior to light off. Open bypass around trap on oil-torch steam-atomizing line an hour before light off, and leave open until all torches are taken out of service after the fire-up is completed.

During shutdown period when corrected generator-field-winding temperature drops to 62 C, apply enough field current to raise winding temperature at a rate not exceeding 5 to 10 C per hr. Remove field, when winding temperature reaches 85 C. At time of turbine roll, field-winding temperature should be about 75 C.

Time when turbine is rolled will be designated $t = 0$.

Operation	Clock time: Gen. on line 6:50 a.m.	Gen. on line 7:00 a.m.	Gen. on line 7:10 a.m.	Gen. on line
At $t = 0 - 76$ min, open radiant-superheater intermediate drains wide.	5:14	5:24	5:34	
At $t = 0 - 76$, start both sets of ID and FD fans..	5:14	5:24	5:34	
At $t = 0 - 75$, light off 1, 2, 5, and 6 oil torches 70 psi oil pressure, burner registers 45 per cent..	5:15	5:25	5:35	
At $t = 0 - 74$, open 1-in. mixing-chamber drain 1 turn to drip flash-tank vent line.....	5:16	5:26	5:36	
At $t = 0 - 73$, open 4-in. inner mixing chamber drain wide.....	5:17	5:27	5:37	

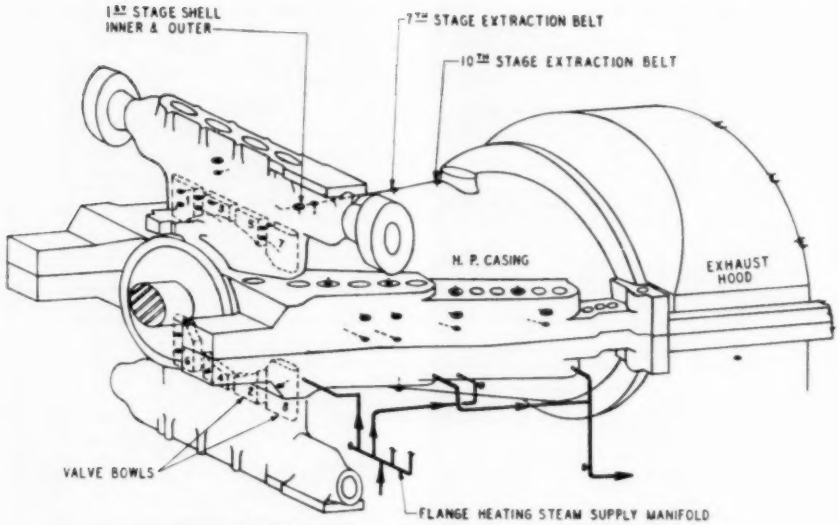

Fig. 22 Principal turbine thermocouple locations, Martins Creek No. 1 unit

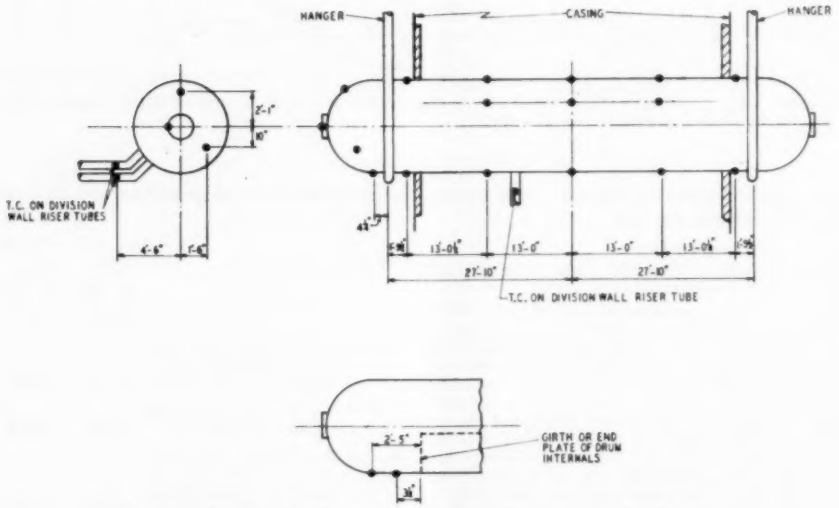

Fig. 23 Boiler drum thermocouple locations, Martins Creek No. 1 unit

paid off well in view of the regular weekend starts to which the two units are subjected.

Effect of Load Soak Period on Metal Temperature-Rise Rates. Referring again to Fig. 18 which depicts a start after weekend or two-day shutdown, it will be noted that the generator load was held constant at 7 mw for the first 10 min after going on line. This produced a maximum rise rate in inner first valve-bowl temperature of about 560 F per hr—too high. On the preceding weekend trial start—not shown—a hold period of 20 min at 7 mw produced a metal temperature rise rate of only 360 F per hr—a little low. The final schedules were therefore set up for a soak at 7 mw of 15 min and have consistently produced temperature-rise rates of 475 to 500 F per hr on all routine weekend starts in the two years which have elapsed since the final schedules were prepared. This is mentioned here to show how the load hold or soak periods can be used to get just about any rise rate desired.

Starting Schedules. Table 4 shows portions of a typical step-by-step procedure for the controlled starting of a unit from overnight shutdown. Schedules of this type are furnished to operating personnel throughout the plant for each start. The number of different types prepared is dependent on the operating conditions which are encountered for the given unit.

Martins Creek, as an example, has five different start schedules as follows: (*a*) Boiler and turbine cold, turbine temperature 50 to 160 F; (*b*) boiler cold, turbine warm, over 160 F; (*c*) one to four-day shutdown boiler bottled, turbine warm; (*d*) overnight shutdown boiler bottled—early automatic operation of boiler; (*e*) overnight shutdown boiler bottled, late automatic operation of boiler.

A schedule such as the one shown for a modern unit which is to be subjected to frequent starting is absolutely essential if turbine temperatures and stresses are to be controlled accurately. Fast-printing turbine-metal temperature recorders are used for backup

and the charts are inspected by an engineer at frequent intervals to see that rates of temperature change are maintained within the limits specified.

Conclusions

From the records of many controlled starts which were made on major units of central-station equipment of different types, both old and new, and from careful inspection of the equipment the following conclusions may be drawn:

1 Rates of change in turbine-metal temperature up to 500 F per hr on modern high-pressure turbines of the types tested will not cause cracking in the heavy shell and chest sections. These rates produce temperature differentials across chest and first valve-bowl sections of about 125 F. Differentials across later valve-bowl sections because of valve-opening sequence, however, may run as high as 185 F for 500-F-per-hr rise rates.

All of the starts on Martins Creek No. 2 unit (1250 psi, 950 F, 132.5 mw, initial operation June, 1956) were made with rates of change under 500 F per hr and no casing cracks of any kind were found during the June-July, 1957 outage.

The front end of this turbine differs slightly from No. 1 turbine in that the downstream faces of the nozzle bridges were drilled out and fitted with pins to allow a small amount of radial movement of the bridge faces; and the inner turbine-shell surface under the nozzle block was relieved by a circumferential groove at the notch change in section.

2 Rates over 500 F per hr are suspect. A few of the starts on Martins Creek No. 1 unit (same size as No. 2 unit) were made with rates of change in bowl metal temperature up to 1200 F per hr, and one cold start showed a change rate as great as 6000 F per hr prior to roll in valve-chest metal when using conventional chest-heating methods.

Upon inspection of the turbine after one year of peaking operation three small circumferential cracks were noticed in the top half inner-shell surface under the nozzle block just radially beyond the nozzle-bridge faces.

During the inspection of Sunbury No. 2 turbine (75 mw, 1250 psi, 950 F) in May, 1957 after almost 8 years of base-load operation, severe cracking was found in nozzle bridges and in inner-shell surface under the nozzle block.

It is believed that much of the shell cracking in modern turbines takes place during starts from cold. This is more certain when the cold unit is on a header system and subjected to impact of full boiler temperatures.

3 Initial load application and subsequent loading rates are the two most important considerations in controlling temperature-rise rates in front-end turbine elements because of the influence of the boiler-turbine main steam leads on turbine-end temperatures. The lead temperatures drop rapidly to saturation point as soon as the flow of superheated steam through them is interrupted when a unit is taken off the line.

It has been found that a short soak period immediately after synchronizing at a constant load in the order of 4 to 5 per cent of name plate rating is an excellent device for controlling metal-temperature-rise rates, the control lying in the length of the soak period. On this unit, length of soak periods required for 300 to 500-F-per-hr metal temperature rise turned out to be 5 min for the overnight start, 15 min for the start from one or two-day shutdown, and 25 min for the start from cold.

The concern which was felt in regard to possible erosion of main nozzles and first-stage wheel components, seal strips, and so on, due to expansion of steam into the wet region when operating at extremely low ratings during the starting soak periods was dispelled on both of the Martins Creek turbines when inspection after a year of peak-load operation in each case showed not the least sign of erosion in the first-stage region.

A small initial load application is also beneficial in holding down the rate of cooling of exhaust end metal.

Each boiler-steam lead system should be given individual study to determine the turbine-end steam-temperature characteristic under the various starting conditions encountered.

4 Confirming the work of other investigators in controlled starting, the study shows that steam temperatures at turbine should be 50 to 100 F above turbine bowl and chest metal before rolling turbine. This is especially desirable for starts from overnight shutdown when turbine metal is hot, because it minimizes the dip in first valve-bowl temperature and the fast reversal in bowl-metal-temperature differential; it reduces possibility of rubbing because of spindle shrinkage; and it allows faster loading for the same temperature-rise rates and differentials.

The dip in first valve-bowl temperature can be entirely eradicated on overnight starts, if the margin of steam over turbine metal is increased to about 150 F, or if the roll period is reduced to something like half of the 20 min used in this program.

5 Heating of horizontal flanges on single-shell turbines is justified on units which are to be shut down weekly. Steam from the first turbine stage makes an ideal, more or less foolproof heating medium, since the flange bolts and outer flanges cannot be overheated by using it, while later valve-bowl behavior makes it unwise to raise loading rates further through use of hotter steam for flange heating.

6 Temperature differences between inner and outer turbine horizontal-flange surfaces in single-shell machines up to 250 F appear to be satisfactory, but anything higher should be avoided. The horizontal joint of Martins Creek No. 2 unit is in good condition after many weekend and overnight starts with flange temperature differentials running under 250 F. That of Martins Creek No. 1 unit on the other hand is leaking. This is believed to be due to the fact that a few of the earlier starts were made with flange temperature differentials over 250 F, one of which actually reached 323 F.

7 Hogging facilities for scavenging turbine-condenser system should be amply sized and designed to produce at least 24-in. mercury vacuum or better with turbine on turning gear to prevent overheating of exhaust-end components as the turbine reaches full speed, and to minimize the cooling shock which takes place as load is applied.

In reheat installations where the volumes to be scavenged are very large, the hogging equipment is often found to be undersized.

The cost of one set of cracked last-stage diaphragms would go far toward paying for the difference between air-removal equipment which produces a weak 17 to 20-in. mercury vacuum over a long time and that which produces an adequate 24 to 28-in. mercury vacuum quickly when needed.

Although the hogging jets and steam-jet air extractors on the Martins Creek units are good by comparison with similar equipment in some other Pennsylvania Power & Light Company stations, being capable of producing turning-gear vacuum of 23 in. mercury and scaling speed vacuum of 26 in. mercury, their limited capacities are the only thing standing in the way of further reductions in starting time especially on starts from overnight and weekend shutdowns.

Front-end turbine-temperature considerations, as all the start data show, would permit much higher accelerations in bringing the turbine to speed if exhaust-end temperatures could be kept down.

The problem may resolve itself into specifying jets that will give optimum performance at the lower steam pressures which are encountered in starting operations.

8 Operation at very light loads below 25 per cent of rating

for long periods is not recommended because of cooling of metal under the closed control valves, which tends to distort the entire valve chest and bowl mass. Permissible load pickup rates after overnight operation at these ratings is lower than it would be if the unit were taken off the line, because natural cooling of later valve bowls is less during a 7-hour shutdown than it would be with the turbine in service carrying 25 per cent rated load.

9 Spelled-out minute-by-minute starting schedules which are experimentally determined for each type of start condition have been used throughout the entire program. They have been found to be beneficial in assuring uniformity and adherence to prescribed procedures as well as in easing the work load on plant operators. For each step in the process the operator is obliged to insert only the time when it was done. The notated schedule is then turned in as a log of the start operation.

10 The use of dry-vacuum pumps or any other air-scavenging equipment which is capable of raising condenser vacuum on unit systems independently of the boiler steam pressure is worth consideration in reducing the temperature shock to which turbines are subjected on starting from cold conditions. The turbine can be rolled with steam which is at lower temperatures, and on some turbine types the lower rolling pressure will allow more even heating of the front-end turbine sections.

Where there are duplicate units, a tie steam line between hogging jets, or a common set of jets centrally located between the two condensers will do the same thing.

11 Changes in design are indicated in some types of turbines in regard to provisions for heating valve chests, more even heating of valve bowls, and in valve-opening sequence.

12 The idea of blowing preroll steam through large drains on turbine ends of steam leads for getting proper steam-to-turbine-metal relationship on starts from overnight shutdown in place of the more expensive bypass line-heat exchanger combination is good provided blowdown tank, silencer, vent stack, and water-separating dome are amply sized and well enough anchored to take large quantities of high-temperature steam. For an installation such as either of the Martins Creek units the ideal preroll flow to atmosphere would be about 200,000 lb per hr which would require about $^1/_2$ hr of preroll firing to accomplish proper margin of steam over turbine-metal temperatures for overnight starts, instead of the full hour required with existing facilities.

13 Many of the waterwall-tube failures in modern boilers have their origins in improper starting procedures. An example is the tendency of operators to increase firing rates at the moment the generator is synchronized or when the boiler nonreturn valves open. A sudden small increase in firing rate at this stage when the total heat input is low becomes a large percentage increase which may result in the weakening or rupture of a waterwall tube near the top of the furnace because the water circulation induced by the small heat input to lower furnace reaches is not good enough.

Also for this reason as well as for better ignition, the practice of going to complete automatic boiler operation too early in the start cycle is not recommended, because sharp increases in firing rate may take place when the switch is made from manual to automatic control.

Acknowledgments

The author gratefully acknowledges the help and advice of Messrs. John M. Driscoll and Maurice Salvage of Consolidated Edison Company of New York, Inc.; Messrs. R. A. Lorenzini, W. W. Ward, L. Green, and P. Ferrari of Foster Wheeler Corporation; Mr. C. S. Peace of Ebasco Services Inc.; and Messrs. S. B. Coulter and L. J. Adams of General Electric Company; and the encouragement of Messrs. Harry Ferguson, George M. Keenan, and Melvin D. Engle of the Pennsylvania Power & Light Company. Special thanks also must be extended to the many men in the Pennsylvania Power & Light Company organization for the able assistance rendered throughout the program.

References

1 "Latest Techniques for Quick Starts on Large Turbines and Boilers," by J. C. Falkner, D. W. Napier, and C. W. Kellstedt, TRANS. ASME, vol. 72, 1950, pp. 1111–1136.

2 "Quick Starting of Large High-Pressure, High-Temperature Boilers," by J. C. Falkner, TRANS. ASME, vol. 75, 1953, pp. 1407–1460.

3 "Controlled Starting of Steam Turbines," by R. L. Reynolds, TRANS. ASME, vol. 75, 1953, pp. 1461–1464.

4 "Factors Involved in Starting and Subsequent Loading of Modern Steam Turbines," by C. W. Elston, TRANS. ASME, vol. 75, 1953, pp. 1465–1468.

5 "Quick Starting of High-Temperature, High-Pressure Boilers," by A. R. Weismantle, TRANS. ASME, vol. 75, 1953, pp. 1469–1472.

6 "Quick Starting of Steam Turbines," discussion by C. D. Wilson, TRANS. ASME, vol. 75, 1953, pp. 1473–1475.

7 General discussion by W. H. Rowand, B. J. Cross, and E. H. Krieg, TRANS. ASME, vol. 75, 1953, pp. 1476–1477.

8 "Accelerated Loading of Large High-Pressure, High-Temperature Turbine Generators," by W. C. Beattie, J. M. Driscoll, and M. Salvage, ASME Unpublished Paper No. 55—SA-63.

9 "Importance of Matching Steam Temperatures With Metal Temperatures During Starting of Large Steam Turbines," by R. L. Jackson, S. B. Coulter and R. Sheppard, TRANS. ASME, vol. 79, 1957, pp. 1669–1678.

Discussion

C. W. Bell, Sr.[2] The author is to be commended for having brought out definite positive recommendations for starting certain high-pressure, high-temperature turbines. Probably the most useful features of this paper are the precautionary or negative points made.

We wish to indorse particularly the recommendation that means be provided for establishing close to full operating vacuum early in the start-up sequence. The matter of good vacuum during starting has seldom had as much consideration as it deserves. The excessive temperatures frequently found at the exhaust ends of turbines may be due simply to natural cumulative build-up of temperature from inlet to exhaust; however, additional heating may occur at random locations if and when air stagnates. This may become dangerous. Evidence of this sometimes can be found during internal inspections. It is usually found in the lower stages in the form of discolored or deformed metal parts but the writer has never found it on the last wheel or last blade row.

On machines with shaft-mounted wheels (with only one or two keys) transient vibration during starting was further evidence of this condition.

A natural steam-temperature gradient cannot be established until partial air pressure is reduced to a very low value.

Even without hot spots the low-pressure ends of turbines will be above natural operating steam temperatures during starting and are often subjected to severe thermal shock when normal operating vacuum becomes effective.

Temperature measurements taken of the inner surface of turbine-blade rings or turbine shell will always lag in time, the temperatures imposed on the smaller blading and sealing members.

Design of high-pressure units with their regenerative heating (and reheat) equipment should include very careful attention to any possible source of air leakage under vacuum. Packing of all valve stems and pump shafts must be effective both above and below atmospheric pressure. Vent connections are hazards to be

[2] Engineering Consultant Central Heating and Power Plants, Drums, Pa. Mem. ASME.

studied particularly if they are of the "breather" variety where no check valve or nonreturn can well be applied.

Air-exhausting equipment of sufficient capacity to produce a good start-up vacuum will, of course, increase refrigeration in the high-pressure zones. This may tend to increase required loading time.

Fig. 24 in the preprint (omitted in the final paper) showing temperature decay on drop of load indicates that metal temperatures can be forced down rapidly. External temperatures of valve bowls Nos. 6, 7, and 8, would show the greatest immediate effect.

J. C. Falkner.[3] The author should be highly commended for the excellent work he has done. The writer is familiar with the large amount of time and work required to make the necessary tests, analyze them, and then write the findings.

As stated in the paper, the writer also believes that many cracks found in turbine casings can be eliminated by changes in operating practices.

When bypass lines or other means are provided, such as large vents from the superheater and reheater lines, and so on, the procedure for shutting down the turbine should be done by lowering the load on the generator to a point where the superheat temperature begins to drop from normal. Trip the turbine at this point. The temperature of the turbine parts will gradually lower, but as it started from the highest temperature, the starting temperature also will be high and the normal operating temperature can be reached in the quickest time, with resultant saving in turbine efficiency.

Another important point which may not be known generally is that in taking a boiler off the line for a weekend shutdown or for overhaul, the boiler drum should be kept filled with water, so as to keep the temperature of the boiler drum from having more than 100 F differential top and bottom which is prescribed by the boiler manufacturers. Temperature differences as high as 180 to 200 F were found before the filling procedure was started. The temperature differential of the drum heads from top to bottom also showed more than the 100 F allowable. Changes have been made in the boilers now purchased so that this high differential does not occur. The cost of a long water column would be excessive but either thermocouples peened in the saturated-steam tubes from the drum to the superheater header or remote high-range level recorders gave quick indication when the boiler is filled with water. It is usually necessary to fill the drum several times during the shutdown before normal conditions are reached.

An interesting incident at the Waterside Station occurred while the writer was present several years ago. A 50,000-kw topping turbine using 1,000,000 of steam per hr at 950 F, 1600 psi was tripped accidentally by an electrician changing a pilot-exciter carbon brush. The turbine was ready to start in five minutes and the boiler in 15 minutes. No steam bypass on this unit had been provided at the time of the tripping. With the turbine at 950 F, the highest steam temperature obtainable from the boiler on the start was 750 F. The station engineer was ordered to take plenty of time in admitting the low-temperature steam into the turbine. Two hours were taken in gradually cooling the turbine and then bringing it up to full speed.

Faster loading turbines can be done safely by using external flange and bolt heating. This also should eliminate the warping of the turbine shell and crushing of the flange joints.

As the gages, thermometers, and so forth, for a high-pressure, high-temperature boiler give poor indications at the lower ranges, a method at Consolidated Edison was developed so that by measuring the temperatures of the boiler-drum water by means of a thermocouple located in the continuous blow-down system, the need of low reading was eliminated. This temperature of the boiler water plotted as a straight line from the starting temperature to normal temperature at full pressure, against the time allotted for starting the boiler, gave the operator all of the information required. The superheater, reheater, drum-temperature differential (top and bottom), and the expansion downward of the boiler, all came within the prescribed safe limits. The superheater and reheater drains or a special bypass line around the turbines or to atmosphere should be opened during the start. This procedure was not tried on boilers having radiant superheaters.

Again I wish to commend the author for a good job well done.

R. L. Jackson.[4] The author is to be congratulated for a fine paper. He has most thoroughly covered a subject in which so many variables are involved.

The complete treatment of all the phases of starting and loading a power plant is not possible for the manufacturers of the individual pieces of equipment, and it is through the efforts and cooperation of such companies as Pennsylvania Power and Light and the interest of such people as the author that essential data must be obtained. The information from such tests plus the condition of equipment as observed after service experience is relied on greatly in making new designs.

There have been, of course, numerous cases of cracked turbine shells in the past several years. We are sure most of them could have been avoided if operating conditions and practices had been studied as carefully and controlled as they were on the starts described in this paper. We are particularly gratified to note the author's statement that the only way to establish correct starting procedures is for the owner company to conduct a thorough investigation on that unit (boiler leads, turbine generator), using only the best instrumentation available. This is necessary because of the individual equipment characteristics and local conditions which necessarily make general rules inadequate.

In so far as the turbine is concerned, the ultimate measure in starting and loading is stress caused by temperature differences set up in various critical parts. As stated in the paper and supported by the evidence of cracking experience, the most critical parts are in the region of the admission ports in the shells. If temperature differences in these regions are held to acceptable limits, then the remainder of the unit should be secure. We would like to point out that rates of temperature change are only important as an indirect expression of temperature differences and for small total temperature changes rates can be very high without excessive stress.

We cannot agree that rates of cooling of turbine-exhaust ends are limiting. A very large percentage of turbines in service customarily experience exhaust-hood temperatures in the order of 175 F during starting and, even though many of them have been started frequently for several years, no failures traceable to temperature quenchings in exhaust hoods have been experienced.

In discussing temperature reductions in valve bowls the author states that control valves are not shut-off valves and, therefore, do not seal off bowls from chests effectively when in the closed position. This is not intended to be so and even though there have been cases where control valves do not seal completely, they are in general as tight as any valves made.

Flange heating is discussed and conclusions are drawn that the reduction in flange-temperature gradients by 50 to 75 F is the difference between crushing or not on the flange faces. We believe that such conclusions are too broad and not necessarily proven. First, there was no steam leakage to atmosphere and, as far as we

[3] The Kissick Company, Power Plant Equipment, New York, N. Y. Fellow ASME.

[4] Mechanical Design Engineer, Large Steam Turbine-Generator Dept., General Electric Company, Schenectady, N. Y. Mem. ASME.

know, no permanent distortion of the flanges could be detected. The presence of the pressure and the leakage into the flange-heating piping could be accounted for by an extremely small opening which might be due to several reasons besides the observed temperature gradients. Many hundreds of turbines are in service without flange heating and do not show evidence of crushing.

It is reassuring to observe that there is a realization of the importance of matching steam temperatures to metal temperatures and that a careful study shows much can be done to obtain this matching without very expensive or elaborate systems. In addition to the ideas presented in this paper, we believe that many situations can be improved by the use of a small bypass valve around the boiler stop valves to control the speed of the turbine which would allow the stop and control valves to be wide open. This would transfer the throttling effects described in the paper to a relatively thin-walled valve of more symmetrical shape which can better tolerate the temperature shocks. In addition, it can be considered more readily expendable than a turbine shell. Under such operation the steam densities and velocities are lower in the turbine shell making for lower heat-transfer coefficients and consequently less drastic shell-temperature changes. Some installations are being equipped with such valves and tests to be run will show how much can be accomplished in this direction.

Progress is being made in new turbine designs that will assure units better able to handle increased starting and loading rates. New turbines being supplied by the writer's company are all steam-sealed units in order that full vacuum may be developed on turning gear; all are supplied with automatic water sprays in exhaust hoods to keep hood temperatures down during starting. Materials have greater rupture ductility, tolerating more cycles of temperature strain without cracking, and the higher pressure units will all have the steam admission in separate small pressure vessels independently mounted and center line-supported, free to expand or contract while being held concentric.

Again may we congratulate the author and suggest that an approach to the frequent starting and loading problem as outlined should go far towards making such starts easy and trouble-free.

R. L. Reynolds.[5] The author and his associates have done an excellent job in measuring the conditions existing on the Martins Creek turbine during various types of controlled starts and in analyzing and controlling these conditions to minimize thermal stresses in the turbine elements.

He has encountered the same problem as other investigators in that, on unit systems, the normal steam temperature ahead of the stop valves following an overnight shutdown is considerably cooler than the metal in the high-temperature parts of the turbine. This temperature differential is further increased by the throttling of steam through the control valves to a subatmospheric pressure.

This condition results in the high-temperature parts of the turbine being cooled during the initial part of the starting cycle, making it necessary to heat these parts from a lower level and to extend the time required for heating in order to avoid undesirable rates of heating and, therefore, excessive thermal stresses.

An additional drop in temperature will occur when the steam expands through the nozzles. This accentuates the thermal shock occurring when the cool steam issuing from the nozzles strikes the impulse blades which have been kept hot during the overnight shutdown by being housed within the turbine casing. Again, these nozzle vanes and impulse blades are subjected to a severe thermal shock when steam is first admitted to the turbine following a short shutdown.

In order to reduce this thermal shock in the high-temperature casing and blading it is evident that it is necessary either to make the steam hotter or the metal cooler at the beginning of the starting cycle after a short shutdown.

The author describes the means taken to increase the steam temperature at the start of the rolling period. These include adjustment of burners, use of oil, and increase in size of steam-lead drains.

Cooling of the metal, to some degree, can be accomplished during the shutting-down cycle when it is known that the unit will be restarted after a short shutdown. This can be done by dwelling at a light load during the load-reducing cycle, holding this load for 30 to 45 min and, at the same time, reducing steam temperature if possible by adjustment of boiler controls.

Although this cooling means that the high-temperature parts of the turbine must be heated from a lower temperature level, this is preferable to subjecting these parts to a severe thermal shock which not only overstresses the parts but also causes them to be heated from this same low-temperature level.

Another point brought out in the paper, and one worth repeating, is that little heating is accomplished during the speed-increasing cycle whereas the critical period in the heating cycle occurs immediately after synchronizing. This dictates the need for applying as small a load as practicable immediately after synchronizing, holding this load until conditions have become somewhat stabilized and then increasing it at a slow rate at first and then at a gradually faster rate as the parts become heated. Furthermore, steam temperature should be held down as much as practicable during this minimum-load period.

In many cases, temperature gradients across partition walls can be reduced materially by bypassing steam from the active to the inactive inlet chambers. The small loss in efficiency at light loads suffered by the bypassing of this small amount of steam can be amply justified by the reduction in thermal stresses and increase in reliability obtained by this heating of the cold side of these partition walls.

During the cold starts, or starts after long shutdowns, the author points out the desirability of heating the flange, and its bolts, by circulating steam from the impulse chamber to the exhaust. As he states, this steam can be more closely controlled by the use of steam from the impulse chamber rather than from the main steam leads. He further states that better results are obtained by passing this steam through the flange in parallel rather than in series. This is usually true, but there may be cases where the heating of the flange should be graduated, making the series arrangement preferable, provided the number of steps in each circuit is not too large. Each unit should be studied individually to determine which arrangement is better.

Again, we wish to point out that this paper is definitely a worth-while addition to the published information on controlled starting and the author and his associates are to be commended on their excellent treatment of this subject.

A. R. Weismantle.[6] The author and his associates are to be commended for providing the power industry with a detailed engineering report on a subject which is becoming increasingly important. It will certainly be of value to the many engineers faced with similar problems.

This discussion will deal only with that phase of the paper which concerns the steam-generating unit. For this apparatus the principles of "controlled starts" are identical with those employed in the well-known "quick-start" technique. Both start-up methods have the same desired end result of maximum safety and

[5] Manager, Steam Division, Large Turbine Apparatus Section, Westinghouse Electric Corp., Philadelphia, Pa. Mem. ASME.

[6] Foster-Wheeler Corp., New York, N. Y. Mem. ASME.

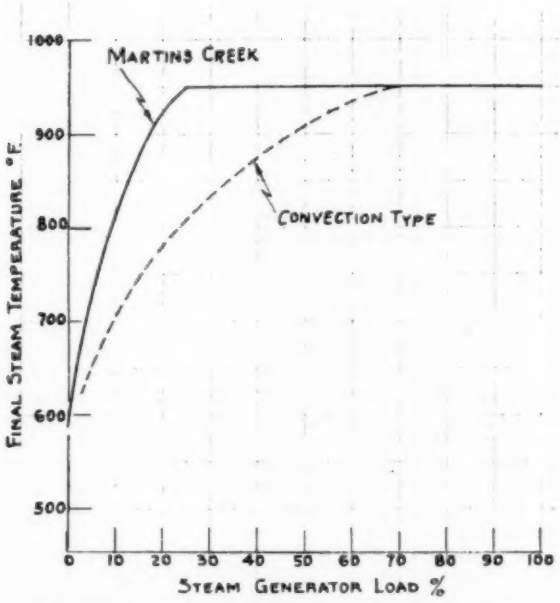

Fig. 24 Comparison of steam temperature characteristics, Martins Creek unit versus conventional convection type

service life for the equipment involved. The application of these principles in the author's investigations differed mainly in that a bypass line-heat exchanger combination, which other investigators had concluded was desirable, was not employed. Such a bypass system permits simple operation of a steam-generating unit under equilibrium conditions in order to obtain the desired steam temperature, and its application minimizes fuel losses, personnel required, and time used for the start. However, it is expensive to install and cannot always be economically justified, as the author's company must have found out.

The author has stated properly that one of the requirements for successful controlled starts is the ability of the steam generator to provide steam to the turbine at from 50 to 100 F above the front-end turbine-metal temperature before rolling. It seems pertinent, therefore, to point out the tremendous advantage of a steam generator with radiant-superheating surfaces for controlled or quick-starting service. This is illustrated by the steam-temperature characteristic provided with the combination radiant and convection superheater of the Martins Creek unit as compared to that from a conventional convection type, Fig. 24 of this discussion. In this example, full steam temperature is obtained at all loads above 70 per cent. Let us say that after an overnight shutdown it is desired to provide steam to the turbine at 875 F. This temperature may be obtained from the Martins Creek type by bringing the unit up to a load of 15 per cent. For the same temperature a unit with a straight convection superheater must be brought up to a load of 40 per cent. It is obvious that fuel and time are saved under either controlled or quick-starting conditions with the Martins Creek-type unit. Also, if it were desired to take maximum advantage of the quick-start concept, then the bypass line-heat exchanger system needed would be much smaller for the Martins Creek type as compared to the conventional convection type.

This paper clearly outlines the various operating problems encountered during the investigations and advises in much detail as to the solutions applied. In connection with the difficulty of minimizing radiant-superheater metal temperatures at Martins Creek, it also should be mentioned that the greatest help was obtained through operation of the coal burners with maximum quantities of auxiliary air and with the widest possible openings used on the secondary-air vanes. Both of these factors increase the axial component of the fuel-air mixture and thus tend to narrow the flame angle. The author has called attention to his finding that the influence of ignition-torch oil pressure on steam-temperature and steam-pressure appreciation is all out of proportion to the change in oil quantities introduced and that radiant-tube metal temperatures are independent of this effect. It is suggested here that the pressure and temperature changes noted are probably due to the pulverized-coal flame-propagation effects and that the radiant-tube metal temperatures are unaffected because of the narrow flame angle mentioned.

The author also reports failure to achieve control of turbine steam-temperature-rise rates by manipulating convection-superheater inlet drains or by using the control condenser. This was to be expected. It is felt that the application of a special spray nozzle in the steam lead before the turbine would be a more sound and effective solution to this problem.

The relatively simple corrections employed for minimizing the influence of the steam leads on turbine-end temperatures and decreasing drum-metal temperature differentials are of interest. In connection with the latter it is well to recall that the greatest drum-metal temperature differentials can occur when a steam-generating unit is being taken out of service. It is felt that this should be kept in mind in any investigation along similar lines which may be carried out by others in the future.

Author's Closure

The author wishes to thank all those distinguished authorities who took time out of their busy schedules to study and discuss this work. Their contributions are very helpful and sincerely appreciated.

The air leakages which Mr. Bell mentions at pump shafts, valve stem packing, and through the multitude of small vents must, of course, be kept to an absolute minimum on large installations because of their effect on the fuel bill during on-line operation.

The leakage with which we are most concerned in the starting operation, however, is that which takes place along the main turbine shaft on steam-water sealed units below half speed and before the water seals become effective. On the necessarily well-kept units of the present day, the comparatively low capacity steam jet air pump is entirely adequate to produce excellent vacuum above sealing speed if it must deal only with the small leakages mentioned by Mr. Bell, but the hogging jets are often too small to properly scavenge the huge quantities of air which enter along the poorly sealed turbine shafts and produce a reasonably high vacuum, with resulting overheating below half speed. After sealing speed is passed the hot turbine then imposes an added burden on the steam jet air pump in removing the lower density hot air which can only be properly cared for by extending the rolling period. In addition to undesirable heating of the whole low-pressure turbine mass, the undersized hogging jet then unnecessarily prolongs the starting operation which is particularly bad on starts from overnight shutdown when, for other reasons, it is beneficial to shorten the roll period as much as possible. Fortunately, for operators, the trend on newer installations is toward steam-sealed units on which full vacuum is attainable on turning gear.

It is difficult to conceive of air stagnation in any of the active regions of the turbine during starting conditions in view of the high velocities existing. Peripheral velocities are in the sonic region. Rough calculations on a typical start of one of the

Martins Creek units indicate that axial velocity of the steam alone in the second last stage annuli occupied by the blading must be in excess of 80 miles per hour toward the end of the rolling operation. Since the vacuum carries well up to the front of the turbine and the annulus areas of the stages increase progressively toward the exhaust end, the axial velocities in upstream stages may actually be higher than those in the low-pressure section.

In this connection, on a recent start from cold of a Westinghouse 100-mw turbine an unusual interruption of the smooth temperature rise of the lower shell at the seventh stage drain belt took place just as the water seals became effective at about 1800 rpm speed. The temperature dropped abruptly from 320 F to 273 F and recovered to 305 F all in a period of six minutes. There was a simultaneous sharp increase in vacuum from 17 to 20 in. Hg as the turbine became sealed. This may have been caused by the sudden flushing of water lying in the quiescent zone between blade ring and outer shell across metal in the area of the temperature sensing device, although it is hard to explain the presence of water at these temperatures and subatmospheric pressures.

Mr. Falkner cites a sound reason for maintaining the turbine metal temperature at a high level prior to removing unit from service for an overnight shutdown which we had overlooked, viz., that the resulting high front end metal temperature on start-up would allow the unit to be brought to normal operating temperatures in shorter time with a resulting saving in turbine efficiency.

We were obliged to live with the higher shutdown steam temperature because of: (1) The flat temperature characteristic of the radiant-convection steam generator which delivered steam to the turbine at 875 F (only 75 F under full load temperature) at minimum practical operating load of 25 mw on the 160 mw unit; this would have reduced the temperature in only the first two of eight valve bowls; and (2) the integral steam chest and stop valve-control valve design which did not permit uniform cooling of the entire chest, bowl, and packing hub sections.

He also mentioned an important point that should be kept in mind by all those responsible for operation of modern units which concerns the caution that must be exercised in matching steam and metal temperatures when returning a unit to service after a very short outage.

Our experience in one case parallels that of Mr. Falkner. In the haste to meet operating deadlines on a new unit, a plug had been screwed hand-tight into one of the extraction lines and forgotten. After a few days of commercial service, the plug blew out, which required the immediate shutting down of the turbine. The theromometer well which was to have gone into the extraction line in the first place instead of the plug, was located and everything was readied for a short shutdown. The unit was unloaded, the fires were removed from the furnaces, and the thermometer well was inserted during a shutdown which should have lasted less than five minutes.

Before the turbine was rolled after the shutdown, it was found that steam temperature ahead of stop valves had dropped 100 F. To start up immediately would have caused a dangerous shrinkage of the hot spindle. It took over three hours of firing before the steam temperature reached that of the steam chest metal to allow the unit to be returned to service.

Our mistake in this case was to stop the firing operation, which caused the delivery steam temperature to decay at once toward saturation level. Proper procedure would have been to continue firing and venting at the turbine end of the leads during the short turbine shutdown.

In the matter of drum temperature differentials during shutdowns, the Martins Creek units are provided with top drum level indicators to allow complete filling when the pressure is to be taken off the boiler. For week-end shutdowns we have followed the lead of Consolidated Edison Company of New York in not allowing the pressure to drop below 40 per cent of operating levels. Our drum thermocouples have shown that the use of this device keeps drum temperature differentials within the 100 F recommendation of the boiler manufacturers during the bottled period. (The foregoing also answers a point raised in Mr. Weismantle's discussion.)

In fact, Mr. Falkner and his former associates, Mr. John M. Driscoll and Mr. Maurice Salvage at Consolidated Edison, have provided us solid direction and precedent in all phases of the work.

Mr. Jackson in his thorough discussion states that our concern in regard to rate of exhaust end cooling is not supported by any broad record of failures in units which have had repeated starts with hood temperatures running to 175 F. Our interest in the matter stemmed from cases on our system where much higher temperatures were reported before any comprehensive controlled start studies had been made. We cited cracked last-stage diaphragm rings on one unit which may possibly have been connected with the severe treatment, and on others we thought that persistent failures of wheel blading in the latter stages could be traced in part to the rapid quenching experienced during the start-up.

In beginning the Martins Creek work then, we felt that the metal components in the exhaust sections were just as massive as those in the high-pressure turbine, albeit not as complex and irregular in shape, and therefore should be treated with a modicum of respect. Operations, such as the draining of hot steam for heating the leads into the condenser, were controlled as much as possible, and finally discontinued when their effects on exhaust end temperatures were realized.

As an example of the quenching which took place on the Martins Creek unit even under closely controlled conditions, we list hood temperatures from the original data sheets taken at one minute intervals before and after the generator was synchronized for the start shown in Fig. 11 in the paper. The generator was synchronized at 7:10 a.m. From 7:05 a.m. to 7:16 a.m., inclusive, hood temperatures on the west side in degrees F were: 187, 192, 197, 195, 199, 200 (at 7:10 a.m.), 160, 110, 95, 89, 83, and 76. The drop of 124 F from 7:10 a.m. to 7:16 a.m. was then at a rate of 1240 F per hour, which we thought was excessive and which we made every effort to reduce.

When the hoods were cooled too fast, as in this case, the operation was also invariably accompanied by a series of heavy dull thuds emanating from the low pressure sections which, to say the least, was not very reassuring. There definitely should be more investigation along these lines.

The new turbine designs mentioned by Mr. Jackson will find ready application in the coming years as the industry is forced into frequent cycling and shutting down of the larger machines.

The use of a small bypass around the boiler lead valves for controlling the speed and early loading operations, and for uniform heating of integral chest turbines, especially on starts from cold, is an excellent idea. For our outdoor installation, it would probably be more desirable to install the bypass at the stop valves in order to maintain the benefits of heated leads during overnight shutdown. The stop valve tripping features would then have to be incorporated into the bypass.

The return to steam seals which will allow full vacuum on turning gear is an unmitigated blessing for the starting operation.

In connection with Mr. Jackson's warm agreement with our statement that each new installation should undergo thorough on-the-job investigation in order to establish correct starting procedures, we might say editorially that both operating and design people within the utility industry, in our opinion, are

often too prone in their fervor to exchange experiences to take the other fellow's word as gospel, to the exclusion of down-to-earth analysis of their specific problems. Design sometimes gets to be a canvass and sublimation of majority opinion rather than a study of individual requirements. A tremendous opportunity exists for the operating engineer to roll up his sleeves and delve into problems in this field to find the relatively simple solutions which are so urgently needed.

Mr. Reynolds speaks of the advantages of precooling the turbine before taking it off the line in making the starting process easier after overnight shutdowns. The reasons why this procedure did not lend itself readily to the Martins Creek installation were brought out in the closure to Mr. Falkner's discussion.

The idea of bypassing steam from the active to the inactive chambers under the steam chest to reduce temperature gradients across partitions is a very good one. It would probably allow faster load applications on all types of starts and would be especially beneficial in uniform heating of the front elements on starts from cold.

We are currently assembling the necessary material to install this type of bypass on a Westinghouse 100-mw, 7-valve integral steam chest turbine which will shortly be subjected to repeated shutdowns.

We agree with Mr. Reynolds that in some cases the series piping arrangement in a two-step flange heating system would be more desirable since it would provide a natural graded temperature line in the bolt holes to parallel that existing on the inner flange surface. In fact, we would have chosen to use the series arrangement for that reason, but found it to be inadequate in the lower reaches of the system. The routing of the spent steam to a region of higher pressure than the condenser, as in this case, and provision of larger cross-sections for steam paths should have made this possible.

We agree with Mr. Weismantle in everything but the statement that the greatest help was obtained in minimizing the difficulty with high radiant superheater metal temperatures through operation with the widest possible opening of secondary air vane dampers.

Historically, all of the September, 1954, runs had to be made with steam temperature well below turbine metal temperature due to inability (because of high radiant tube metal temperatures) to fire at the 1.8-in. minimum classifier differentials specified for the needed steam temperature raising operation before rolling the turbine. Fig. 8 illustrates one of the last of these runs.

For the January, 1955, and succeeding runs, a minimum classifier differential of 1.3 in. was found to be satisfactory for two-burner-per-exhauster operation since it did not reduce the coal-air velocities through burner tubes below that when firing at 1.8-in. classifier differential for three-burner-per-exhauster operation. This made it possible to fire with coal to bring steam temperature to proper levels at or above front end turbine metal temperature before rolling the turbine.

It is true that further opening of the vanes in April, 1955, from 65 to 75 per cent reduced the radiant superheater metal temperature on the overnight starts, an average of about 90 F and was distinctly beneficial, but the big step was made in going to the lower firing rate without running the risk of coked burners.

In so far as auxiliary air supply to burners was concerned, the practice was always to keep this as high as possible during starts consistent with stable flame propagation.

We heartily confirm the case Mr. Weismantle makes for the radiant and convection superheater for the start-up phases of Central Station operation. It gets the steam temperature up to where we want it to be with a minimum of pre-roll firing. The steam generator behaved very well in other respects, such as circulation, turn-down characteristics, the ability to start up smoothly with low volatile coals, in addition to good response to controls and high over-all efficiency.

A point well worth mentioning is the keen interest, patience, and co-operation displayed by all the service representatives of Mr. Weismantle's company in this work. There was never any hint of dictation because of their greater boiler operating experience, but a willingness to go along in every reasonable experiment. Without this spirit, it is doubtful that the investigations could have been pursued to their logical conclusions.

Operating Experience With High-Temperature Steam-Turbine Rotors and Design Improvements in Rotor-Blade Fastening[1]

By JOSEPH D. CONRAD[2] AND N. L. MOCHEL,[3] LESTER, PA.

Introduction

At the conclusion of the presentation of a paper [1][4] dealing with turbine and generator rotor forgings, at the 1955 Annual Meeting of the Society in Chicago, it was stated that, after the paper had been printed, there had been two experiences on the part of the authors' company, involving cracking in turbine rotor-blade groove walls. Both were in the intermediate-pressure rotors of single-shaft, tandem-compound, three-casing, triple-exhaust, reheat turbines. The first had taken place in a nickel-chromium-molybdenum-vanadium steel rotor at TVA Shawnee Station, Unit No. 1; and the second, just a week before the Chicago meeting, in Consumers Power Company's Weadock Station Unit No. 7. In the latter case, the forging was of chromium-molybdenum-vanadium steel. It is the purpose of this paper to report the results of the investigations arising from these experiences, and the examination of similar rotors in other Westinghouse-built turbines.

The Weadock Rotor

The mishap on the Weadock No. 7 turbine took place on November 6, 1955. It consisted of a groove-wall failure at the second blade row of the i-p spindle. Weadock No. 7 is a 156,250 kw single-shaft, tandem-compound, three-casing triple-exhaust, 3600-rpm turbine-generator unit designed for steam conditions of 2000 psi, 1050 F, reheating to 1000 F. The reheated steam is admitted ahead of the first stage of this spindle. A cross section of the entire turbine is shown in Fig. 1, and an enlargement of the i-p element is shown in Fig. 2. This i-p element contains all of the intermediate-pressure stages following the reheat point and one of the three sets of low-pressure exhaust blades. This machine had been in service for seven months when the mishap occurred.

Temporary Repair of Weadock Rotor. Eight stages of blading immediately following the reheat point were sufficiently damaged to require removal. The material between the blade-root grooves was machined out to provide specimens for a full metallurgical investigation. The machine was returned to service in five weeks without these 8 stages and with the reheat temperature limited to 850 F. The interceptor valves were adjusted to prevent them opening wide in order to compensate for unbalance in thrust brought about by omission of the 8 stages. The machine was found to operate satisfactorily up to 170,000 kw. However, to provide a large margin of safety, the load was limited to 145,000 kw (93 per cent of rated capability) until the rotor was replaced about one year later.

Description of the Weadock Rotor Mishap. The machine had been operating very smoothly. However, it developed an increasing amount of vibration over a period of five days immediately before the mishap occurred. The vibration was somewhat spasmodic in magnitude finally reaching a double amplitude of 7 mils, thus demonstrating that this was a progressive failure rather than an explosive one. Successive surges of vibration were probably created as progressive cracking allowed the blades to lean and permitted shrouds to rub.

The fracture was of the creep-to-rupture type, and took place along the sections AA, BB, and BC in Fig. 3 and extended around the circumference about 8 in. The part above AA was completely broken out and that above BC almost broken out in a manner to let 9 blades come out of the rotor. The blade-entering slots for successive rotating rows are diametrically opposite one another. This fracture, adjacent to row 2, was at the location of entering slots of rows 1 and 3 shown by dotted lines in Fig. 3. Groove-wall stresses are higher than average at this circumferential location. The stress across section BB is increased by the extra load of the closing blade in row 3, transmitted through the serrated breech block. The stresses across section AA and BC are increased by the cutting of these sections for the entering slots of rows 1 and 3, respectively. The detail of this construction is illustrated by Fig. 4. Photographs of the failed-rotor groove wall are shown in Figs. 5 and 6.

The stresses at the point of failure were higher than normally allowed at this reheat operating temperature due to an unusual combination of blade size, row spacing, and radial step-up between rows. In combination, this resulted in too thin a wall at both AA and BB. This condition was created and not fully checked when a previously established design was modified for lower reheat and crossover pressures. The concentration of load due to breech-block loading was also above normal, due to use of a wider-than-necessary entering slot taken from a larger pitch blade using the same fastening.

Weadock Rotor Material. The rotor was made of chromium-molybdenum-vanadium steel of the following composition:

	Per cent
Carbon	0.32
Manganese	0.74
Phosphorus	0.037
Sulfur	0.036
Silicon	0.25
Chromium	1.04
Molybdenum	1.20
Vanadium	0.24
Nickel	0.34

The forging had been treated during manufacture as follows:
1 After all forging had been completed, it was equalized at 1450

[1] The preprints and presentation of this paper also contained a description of operating experience on high-pressure rotors which has been omitted in the interest of conserving publication space. The experience was similar to that with the intermediate-pressure rotors.

[2] Assistant Manager, Large Turbine Engineering, Westinghouse Electric Corporation. Mem. ASME.

[3] Manager, Metallurgical Engineering, Westinghouse Electric Corporation. Mem. ASME.

[4] Numbers in brackets designate References at end of paper.

Contributed by the Power Division and presented at the Power Conference, Allentown, Pa., October 21–23, 1957, of The American Society of Mechanical Engineers.

Note: Statements and opinions advanced in papers are to be understood as individual expressions of their authors and not those of the Society. Manuscript received at ASME Headquarters, October 21, 1957. Paper No. 57—PWR-10.

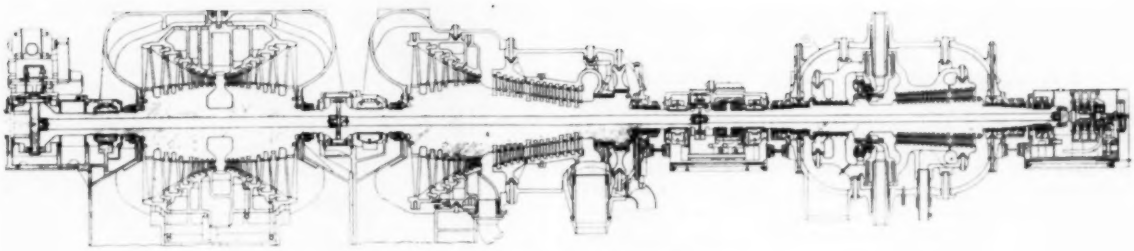

Fig. 1 Cross section of Weadock turbine

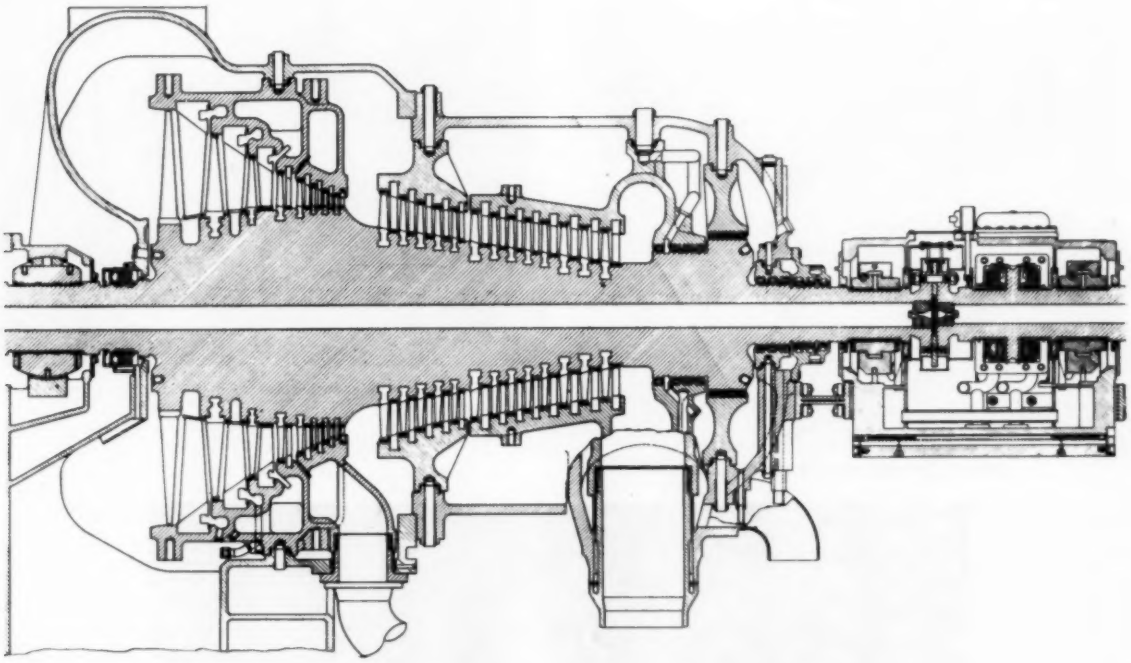

Fig. 2 Cross section of i-p element of Weadock turbine

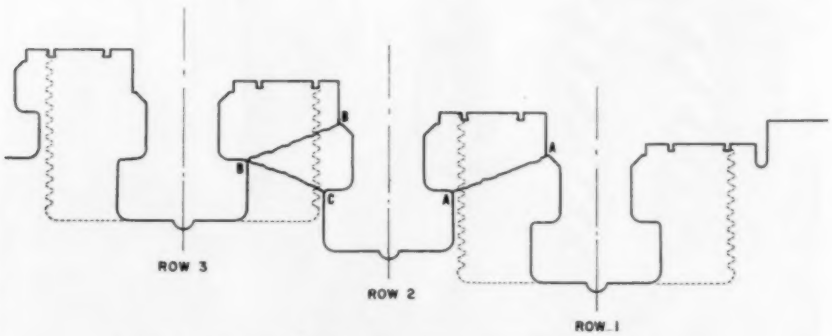

Fig. 3 Enlarged section of Weadock rotor showing location of fracture

F for 10 hr, then cooled at a rate of 30 F per hr to 450 F, held 12½ hr. It was then reheated to 1750 F, held for 23 hr, and cooled in the furnace to 450 F, and held 12½ hr. It was then reheated to 1300 F, held for 31 hr, cooled slowly in the furnace to below 400 F, and air cooled to room temperature. The forging was then rough turned, faced, and bored.

2 It was then reheated at a rate of approximately 40 F per hr to 1850 F, held for 12½ hr, air cooled quickly with fans to 1000 F, cooled normally in air to 450 F, and equalized at 450 F for 12½ hr. It was then reheated at a rate of about 30 F per hr to 1225 F, held for 23 hr, furnace cooled at about 30 F per hr to 450 F, and cooled to room temperature in air.

3 After being rough machined to drawing size, it was stress relieved by reheating to 1225 F, held for 36 hr, cooled at about 30 F per hr to 400 F, and cooled to room temperature in air.

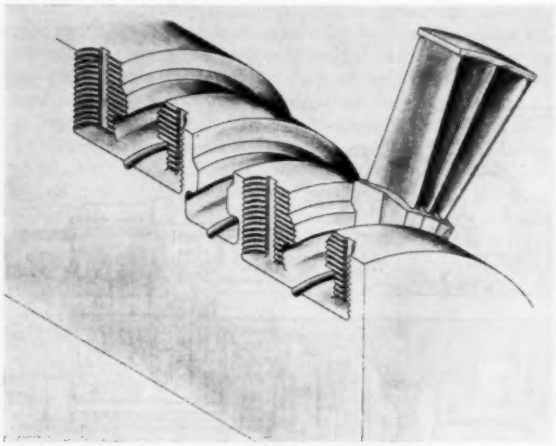

Fig. 4 Entering slots for rotor blades

Fig. 6 Close-up of Weadock rotor with partially fractured section removed

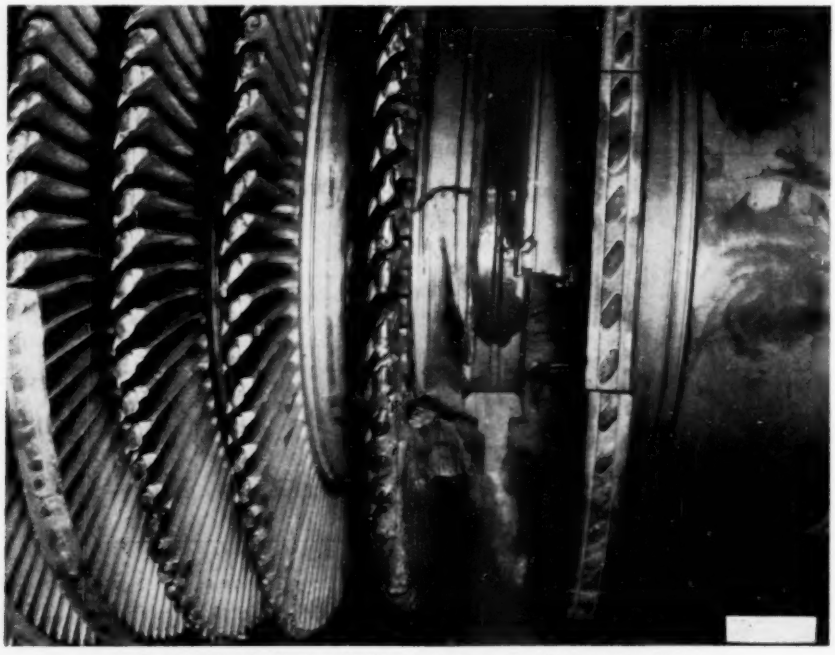

Fig. 5 Weadock rotor showing partially fractured segment in place

Table 1 Weadock rotor—notched-bar creep-rupture tests at 1000 F

Specimen no.	Stage	Direction	Stress	Notch radius	K^a T	Rupture time, hr
1	1	Tang.	96,000	0.005	4.8	0.9
2	7	Tang.	96,000	0.005	4.8	1.2
3	3	Radial	62,000	0.005	4.8	18.5
4	3	Tang.	62,000	0.005	4.8	20.0
5	1	Tang.	48,000	0.005	4.8	44.1
6	3	Tang.	48,000	0.005	4.8	47.5
7	7	Tang.	48,000	0.005	4.8	63.6
8	3	Radial	40,000	0.005	4.8	230
9	3	Tang.	40,000	0.005	4.8	449
10	1	Tang.	35,000	0.005	4.8	410
11	7	Tang.	35,000	0.005	4.8	252
12	3	Tang.	32,000	0.002	8.8	452
13	3	Tang.	32,000	0.005	5.8	419
14	3	Tang.	32,000	0.020	3.0	816
15	3	Tang.	32,000	0.005	4.8	517
16	3	Radial	30,000	0.005	4.8	1076
17	3	Tang.	30,000	0.005	4.8	440
18	3	Tang.	28,000	0.005	5.8	1070
19	3	Tang.	28,000	0.002	8.8	517
20	3	Tang.	25,000	0.002	8.8	2201
21	3	Tang.	25,000	0.005	5.8	1792

[a] Theoretical stress concentration factor.

The acceptance-test physical properties of the forging were as follows:

Tangential test specimens	Yield strength 0.2 per cent plastic deformation, lb per sq in.	Ultimate tensile strength, lb per sq in.	Elongation in 2 in., per cent	Reduction area, per cent
X-1	99,000	122,500	15	35
X-2	102,000	124,500	16	39
X-3	99,500	122,500	16	41

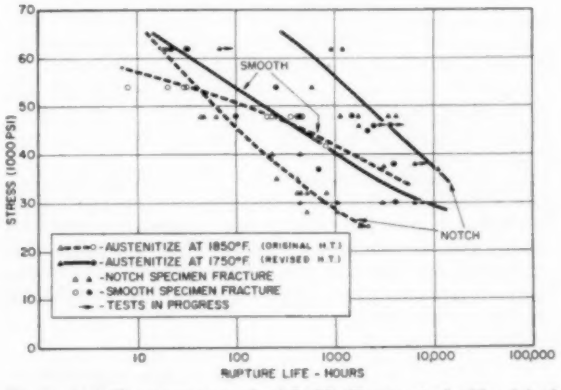

Fig. 7 1000-F rupture strength of Cr-Mo-V rotor steel with original and revised heat-treatments

Table 2 Weadock rotor smooth-bar creep-rupture tests at 1000 F

Specimen number	Stage	Direction	Stress	Rupture time, hr	Per cent elongation in $1^1/_2$ in.	Per cent reduction of area
1	1	Tangential	54,000	8	11	30
2	3	Radial	54,000	29.8	10	18
3	3	Tangential	54,000	20.0	9.2	27
4	7	Tangential	54,000	31.5	11	28
5	1	Tangential	48,000	204	6.3	14
6	3	Radial	48,000	230	5.9	12
7	3	Tangential	48,000	354	4.8	11
8	7	Tangential	48,000	475	4.9	11
9	3	Tangential	42,000	807	2.8	10

Table 3 Cr-Mo-V rotor material with revised heat-treatment combination specimen creep-rupture-tests at 1000 F

Specimen no.	Tempering temperature, F	Stress	Smooth bar: Rupture time, hr	Smooth bar: Per cent elongation in $1^1/_2$ in.	Smooth bar: Per cent reduction of area	Notch-bar rupture time, hr
			Weadock rotor—retreated			
1	1225	62,000	32	23	48	68[a]
2	1225	48,000	433	17	48	1124
3	1300	48,000	100	18	67	1722
4	1225	37,500				3090
			Test rotor forging—31 in. diam			
5	1225	62,000	31.9	17	69	928
6	1225	54,000	266	22	72	597
7	1225	48,000	461	14	67	3661
8	1225	38,000	4002	16	56	6490[b]
9	1300	37,500	698	28	77	11029
10	1300	30,000	4112	21	76	6530[b]
			Production rotor forgings			
11	1225	62,000	22	18	79	1218
12	1225	48,000	1489	14		4085
13	1225	45,000	2209	14	52	2209[b]
14	1200	46,000	3610	10		3000[c]
15	1210	46,000	2500	8		1811[c]

[a] Stripped threads in notch bar. [b] Notch bar test still running.
[c] Smooth bar test still running.

Smooth-bar and notched-bar creep-rupture tests were made on the material which had been removed from the rotor before it was returned to temporary service. The results of these tests are given in Tables 1 and 2 and are plotted in Fig. 7, with broken lines showing the locus of points. It is evident that this forging was particularly notch sensitive.

Between the time the forging for this rotor was made and the groove-wall failure took place, a change in the heat-treating procedure for chromium-molybdenum-vanadium forgings had been put into effect. The change in heat treatment consisted essentially in reducing the previously specified austenitizing temperature of 1850 F to 1740/1750 F, for purposes of securing improved ductility both at room and elevated temperatures.

As part of the investigation, a portion of the material cut from the Weadock rotor was retreated in line with the more recent practice given above, and creep-rupture tests were made. Results of these tests are given in Table 3.

Also, as part of the investigations, use was made of a 31-in-diam × 9-in-thick disk section, sliced from the 31-in-diam body of a chromium-molybdenum-vanadium steel forging, rejected during an early stage of manufacture for unsoundness at a location quite remote from the section secured for test purposes. The forging had been produced from a 92-in. ingot, and had the following chemical composition:

	Per cent
Carbon	0.34
Manganese	0.86
Phosphorus	0.010
Sulfur	0.009
Silicon	0.29
Chromium	0.97
Molybdenum	1.21
Vanadium	0.25
Nickel	0.10

As secured by us, it had received only the preliminary treatments given before rough machining.

A section of this rotor was heat-treated to the revised specifications and creep-rupture tests were made. The results of these tests are given in Table 3. At the bottom of Table 3 are also given the results of creep-rupture tests from cored specimens taken from several production rotor forgings using the revised heat-treatment.

The data in Table 3 are also plotted in Fig. 7, with solid lines showing the locus of points. These results show clearly that the revised heat-treatment gives a considerably improved material from the standpoint of notch sensitivity.

In order to obtain a comprehensive picture of the creep-rupture strength of this material, representative test data from cored

Table 4 Inspection and stress reports on Cr-Mo-V rotors

SPINDLE		A	B	C	D	E	F	G	H	J	K	L
Start up Date Hrs. Full Reheat Temp. Machine Type Austenitizing Temp. F Tempering Temp. F Notes		9/22/54 13000 2 cyl 1850 1230	10/25/54 9000 3 cyl 1850 1220 3	11/26/54 10000 2 cyl 1850 1240	2/7/55 6500 3 cyl 1850 1220 3	3/31/55 5000 3 cyl 1850 1225 2,4	6/8/55 4000 3 cyl 1750 1210	6/10/55 9000 3 cyl 1850 1230 1	6/23/55 3500 3 cyl 1750 1190	8/20/55 9000 3 cyl 1750 1220 1	9/24/55 13000 3 cyl 1850 1230	12/30/55 6500 2 cyl 1850 1230
Row 1 Inlet	Temperature Nominal Stress Multiplier Max Stress Crack Length Crack Depth	830 11500 1.53 17600 NONE	990 11700 1.73 20200 360° .25	830 10640 1.535 16350 NONE	990 14100 1.81 25400 NONE	990 14100 1.81 25400 2.6	990 13100 1.81 23700 NONE	960 9800 1.36 12500 NONE	990 10900 1.73 18900 NONE	960 8600 1.36 11700 NONE	990 11400 1.58 18000 NONE	830 13000 1.38 18000 NONE
Row 1 Outlet	Temperature Nominal Stress Multiplier Max Stress Crack Length Crack Depth	935 11500 1.53 17600 NONE	975 11700 1.73 20200 360° .095	935 9870 1.56 15400 NONE	975 21400 1.68 35900 NONE	975 21400 1.68 35900 6.1	975 21000 1.68 35300 NONE	950 16300 1.56 25500 NONE	975 10900 1.73 18900 NONE	950 15600 1.56 24300 NONE	975 10500 1.43 15000 NONE	935 13400 1.26 16900 NONE
Row 2 Inlet	Temperature Nominal Stress Multiplier Max Stress Crack Length Crack Depth	935 11700 1.54 18000 NONE	975 12100 1.70 20600 NONE	935 10800 1.56 16800 NONE	975 18900 1.85 35000 2.6 .010	975 18900 1.85 35000 18	975 17100 1.85 31660 NONE	950 15800 1.72 27200 NONE	975 11300 1.70 19200 NONE	950 14600 1.72 25100 NONE	975 12200 1.57 19200 NONE	935 14800 1.38 20400 NONE
Row 2 Outlet	Temperature Nominal Stress Multiplier Max Stress Crack Length Crack Depth	930 12600 1.41 17800 NONE	955 13000 1.55 20000 NONE	930 10800 1.56 16800 NONE	955 20400 1.84 37500 NONE	955 20400 1.84 37500 15	955 19900 1.84 36600 NONE	945 16800 1.56 25900 NONE	955 13000 1.55 20000 NONE	945 16400 1.56 25900 NONE	955 12500 1.42 17800 NONE	930 13400 1.26 16900 NONE
Row 3 Inlet	Temperature Nominal Stress Multiplier Max Stress Crack Length Crack Depth	930 12200 1.55 19000	955 13400 1.70 22800 NONE	930 11150 1.56 17300	955 20600 1.84 37900 NONE	955 20600 1.84 37900 18	955 19000 1.84 35000 NONE	945 16950 1.72 29100 NONE	955 11800 1.70 20000	945 15600 1.72 26800 NONE	955 15300 1.56 24000	930 13400 1.26 16900
Row 3 Outlet	Temperature Nominal Stress Multiplier Max Stress Crack Length Crack Depth		930 14900 1.55 23200 NONE		NONE	11	NONE	910 13300 1.63 21700 NONE	930 14900 1.55 23200	910 12400 1.63 20800 NONE		
Row 4 Inlet	Temperature Nominal Stress Multiplier Max Stress Crack Length Crack Depth							910 29400 1.56 45900 NONE		910 27800 1.56 43400 NONE		
Row 4 Outlet	Temperature Nominal Stress Multiplier Max Stress Crack Length Crack Depth							875 14900 1.69 25200 NONE		875 14100 1.69 23800 NONE		
Row 5 Inlet	Temperature Nominal Stress Multiplier Max Stress Crack Length Crack Depth							875 40600 1.48 60000 NONE		875 38200 1.48 56600 NONE		

NOTES: 1. Cross compound machine, cooling provided in original design.
2. Total length of cracks when more than one crack present.
3. Maximum depth given where crack varied in depth.
4. Weadock Spindle, see text for full extent of fractures.

specimens of many rotors have been plotted with stress to rupture versus a time-temperature parameter [2] in Fig. 8.

Inspection of Chromium-Molybdenum-Vanadium Steel Rotors

Immediately after the Weadock experience, owners of similar machines were requested to reduce the reheat temperature about 50 F until an inspection could be made. During the past two years, ten other rotors made of the chromium-molybdenum-vanadium-steel material have been inspected after service periods up to 13,000 hr. Pertinent design data, operating conditions, and results of inspection are given in Table 4. In this table, rotor E is Weadock and D and F are very nearly duplicates of that machine. Since two different heat-treatments were used on this material, this is designated in the table.

It will be noted that two other rotors, B and D, had cracks and both used the 1850 F heat-treatment. No rotor using the 1750 F heat-treatment had any cracks including rotor F, one of the near duplicates, which ran almost as long as Weadock. Also, one of the rotors which cracked, rotor B, had considerably less stress than Weadock and ran less than twice as long. Rotors A, C, and G used the 1850 F heat-treated steel; however, the combination of stress and temperature in these cases gave a more favorable condition than in B or E.

Operating Experience With Nickel-Chromium-Molybdenum-Vanadium Steel Rotors

Prior to 1953, all high-temperature rotors used by Westinghouse were made of a nickel-chromium-molybdenum-vanadium steel. This material was made with some variations in chemical composition and heat-treatment. In general, it had been found to be very satisfactory with metal temperatures from 850 to 950 F.

One form of this material had been made in 18-in-diam forgings and extensively tested at 1000 F with very good results. Prior to the adoption of the chromium-molybdenum-vanadium steel just described, this form of the nickel-molybdenum-vanadium steel was applied to a number of rotors for operation with metal temperatures near 1000 F. Among these machines was the i-p element of the Shawnee No. 1 unit of the TVA system. This machine is similar in design to Weadock except the i-p groove-wall stresses are much lower.

Table 5 Inspection and stress reports on Ni-Cr-Mo-V rotors

SPINDLE		A	B	C	D	E	F	G	H	J	K
Start up Date Hrs. Full Reheat Temp. Machine Type		8/15/49 58000 3 cyl	7/51 40000 3 cyl	4/1/53 24000 3 cyl	6/15/53 20000 3 cyl	6/15/53 20000 3 cyl	8/15/53 19000 3 cyl	9/21/53 16000 3 cyl	11/53 20000 3 cyl	1/1/54 16000 3 cyl	1/54 20000 2 cyl
Notes			1	1	1	1,2	1	1,2		1,2	
Row 1 Inlet	Temperature Nominal Stress Multiplier Max Stress Crack Length Crack Depth	990 6300 1.59 9960 NONE	990 12100 1.55 18700 5 .265	990 12000 1.54 18500 1.125 .020	990 10900 1.73 18900 360° 1.00	990 10900 1.73 18900 360° 1.25	990 12000 1.54 18500 360° .090	990 10900 1.73 18900 360° .125	990 3510 1.55 5450 NONE	990 10900 1.73 18900 360° .25	830 7500 1.55 11600 NONE
Row 1 Outlet	Temperature Nominal Stress Multiplier Max Stress Crack Length Crack Depth	975 6700 1.59 9000 NONE	975 15200 1.55 23600 1.25 .110	975 13600 1.54 20900 3.25 .020	975 10900 1.73 18900 6 .38	975 10900 1.73 18900 360° .425	975 12100 1.54 18600 1 .080	975 10900 1.73 18900 8.5 .070	975 3510 1.55 5450 NONE	975 10900 1.73 18900 360° .35	935 8700 1.42 12400 NONE
Row 2 Inlet	Temperature Nominal Stress Multiplier Max Stress Crack Length Crack Depth	975 6340 1.59 10050 NONE	975 11500 1.58 18100 NONE	975 10400 1.57 16300 NONE	975 11300 1.70 19200	975 11300 1.70 19200 360° .50	975 11600 1.58 18300 NONE	975 11300 1.70 19000 12	975 3560 1.55 5500 NONE	975 11300 1.70 19200 360° .25	935 8700 1.42 12400 NONE
Row 2 Outlet	Temperature Nominal Stress Multiplier Max Stress Crack Length Crack Depth	955 6500 1.44 9400 NONE	955 9200 1.44 13300 NONE	955 10800 1.45 15600 NONE	955 13000 1.55 20000	955 13000 1.55 20000 360° .125	955 10800 1.45 15600 NONE	955 13000 1.55 20000 4	955 5000 1.57 7850 NONE	955 13000 1.55 20000 17 .110	930 8800 1.42 12500 NONE
Row 3 Inlet	Temperature Nominal Stress Multiplier Max Stress Crack Length Crack Depth	955 6500 1.59 10300	955 11700 1.58 18500	955 11200 1.60 17900	955 11800 1.70 20000	955 11800 1.70 20000 360° .290	955 11300 1.60 18000	955 11800 1.70 20000 360° .128	955 2200 1.57 3480	955 11800 1.70 20000 360° .185	930 8800 1.42 12500
Row 3 Outlet	Temperature Nominal Stress Multiplier Max Stress Crack Length Crack Depth					930 14900 1.55 23200 360° .030		930 14900 1.55 23200 NONE		930 14900 1.55 23200 NONE	
Row 4 Inlet	Temperature Nominal Stress Multiplier Max Stress Crack Length Crack Depth					930 14700 1.71 25000 8 .60		930 14700 1.71 25000 NONE		930 14700 1.71 25000 360° .230	
Row 4 Outlet	Temperature Nominal Stress Multiplier Max Stress Crack Length Crack Depth					910 18600 1.71 31700 6 .375		910 18600 1.71 31700 NONE		910 18600 1.71 31700 8 .060	
Row 5 Inlet	Temperature Nominal Stress Multiplier Max Stress Crack Length Crack Depth					910 13200 1.73 22900 15.5 .25				910 13200 1.73 22900 10 .150	
Row 5 Outlet	Temperature Nominal Stress Multiplier Max Stress Crack Length Crack Depth					890 12600 1.56 19700 1.00 .185				890 12600 1.56 19700 NONE	
Row 6 Inlet	Temperature Nominal Stress Multiplier Max Stress Crack Length Crack Depth					890 12900 1.72 22200 7.75 .22				890 12900 1.72 22200 2 .050	

NOTES: 1. Maximum depth given where crack varied in depth.
2. Total length of cracks when more than one crack present.

Shortly before the Weadock mishap, this TVA machine was being modified for reasons unrelated to the rotor problem. At that time rotor blades in the first row were found to be leaning. On removal of the blades, the groove walls on each side of the row were found to be cracked. The crack extended the entire circumference on the inlet side and was about halfway through the wall adjacent to the entering slot. The crack on the outlet side was of short length and relatively shallow.

The chemical composition of this rotor forging is as follows:

	Per cent
Carbon	0.28
Manganese	0.75
Phosphorus	0.030
Sulfur	0.027
Silicon	0.25
Nickel	2.71
Chromium	1.07
Molybdenum	0.56
Vanadium	0.21

The forging was heat-treated during manufacture as follows:

1 After all forging had been completed, the forging was equalized at 1300 F for 14 hr, and control cooled to 460 F, and held at 460 F for 24 hr. It was then reheated to 1640 F and held for 36 hr, and air cooled to 1200 F, then control cooled to 460 F, and equalized at 460 F for 24 hr. It was then reheated to 1220 F and held for 36 hr, and control cooled to 400 F, and then air cooled.

2 The forging was then rough turned, faced, and bored. It was then reheated to 1600 F, held for 32 hr and air cooled to 460 F, and equalized at 460 F for 30 hr. It was then reheated to 1140 F, held for 45 hr, and furnace cooled to 600 F, followed by cooling to room temperature in air.

3 The forging was then rough machined to forging drawing size. It was then stress-relieved by heating to 1150 F, held for 38 hr, and furnace cooled to 450 F, then air cooled to room temperature. Failing to meet the specified physical properties, the forging was retreated as follows. The forging was reheated to 1600 F, and held for 32 hr, and air cooled to 450 F, and equalized at 450 F for 16 hr. It was then reheated to 1160 F, held for 38 hr, and

Table 5 (cont.) Inspection and stress reports on Ni-Cr-Mo-V rotors

SPINDLE		L	M	N	O	P	Q	R	S
Start up Date Hrs. Full Reheat Temp. Machine Type		1/26/54 15000 3 cyl	4/24/54 13000 3 cyl	6/3/54 12000 3 cyl	7/22/54 16000 3 cyl	9/19/54 10000 3 cyl	12/18/54 8000 3 cyl	2/9/55 7000 3 cyl	6/10/55 5000 3 cyl
Notes		1	1	1	1,2	1,2			3
Row 1 Inlet	Temperature Nominal Stress Multiplier Max Stress Crack Length Crack Depth	990 10900 1.73 18900 6 .040	990 10900 1.73 18900 240° .025	990 10900 1.73 18900 360° .090	990 10900 1.73 18900 360° .180	990 10900 1.73 18900 2.5 .125	990 10900 1.73 18900 NONE	990 10900 1.73 18900 NONE	860 15900 1.61 25600 NONE
Row 1 Outlet	Temperature Nominal Stress Multiplier Max Stress Crack Length Crack Depth	975 10900 1.73 18900 NONE	975 10900 1.73 18900 6.5	975 10900 1.73 18900 4 .030	975 10900 1.73 18900 360° .125	975 10900 1.73 18900 1.75 .063	975 10900 1.73 18900 NONE	975 10900 1.73 18900 NONE	930 18800 1.76 33100 NONE
Row 2 Inlet	Temperature Nominal Stress Multiplier Max Stress Crack Length Crack Depth	975 11300 1.74 19800 NONE	975 11300 1.74 19800 1.25 .060	975 11300 1.74 19800 4 .060	975 11300 1.74 19800 9.5 .060	975 11300 1.74 19800 4 .060	975 11300 1.74 19800	975 11300 1.74 19800	930 19800 1.76 34800 NONE
Row 2 Outlet	Temperature Nominal Stress Multiplier Max Stress Crack Length Crack Depth	955 13000 1.55 20000 NONE	955 13000 1.55 20000 NONE	955 13000 1.55 20000 NONE	955 13000 1.55 20000 1.375 .060	955 13000 1.55 20000 NONE	955 13000 1.55 20000	955 13000 1.55 20000	944 18700 1.76 32900 NONE
Row 3 Inlet	Temperature Nominal Stress Multiplier Max Stress Crack Length Crack Depth	955 11800 1.70 20000 NONE	955 11800 1.70 20000	955 11800 1.70 20000 NONE	955 11800 1.70 20000 22.375 .060	955 11800 1.70 20000 NONE	955 11800 1.70 20000	955 11800 1.70 20000	944 18700 1.76 32900
Row 3 Outlet	Temperature Nominal Stress Multiplier Max Stress Crack Length Crack Depth	930 14900 1.55 23200 NONE		930 14900 1.55 23200 NONE	930 14900 1.55 23200 1.625 .020				930 18700 1.76 32900
Row 4 Inlet	Temperature Nominal Stress Multiplier Max Stress Crack Length Crack Depth				930 14700 1.71 25000 4.50 .060				
Row 4 Outlet	Temperature Nominal Stress Multiplier Max Stress Crack Length Crack Depth				910 18600 1.71 31700 2 .020				
Row 5 Inlet	Temperature Nominal Stress Multiplier Max Stress Crack Length Crack Depth				910 13200 1.73 22900 NONE				
Row 5 Outlet	Temperature Nominal Stress Multiplier Max Stress Crack Length Crack Depth								
Row 6 Inlet	Temperature Nominal Stress Multiplier Max Stress Crack Length Crack Depth								

NOTES: 1. Maximum depth given where crack varied in depth.
2. Total length of cracks when more than one crack present.
3. Cooling provided in original design.

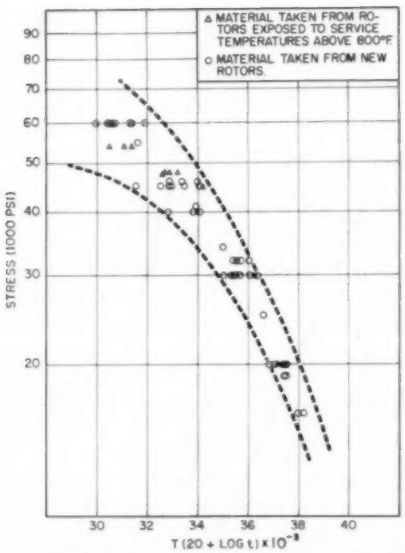

Fig. 8 Smooth-bar rupture strength of Cr-Mo-V rotor steel

furnace cooled to 450 F, then air cooled to room temperature.

The room-temperature physical properties of the forging were then as follows:

Tangential test specimens	Yield strength 0.2 per cent plastic deformation, lb per sq in.	Ultimate tensile strength, lb per sq in.	Elongation in 2 in., per cent	Reduction of area, per cent
X-1	106,500	125,500	16	43
X-2	108,000	126,500	17	44
X-3	107,000	126,000	16	41

Seventeen other rotors made of this material have been inspected during the past two years. These rotors had been in operation for periods up to 58,000 hr. For most machines, the operating time was considerably longer than for the previously discussed group of machines. The results of these inspections are given in Table 5. Rotor D, in this table, is TVA Shawnee Unit No. 1 described above. Eleven of the additional rotors had cracks and six had none. The depth of the cracks varied from 0.020 in. in rotor C to 1¼ in. in rotor E. Two machines, E and J, had cracks as far down the rotor as the 900-F zone.

A study of the stresses, operating temperatures, and time before cracking occurred, shows that this material must have a wide scatter in creep-rupture properties. Core specimens were taken from all rotors inspected and creep-rupture tests are being made. Results from these tests also indicate a wide variation in the creep-rupture properties of these rotors.

Results of these tests are shown in Fig. 9. Rupture time is plotted versus a time-temperature parameter. Also on this plot are shown test data obtained from specimens taken from 18-in-diam forgings previously mentioned. These later results were the best available data at the time the subject rotors were designed. Two things are significant from these data. First, there is a wide scatter in the high-temperature properties of this material. Second, the data available at the time these rotors were designed indicated creep-rupture strength considerably higher than that found in subsequent tests of specimens taken from actual rotors.

From one rotor which had operated about 2½ yr, specimens were taken from the hot end and the cold end, both from points of low stresses. Those from the hot end showed about ½ lower

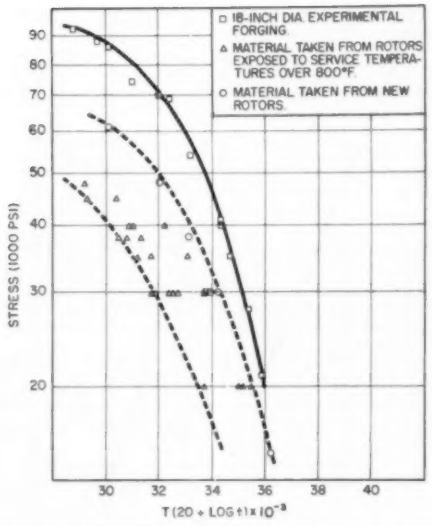

Fig. 9 Smooth-bar rupture strength of Ni-Cr-Mo-V rotor steel

rupture strength than those from the cold end. There appears to be a deterioration of this material with time and temperature at least in the 950 F to 1000 F zone.

Stress Analysis

It is not within the scope of this paper to go into the many aspects of the stress problem where biaxial strain affected by time is involved; however, the paper would be incomplete without some form of stress analysis.

The general approach used to compare the stress levels in the various rotors covered in this paper is given in the Appendix. While this is an oversimplification of the problem, it is believed to result in a valid comparison of stress levels in various rotors.

The stresses in Tables 4 and 5 are first given for the groove wall away from any locking piece; a factor is given for stress and load concentrations at the locking device; finally, a resultant stress at the locking device is shown. The most intangible part of this calculation is the selection of an effective stress-concentration factor. This factor is a function not only of the groove geometry, but also of the notch sensitivity of the rotor material under the particular stress system, stress level, and temperature.

In Figs. 10 and 11, the stresses at the locking device calculated by this method are plotted versus a parameter representing operating temperature and length of service before cracks were found. In most cases, the points fall well within the scatter band of creep-rupture tests made with cored samples from this group of rotors. Significantly, the points falling outside the scatter band all represent the notch-sensitive variety of Cr-Mo-V rotors. For such rotors, it is essential to relate the stress analysis to notch-bar tests run under representative stresses and temperatures.

The development of a high-strength rotor material which is fully notch insensitive under all conditions of stress and temperature is still a goal in the fields of metallurgy and steel-making. Until this goal is achieved, the correction evaluation of the effect of unavoidable stress concentrations on the rupture life remains an important part of the stress analysis.

Solution of the I-P Rotor Problem—Steam Cooling

Three-cylinder triple exhaust machines of both the TVA basic frame and the Weadock modification have an important difference as compared to our two-cylinder reheat machines. Re-

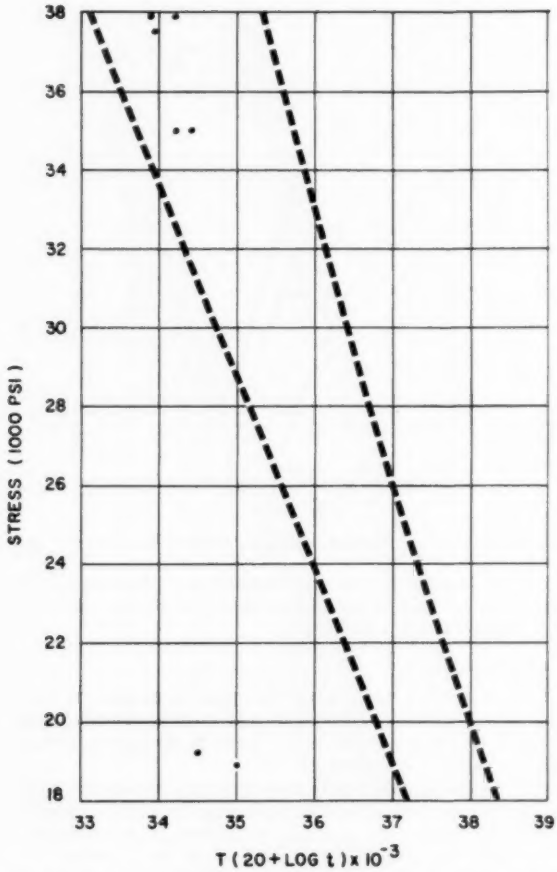

Fig. 10 Relation between stresses in cracked Cr-Mo-V rotors and test-scatter band

ferring to Fig. 1, it will be seen that a portion of the rotor is exposed to the full 1000-F reheat steam between the first stage and dummy. In the two-cylinder machine (see Fig. 12), the 1000-F reheat steam passes through the first stage and decreases in temperature before contacting the rotor. Also, the rotor right up to the first stage is cooled by the gland steam leakage from the h-p exhaust (cold reheat steam.) This reduces the temperature at the point of highest stress on the inlet side of the first row. Stratification of this leakage steam along the tips of stationary blades can effect some cooling for several stages. Also, heat flow in the spindle toward the cooler sections in both directions creates a gradient which gives a lower temperature at the higher stressed points between rows one and two.

Fig. 13 shows the results of a heat-flow calculation giving metal temperatures in a typical two-cylinder i-p rotor using 1000-F reheat steam. Fig. 14 shows the results of similar calculations in the i-p rotor of three-cylinder machines of the Weadock and TVA design. It will be noted that the temperature at the critical point is about 50 F lower in the two cylinder machine. It is noteworthy that no cracking has thus far taken place in any two-cylinder rotor of this design.

A fairly simple modification has been made on three-cylinder machines to accomplish this cooling. Fig. 15 shows this modification. These machines already had cold reheat steam from the h-p exhaust introduced at A to supply the dummy leakage,

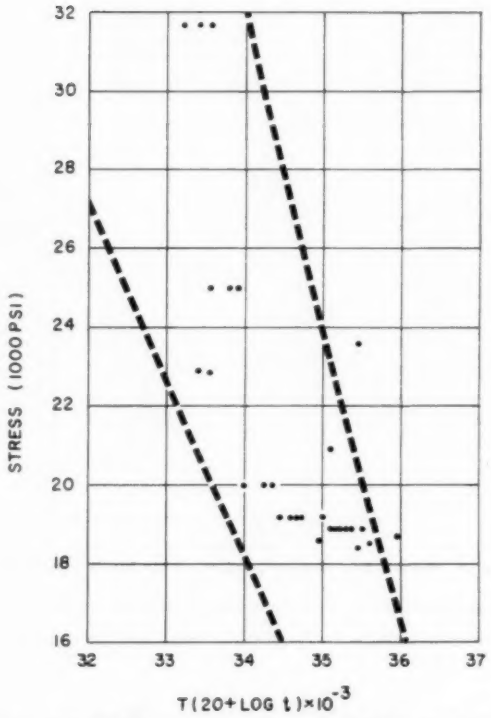

Fig. 11 Relation between stresses in cracked Ni-Cr-Mo-V rotors and test-scatter band

thereby reducing the temperature of the dummy seals, gland seals, and cylinder end wall. The modification consists of:

1 Addition of baffle B.
2 Increase of seal clearance at C.
3 Elimination of seals at D.
4 Enlarging the orifice in cooling-steam supply line.
5 Drilling of holes through base of blades at E.
6 Installation of thermocouples at F, G, H, and I to determine the amount of cooling.

Temperature readings on a machine so modified shows the following:

Thermocouple F:	800 F
Thermocouple G:	850 F
Thermocouple H:	930 F
Thermocouple I:	945 F

Using these readings, metal temperatures were computed in the rotor. These are shown in Fig. 16. By comparing with Fig. 14, it will be noted that the temperature at critical points is reduced about 50 F.

Stress Reduction

In addition to cooling, several modifications were made to reduce the stress. These include:

1 The replacement of several critical rows with lighter blades made of higher-strength material.
2 Alteration of blade roots to reduce weight.
3 Omission of closing blade in critical rows.
4 Alteration of locking pieces to reduce weight.
5 Increase of groove fillets and improvement of groove-wall finish to reduce stress concentration.

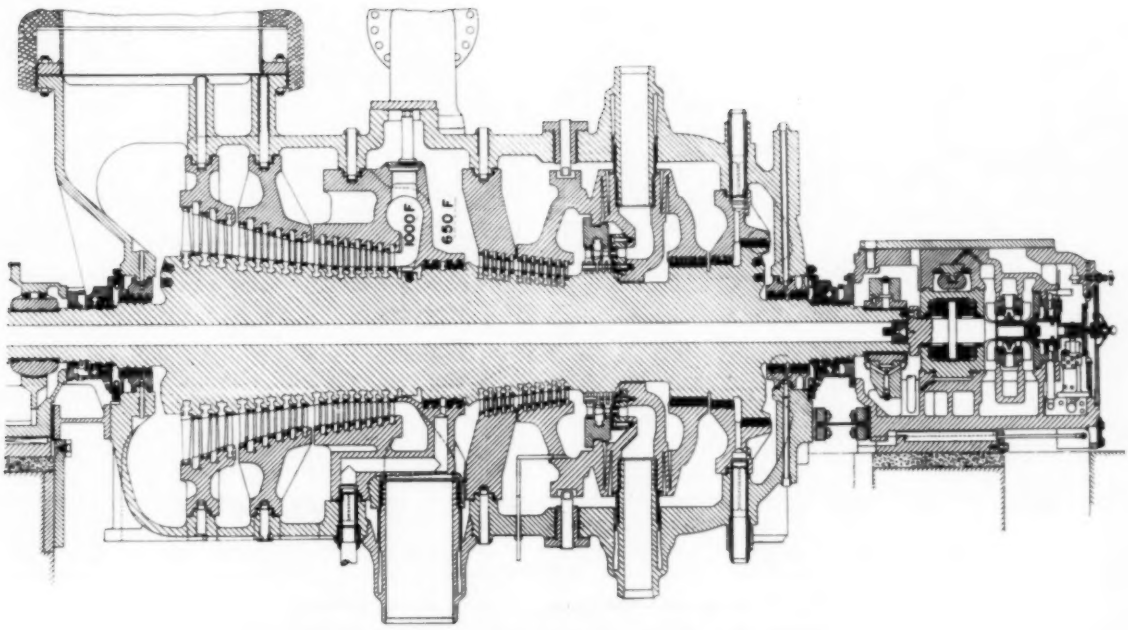

Fig. 12 Cross section of h-p—i-p element of 2-cyl turbine

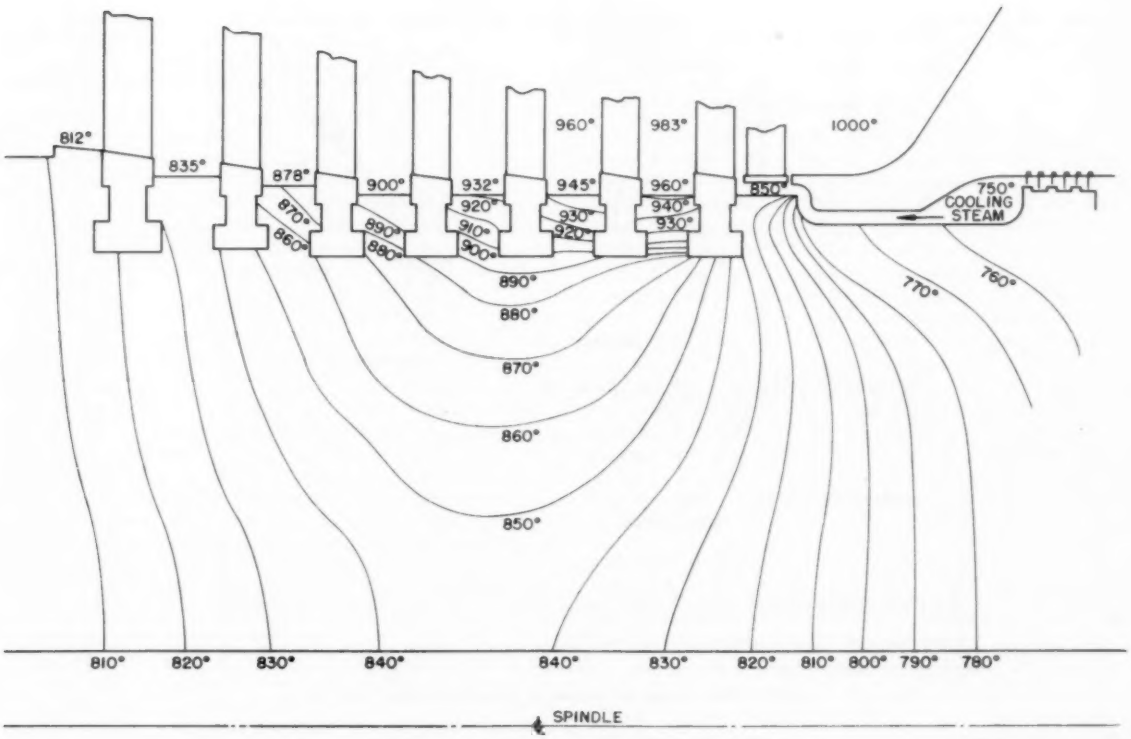

Fig. 13 Temperature distribution in h-p—i-p rotor of 2-cyl turbine

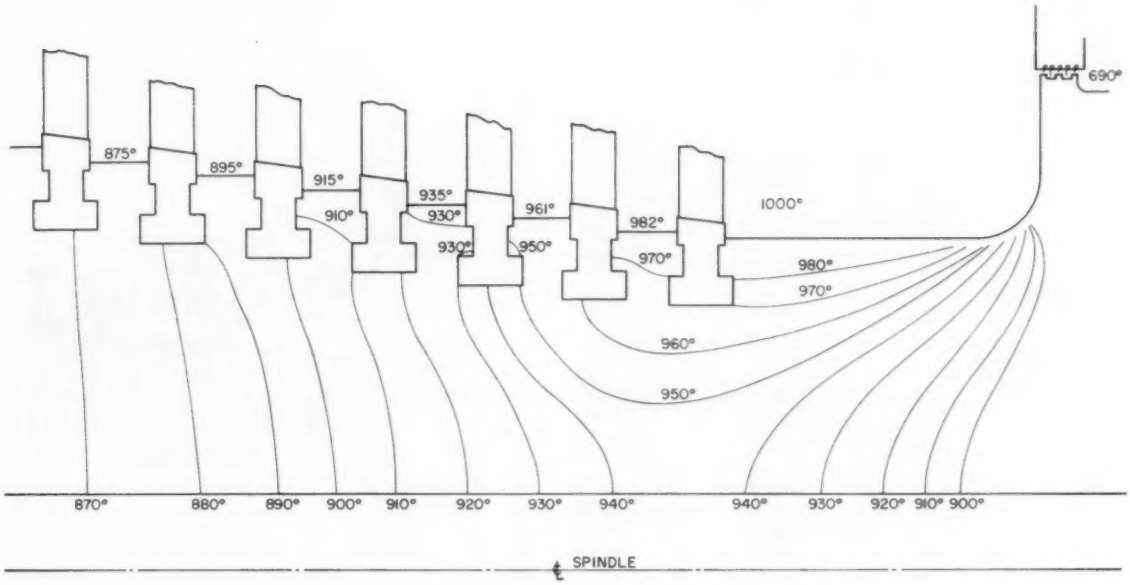

Fig. 14 Temperature distribution in i-p rotor of 3-cyl turbine

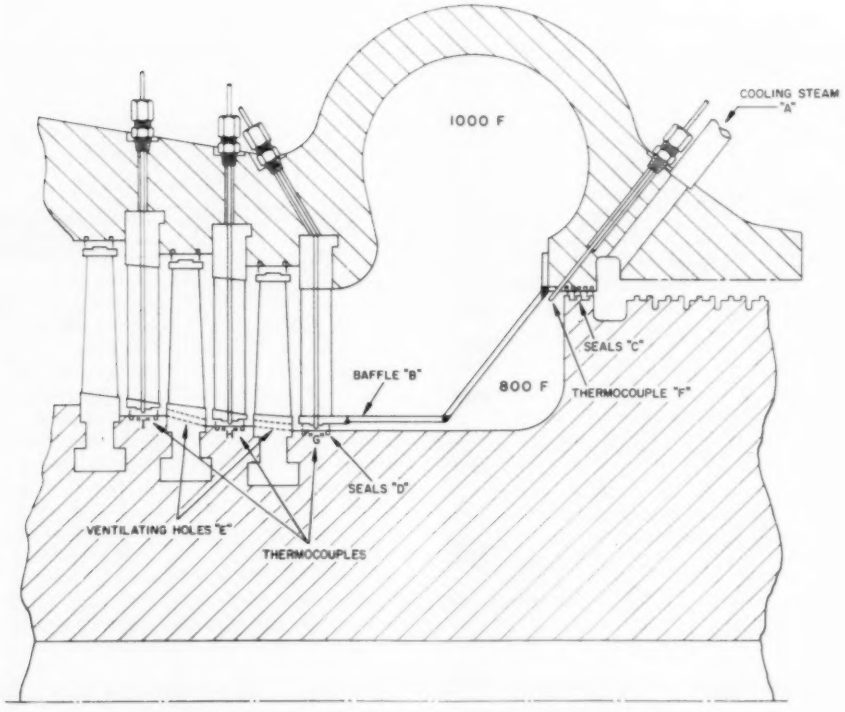

Fig. 15 Modification for cooling of i-p rotor on 3-cyl turbine

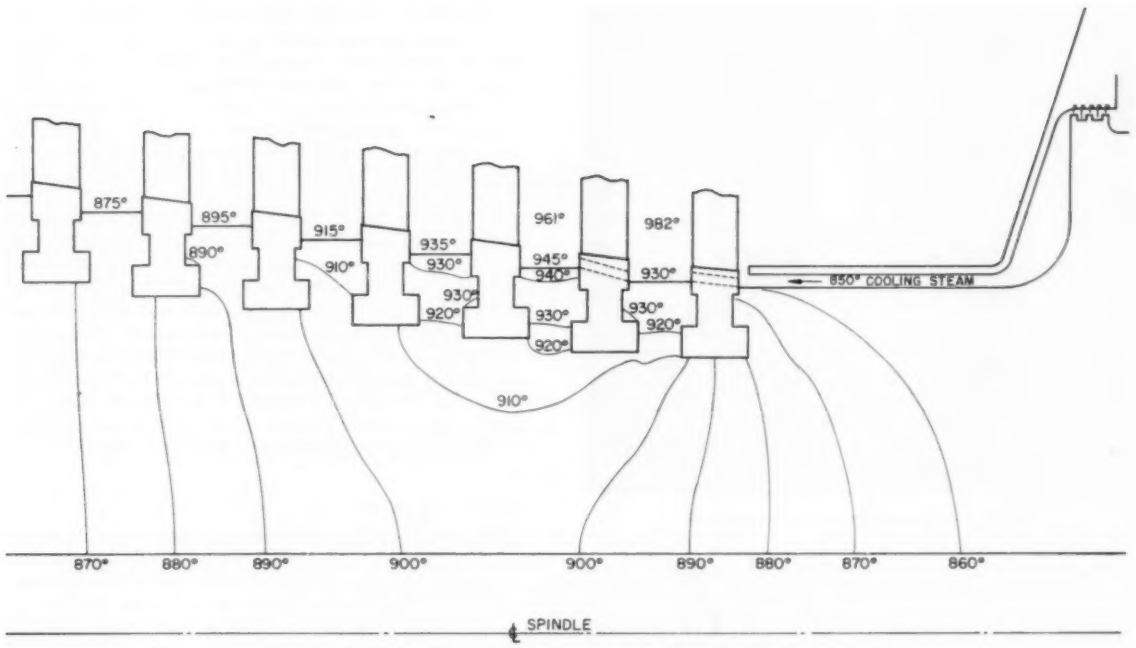

Fig. 16 Temperature distribution in i-p rotor of modified 3-cyl turbine

6 Addition of a fillet in the bottom of the serration in entering slots to reduce stress concentration.

Operating Experience With Modified I-P Rotors

Machine C (Table 4) was modified in January, 1956. This was the first machine modified and the control of cooling steam and measurement of temperature at points F, G, H, and I (see Fig. 15) had not been perfected. Some cooling during the subsequent period of operation was evident from the temperature readings at F. However, the more indicative reading at G was lost after a brief period of operation because of a defective thermocouple connection. Prior to the loss of the thermocouple reading, there was an indication that the cooling was only about 25 F. The stress had been markedly reduced at the two points of cracking by omission of blades in each row at the entering-slot locations. This machine was inspected again in August, 1957, after 18 months of additional operation at full-reheat temperature and with the stress reduction and somewhat indeterminate cooling described above. At the identical locations of cracks found previously, there were again faint traces of cracks each about $^3/_8$ in. long. They were removed by local grinding about 0.025 in. deep. After apparently removing one of these cracks by grinding, a trace was still found after etching. These cracks are very hard to find because of the presence of a hard oxide inside of them. It is difficult to get any of the penetrant oils to penetrate this oxide. It is, therefore, not certain that the cracks were completely removed at the time of modification in January, 1956. Therefore, no specific conclusion is possible on this machine.

Another machine (P in Table 5) was modified in May, 1956. The cooling and temperature-measuring features on this machine were made with the benefit of the experience gained on the earlier turbines and the results were more effective. Most of the stress-reducing features were included. Full-reheat temperature operation was restored at that time. Another inspection was made in August, 1957, after 15 months of additional operation. There was no further cracking of this rotor. Apparently, the combination of stress reducing at the locking slot and the cooling was effective in solving the problem on this rotor.

Material Used on New Machines

On new machines, we are restricting the use of the nickel-chromium-molybdenum-vanadium steel to rotors where the metal temperature is 900 F or less and have reduced the allowable stress in the temperature bracket from 800 F to 900 F. For rotors with metal temperatures over 900 F, we are using the chromium-molybdenum-vanadium steel with the revised heat treatment. Research work is now in progress to determine the optimum heat treatment. There is already some evidence that the notch sensitivity can be further reduced with an additional modification of heat treatment, but with some reduction in room-temperature yield strength. This, of course, would affect the design of the lower temperature zones of such rotors. All new designs are now being worked out on the basis of a minimum-room-temperature yield strength of 80,000 psi instead of the 95,000 psi now specified. We are therefore prepared, on most machines, to change to a lower room-temperature yield strength should this make it possible to produce a forging with better high-temperature properties.

Design Improvement

We have also changed the design in the high-temperature zones in a manner to further lower the stresses in groove walls. These design changes include the following:

1 Use of more efficient blade fastening.
   (*a*) Double-T circumferential groove.
   (*b*) Fir-tree side-entry groove.

2 Improved entering slot and locking device on circumferential grooves, of either the double-T or single-T type.

Fig. 17 shows three types of fastening. The first is the con-

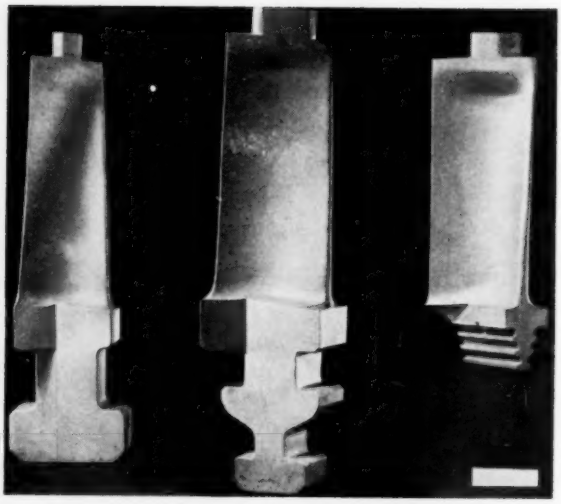

Fig. 17 High-temperature blade fastenings

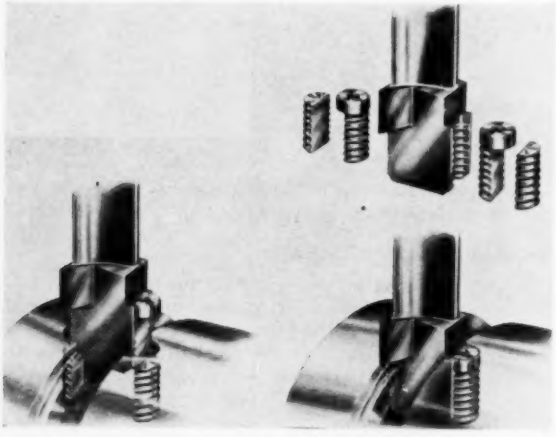

Fig. 18 New blade-locking device

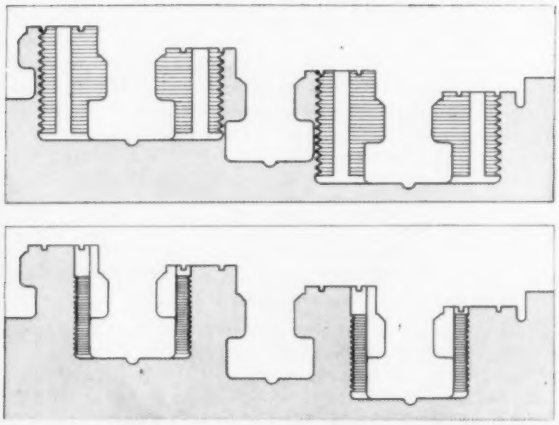

Fig. 19 Contrast of groove-wall slotting using old and new locking device

ventional single "T" circumferential fastening. The second is the double "T" circumferential fastening which will give a moderate reduction in spindle stress for the same spacing of blade rows. The third is the fir-tree side-entry fastening. This gives the lowest rotor stress for a given spacing of blade rows. Its use is limited to critical points in machines because of the greater machining accuracy required and the longer time necessary for production. Also, the stress in the blade root is somewhat higher than in the other types of fastenings.

Fig. 18 shows the new locking device. This device is shown in three stages of assembly. The two pairs of half-round pieces are made in jig fixtures to assure accuracy of matching of serrations between the parts. The closing blade of a row is inserted radially with the shorter serrated pieces in the rotor notch and the longer serrated pieces in the blade-root notch. The projection at the top of each piece in the blade root allows the assembly to be brought into exact position for rotating the parts and closing the lock. Fig. 19 shows the contrast of groove-wall slotting for the old and the new locking device. It is believed that the maximum stress at the locking device is reduced by $^1/_3$ by use of this device.

Conclusion

The nickel-chromium-molybdenum-vanadium steel has a wide scatter in creep-rupture strength above 900 F and in some cases may undergo metallurgical changes above 950 F. Modifications employing a combination of cooling and reduction of stress appear to have been effective in protecting rotors where operating metal temperatures were over 900 F. This material is no longer used for designs in which metal temperatures in excess of 900 F are expected.

The chromium-molybdenum-vanadium steel using the earlier heat treatment with an austenitizing temperature of 1850 F is particularly notch sensitive. Cooling and reduction of stress concentration are important factors in raising the margin of safety of rotors using this material and heat treatment.

The chromium-molybdenum-vanadium steel using the later heat treatment with an austenitizing temperature of 1750 F is a much improved material with respect to notch sensitivity at elevated temperature.

Greatly accelerated development studies have led to an improvement in blade fastenings, locking devices, and the application of cooling to critical zones resulting in lower stresses and better use of available materials.

Acknowledgments

It will be appreciated that the many experiments, evaluations, and design considerations involved in this report required the work of many persons. Engineers and technicians of the Steam Division, the Westinghouse Research Laboratories, and Materials Engineering Department contributed in important ways. The co-operation of our forging suppliers and the operators of the power plants should not be overlooked. The appendix was prepared by D. D. Rosard of the Large Turbine Department.

References

1 N. L. Mochel, R. E. Peterson, J. D. Conrad, and D. W. Gunther, "Large Rotor Forgings for Turbines and Generators," TRANS. ASME, vol. 78, 1956, pp. 1585–1601.

2 F. R. Larson and James Miller, "A Time-Temperature Relationship for Rupture and Creep Stresses, TRANS. ASME, vol. 74, 1952, pp. 765–775.

3 R. W. Bailey, "Utilization of Creep-Test Data on Engineering Design," *Proceedings of The Institution of Mechanical Engineers*, vol. 131, 1935, pp. 131–254.

4 B. G. Neal, "The Plastic Methods of Structural Analysis," John Wiley & Sons, Inc., New York, N. Y., 1956, pp. 217–223.

5 D. C. Drucker "The Effect of Shear on the Plastic Bending of

Beams," *Journal of Applied Mechanics*, vol. 23, TRANS. ASME, vol. 78, 1956, pp. 509–514.

6 P. G. Hodge, Jr., "Interaction Curves for Shear and Bending of Plastic Beams," *Journal of Applied Mechanics*, vol. 24, TRANS. ASME, vol. 79, 1957, pp. 453–456.

APPENDIX

The groove-wall stresses are calculated by consideration of the various possible modes of failure. Along the planes of highest stress, the loading is generally such that tension, bending, and shear are acting simultaneously, such as, on planes AA and BB in Fig. 20.

The stress analysis is made by considering a stress-strain relation of the form $\epsilon = B\sigma^n$, where ϵ is the strain at a given time, B is a constant dependent on the material properties and temperature, σ is the tensile stress, and n is an exponent which again depends on material and temperature. The differences in stress distribution for the elastic, plastic, and creep cases are illustrated in Fig. 21.

For temperatures below the creep range and for stresses below the elastic limit, n is equal to 1, and the analysis reduces to the familiar elastic-stress calculation.

For an idealized stress-strain diagram above the elastic range where the stress remains constant as the strain increases (no strain hardening), n becomes infinite, and the analysis reduces to a plastic-stress analysis (or limit design).

At high temperatures, under creep conditions, the relation between strain-rate and stress is approximated by a power function where the exponent n normally varies between 2 and 10. A low value of n indicates a tendency to brittleness, a high value of n a tendency to ductility. The maximum stress in a beam subjected to tension and bending can be calculated from the following relation

$$\sigma_n = C_n(\sigma_d + \sigma_b)$$

where σ_n is the maximum stress on the beam, σ_d is the tension stress, σ_b is the bending stress, and C_n is the coefficient dependent on n and the ratio of σ_d to σ_b, as shown on Fig. 22.

No exact theory on the effect of superposition of shear to tension and bending stresses on creep-rupture life has yet been developed. Several approximations have been made for the plastic case [4, 5, and 6]. In this paper, to include the effect of shear, an equivalent combined stress is calculated from the empirical relation

$$\sigma_e = (\sigma_n^2 + 3\tau^2)^{1/2}$$

where τ is the average shear stress in the plane in question.

This relation has been verified by a number of tests, and is expected to give a good approximation to the rupture life when compared to creep-rupture results on standard test specimens.

The locking-device construction is such that the centrifugal load of the closing blade is transferred to the rotor by edge loading along serrations cut parallel to the axis of the rotor as shown on Fig. 4. This load was found by photoelastic tests to decay in about three blade pitches. The load concentration at the edge of the lockslot can then be calculated.

The effect of stress concentration at the groove fillet is dependent on the notch sensitivity of the material. For every ductile material, this stress concentration would not affect the rupture life. For brittle materials, this stress concentration can reduce the rupture life appreciably.

A continuing study is being carried out to determine the effect of stress concentrations on creep-rupture life under complex loading for materials with various values of notch sensitivity.

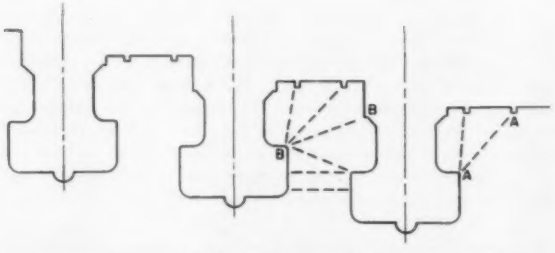

Fig. 20 Location of calculated stress planes in rotor grooves

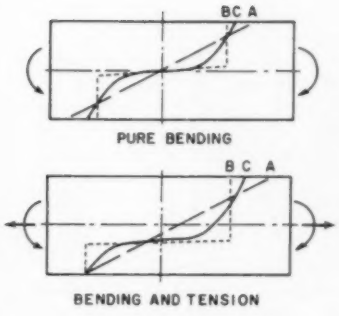

Fig. 21 Comparison of elastic, plastic, and creep stresses

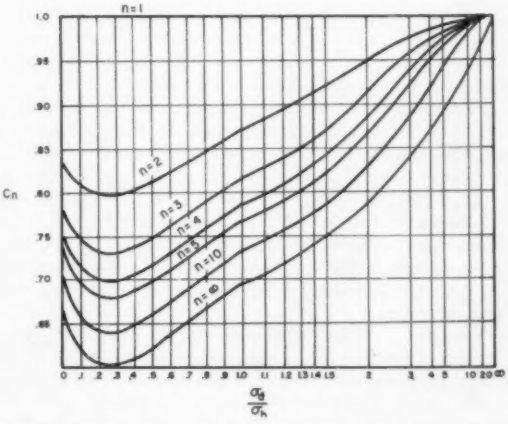

Fig. 22 Ratio of creep stress to elastic stress for various values of n

Discussion

T. G. Foulkes.[8] This paper presents a straightforward story of difficulties observed in service and steps taken to correct them. We have here a demonstration of the most reliable research possible—full scale research. It is unlikely that research on small laboratory processed specimens would have resulted in the metallurgical decisions arrived at in this instance. Here is evidence of how close design engineering comes to the ultimate of the range of

[8] Metallurgical Engineer, Bethlehem Steel Company, Bethlehem, Penna.

properties of the material and how design improvement results in performance improvement.

The decision to reduce the final austenitizing temperature from 1850 F to 1750 F is gratifying to the forging industry. It means less distortion hazard, less scaling tendency, greater refinement of microstructure. The decision to lower the yield strength requirement is also gratifying to the forging industry. This permits higher tempering temperatures with the accompanying trend toward less residual stress and greater uniformity of mechanical properties.

A. W. Rankin.[6] The power-generation industry should, and I am sure does, appreciate the frankness and directness with which the authors have discussed their operating experiences with high-temperature steam turbine rotors. The construction of precision equipment of this size presents many unique challenges, some of which cannot be fully appreciated until they are bared by the ultimate test of relatively long-time operation. More specifically, in high-speed, high-temperature rotors, we must withstand high operating stresses for life periods unmatched in any similar high-temperature equipment, within a reliability which will permit almost no margin of error because of the serious consequences of a major rotor failure, and we must do this with the materials which the industry can produce in the required sizes and within the limitations of available technical knowledge. Over all this hangs the specter of "adequate" ductility, whatever adequate is, and the knowledge that laboratory tests of sufficient life periods are of little avail since at their conclusion one has either committed many tons of material to production and operation, or has superseded such material with stronger and more complex alloys. With these thoughts in mind, the forthright treatment of any operating experiences should be appreciated fully since it aids both manufacturers and operators to meet the challenges which will come with this industry's expected future growth and Brobdingnagian units.

As pointed out in our own report on the turbine wheel fracture at Tanners Creek,[7] we were also concerned about the rupture ductility of the chromium-molybdenum-vanadium alloy when austenitized from 1850 F, and early in 1953 we introduced the 1750 F austenitizing treatment. Following the Tanners Creek fracture, we also introduced the practice of making high-temperature rupture tests for estimates of ductility through parameter evaluations on every production turbine rotor, and specific ductility levels must be obtained before such rotors are released for complete processing. By this means we have ensured that the superior rupture ductility obtainable with the 1750-F treatment will be maintained in continued routine production.

The scatter which seems inherent in long-time high-temperature strength will be bothersome to designers until high-temperature rupture is itself better understood. We have combated this for many years by taking rupture specimens from every high-temperature rotor in manufacture before release for final machining. In addition, we have attempted to obtain relatively complete data on new or modified alloys before committing them to production use, although sometimes it is difficult to determine what "complete" is, and in rotor design our most important specimens are taken from full-size rotors since only in such sizes can one be certain that the correct cooling rates have been obtained. As a matter of interest, before we introduced the chromium-molybdenum-vanadium alloy, we had three full-diameter forgings available for test specimens, these three forgings being: (1) Molybdenum-vanadium; (2) nickel-molybdenum-vanadium; and (3) chromium-molybdenum-vanadium. In addition, in our current Rotor Development Program, we are also utilizing full-size rotor forgings, of new compositions and/or heat treatments, to obtain our evaluation test specimens.

The maintenance of an adequate safety factor for high-temperature design stresses is of considerable difficulty, particularly in this field of expected long life in which the designer may not know for several years that his safety factors are not adequate to withstand design, manufacturing, and operating misadventures. One requires for this not only a competent stress-analysis group with full studies on each machine, but also a safety-factor policy that recognizes human limitations in visualizing all the points of major stresses. In our own case, our Tanners Creek incident caused us to recognize the stress intensifications which could result at bucket gates in wheels, and early in 1953 we introduced specific allowable stresses for these important points, and also introduced new and lower-stress designs for the closing pieces at these points.

In conclusion, the writer expresses his appreciation to the authors for their complete discussion of these operating experiences, and his sympathy on the concatenation of events which resulted in these failures. Through these discussions of our mutual problems, we will all be better able to provide the power-generation equipment needed by the country in this disturbed period.

Authors' Closure

The authors appreciate the gracious comments of Messrs. Foulkes and Rankin, especially since each is intimately associated with the problems of supply and application of rotors for the exacting service involved in modern steam turbines.

Developments must go hand in hand with our ability to obtain satisfactory alloy forgings. Only by advances in the field of metallurgy can we hope to secure those economic gains promised by increasing turbine unit size and increasing operating steam temperature. As manufacturers, we must, of course, assess our requirements realistically and from that point forward must look to the steel supplier to co-operate closely in developing compositions and treatments which are adequate for the purpose intended.

The i-p—l-p rotor, largely dealt with in this paper, presents an unusual problem, in a large mass of steel, in that we desire a forging with excellent high-temperature properties at one end along with very high strength at low operating temperature at the other end. As is so often the case in engineering design, this situation leads us into a compromise with the optimum solution available for either end condition if it were considered alone.

That we encountered difficulty here is a matter of considerable disappointment. We extended the Ni-Cr-Mo-V alloy application to operating temperatures for which subsequent experience shows it unsuitable.

Fortunately, the resulting groove wall cracks progressed slowly, were detected, and corrective action was taken. In contrast, the only alternative material available at the time was the Cr-Mo-V alloy with the early 1850-F heat-treatment, which has proved susceptible to rapidly propagating fractures with the possibility of more serious damage. In retrospect, it appears better to have overstepped the limitations of the nickel alloy in a number of rotors than to have more widely applied the notch-sensitive variety of the Cr-Mo-V steel.

[6] Manager, Turbine Structural Engineering, Large Steam Turbine-Generator Department, General Electric Co., Schenectady, N. Y. Mem. ASME.

[7] "Report of the Investigation of the Turbine Wheel Fracture at Tanners Creek," by A. W. Rankin and B. R. Seguin, TRANS. ASME, vol. 78, 1956, pp. 1527–1546.

The Propagation of Cracks and the Energy of Elastic Deformation

By H. F. BUECKNER,[1] SCHENECTADY, N. Y.

The Griffith-model of brittle fracture of elastic solids and the model by Irwin and Orowan for the brittle fracture of elastic-plastic solids predict the propagation of cracks on the basis of energy supplied by the work of externally impressed forces and by the change of strain energy. Previous discussions have neglected the three-dimensional viewpoint and the body forces. Since the Irwin method of fracture-strength analysis has become of increased interest, especially with respect to rotor fracture, a general analysis of energy supply is presented. The analysis uses Clapeyron's theorem and Betti's reciprocal theorem. One of the results is that the energy supplied for crack extension equals the strain energy of the difference of the two stress fields before and after crack extension.

Introduction

THE following considerations deal with the change of strain energy and with the work of impressed forces during crack extension. It is assumed that the strains are small and that stresses and strains are correlated by Hooke's law. The following models of crack propagation are assumed:

The Griffith-Model. It has been demonstrated by Griffith (1)[2] that the onset of crack propagation in brittle material like glass can be explained by considering an elastic body with two forms of potential energy. These are the strain energy and the surface energy, the latter one stored with constant density H along the surface of the body. As an example we consider, Fig. 1, a plate of uniform thickness h and of rectangular shape with two opposite sides subject to a constant tension σ. Let there be a crack of length $2c$ (blacked area) parallel to the loaded sides. Let us assume that the crack extends to length $2c'$ while the two loaded sides are kept by fixed grips. The external forces will do no work. The extension creates new surfaces with $4(c' - c)h$ as gain in area. This requires the surface energy to increase by $4(c' - c)hH$. The strain energy U decreases to an amount U', and

$$U - U' \geq 4(c' - c)h \cdot H \quad \ldots\ldots [1]$$

is a necessary condition in order to make the crack extension possible. The difference between the two sides of Inequality [1] will appear as kinetic energy at a real crack propagation. In the limit $c' \to c$ a certain strain-energy release rate

$$U^* = \lim_{c' \to c} \frac{U - U'}{2(c' - c)h} \quad \ldots\ldots [2]$$

is obtained. Condition [1] implies

$$U^* \geq 2H \quad \ldots\ldots [3]$$

Assuming a virtual crack extension for any pair of parameters σ, c Griffith found

$$U^* = \pi c \sigma^2 / E \qquad E = \text{Young's modulus} \quad \ldots\ldots [4]$$

which holds for a state of plane stress and for c small against the dimensions of the plate. For constant c and sufficiently small values of σ the release rate U^* is below $2H$. There will be no crack propagation. For a critical value of σ, namely

$$\sigma^* = (2HE/\pi c)^{1/2} \quad \ldots\ldots [5]$$

the equality sign in [3] is reached. At this value crack propagation can start and, indeed, this was observed by Griffith.

The Model of Irwin and Orowan for the Brittle Fracture of Mild Steel. The experiment of Fig. 1 can be repeated with mild steel rather than glass as material of the plate. There is experimental evidence to support the existence of a critical stress σ^* and even the type of the law [5], (9). However, H has to be substituted by another quantity, say $^1/_2 G_c$, which is much larger than H, in some cases by a factor of 1000. Clearly the surface energy plays no role whatsoever. Due to Orowan (2, 3) the phenomenon can be explained by plastic deformation of a certain surface layer along the crack. In the realm of elasticity the stresses become infinitely large at the root of the crack. In reality a zone 1 of contained plastic deformation will appear at the root (see shaded area of Fig. 2). As the crack propagates zone 1 will be unloaded but some permanent plastic deformation will be left. Another zone 2 of plastic deformation will be set up, thereafter partially relieved, and so forth. Thus a surface layer of permanent plastic deformation is generated along the crack. This process is dis-

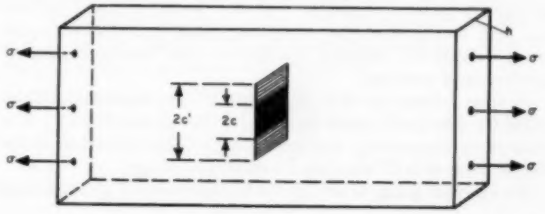

Fig. 1

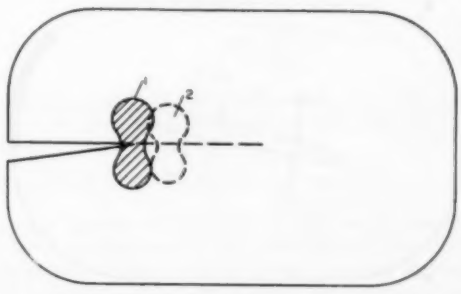

Fig. 2

[1] Engineering Mathematician, Large Steam Turbine and Generator Department, General Electric Company.

[2] Numbers in parentheses refer to the Bibliography at the end of the paper.

Contributed by the Power Division and presented at the Annual Meeting, New York, N. Y., December 1–6, 1957, of THE AMERICAN SOCIETY OF MECHANICAL ENGINEERS.

NOTE: Statements and opinions advanced in papers are to be understood as individual expressions of their authors and not those of the Society. Manuscript received at ASME Headquarters, September 5, 1957. Paper No. 57—A-189.

sipative as mechanical energy is transformed into heat. If the layer is thin and of constant thickness then one may calculate the dissipated energy in proportion to the gain in crack surface. This makes it plausible why Formula [5] would stay valid with a dissipation density G_e substituted for $2H$. In this way the following model for the brittle fracture of mild steel is obtained:

The rupturing body is considered to be elastic; energy dissipation goes with the creation of new crack surfaces, and it is proportional to the area gained times a certain density factor $^1/_2G_e$.

An extensive application of this model as well as theoretical results about the release rate of strain energy are due to Irwin (4 to 8). The model is simple, and it cannot be expected that it will explain all phenomena which occur in fractures. Even so it will be useful in order to separate one cause of crack propagation from others. Regardless of what the area of applicability of the model will turn out to be, it is useful to analyze the changes of elastic strain energy for virtual crack extension. This is the objective of the following investigation. Dynamical effects will not be considered. The results are applicable to the onset of crack propagation.

Release of Energy in General

With respect to Fig. 3 we consider an elastic body V with a crack inside. The two crack surfaces are C_1, C_2. The other part of the surface of the body is denoted by $O = O_1 + O_2$. Here O_1 may be subject to tractions T (T is a vector) while the displacements are prescribed along O_2. We also admit a distribution of body forces given by a vector field X. With respect to a cartesian co-ordinate system (x_1, x_2, x_3) we introduce the displacement vector $u = (u_1, u_2, u_3)$ and the following components of the strain tensor

$$e_{ik} = \frac{1}{2}\left(\frac{\partial u_i}{\partial x_k} + \frac{\partial u_k}{\partial x_i}\right) \quad \ldots\ldots\ldots\ldots [6]$$

The components of the stress tensor may be denoted by σ_{ik}. It is assumed that C_1, C_2 are separated by the displacements and that they are free from tractions.

Let us consider a virtual crack extension which adds a new surface C_1' to C_1 and a new surface C_2' to C_2 (dotted lines in Fig. 3). With body forces and surface conditions unchanged, a new displacement vector u' together with new strains e_{ik}' and stresses σ_{ik}' will characterize the state that goes with the extended crack. Again it is assumed that the crack surfaces are separated and free from tractions.

In what follows the state of stresses σ_{ik} and strains e_{ik} will be called the first state; its strain energy will be denoted by U. The state of the stresses σ_{ik}' and strains e_{ik}' will be referred to as the second state with U' standing for its strain energy.

We are now going to set up the virtual work of all impressed forces due to crack extension. The virtual work of the externally impressed forces is

$$W_a = \iint_{O_1} T(u' - u)do + \iiint_V X(u' - u)dV$$

do = surface element, dV = volume element..... [7]

The virtual work of the internal forces is

$$W_i = U - U' \quad \ldots\ldots\ldots\ldots\ldots [8]$$

The total virtual work is $W = W_a + W_i$, and the condition of crack propagation becomes

$$W = W_a + W_i > G_c \cdot |C_1'|; \quad |C_1'| = \text{area of } C_1' \ldots. [9]$$

If Equation [9] holds for at least one virtual crack extension then the crack C_1, C_2 cannot be stable and crack extension is bound to follow.

The following considerations are not restricted to infinitely small crack extensions which are attributed to the principle of virtual work. The strain energies U, U' are explicitly

$$U = \frac{1}{2} \cdot \iiint_V \sum_{i,k} \sigma_{ik} e_{ik} \cdot dV;$$

$$U' = \frac{1}{2} \cdot \iiint_V \sum_{i,k=1}^{3} \sigma_{ik}' e_{ik}' \cdot dV \ldots\ldots [10]$$

It is also useful to introduce the mixed energy

$$U_m = \frac{1}{2} \cdot \iiint_V \sum_{i,k} \sigma_{ik}' \cdot e_{ik} \cdot dV$$

$$= \frac{1}{2} \cdot \iiint_V \sum_{i,k} \sigma_{ik} \cdot e_{ik}' \cdot dV \ldots\ldots [11]$$

The two integrals in Equation [11] are equal to one another as a consequence of Hooke's law. From Equations [10] and [11] it follows

$$-W_i = U' - U$$

$$= \frac{1}{2} \cdot \iiint \sum_{i,k} (\sigma_{ik}' + \sigma_{ik})(e_{ik}' - e_{ik})dV \ldots\ldots [12]$$

In addition to the first and second states of stress and strain two more states will be introduced. These are the sum-state with the stresses $\sigma_{ik}' + \sigma_{ik}$ and strains $e_{ik}' + e_{ik}$ and the difference-state with the stresses $\sigma_{ik}' - \sigma_{ik}$ and strains $e_{ik}' - e_{ik}$. The displacement vectors are $v_s = u + u'$ and $v_d = u' - u$, respectively.

From now on the first state will be reinterpreted as a state of the body V with the extended crack. The stresses of the first state result in certain tractions T^* along C_1',C_2' (see Fig. 3). Vice versa, the first state is determined by the condition on O_2, by the distribution of the tractions T, T^* and by the body forces X, applied to the body V with the extended crack. It is to be noted that the vector T^* preserves its length but jumps into the opposite direction as we go from a point of C_1' to the opposite point of C_2'. The displacement vector u remains unchanged.

With the first state reinterpreted, the sum-state and the difference-state find a corresponding interpretation. The sum-state is the response to the body forces $2X$, to the surface tractions $2T$ on O_1, zero-tractions on C_1, C_2, and tractions T^* along C_1', C_2'; along O_2 the displacements are prescribed. The difference-state is the response to no body forces, no tractions on

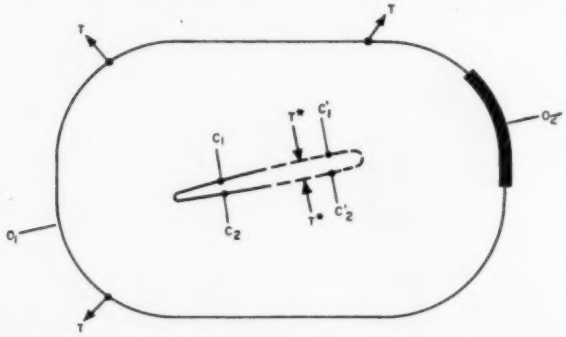

Fig. 3

O_1, C_1, C_2, tractions $-T^*$ along C_1', C_2', and no displacements along O_2.

The integral in Equation [12] is the mixed energy of the sum-state and of the difference state. According to Betti's theorem (10) the mixed energy equals one-half of the work done by the external forces (impressed and reactionary) of one state through the displacements of the other, no matter from which state the forces are taken. We decide to take the forces from the sum-state and the displacements from the difference-state. There is no contribution from the reactionary forces of the sum-state along O_2, since they go with zero-displacements of the difference-state; the externally impressed forces of the sum-state give rise to the work

$$U' - U = \iiint_V X v_d \cdot dV + \iint_{O_1} T \cdot v_d \cdot do + \frac{1}{2} \cdot \iint_{C_1' + C_2'} T^* \cdot v_d \cdot do \quad [13]$$

whence in combination with Equations [7] and [8]

$$W = W_e + W_i = -\frac{1}{2} \cdot \iint_{C_1' + C_2'} T^* \cdot v_d \cdot do \quad [14]$$

On the other hand the integral expression on the right-hand side equals the strain energy U_d of the difference-state

$$U_d = \frac{1}{2} \cdot \iiint_V \sum_{i,k} (\sigma_{ik}' - \sigma_{ik})(e_{ik}' - e_{ik}) dV = -\frac{1}{2} \cdot \iint_{C_1' + C_2'} v_d \cdot T^* do \quad [15]$$

This follows from Clapeyron's theorem (10), according to which the strain-energy equals one half of the work done by the externally impressed forces through the displacements. The energy U_d is always non-negative. In general the same is not true for either W_e or W_i. Relations [14] and [15] are useful for a practical discussion of the Condition [9].

Since the strain energy of the difference-state is all that counts for crack propagation, it does not matter if a certain reference state of stress and strain is subtracted from both the first and the second state. As reference state one may take the state of the body V *without any crack* subject to the constraints and externally impressed forces of the first state. Subtraction of this special reference state from the first and second state will lead us to the modified first and the modified second state.

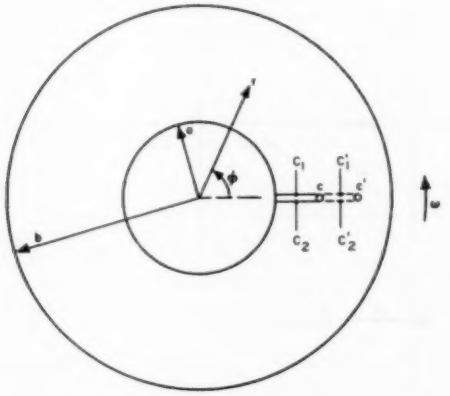

Fig. 4

The reference state gives rise to tractions T_0 along C_1, C_1', C_2, C_2'. Each of the modified states is the response to these conditions: No body forces, no tractions along O_1, no displacements along O_2, and traction $-T_0$ along its crack surfaces. This makes it clear that the crack extension depends on T_0 only. Once T_0 is known along $C_1 + C_1'$, $C_2 + C_2'$ one may forget everything about the body forces X and the tractions T.

As an example we consider the state of plane strain of a rotor with a borehole, as shown in Fig. 4. Let ω be the angular velocity, a the inner and b the outer radius. With respect to polar co-ordinates r, ϕ a radial crack C_1, C_2 along a radial interval $a \leq r \leq c$ and a crack extension C_1', C_2' along the interval $c \leq r \leq c'$ of the same direction is assumed. No surface tractions and no constraints are prescribed.

As is well known the tangential stress of the uncracked rotor is

$$\sigma_\phi = \frac{3+\nu}{8} \rho\omega^2 \cdot \left(b^2 + a^2 + \frac{a^2 b^2}{r^2} - \frac{1+3\nu}{3+\nu} \cdot r^2 \right) = F(r)$$

ν = Poisson's ratio
ρ = mass density [16]

The shear stress $\tau_{r\phi}$ vanishes.

The two modified states are determined by the following impressed forces: No body forces; no tractions along the surfaces $r = a$, $r = b$; normal tractions along the cracks as given by $\sigma_\phi = -F(r)$.

Therefore the difference state and its strain energy are entirely determined by the function $F(r)$ along the interval $a \leq r \leq c'$. Especially for very short cracks, that is $c' - a \ll a$ it is the value $F(a)$ which together with c, c' determines U_d with sufficiently good approximation.

Crack Extension Under Constant Load and Under Fixed Grips

We consider the special case where O_2 vanishes; $O_1 = O$ represents the full surface of the body V without cracks. This situation will be referred to as the case of constant load. The integral of Equation [12] will now be transformed by means of Betti's theorem in the other way; i.e., we will calculate the work done by the forces of the difference-state through the displacements of the sum-state. This results in

$$U' - U = \iint_{C_1' + C_2'} -\frac{1}{2} T^* \cdot v_s \cdot do \quad [17]$$

But

$$\iint_{C_1' + C_2'} T^* \cdot u \cdot do = 0 \quad \text{and} \quad \iint_{C_1' + C_2'} T^* \cdot v_d \cdot do = \iint_{C_1' + C_2'} T^* \cdot v_s \cdot do \quad [18]$$

as u is the same and as T^* differs in direction at opposite points of C_1', C_2'. By comparison of Equations [13], [14], [17], and [18] we find

$$W_e = 2U_d \qquad W_i = U - U' = -U_d \quad [19]$$

This means that the strain energy *increases* as the crack extends. But the virtual work of the externally impressed forces equals twice the increase of strain energy, and the surplus of energy is available for crack propagation. An example of crack propagation under constant load is the rotor of Fig. 4. Another

facet of crack extension under constant load is expressed by the relation

$$\iiint_V \sum_{i,k} \sigma_{ik}(e_{ik}' - e_{ik})dV = 0 \quad \ldots\ldots [20]$$

The difference-state and the first state σ_{ik}, e_{ik} have no mixed energy; they are orthogonal. Relation [20] can be proved by means of Betti's theorem, if the forces are taken from the difference-state and the displacements from the first state. The proof uses Equation [18] and may be left to the reader. A special case of Equation [20] is

$$\iiint_V \sum_{i,k} \sigma_{ik}^{(0)} \cdot (e_{ik}' - e_{ik}^{(0)})dV = 0 \quad \ldots\ldots [21]$$

where $\sigma_{ik}^{(0)}$, $e_{ik}^{(0)}$ characterizes the state of the body without any crack. Hence from Equation [12] and from [21]

$$\left\{\begin{aligned} U' - U_0 &= \frac{1}{2} \cdot \iiint_V \sum_{i,k} (\sigma_{ik}' + \sigma_{ik}^{(0)})\,(e_{ik}' - e_{ik}^{(0)})dV \\ &= \frac{1}{2} \iiint_V \sum_{i,k} (\sigma_{ik}' - \sigma_{ik}^{(0)})(e_{ik}' - e_{ik}^{(0)})dV \\ U_0 &= \frac{1}{2} \iiint_V \sum_{i,k} \sigma_{ik}^{(0)} e_{ik}^{(0)} dV \end{aligned}\right. \quad \ldots\ldots [22]$$

Therefore the difference $U' - U = U_d$ of Equation [19] can be computed as the difference of the strain energies of the modified states $(\sigma_{ik}' - \sigma_{ik}^{(0)})$ and $(\sigma_{ik} - \sigma_{ik}^{(0)})$. This applies especially to the rotor of Fig. 4 which was studied in section 2 by means of the modified states.

Sometimes crack extension is considered under the condition of fixed grips. This means that the first state is defined by the general configuration of Fig. 3. One takes the displacements which this state induces along O_2, and it is required that the second state have the same displacements along O_1 and in addition the prescribed displacements along O_2. In this case the vector v_d of the difference-state vanishes along O_1 and O_2. Again Relations [14] and [15] are valid, but W_a represents the virtual work of the body forces only. If there are *no* body forces, then

$$W = U_d = U - U' \quad \ldots\ldots [23]$$

The strain energy *decreases* as the crack extends. The difference in the strain energies is available for crack propagation. The analog of Equation [20] turns out to be

$$\iiint_V \sum_{i,k} \sigma_{ik}'(e_{ik}' - e_{ik})dV = 0 \quad \ldots\ldots [24]$$

which is a direct consequence of Equations [9], [15], and [23]. Relation [24] says that the mixed energy of the difference-state and of the second state vanishes if no body forces exist.

It is useful to compare the difference-states of crack propagation under constant load and under fixed grips with one another. In both cases we have the same tractions $-T^*$ along C_1', C_2'; there are no tractions along C_1, C_2. In the case of constant load the tractions along O vanish; in the case of fixed grips the displacements along O vanish.

According to the so-called minimum principle of stresses the energy U_d in the case of fixed grips is smaller than the energy of any other stress field where the stresses satisfy the equilibrium conditions and the boundary conditions on the impressed forces. Therefore the strain energy of the difference field of fixed grips is *smaller* than the strain energy of the difference field of constant load.

Yet the difference between the two cases seems to become insignificant for infinitely small crack extensions as can be seen from the one-dimensional model of a spring subject to a tensile force F. The reciprocal spring constant M may characterize a crack. M increases as the crack extends. With $u = MF$ denoting the elongation, the strain energy of the spring is

$$U = uF/2 = MF^2/2 = u^2/2M \quad \ldots\ldots [25]$$

If M increases up to M' as the crack extends one finds

$$U_d = (M' - M)F^2/2 \quad \ldots\ldots [26]$$

for the case of constant load and

$$U_d = (M' - M)\frac{M}{M'}F^2/2 \quad \ldots\ldots [27]$$

for the case of fixed grips. The energy [27] is smaller than the energy [26]. However, the limit

$$\lim_{M' \to M} \frac{U_d}{M' - M} = F^2/2 \quad \ldots\ldots [28]$$

is the same for both cases.

It is to be mentioned that the difference between the two cases has been pointed out by Orowan (2 and 3) in connection with the spring model. He also found the results, Equations [19] and [23], for this special case. The identity of the limits, Equation [28], was observed by Irwin and also conveyed to this writer.

Another class of cases will be discussed in the next section. However, for a study of crack propagation in the large the emphasis should be on the case of constant load.

Irwin's Formula

We consider a state of plane strain of a cylindrical body V, of which Fig. 5 shows a cross-section V^*. Let σ_x, σ_y, τ_{xy} denote the stresses and u, v the displacements in x and y-direction respectively.

The following simplifying assumptions will be made:

1 The cross-section is symmetric with respect to the x-axis.

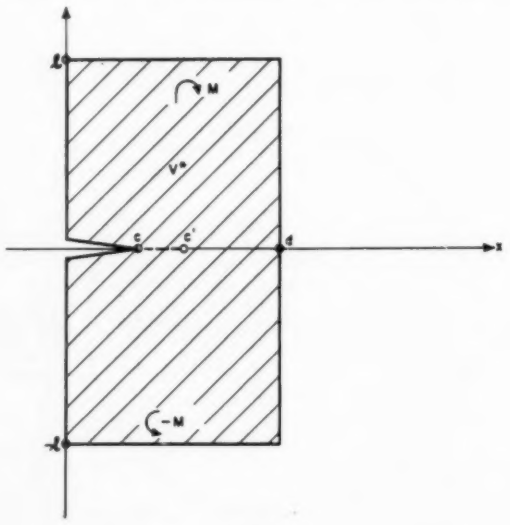

Fig. 5

2 The distribution of load is symmetric with respect to the x-axis.

3 The crack runs along part of the x-axis.

Consequently there will be no shear stress along the x-axis. Fig. 5 shows an example. We have a bar of length $2l$ and of width d. The crack shall run from $x = 0$ to $x = c$; its extension will run from $x = c$ to $x = c'$. The bar is bent by two moments M and $-M$, as indicated in Fig. 5.

Let us consider the case of the crack $0 \leq x \leq c$. In general the stress σ_y for $x > c$, $y = 0$ follows the law

$$\sigma_y = \sigma_y(x, c) = \left[\frac{EG}{(1 - \nu^2)2\pi}\right]^{1/2} \cdot (x - c)^{-1/2} \cdot F_1(x, c); \quad F_1(c, c) = 1 \ldots\ldots [29]$$

where G is a certain constant (introduced by Irwin) and where $F_1(x, c)$ is a continuous function of both x and c. Also the displacement v along the upper side of the crack behaves according to

$$v = v(x, c) = \frac{4(1 - \nu^2)}{E}\left[\frac{E \cdot G}{(1 - \nu^2)2\pi}\right](c - x)^{1/2} \cdot F_2(x, c); \quad F_2(c, c) = 1 \ldots\ldots [30]$$

where F_2 is a continuous function of x and c. Applying Equation [17] for the case of crack extension under constant load we find

$$U(c') - U(c) = \int_c^{c'} \sigma_y(x, c)v(x, c')dx \ldots\ldots [31]$$

where $U(c)$ represents the strain energy per unit thickness of the state with crack length c. With Equations [29] and [30] taken into account we obtain from Equation [31]

$$U(c') - U(c) = \frac{2G}{\pi}\int_c^{c'} (x - c)^{-1/2}(c' - x)^{1/2} \cdot F_1(x, c)F_2(x, c')dx \ldots\ldots [32]$$

Introducting $t = (x - c)/(c' - c)$ we obtain

$$\frac{U(c') - U(c)}{c' - c} = \frac{2G}{\pi}\int_0^1 \left(\frac{1 - t}{t}\right)^{1/2} \cdot F_1[c + (c' - c)t; c] F_2[c + (c' - c)t; c]dt \ldots\ldots [33]$$

and

$$\frac{dU}{dc} = \frac{2G}{\pi}\int_0^1 \left(\frac{1 - t}{t}\right)^{1/2} \cdot dt = G \ldots\ldots [34]$$

This is Irwin's formula. It shows that the energy-release rate depends on the parameter G of the first state only. The same reasoning can be applied to the case of crack extension under fixed grips. Again G is obtained as the energy-release rate. Hence for infinitesimal crack extension there is no difference between the energy-release rates at constant load and under fixed grips. The Formula [34] together with Equations [29] and [30] is a useful tool for the study and prediction of crack propagation. The criterion, Equation [9], of crack propagation takes the very simple form

$$G \geq G_c \ldots\ldots [35]$$

Conclusions

The energy available for crack extension comes from two sources: The work of the externally impressed forces, and the change of the strain energy. The combined energy release from both sources is always positive; it equals the strain energy of the difference of the stress fields before and after crack extension. The difference field stays the same if the fields before and after crack extension are modified by subtracting from both of them the field of the uncracked specimen. The problem of crack extension is thus reduced to a study of the modified fields. These have no body forces; they show surface tractions at the crack surfaces only; these tractions are induced by the field of the uncracked specimen. The effects of different systems of impressed forces (e.g., one system with body forces, another with surface tractions) acting on the same body, can be compared with one another on the basis of the surface tractions, which the modified states display on their crack surfaces.

In addition to these general results, the following special statements can be made. When a crack extends under constant load, the strain energy decreases. However, the work of the externally impressed forces supplies twice the increment of strain energy and the surplus is available for crack extension. When a crack extends under fixed grips without body forces, there is no work of externally impressed forces. The strain energy decreases, and the decrement is available for crack extension. The energy supply for crack extension under constant load is larger than the supply under the condition of fixed grips. However, the energy release rates (energy per unit area of crack extension) are the same at the onset of crack propagation, at least for certain cases of plane strain.

Bibliography

1 "The Phenomenon of Rupture and Flow in Solids," by A. A. Griffith, *Philosophical Transactions of the Royal Society of London*, series A, vol. 221, 1929, pp. 163–198.

2 "Fundamentals of Brittle Behavior of Metals," by E. Orowan, Fatigue and Fracture of Metals (MIT Symposium, June, 1950), John Wiley & Sons, Inc., New York, N. Y.

3 "Energy Criteria of Fracture," by E. Orowan, *Welding Journal*, Research Supplement, March, 1955.

4 "Fracture Dynamics," by G. R. Irwin, Fracturing of Metals, ASM, 1948, p. 152.

5 "Fracturing and Fracture Dynamics," by G. R. Irwin and J. A. Kies, *Welding Journal*, Research Supplement vol. 31, February, 1952, pp. 95s–100s.

6 "Critical Energy Rate Analysis of Fracture Strength of Large Welded Structures," by G. R. Irwin and J. A. Kies, *Welding Journal*, Research Supplement, vol. 33, April, 1954, pp. 193s–198s.

7 "Onset of Fast Crack Propagation in High Strength Sheet and Aluminum Alloys," by G. R. Irwin, Proceedings of Sagamore Conference on High Strength Materials, Syracuse University, vol. 2, 1955, pp. 289–305.

8 "Analysis of Stresses and Strains Near the End of a Crack Traversing a Plate," by G. R. Irwin, *Journal of Applied Mechanics*, TRANS. ASME, vol. 79, 1957, pp. 361–364.

9 "The Relation of Microstructure to Brittle Fracture," by J. R. Low, Jr., ASM Symposium on Behavior of Materials at Low Temperature, American Society for Metals, Cleveland, Ohio, 1953, p. 163.

10 "Mathematical Theory of Elasticity," by I. S. Sokolnikoff, McGraw-Hill Book Company, New York, N. Y., second edition, 1956, pp. 86 and 391.

Discussion

G. R. Irwin.[1] This paper is a welcome contribution for several reasons. The effect of motion of the loading forces during crack extension, although explained in references (3) and (6), has not been well understood. The present paper provides a thorough review of crack-extension energy and strain energy on a 3-dimensional basis, and shows explicitly the applicability of classic theorems by Betti and by Clapeyron. The fact that the paper

[1] U. S. Naval Research Laboratory, Washington, D. C.

shows that the presence of body forces introduces no new type of difficulty into the crack-extension-force determination is of special value.

However, the difficulty of the analysis of stresses near a crack in a rotating cylinder or in a notched-bend specimen should not be underestimated. For example, the stresses in a rotating cylinder as shown by Fig. 4 of the paper are well known when no crack is present. As stated by the author, to obtain the stress system appropriate to a cylinder containing a radial crack, one may add a new stress system which cancels the normal stresses along the crack surfaces. The stresses which must be canceled, $F(r)$, are indeed known. However, it appears unlikely that any simple procedure exists for constructing a stress system which produces pressures equal to $-F(r)$ along the crack and at the same time satisfies free-surface conditions at the inner and outer radii of the cylinder. Of course, for purposes of fracture-mechanics analysis only the stresses near the leading edge of the crack are required. The comments of the author as to the actual difficulty of this stress calculation would be appreciated.

Author's Closure

The calculation of the intensity factor G for cracked specimen with a free boundary is indeed a difficult problem. For the notched bar in bending (Fig. 5) such calculations were carried out by means of an integral equation which relates the displacement v to the stress σ_y along the notch; more precisely an integral operator applied to v produces the stress σ_y. In order to match a prescribed stress distribution along the notch, a linear combination of the responses to four different v-functions was used; this procedure furnished the G-value with engineering accuracy. It appears from this experience that the method of integral equations is a useful tool for other problems as well.

Sulfuric Acid Corrosion in Oil-Fired Boilers —Studies on Sulfur Trioxide Formation

By DONALD R. ANDERSON[1] AND FRANK P. MANLIK,[2] CHICAGO, ILL.

Experimental studies on economizer and air-heater corrosion resulting from the formation of sulfuric acid in residual-oil-fired boilers are described. Factors controlling the oxidation of sulfur dioxide to sulfur trioxide have been investigated in a small experimental boiler. The fuel used was a distillate oil to which synthetic compounds were added to simulate the sulfur and metallic components commonly found in residual oils. The sulfur trioxide content of the flue gases was determined indirectly by measuring the corrosion of and sulfate deposition on a steel specimen maintained at a controlled temperature.

In an initially clean boiler, approximately equal quantities of sulfur trioxide formed in the flame, furnace, and convection sections, while less formed in the economizer-air heater section. Nickel, iron, sodium, and vanadium in the fuel each decreased the corrosion normally experienced by the test specimen, the magnitude of the effect increasing in the order given. Deposits of these metallic fuel-ash components in the boiler had a relatively small effect on the corrosion of the test specimen. Only the iron deposits indicated significant catalytic activity for the oxidation of sulfur dioxide to sulfur trioxide.

Combinations of sodium and vanadium in the fuel were found to decrease corrosion in an initially clean furnace, but boiler deposits from certain combinations of these elements were found to increase corrosion substantially. This catalytic effect is predominant over extended periods of time.

Introduction

DESIGN and operation of boiler plants have attained an amazing level of development. Today, push-button operated boilers, designed for higher superheated steam and lower exit gas temperatures are continually replacing older, less efficient units. Yet, the problem of sulfuric acid corrosion of boiler air heaters and economizers still remains unsolved, and costly manpower and materials are required to maintain the units in continuous operation.

During the combustion process, the sulfur in the fuel oxidizes to sulfur dioxide. A small fraction of gas converts to sulfur trioxide, which in turn combines with the water vapor always present in combustion gases to form sulfuric acid. The amount of sulfuric acid in the flue gases is generally small (20 to 50 ppm) but, because of its high boiling point, it condenses on surfaces maintained at temperatures up to 350 F. The condensate containing up to 80 per cent acid causes severe corrosion of the construction material of the boiler and, consequently, frequent interruption in boiler operation.

Previous work on alleviating low-temperature corrosion falls generally into two categories:

Mechanical—including such items as boiler design, operating conditions of the boiler, particularly in the economizer and air-heater sections, and use of corrosion-resistant materials. The mechanical approach frequently relieves the severity of the problem although the improvement usually is at the expense of the over-all efficiency.

Chemical—which involves the use of chemical additives applied to the fuel or to the combustion gases directly for the prevention of acid corrosion. The large amount of chemical additive required in cases of severe corrosion presently limits the extensive use of this approach. A more economical solution to this problem from the chemical-additive standpoint depends on a better understanding of the problem as it exists in operating boilers. With the knowledge of where and how sulfur in fuel oil is transformed into sulfuric acid, a successful approach to combat low-temperature corrosion should become more perceptible than it has been in the past.

In the broad sense, the process involves two stages, one being the production of sulfuric-acid vapor, and the other the condensation and resulting corrosion. Numerous studies on various aspects of sulfuric-acid condensation and corrosion explain this portion of the process in satisfactory detail (1–11).[3] However, the controversy on where and how the acid vapors originate continues to flourish and, as such, delays the long overdue solution to this problem (12–19).

Recognizing the need to clarify where and by what mechanisms sulfuric acid is produced in a boiler, experimental studies were conducted by the authors' company, results of which are presented in this paper.

Experimental Studies

To narrow the gap between conditions present in large scale boilers, and those in laboratory bench-type equipment, the experimental approach centered around the use of a pilot-plant-size boiler. The test unit incorporated many of the characteristic features of large boilers, such as gas and surface-temperature relations, construction materials, and mass reactions, while retaining the flexibility, accuracy, and economy of laboratory equipment.

Experimental Equipment. The basic unit was a Kewanee steam boiler of the type commonly used for domestic steam heating, Fig. 1. It consisted of a refractory-lined combustion chamber surmounted by a circular-water-wall furnace and a two-pass fire-tube convection section. The burner was a Hauck proportioning oil burner using low-pressure air for atomization and secondary air supply. A continuous analyzer measured and recorded oxygen content of the stack gas, thus providing a convenient means of maintaining reproducible combustion conditions during each series of tests.

A tubular corrosion specimen was positioned in the center of the stack. The operating conditions of this zone corresponded very closely with conditions in the corrosion areas of conventional

[1] Group Leader, Combustion and Engineering Laboratory, National Aluminate Corporation. Assoc. Mem. ASME.

[2] Chemical Engineer, Combustion and Engineering Laboratory, National Aluminate Corporation.

Contributed by the Research Committee on Corrosion and Deposits from Combustion Gases and the Research Committee on Furnace Performance Factors and presented at a joint session with the Fuels Division at the Annual Meeting, New York, N. Y., December 1–6, 1957, of THE AMERICAN SOCIETY OF MECHANICAL ENGINEERS.

NOTE: Statements and opinions advanced in papers are to be understood as individual expressions of their authors and not those of the Society. Manuscript received at ASME Headquarters, August 23, 1957. Paper No. 57—A-199.

[3] Numbers in parentheses refer to the Bibliography at the end of the paper.

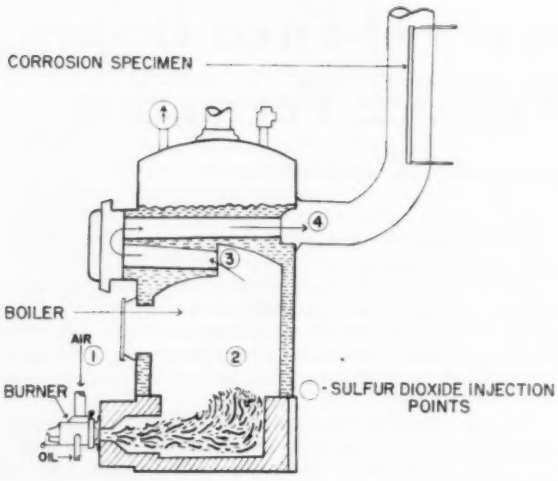

Fig. 1 Experimental boiler used in low-temperature corrosion studies

economizers and air heaters. Flue-gas temperature of the specimen zone was 500 F at the inlet and 450 F at the outlet.

The test specimen was low-carbon, cold-drawn seamless steel tubing, 1/2 in. OD, 24 gage, and 38 1/2 in. long. To simulate the various surface-temperature conditions in full-scale air heaters and economizers, controlled-temperature synthetic oil was circulated through the corrosion specimen. With oil inlet temperatures varying from 150 F to 350 F, surface-temperature variation along the tube averaged 10 F.

Test Procedure. To obtain a standard specimen surface, each tube was cleaned in toluene and sand blasted before determining the initial weight. Prior to each test, the boiler was fired until constant-temperature conditions were reached. The corrosion specimen was then positioned in the duct, and the cooling-oil inlet temperature adjusted to give the desired specimen temperature.

The boiler was fired with distillate oil having a sulfur content of less than 0.1 per cent. Fuel consumption averaged 1.4 gal per hr. The use of distillate oil circumvented many of the difficulties associated with the use of residual fuel oil, particularly since the studies required controlled amounts of sulfur and ash materials in the fuel. Carbon disulfide and the metal soaps of octoic and naphthenic acids were the normal oil-soluble materials used to provide added sulfur and ash to the fuel. Oxygen content of the flue gas was maintained at 5 ± 0.2 per cent, care being taken to seal all boiler and stack openings to prevent air infiltration.

The specimen remained in contact with the corrosive gases for 5 hr, this test period being required to obtain sufficiently accurate and reproducible corrosion data. The tube was then removed and washed for 10 min in hot distilled water to remove the water-soluble deposits and sulfuric acid accumulated during the test. After drying, the tube was reweighed and the difference recorded as weight loss due to corrosion. The weight loss from the washing procedure was less than 0.003 gram from an original weight of 170 grams which corresponded to 0.008 milligram per sq cm per test. Corrections were not made in the experimental results for this negligible weight loss. For most of the tests duplicates were run, the reproducibility being generally very good. When synthetic ash was present in the fuel maximum deviation in the test results did not exceed ±3 per cent.

To determine the amount of sulfuric acid and acid-reaction product on the tube specimen, the sulfate (SO_4) content of the wash water was determined by the conventional turbidimetric method.

Duplication of the Sulfuric Acid Problem in Experimental Equipment

The usefulness of the experimental unit depended largely on the extent to which the test unit duplicated corrosion conditions present in full-scale boilers. To establish some criteria by which the test unit could be judged, published studies on low-temperature boiler corrosion were consulted. It was apparent to the authors that general agreement on low-temperature corrosion conditions in industrial and utility boilers was limited to the following facts:

A Low temperature corrosion is caused by the formation and subsequent condensation of sulfuric acid on the cooler sections of boilers; with normal residual oils containing 1 to 4 per cent sulfur, this condensation can occur on air-heater and economizer surfaces having temperatures up to 350 F.

B The rates of acid condensation and corrosion are a function of the temperature of the condensing surface.

C The amount of sulfur trioxide in the combustion gases is a function of the sulfur content in the oil.

It will be noted that the methods of sulfur-trioxide formation are not included in this list since considerable controversy exists in this phase of the over-all problem (12–19).

To determine whether the experimental boiler could produce the phenomena generally agreed on, a series of boiler tests were made at various specimen temperatures. Carbon disulfide was added to the distillate fuel oil to provide a 2 per cent sulfur content. Fig. 2 shows graphically the corrosion data obtained as the surface temperature varied from 185 to 355 F. The relationship between the sulfatic material on the tubes and the specimen temperature was similar to the general form of the corrosion curve. These relationships are in agreement with the work done by Taylor (7) and others (6, 9) and satisfy the first and second requirements stated previously. Additional tests at a fixed specimen temperature of 230 F confirmed that with an increasing amount of sulfur in the fuel, corrosion increases. At sulfur concentrations of less than 0.1, 1.0, and 2.0 per cent, corrosion values of 0.02, 0.15, and 0.26 were obtained. This relationship was also found and reported by others (15, 19). Since the performance

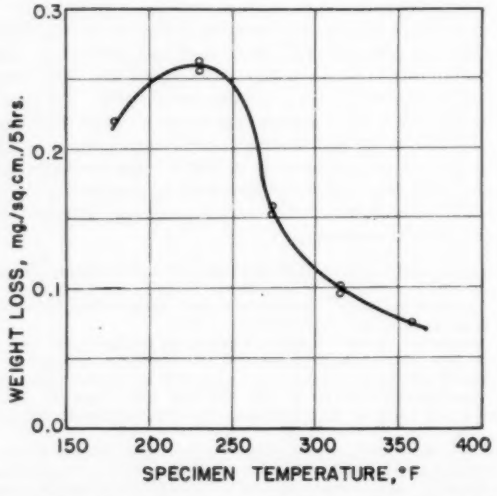

Fig. 2 Effect of temperature on sulfuric-acid corrosion in boilers

of the test unit met all three requirements, it was the authors' opinion that the experimental equipment adequately duplicated the low-temperature corrosion problem existing in full-scale boilers and further studies with this equipment were justified.

Sulfur Trioxide Formation in the Experimental Boiler

The knowledge of where and how sulfur trioxide forms in combustion units has been generally considered fundamental to the solution of the low-temperature corrosion problem. Two mechanisms of sulfur trioxide formation in flue gases have received wide attention, each being claimed as the principal source of the trioxide. Harlow (18) subscribes to the view that the sulfur dioxide formed in the initial combustion is oxidized catalytically to sulfur trioxide on metal and metal-oxide surfaces maintained at high temperatures. Whittingham and his colleagues (1, 17) consider that the atomic oxygen produced in the flame region is responsible for the oxidation of sulfur dioxide to sulfur trioxide. Other research workers (12, 13) expressed the belief that sulfur trioxide is formed when sulfur dioxide contacts the liquid phase already present on air-heater and economizer surfaces, resulting in a self-promoting reaction. To determine where sulfur trioxide forms in the experimental boiler the authors conducted a series of tests based on the introduction of sulfur-dioxide gas into various sections of the boiler.

Description of Special Test Procedure. Measured quantities of sulfur-dioxide gas equivalent to a 1 per cent sulfur content in the fuel were introduced in consecutive tests into the combustion air, the furnace, the convection section, and the stack of the experimental unit. (See Fig. 1, points 1, 2, 3, and 4). The boiler was operated with a fuel essentially free of sulfur (0.1 per cent). The sulfur dioxide injected into the combustion air at point 1 traveled through every section of the boiler. Thus the amount of sulfur trioxide in the stack gases was the total of the amount produced in the individual sections. Sulfur dioxide introduced into the furnace at point 2, however, left the boiler without passing through the flame region, and consequently a smaller total amount of sulfur trioxide was present in the stack gases, the difference being the amount produced in the flame region.

As in previous tests, the sulfur-trioxide content was not measured, but the resulting acid condensation and corrosion of specimens maintained at 230 F were determined.

Results. Fig. 3 shows the amount of corrosion obtained during four separate 5-hr tests. The sulfur dioxide injected into the combustion air ahead of the burner and passing through every section of the boiler caused the most corrosion. As the point of introduction moves toward the cooler sections of the boiler, the corrosion decreases to practically zero at the stack. Comparing the differences in corrosion obtained from two adjacent points of introduction, it becomes apparent that the amount of sulfur trioxide produced in the flame, furnace, and convection sections is approximately equal. Less oxidation of sulfur dioxide to sulfur trioxide occurred in the stack area. The flame region has long been recognized as a potential sulfur-trioxide producer, despite the fact that high temperatures favor sulfur-dioxide formation in the equilibrium reaction $SO_2 + {}^1/_2O_2 \rightleftharpoons SO_3$. The presence of highly reactive atomic oxygen in the flame, however, may be responsible for the formation of larger quantities of the trioxide than indicated by the equilibrium values (1, 17). In the interpretation of these results it should be considered that, although corrosion is a function of the amount of acid condensed, at the higher rates of condensation the proportionate change in corrosion is slightly less than at lower condensation rates. A similar relationship exists between the amount of sulfur trioxide present in the flue gas and the rate of condensation (6, 9). Consequently, an increase in corrosion by 30 per cent from additional trioxide formed in the flame probably corresponds to slightly larger rates of sulfur-trioxide formation than indicated by the test results. Taking into account this higher percentage, the fact still remains that a substantial proportion of the trioxide forms in areas outside the flame. In these zones, the equilibrium favors the conversion to sulfur trioxide; the reaction velocity, however, being a function of temperature, is much less than in the flame zone (20 and 21).

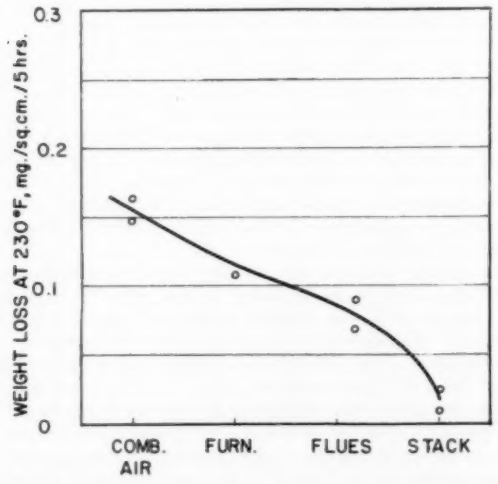

Fig. 3 Sulfuric-acid corrosion resulting from sulfur-dioxide injection into various boiler sections

In the absence of catalytically active surfaces, the actual quantity of sulfur dioxide converted can safely be expected to be small. The fact that a substantial portion of the trioxide does form in the post-flame areas of the experimental unit can only be accounted for by catalytic action. Since the fuel used in these tests was essentially free of ash, the materials capable of catalytic action were limited initially to iron scale present on the boiler walls. It will be shown in later tests that deposits originating from ash materials in the fuel may also increase the amount of sulfur trioxide formed in areas outside the flame region.

Effect of Type of Sulfur on Low-Temperature Corrosion

It is interesting to note that the corrosion value obtained with sulfur dioxide introduced into the combustion air, as shown in Fig. 3, corresponds closely with the corrosion value obtained previously with 1 per cent carbon disulfide in the fuel. Since it is conceivable that the molecular structure of the sulfur compounds present in the fuel may have an effect on the rates of low-temperature corrosion, especially in reactions taking place in the flame, a test series was made to resolve this question. A disulfide, mercaptan, and a thiophene, each representing a known group of sulfur compounds present in oil, were tested at a sulfur level in the fuel of 1 per cent. Tertiary octyl mercaptan, ditertiary butyl disulfide, and thiophene all produced slightly higher rates of corrosion (5 to 10 per cent) than previously obtained with carbon disulfide or sulfur dioxide. However, the magnitude of the changes is sufficiently small to discount the source of sulfur as a significant factor in the over-all problem.

Effect of Fuel-Ash on Low-Temperature Corrosion

Present day residual fuel oils contain a large variety of elements, although the majority of them are present in very small quantities. If those elements which usually appear in concentrations of less than 10 ppm in the fuel are neglected, the main ash-forming constituents in addition to sulfur are iron, vanadium,

sodium, calcium, nickel, and silicon. During the combustion of residual fuel oil, large quantities of these inorganic ash materials are introduced into the boiler. While the largest portion of the ash passes through the boiler at high velocity in the form of fly ash, a small amount deposits on the surfaces in the form of slag. Because of selective deposition of these materials, and longer residence time on the part of the slag deposits, marked differences in physical characteristics and chemical composition exist between slag and fly ash (22). Since the oxides of sulfur contact fly ash and deposits throughout the boiler, it is natural to expect that these materials may affect the reactions leading to low-temperature corrosion. It has been reported, for example, that fly-ash particles, because of their large surface area per unit weight, are very efficient gas absorbents. This has been proposed as one of the primary reasons for the relative immunity from low-temperature corrosion experienced in pulverized-coal-fired boilers (23). Fly ash may also influence the flame reactions in a manner similar to the common use of metal compounds as combustion catalysts to accelerate reactions in the flame. Commercial production of sulfuric acid, by the obsolete Mannheim and modern Contact processes, utilizes iron oxide and vanadium catalysts, respectively. Both of these materials are found in considerable quantities in oil ash and deposits. Finally, several of the newly designed industrial catalytic processes employ finely divided materials which are suspended as dust in the reacting gas stream, an arrangement which is very similar to fly-ash particles passing through a boiler.

Despite these analogies, little practical work has been done on reactions between oil-ash constituents and the combustion gases in general, or the sulfur oxides in particular. Gumz (26) and others (24, 30, 31) point out that in view of the large quantities of vanadium present in most residual fuel oils, a promotion of the sulfur dioxide to sulfur trioxide conversion should be expected. However, from combustion tests using distillate fuel oil containing oil-soluble vanadium as the only ash constituent, Taylor and Lewis (19) concluded that vanadium has no effect on the dew point of the combustion gases, i.e., upon the extent of sulfur trioxide formation. The authors suggested further that, based on their test results, the presence of vanadium in residual oil has no effect on low-temperature corrosion. Harlow (18) points out that iron oxide acts as a catalyst for the oxidation of sulfur dioxide provided that the surface temperature of the material is sufficiently high (approximately 1100 F). In a recent publication, Burnside, et al. (25), of Babcock & Wilcox, Ltd., London, England, described tests on a pilot-plant-size unit, and confirmed that additional trioxide is formed when flue gas passes over superheater tubes, presumably owing to catalytic oxidation. Furthermore, mixtures of ferric and ferrous sulfate formed by either a reaction of sulfuric acid with the metal of the boiler tubes or the iron oxide of the fly ash are powerful catalysts for the same conversion, a fact well known for many years (12, 14).

Experimental Studies on the Effect of Individual Fuel-Ash Elements

The uncertainty of many investigators as to the significance of fly ash and deposits in the reactions leading to low-temperature corrosion suggests that previous studies are inadequate. The authors believe that the ash materials, particularly potentially catalytic vanadium, have not been satisfactorily evaluated under conditions approximating those in actual boilers.

To gain further insight into the effect of ash materials on the formation of sulfur trioxide, additional tests were conducted in the laboratory boiler. The experimental approach consisted of two 5-hr tests for each ash material evaluated. During the first test of each material, the fuel contained 200 ppm of the element in oil-soluble form. Upon combustion, a small amount of ash

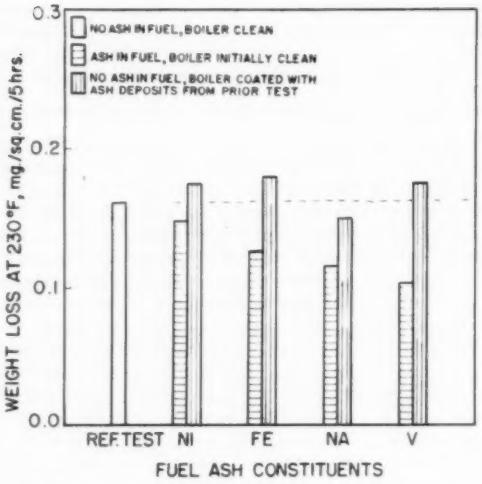

Fig. 4 Reductive and catalytic effects of fuel-ash constituents on sulfuric-acid corrosion

deposited on the boiler surfaces, while the remainder passed through the boiler in the form of fly ash. Thus the ash which was retained on the boiler surfaces was given an opportunity to form catalytically active deposits as well as to neutralize or absorb sulfur trioxide from the combustion gases under conditions relatively close to those prevalent in actual boilers. The acid corrosion obtained in this type of test consequently reflects any flame-inhibiting, absorbing, neutralizing, or catalytic action on the part of the fly ash and deposits, the corrosion observed being the net result of all the actions occurring.

Fig. 4 shows the corrosion resulting from the separate addition of nickel, iron, sodium, and vanadium to the fuel. Although it was expected that sodium and iron would cause a slight reduction in corrosion by sulfate formation in the combustion gases or on the boiler surfaces, values of 29 and 23 per cent respectively were not anticipated. However, the most interesting result in Fig. 4 is the 37-per-cent reduction due to vanadium.

The results with sodium confirm work done by Whittingham (27), who introduced sodium compounds into a gas flame and observed a decrease in the dew point of the combustion gases. Sulzer (28) reports that sodium not only reacts with sulfur trioxide, but also with sulfur dioxide which may account for the relatively small reduction obtained with sodium. Although these tests were not designed to determine whether the corrosion reduction (reductive effect) produced by the fly ash of the metals is a result of an inhibiting process in the flame, absorption, or neutralization, it is interesting to note that analytical tests revealed large quantities of metal sulfate present in the iron, vanadium, and sodium deposits.

Immediately following each of these tests, a second 5-hr test was made using fuel oil containing no ash, but with the standard amount of carbon disulfide to provide 1 per cent sulfur in the oil. The corrosion obtained in these tests represents the residual effect of the boiler deposits formed during the preceding test. Catalytic action of the deposits is indicated when the corrosion rises above that obtained in the absence of ash materials, i.e., above the reference test value. Results of this test series are also presented in Fig. 4. It was found that iron deposits increase corrosion approximately 15 per cent while nickel and vanadium deposits furnish less than 10 per cent additional corrosion. The residual effect of the sodium deposits reduced the corro-

sion below the value for the reference test, definitely showing that these deposits had no catalytic activity.

Experimental Studies on the Effect of Mixtures of Sodium and Vanadium as Fuel Ash

The relatively low catalytic effect of vanadium in the previous series of tests was of particular interest since Taylor and Lewis (19) obtained similar results and concluded that vanadium is relatively harmless. Nevertheless, the numerous references in the literature suggesting vanadium as a significant contributor to low-temperature corrosion in boilers could not be ignored.

A review of the published studies on sulfuric-acid catalysts revealed that the addition of alkali to vanadium oxides greatly increases the activity over that of the pure oxides (29). Since residual fuel oil contains both sodium and vanadium, the formation of catalytic sodium and vanadium mixtures in boilers appeared plausible. Furthermore, it is well known that boiler deposits in oil-fired boilers frequently contain both sodium and vanadium. However, experimental evidence was required to prove that harmful sodium-vanadium catalysts can be formed in a boiler. To accomplish this, boiler tests were performed similar to the previous 5-hr sequential tests, with the exception that the fuel contained various mixtures of oil-soluble sodium and vanadium. The vanadium content remained constant at 200 ppm for all tests involving fuel ash.

Fig. 5 shows the very low corrosion that occurred during the tests with mixtures of sodium and vanadium in the fuel. When the ratios of sodium oxide to vanadium pentoxide were 1:1, 1:3, and 1:6, the net reduction in corrosion varied from 47 to 52 per cent. Comparing these results with the previous work on the effect of individual fuel-ash constituents, Fig. 4, the greater reductive effect of these mixtures is apparent.

The catalytic effects of the residual deposits were determined during the second 5-hr tests. The formation of catalytic sodium-vanadium deposits was immediately confirmed by the pronounced increase in acid-corrosion values, Fig. 5. The sodium-oxide vanadium-pentoxide ratio of 1:1 in the fuel produced a 23-percent increase in corrosion. The maximum corrosion, amounting to an increase of 42 per cent, was obtained with the sodium-oxide vanadium-pentoxide ratio of 1:3 in the fuel whereas the relatively low-sodium mixture with the 1:6 ratio produced no evidence of catalytic activity.

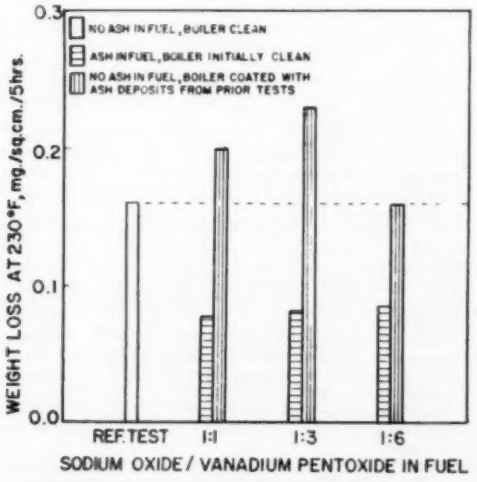

Fig. 5 Reductive and catalytic effects of sodium-vanadium mixtures in fuel oil on sulfuric-acid corrosion

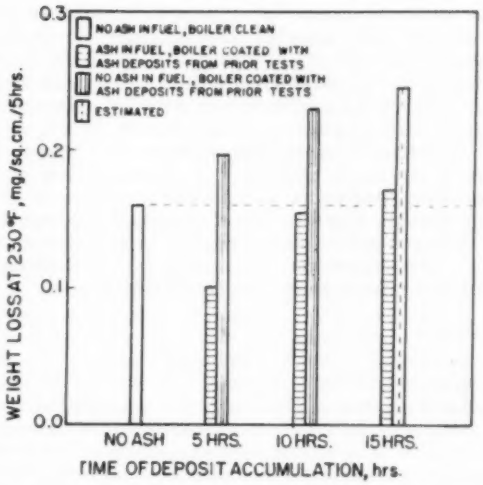

Fig. 6 Influence of progressive catalytic deposit build-up on sulfuric-acid corrosion

Having established that certain ratios of sodium and vanadium in the fuel produce deposits which increase low-temperature corrosion, two additional questions were raised:

(*a*) Can the catalytic effect be increased by the additional build-up of sodium-vanadium deposits, and

(*b*) can corrosion due to these catalytic deposits sufficiently exceed the reductive effect due to the sodium-vanadium fly ash to justify considering such deposits a major factor in acid production? Using fuel containing a sodium oxide to vanadium pentoxide ratio of 1:3 and 1 per cent sulfur, a series of 5-hr tests was made in the following sequence:

A Test with fuel ash (sodium and vanadium compounds added to fuel) and initially clean boiler surfaces.

B Test without fuel ash, but with 5 hr of accumulated deposit from Test A present on the boiler surfaces.

C Test with fuel ash and 5 hr of Test A deposit at the start of the test.

D Test without fuel ash but with 10 hr of accumulated deposit from Tests A and C present on the boiler surfaces.

E Test with fuel ash and 10 hr of Test A and C deposit at the start of the test.

F Test without fuel ash but with 15 hr of accumulated deposit present on the boiler surfaces. (Time did not permit this test to be run. Since the results from Test A, C, and E, however, establish the trend sufficiently, the results of Test F were estimated and reported as such.)

The values shown in Fig. 6 show the decrease in corrosion followed by the gradual rise due to residual catalytic deposits despite the fact that the fuel ash was present, tending to reduce the total corrosion. It is apparent from these data that the net corrosion exceeds the reference test value after ten hours of deposit formation. Fig. 6 also illustrates the corrosion values obtained from the tests run without ash present in the fuel, but with varying amounts of residual deposit present on the boiler surfaces. Under these conditions, the catalytic deposits accumulated during the total 15 hr produced an estimated increase in corrosion of 50 per cent over the reference value obtained with ash-free oil. Inasmuch as the quantity of ash added to the fuel was constant, the trend in Fig. 6 reveals the inability of the ash to counteract the increasing catalytic effect.

The significant increase in corrosion in the relatively short period of 15 hr illustrates the potential danger of sodium and vanadium in residual fuel oil. Furthermore, consideration should be given to the interrelationship between the catalytic and reductive effects and the sulfur content of the fuel. The quantity of fuel ash limits the reductive capacity of the fly ash, but has very little influence on the catalytic effect which increases to a maximum activity as determined by factors such as deposit temperature, composition, and physical structure. It would appear therefore that with fuels of comparable ash content the relative importance of deposit catalytic action increases with higher fuel-sulfur contents since additional sulfur dioxide is available for catalytic conversion to sulfur trioxide.

Conclusions

In this work an attempt has been made to utilize a pilot-plant-size experimental boiler in studying the problem of sulfuric-acid corrosion in air heaters and economizers of residual-oil-fired boilers. The intent has been, first, to provide a useful experimental unit and, secondly, to investigate factors controlling the oxidation of sulfur dioxide to sulfur trioxide during the combustion process of residual fuels. Compared with the general conclusions that have been drawn in the past from work on full-scale boilers, the results from the present work are relatively clear-cut:

1 In the absence of ash compounds in the fuel, the amount of sulfur trioxide produced in the flame, furnace, and convection section of the experimental unit is approximately equal. Less oxidation of sulfur dioxide to sulfur trioxide occurs in the stack area.

It is the authors' opinion therefore that significant quantities of sulfur trioxide are formed both in the flame and on the boiler surfaces, the relative importance of the mechanisms being governed largely by the individual boiler conditions.

2 The form in which sulfur is present in the oil has a negligible effect on the amount of sulfur trioxide formed during the combustion process.

3 The net-effect of certain ash compounds in fuel oil on low temperature corrosion is the result of two conflicting actions: A reductive effect, e.g., neutralization, absorption, or flame-inhibiting action, causing a decrease in the amount of sulfur trioxide available for corrosion and, simultaneously, a catalytic effect of deposits formed on the boiler surfaces resulting in an increase in the amount of sulfur dioxide converted to sulfur trioxide.

(*a*) Nickel, iron, sodium, or vanadium present in fuel oil tends to decrease corrosion by the reductive effect, the magnitude of the effect increasing in the order given.

(*b*) Boiler deposits resulting from the presence of iron in fuel oil tend to increase corrosion due to the formation of catalytically active surfaces. Nickel and vanadium show a similar effect but to a lesser degree.

(*c*) Mixtures of sodium and vanadium present in the fuel (sodium-oxide to vanadium-pentoxide 1:1, 1:3, 1:6) decrease corrosion in a manner similar to that of the individual elements but to a greater extent.

(*d*) Boiler deposits from these two elements, particularly at the oxide ratios of 1:1 and 1:3 in the oil, however, are powerful catalysts.

(*e*) It has been possible to show that, as more deposits form, the catalytic effect increases and surpasses the reductive effect of these ash compounds. It was reasoned that with sulfur contents normally found in residual fuel oils (1 to 4 per cent) the resulting increase in sulfur trioxide can be far greater than indicated by the results of this work.

It is recognized that the results of this work cannot be applied strictly to the operation of full-scale boilers. There, residual oil is burned which contains a large number of ash compounds, some in minute quantities, while the fuel used in the laboratory test unit contained only one or two ash elements at one time. The formation of molten slag, differences in temperature distribution, and the time of deposit build-up complicate the reactions taking place and make it difficult to project these findings to the operation of full-scale boilers. The results of this work indicate clearly, however, that the catalytic action of boiler deposits formed from sodium and vanadium in the fuel are capable of promoting the oxidation of sulfur dioxide to sulfur trioxide and, consequently, may assume the role of a principal contributor of sulfuric acid in residual-oil-fired boilers.

Acknowledgment

The authors wish to acknowledge the help and encouragement received from J. H. Phillips under whose immediate direction this research was conducted.

Bibliography

1 "The Oxidation of Sulfur Dioxide in Gas Flames," by A. Dooley and G. Whittingham, *Trans. Faraday Society*, vol. 42, 1946, pp. 354–362.

2 "The Oxidation of Sulfur Dioxide in Slow Combustion Processes," by G. Whittingham, *Trans. Faraday Society*, vol. 44, 1948, pp. 143–146.

3 "Relation Between Dew Point and the Concentration of Sulfuric Acid in Flue Gases," by A. A. Taylor, *Journal of the Institute of Fuel*, vol. 16, 1942, pp. 25–28.

4 "The Investigation of Dew Point and Related Condensation Phenomena in Flue Gases," by D. Flint, *Journal of the Institute of Fuel*, vol. 21, 1948, pp. 248–253.

5 "The Determination of SO_2 and SO_3 in Flue Gases," by P. F. Corbett, *Journal of the Institute of Fuel*, vol. 24, 1951, p. 247.

6 "The Corrosion of a Steel Surface by Condensed Films of Sulfuric Acid," by D. Flint and R. W. Kear, *Journal of Applied Chemistry*, vol. 1, 1951, pp. 388–393.

7 "The Condensation of Sulfuric Acid on Cooled Surfaces Exposed to Hot Gases Containing Sulfur Trioxide," by H. D. Taylor, *Trans. Faraday Society*, vol. 47, 1951, pp. 1115–1120.

8 "The Corrosion of Heating Surfaces in Boiler Plants: Further Studies in Deposit Formation," by J. R. Rylands and J. R. Jenkinson, *Proceedings of The Institution of Mechanical Engineers*, vol. 158, 1949, pp. 405–414.

9 "The Acid Dew Point," by J. R. Rylands and J. R. Jenkinson, *Journal of the Institute of Fuel*, vol. 27, 1954, pp. 299–309.

10 "The Measurement of the Dew Point and H_2SO_4 Vapour Content of Combustion Products," by W. E. Francis, Gas Research Board Communication GRB 64, June, 1952.

11 "An Investigation into the Air-Heater Corrosion of Oil-Fired Boilers," by B. Lees, *Journal of the Institute of Fuel*, vol. 29, 1956, p. 171.

12 "The Corrosion of Power Plant Equipment by Flue Gases," H. F. Johnstone, University of Illinois Engineering Experiment Station, Bulletin no. 228, June, 1931.

13 "Bonded Deposits on Economizer Heating Surfaces," by J. R. Rylands and J. R. Jenkinson, *Journal of the Institution of Electrical Engineers, London*, vol. 91, April, 1944, pp. 77–88.

14 F. S. Wartmann, R. R. Keyes, U. S. Bureau of Mines Reports, Investigation no. 2839, 1927.

15 "The Formation of Sulfur Trioxide in Flue Gases," by P. H. Crumley and A. W. Fletcher, *Journal of the Institute of Fuel*, vol. 29, 1956, pp. 322–327.

16 "The Catalytic Oxidation of Sulfur Dioxide on Metal Surfaces," by G. Tolley, *Journal of Society of Chemical Industries*, vol. 67, 1948, pp. 369–373.

17 "Flame and Explosion Phenomena," by G. Whittingham, Third Symposium on Combustion, Madison, Wisconsin, 1948.

18 "The Formation of Sulfuric Acid in Boiler Flue Gases," by W. F. Harlow, TRANS. ASME, vol. 80, 1958, pp. 225–234.

19 "SO_3 Formation in Oil Firing," by R. P. Taylor and A. Lewis, IV Congrès International du Chauffage Industriel, Groupe II, Section 24, no. 154, 1952.

20 "Sulfur in Fuel and the Dew Point of Combustion Gases," by W. Gumz, *Brennstoff-Wärme-Kraft*, 5, 8, 1953, pp. 264–269.

21 "Formation of Sulfur Trioxide in Flue Gas," by Torsten Widell, *Combustion*, vol. 24, 1953, pp. 53–55.

22 "Fireside Deposits in Oil-Fired Boilers," by C. Jacklin, D. R. Anderson, and H. Thompson, *Industrial and Engineering Chemistry*, vol. 48, no. 10, 1956.

23 "The Reduction of Sulfur Trioxide by Constituents of Boiler Flue Dust," by H. E. Crossley, A. Pollard, and F. Sweett, *Journal of the Institute of Fuel*, vol. 21, 1948, pp. 207–209, 213.

24 "Properties of Residual Petroleum Fuels," by W. Sacks, TRANS. ASME, vol. 76, 1954, pp. 375–379.

25 "The Influence of Superheater Metal Temperature on the Acid Dew Point of Flue Gases," by W. Burnside, W. G. Marskell, and J. M. Miller, *Journal of the Institute of Fuel*, vol. 29, 1956, pp. 261–269.

26 "Fouling of Heating Surfaces as a Function of Fuel, Fuel Ash, Operation, and Design of Boilers," by W. Gumz, *Mitteilungen der Vereinigung der Grosskesselbesitzer*, vol. 27, 1954, pp. 1–24.

27 "Formation of Sulfate Deposits and Acid Condensates During Combustion," by G. Whittingham, Eleventh International Congress of Pure and Applied Chemistry, London, England, July, 1947.

28 "The Influence of Combustion Control on Oil Ash Deposition Occurring in Industrial Gas Turbine Plants," by P. T. Sulzer, *Schweizer Archiv für angewandte Wissenschaft und Technik*, vol. 20, 8, 1954, pp. 1–9.

29 "The Role of Alkali Sulfates in Vanadium Catalysts for Sulfur Dioxide Oxidation," by G. H. Tandy, *Journal of Applied Chemistry*, vol. 6, 1956, pp. 68–74.

30 "The Gas Turbine and Its Fuels," by E. L. Bass, I. Lubbock, and C. G. Williams, *Shell Aviation News*, no. 156, June, 1951.

31 "Erosion and Corrosion Damage Through Use of Heavy Heating Oils as Fuels for Engines, Boilers, and Gas Turbines," by B. Engel, *Erdöl und Kohle*, vol. 3, 1950, pp. 321–327.

Discussion

J. R. Jenkinson.[4] The experiments described in this paper are useful in that they have confirmed previous work done by other research workers, but as far as this discusser is aware the results obtained by the addition of various elements to study their effect on SO_3 formation is new. The authors say that the results cannot be strictly applied to the operation of full-scale boilers because of the numerous variants that are possible, but this does not detract in any way from the value of the work done and the results obtained.

Fig. 2 could have been correlated with the results given in the discusser's ASME Paper No. 56—A-184, "Low Temperature Deposits and Corrosion in Boilers," November, 1956. This same paper mentioned the possible reactions of vanadium compounds on surfaces rather than in the gas stream, and indicated that catalytic reactions are possible after deposits have formed on the metal surfaces.

Further work could well be done with the same apparatus at much lower temperatures than those used, for the results indicate that metal temperatures below 230 F are attacked less.

Many airheaters do have metal temperatures round about 230 F. It cannot always be avoided, but attack is not severe during service, as the deposited acid is concentrated and renders the metal surfaces passive. Unfortunately when the unit cools down this acid becomes diluted and attack occurs. It is quite possible that some of the corrosion of the specimen occurred during the time it was taken out of the apparatus and washed with hot water.

Everyone seems to strive to raise the metal temperature, but the work described in this paper does suggest that much lower temperatures can be used. The question is how far a designer can safely go. The discusser indicated in the ASME paper already referred to that 140 F appeared to be a critical temperature, below which metal surfaces were in danger of excessive corrosion, and the results of experiments still to be published tend to confirm this statement.

Hilmer Karlsson.[5] The authors, by processes of adding and eliminating contaminating variables, developed results which warrant considerable thought in controlling SO_3 formation. We wonder, however, in considering the reductive effects of single constituents, in contrast to combined effects as in sodium-oxide vanadium-pentoxide ratios, whether additions of water vapor would not have altered results during the single-effect tests.

Furthermore, the contention of a catalytic effect produced by deposits limited to test period of 5 to 15 hr presumes a proportionate increase with time. Our work on corrosion rates generally indicated reduced rates developed with time, concluding that reaction was more rapid on initially clean plates. From this the writer hypothesized that deposits acted as a buffer with time although during the initial stages contaminants could conceivably have reacted more rapidly in promoting corrosion.

The authors have made an excellent approach to the evaluation of effects of contaminants generally considered to be responsible for aggressive corrosion. It is hoped that these efforts will be continued along lines of combined effects so that a more exact appraisal of field operation can be made.

Authors' Closure

Messrs. Jenkinson and Karlsson present in their discussions some very interesting and certainly thought-provoking comments. The authors appreciate the interest both discussers have shown in the paper.

Progress toward lower economizer and air-heater surface temperatures for boilers burning residual fuel oil will be delayed by several factors, not the least of which is the companion problem of excessive deposits. Nevertheless, the authors agree with Mr. Jenkinson that this approach opens promising possibilities and certainly warrants further efforts and studies.

The view expressed by Mr. Jenkinson that very little corrosion occurs at 230 F may be true under certain conditions. More recent 20-hr studies by the authors have shown that sulfuric acid condensate may or may not attack metal surfaces at this temperature. Tests in which the fuel contained 2 per cent sulfur resulted in high corrosion values. The addition of ash to the same fuel essentially stopped the corrosion at 230 F. With high rates of attack, the specimen surfaces were dry when removed from the test area whereas, with very low corrosion rates, the tubes were visibly wet. Considerable attack occurred on the latter tubes during the water-washing operation as evidenced by vigorous bubble formation. Wet and dry specimens did not differ appreciably from each other in sulfate measurements. Since all of the results presented in this paper were obtained from specimens removed in a dry state, it is unlikely that the weight-loss data presented were significantly influenced by water-washing as Mr. Jenkinson proposes. However, the more recent results also illustrate the condition mentioned by this discusser where sulfuric acid condenses during service, but does not cause aggressive attack. For such cases, corrosion can then be severe as the acid becomes more dilute during the shutdown or subsequent water-washing periods.

Mr. Karlsson raises the question of whether or not additions of water vapor would alter the results of the single effect tests. The authors agree that water-vapor content could have some effect and should be investigated.

On the point that the reported data imply that the corrosion rate increases proportionately with the formation of catalytic deposits, it is important to remember that the catalytic effect of high-temperature slag has limiting factors which determine its ultimate influence on corrosion. This can be seen from the values in Fig. 6 where the incremental increase in corrosion became less pronounced with each additional period of operation. The results are presented not to imply a continuously increasing corrosion rate over extended periods of time, but to merely

[4] E. Green & Son, Ltd., Wakefield, England.

[5] Technical Manager, The Air Preheater Corporation, Wellsville, N. Y. Fellow, ASME.

establish that a higher sulfuric acid production level can result from the presence of certain fuel ash constituents. No attempt was made to assess the influence of low-temperature economizer and air-heater deposits which probably do alter the rate of attack at the interface as suggested by Mr. Karlsson. This, we agree, is an area which needs further investigation. Future studies on the relationship between fuel ash and visibly wet surfaces, sulfuric acid mist formation, acid concentration, and deposit formation should provide much of this needed information.

In the work which followed the studies reported in this paper, a search was begun for new chemical methods of preventing low-temperature boiler corrosion. Some of the results on effects of chemical interference in flame and catalytic deposit mechanisms have been encouraging in both laboratory and field tests. It is hoped that through continued efforts, improved methods of combating the problem can be reported at a later time.

An Investigation of the Variation in Heat Absorption in a Pulverized-Coal-Fired Slag-Tap Steam Boiler at Blaine Island, Charleston, W. Va.[1]

By A. A. ORNING,[2] M. WEINTRAUB,[3] C. H. SCHWARTZ,[3] E. A. MIHOK,[3] C. R. McCANN,[3] AND W. C. HARROLD,[3] PITTSBURGH, PA.

This paper resulted from the sixth in a series of investigations of heat absorption in large steam-boiler furnaces, sponsored by THE AMERICAN SOCIETY OF MECHANICAL ENGINEERS Special Research Committee on Furnace Performance Factors. The furnace heat absorption was determined from the furnace exit-gas composition and temperature in 18 tests on a steam generator rated at 250,000 lb of steam per hr at 675 psi and 670 F. The furnace was fired with pulverized coal, through opposed burners with reinjection of fly ash, over a refractory-insulated slagging bottom. Furnace heat absorption, at various loads and excess air values, was correlated with the adiabatic flame temperature and the residence time of combustion products in the furnace. The furnace performance was found to depend upon burner adjustments, but did not significantly depend upon recirculation of fly ash.

Former investigations were conducted on a spreader-stoker-fired furnace (1),[4] a natural-gas-fired furnace (2), and dry-bottom pulverized-coal-fired units with various burner arrangements (3). The present investigation concerns a pulverized-coal-fired slag-tap furnace, normally operated with fly-ash recirculation and having a steel-clad refractory-insulated bottom.

This paper presents an estimation of furnace heat-absorption efficiency by the Combustion Section of the Bureau of Mines, as part of the research program of the Special Research Committee on Furnace Performance Factors.

Description of Tests

Eighteen tests were made to determine the effect on furnace heat absorption of variation of load, excess air, and fly-ash recirculation. Tests 1–12 were conducted November 4–20, 1956, and tests A1–C2, July 10–12, 1957. Furnace heat absorption was estimated as the difference between the net heat available and the heat losses, the first including an estimate of heat in recirculated ash and the latter including sensible heat in the products of combustion, and the radiation and convection losses. Method (*b*), paragraph 7, of the ASME Test Code for Stationary Steam-Generating Units was followed wherever applicable.

Since coal scales were not used, the net heat available was obtained by an over-all heat balance of the entire unit, using the flow rate and enthalpy of steam generated, the flow rate and enthalpy of feedwater, the flue-gas temperature at the air-heater outlet, and the gas composition at the furnace outlet. The last was found to agree with gas composition at the induced-draft-fan outlet as determined immediately before and after each test. Sensible heat in the gases leaving the furnace, for the first twelve tests, was estimated from measurements of gas temperature and composition ahead of the screen at the furnace outlet, using techniques developed by the Bureau of Mines (4). The temperatures used for the first twelve tests were those measured by high-velocity thermocouples with Bureau of Mines type-G thermocouple shields (4). The gas temperature for the last six tests was determined on the basis of correlations developed between superheater performance and furnace-outlet conditions. The feedwater temperature was 385 ± 2 F for the first twelve and 330 F for the last six tests.

Data on gas temperature and composition and on dust loadings were also obtained within the furnace above the flame. Dust loadings at the air-heater inlet and at the stack were obtained by the Western Precipitation Corp. These data, together with temperature data at the entrance and exit of the air heater, were used for computation of over-all heat balances and estimation of the heat returned to the furnace in recirculated fly ash and preheated air.

Description of Furnace

The boiler has been previously described (5). Fig. 1 is a sectional side elevation of the unit. The design capacity was 250,000 lb of steam per hr at 675 psi and 670 F with a heat release of 15,800 Btu per cu ft. The furnace is approximately 61 ft high from the bottom wall headers to the top of the furnace outlet. The width is 19 ft 8 1/4 in. and the depth is 20 ft 9 3/4 in. The depth, just above the burners, is constricted to about 16 1/2 ft. The projected wall area including the furnace outlet is 4672 sq ft, and the furnace volume is 20,600 cu ft. The furnace-wall tubes are 3 1/2-in. diam set on 3 3/4-in. centers. The bottom is a steel-clad, refractory-insulated hearth. The furnace is fired with pulverized coal through three burners in the rear wall and three in the front wall. Opposed burners are slightly offset and directed 20 deg below horizontal.

The furnace depth narrows to 15 ft 2 1/4 in. ahead of the furnace outlet. Gas flows downward from the furnace outlet through the superheater, up through the boiler section, and down through tubes of the vertical air heater to the induced-draft fan.

---

[1] Work on manuscript completed August, 1957.

[2] Chief, Combustion Section, Branch of Bituminous Coal, Division of Solid Fuels Technology, Bureau of Mines, U. S. Department of the Interior. Mem. ASME.

[3] Chemical Engineer, Combustion Section, Branch of Bituminous Coal, Division of Solid Fuels Technology, Bureau of Mines, U. S. Department of the Interior.

[4] Numbers in parentheses designate References at end of paper.

Contributed by the Research Committee on Furnace Performance Factors and presented at a joint session with the Fuels Division and the Research Committee on Corrosion and Deposits From Combustion Gases at the Annual Meeting, New York, N. Y., December 1–6, 1957, of THE AMERICAN SOCIETY OF MECHANICAL ENGINEERS.

NOTE: Statements and opinions advanced in papers are to be understood as individual expressions of their authors and not those of the Society. Manuscript received at ASME Headquaters, November 27, 1957. This paper was not preprinted.

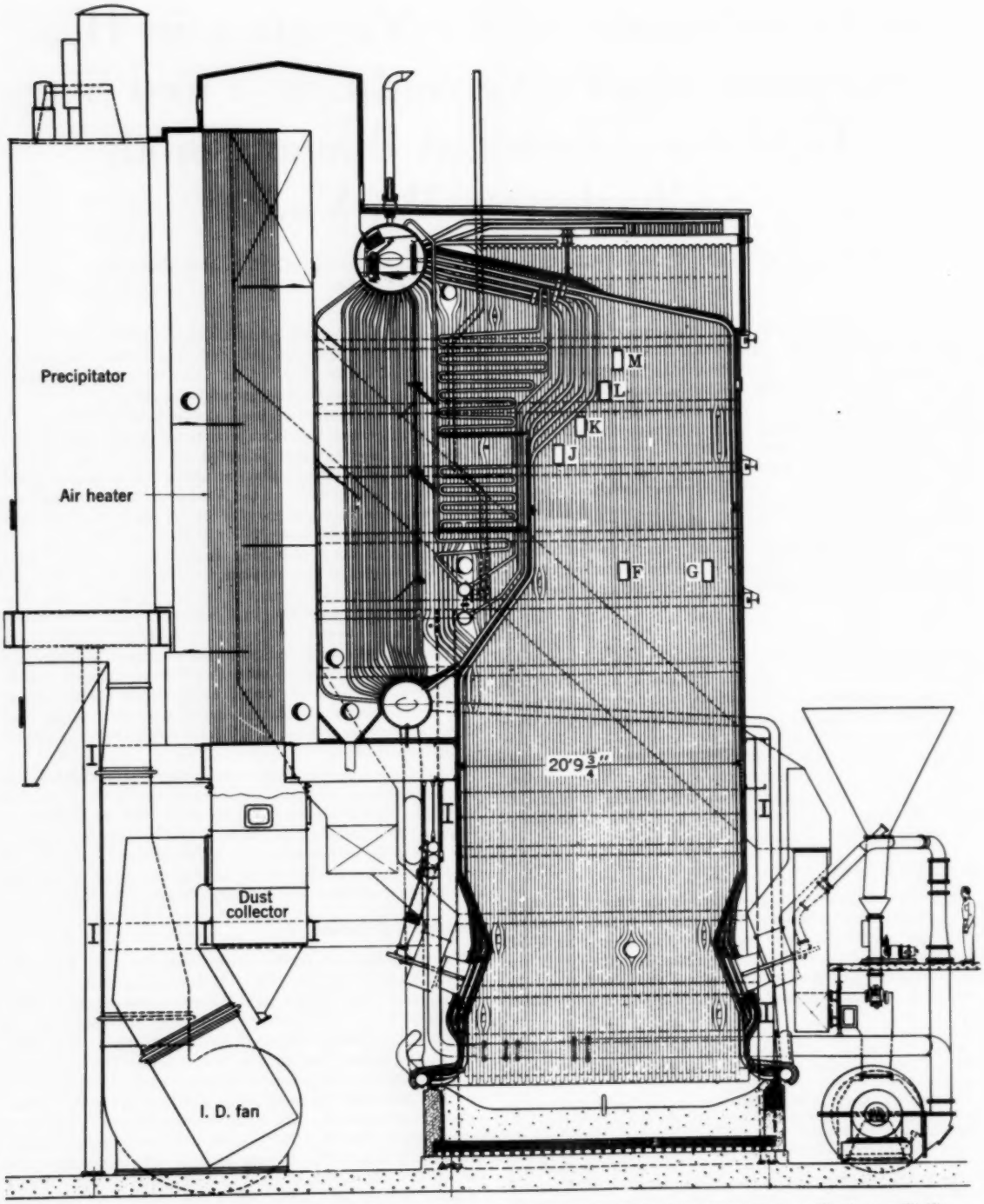

Fig. 1 Sectional side elevation of boiler 25, Blaine Island plant, Carbide and Carbon Chemical Company, Charleston, W. Va.

Fly ash is returned through nozzles into the rear of the furnace from hoppers at the base of the boiler section, the mechanical collectors at the base of the air heater, and the electrostatic precipitator. Fly ash is reinjected with air from a high-pressure fan taking air from the end of the rear secondary air duct.

Location of Survey Points

Gas temperature and composition surveys were made at the furnace outlet by means of a high-velocity thermocouple probe. Measurements were made at eight positions, spaced at 30-in. intervals across the width of the furnace, at each of four levels. The positions, as indicated by door locations in Fig. 1, were in the furnace about 10 to 18 in. from the first row of screen tubes. Dust loadings and gas samples were also taken at a lower level in the furnace, covering only the left half of the furnace.

Instrumentation and Analytical Methods

The instrumentation and techniques used for estimating gas temperature and composition have been previously described (4).

Since the coal flowed directly from bunkers into the coal feeders, heat input could not be determined by direct weighing of fuel. Data on composition and on temperatures at the air-heater outlet, and the flow rate and enthalpy of steam generated were used, through an over-all heat and mass balance, to estimate mass flow rates and thermal input.

The steam flowmeter and steam-superheat indicator were calibrated just before the tests. Plant instruments showed temperatures in air and flue gas at the air-heater inlet and outlet. These instruments were checked and found satisfactory by a traverse across the gas stream with an unshielded thermocouple.

The humidity of the air was determined by wet and dry-bulb measurements at the forced-draft-fan inlet. Coal samples were taken at 10-min intervals throughout the test period. Coal analyses were made by the Coal Analysis Section of the Bureau of Mines.

Methods of Calculation

Flue-Gas Temperature. The flue-gas temperature at the furnace outlet was taken as a weighted average of individual readings at the survey positions. It was planned to take readings at five levels in front of the screen tubes. Due to structural difficulties, the uppermost opening was not provided. Readings for each position across the furnace were plotted against the distance between levels, and the temperature at the fifth and uppermost level was estimated by extrapolation. Readings at each position were weighted in proportion to the area of the furnace outlet represented by that position. Temperatures at the furnace outlet, for tests A1 through C2, were estimated from superheater performance by means of Equation [4], which was developed on the basis of data for the first twelve tests.

Adiabatic Flame Temperatures. The adiabatic, or theoretical, flame temperatures were calculated by methods developed by Myers, Goldberg, and Smith (6). These temperatures may not exist anywhere in the furnace, owing to heat being transferred before combustion is complete, but they are nevertheless a useful measure of the intensity of radiation.

Gas Composition. The gas composition at the furnace outlet varied with sampling location; the excess air varied with location over a range of 20 to 30 per cent for a given test. Except for some trend to lower values at the lower right corner, the variation appeared erratic. Data for the upper portion of the outlet, therefore, could not be obtained by extrapolation. For these reasons an average for the 32 positions, without weighting, was used.

The average oxygen concentration at the furnace outlet correlated well with that of samples taken before and after each test at the induced-draft-fan outlet with the same instrument. The average oxygen concentration, from samples taken at the furnace outlet during the test, was used for estimating excess air, except for test 1, where the estimate was based on samples taken at the induced-draft-fan outlet.

Heat Balance on Entire Unit. No means were available for direct estimation of the coal-feed rate. The excess air, and hence air-to-coal ratio, was determined from the coal analysis and the flue-gas composition. The heating value of the coal, the temperature of the preheated air, and estimates of heat returned in recirculated ash gave the net heat available per lb of coal fired. A balance with heat lost in the products of combustion, lost as radiation, and transferred to steam produced gave the firing rate in lb of coal per hr.

The net heat available is the sum of the lower heating value of the fuel (corrected for unburned combustible), heat returned in recirculated fly ash, and the enthalpy above 80 F of the air used for combustion. It was assumed that 50 per cent of the ash left as fly ash with nonreinjection and a multiple of this amount, in proportion to indicated dust loadings in the furnace and the air-heater inlet, was recirculated with reinjection.

Radiation and convection losses were estimated from the ABMA Standard Radiation Loss Chart, shown in the ASME Power Test Code for Stationary Steam Generating Units (1946). For the furnace, the radiation loss was taken as one-half that of the entire unit.

Heat Balance on Furnace. Heat absorption in the furnace was estimated as the difference between the net heat available and heat carried out of the furnace in combustion products plus furnace-radiation losses. It was assumed that the temperature of ash at the furnace outlet was the same as that of the gases, and that of the slag tapped was 2700 F. A mean specific-heat value of 0.27 Btu per lb deg F was used for ash and slag. Heat content of furnace-exit gases was based on tables of Heck (7).

Results of Tests

Eighteen tests were run to study the effects of steam load and excess air with and without reinjection of fly ash. Operating data and results of the tests are shown in Table 1. The number of significant figures, given for derived data, is not an indication of precision; the precise figures are given in order that numerical relations should not be confused with rounding errors.

Tests 3 and 4 were planned without fly-ash reinjection. For these tests the fly-ash feeders were stopped and ducts without feeders were blocked by inserting plates inside the bolt circles of flange connections. Because it appeared that fly-ash recirculation was not stopped for these tests, blocks were placed in all lines, including those with feeders, before test 8, and recirculation was stopped throughout the 5-day period for tests 8 through 11, and tests 3 and 4 are shown in Table 1 as tests with fly-ash recirculation. Operating problems led to excess-air values distributed over the range from 13 to 36 per cent. The fuel was a West Virginia high-volatile bituminous coal.

Distribution of Temperature and Gas Composition. The furnace outlet temperatures at the indicated test points, for the first twelve tests, are given in Table 2. Excess air values for these tests are given in Table 3. Typical plots of temperature and of excess-air distribution are given in Fig. 2. The temperature patterns showed moderate variation with test conditions. There was a general tendency for higher temperatures to extend into the lower right corner of the furnace outlet. The excess air was generally higher on the left than on the right side. Allowing for greater cooling of gases flowing nearer the furnace walls, there was approximate correlation between high temperatures and low excess air. It appears, however, that rotational flow, and a shorter flow path may have contributed to higher temperatures in the lower right corner of the furnace outlet.

Table 1 Summary of data and results, ASME Furnace Heat-Absorption Tests, Boiler 25, Blaine Island Station, Charleston, W. Va.*

		1	2	3	4	5	6	7	8	9	10	11	12	A1	A2	B1	B2	C1	C2
1	TEST NUMBER																		
2	DATE	11-6	11-7	11-8	11-9	11-13	11-14	11-14	11-15	11-16	11-17	11-19	11-20	7-10	7-10	7-11	7-11	7-12	7-12
3	START OF TEST, EST, Daylight hours	10:52	10:05	9:35	10:10	11:15	8:50	1:30	10:00	10:00	10:15	10:15	9:00	5:00	7:00	10:30	12:45	10:00	12:45
4	END OF TEST, EST, Daylight hours	4:22	4:05	2:35	3:40	3:45	11:50	3:30	3:30	2:00	2:45	1:45	12:30	6:00	8:00	11:45	1:45	11:00	1:45
5	REINJECTION or NON-REINJECTION	R	R	R	R	R	R	R	N	N	N	N	R	R	N	R	N	R	N
6	STEAM FLOW, M lb per hr	285.6	196.1	204.5	287.0	284.3	285.4	197.0	290.4	285.3	213.0	207.9	291.0	251.4	252.1	285.8	283.8	261.2	254.8
7	RATE OF BLOWDOWN, M lb per hr	18.8	17.9	16.9	17.0	17.7	21.2	15.6	16.8	17.0	16.6	18.1	17.4	18.4	17.1	18.9	18.7	15.4	15.5
8	SUPERHEATER OUTLET HEADER PRESSURE, psig	619	618	618	623	620	622	618	625	619	618	619	623	616	613	616	621	618	619
9	STEAM TEMPERATURE AT SUPERHEATER OUTLET HEADER, °F	678	663	653	674	679	676	653	683	701	666	684	674	679	681	677	671	672	678
10	COAL FEED RATE, AS FIRED WEIGHT, lb per hr	25,806	17,661	18,143	25,624	26,013	25,997	18,070	26,575	26,606	19,536	19,308	26,720	24,553	24,973	28,291	27,626	25,629	25,345
	COAL, PROXIMATE ANALYSIS, percent as fired																		
11	MOISTURE	5.1	4.7	4.6	4.0	4.6	4.6	5.4	4.9	5.5	5.0	5.0	5.6	5.1	5.5	6.2	5.9	6.6	5.9
12	VOLATILE MATTER	37.4	38.2	37.7	37.1	37.0	36.9	36.6	35.8	36.8	36.8	36.7	37.2	38.0	37.5	36.8	37.3	37.2	37.3
13	FIXED CARBON	46.7	47.2	47.4	48.1	46.8	46.8	46.2	47.8	46.7	46.1	46.8	46.2	45.7	46.1	45.5	46.0	45.7	46.2
14	ASH	10.8	9.9	10.3	10.8	11.6	11.7	11.8	11.5	11.0	11.9	11.5	11.0	11.2	10.9	11.5	10.8	10.5	10.6
	COAL, ULTIMATE ANALYSIS, percent as fired																		
15	HYDROGEN	5.3	5.4	5.3	5.3	5.2	5.2	5.3	5.2	5.4	5.2	5.3	5.4	5.4	5.4	5.4	5.4	5.4	5.4
16	CARBON	68.6	69.2	69.0	69.3	67.7	68.0	67.0	67.9	67.7	67.2	67.4	67.3	68.0	68.2	66.9	67.1	67.5	68.1
17	NITROGEN	1.3	1.3	1.3	1.3	1.3	1.3	1.2	1.2	1.2	1.2	1.3	1.3	1.3	1.3	1.3	1.3	1.3	1.3
18	OXYGEN	11.6	11.8	11.6	11.0	11.6	11.0	12.6	11.9	12.4	11.9	12.2	12.8	11.8	12.0	12.8	13.2	13.4	12.7
19	SULFUR	2.4	2.4	2.5	2.3	2.6	2.8	2.1	2.3	2.3	2.6	2.3	2.2	2.3	2.2	2.1	2.2	1.9	1.9
20	HIGH HEATING VALUE, AS FIRED, Btu per lb	12,350	12,530	12,460	12,490	12,270	12,310	12,000	12,230	12,170	12,160	12,190	12,160	12,300	12,290	12,010	12,200	12,080	12,150
	ASH CONE FUSION TEMP., °F (ASTM)																		
21	I.D.T.	2050	2020	1950	2080	2020	2080	2080	2150	1990	1990	2030	1970	2080	2130	2250	2200	2180	2100
22	S.T.	2230	2170	2190	2220	2150	2190	2250	2270	2250	2240	2260	2270	2470	2450	2520	2510	2460	2470
23	F.T.	2470	2420	2380	2470	2440	2360	2470	2450	2470	2470	2520	2520	2600	2600	2620	2620	2620	2640
24	DUST LOADING AT STACK, lb per lb of coal	.0108a/	.0099	.0103	.0108	.0116b/	.0117	.0118	.0076	.0115	.0128	.0063	.0110	-	-	-	-	-	-
25	ASH-PIT REFUSE, lb per lb of coal	.0972b/	.0891b/	.0921b/	.0972b/	.1044b/	.1053b/	.1062b/	.0575b/	.0550b/	.0599b/	.0575b/	.0990b/	.0101b/	.0055b/	.0104b/	.0054b/	.0945b/	.0853b/
26	TOTAL CARBON LOSS, lb per lb of coal	.0009	.0005	.0009	.0010	.0003	.0006	.0004	.0040	.0032	.0046	.0030	.0009	0	.0020	0	.0060	.0010	.0160
27	DUST REINJECTED IN FURNACE, lb per lb of coal c/	.1215	.3738	.4820	.1053	.2084	.2963	.5416	0	0	0	0	.1845	.5634	0	.3818	0	.3833	0
28	AVERAGE TEMPERATURE OF GASES LEAVING FURNACE, °F d/	1802	1580	1562	1797	1769	1770	1617	1875	1934	1727	1837	1787	1623	1647	1723	1706	1618	1645
	AVERAGE COMPOSITION OF GASES LEAVING FURNACE, percent dry gas																		
29	$CO_2 + SO_2$	15.11	13.55	14.11	15.11	13.82	14.12	14.93	14.72	14.33	15.19	14.24	15.33	13.88	13.90	16.03	16.13	15.10	15.23
30	O_2 e/	3.90e/	5.67	5.03	3.90	5.36	5.02	4.10	4.34	4.78	3.81	4.89	3.65	5.24	5.24	2.83	2.73	3.94	3.72
31	N_2	80.99	80.78	80.86	80.99	80.82	80.86	80.97	80.94	80.89	81.00	80.87	81.02	80.88	80.86	81.14	81.14	80.96	81.05
32	EXCESS AIR AT FURNACE OUTLET, percent	22.02	35.85	30.17	21.65	33.22	30.44	23.52	24.70	28.13	20.83	28.68	20.31	32.32	31.91	15.12	13.62	22.27	18.48
33	DRY AIR FOR COMBUSTION, lb per lb of coal as fired	11.36	12.76	12.19	11.43	12.26	12.07	11.22	11.49	11.77	11.03	11.79	10.98	12.25	12.23	10.45	10.33	11.14	10.92
34	WET FLUE GAS AT FURNACE OUTLET, lb per lb of coal as fired	12.27	13.68	13.06	12.30	13.10	12.94	12.10	12.36	12.64	11.94	12.65	11.86	13.18	13.16	11.39	11.27	12.13	11.90
35	AVERAGE TEMPERATURE OF GAS ENTERING AIR HEATER, °F	658	608	612	669	672	657	603	678	708	630	659	636	661	675	652	671	638	669
36	AVERAGE TEMPERATURE OF GAS LEAVING AIR HEATER, °F	342	335	318	332	332	334	330	338	343	324	332	332	351	351	351	351	351	342
37	AVERAGE TEMPERATURE OF AIR ENTERING AIR HEATER, °F	75	70	50	48	57	60	77	73	54	42	53	47	86	86	81	85	87	96
38	AVERAGE TEMPERATURE OF AIR LEAVING AIR HEATER, °F	534	523	517	542	541	534	527	550	571	545	560	540	551	570	544	560	536	572
39	LOW HEATING VALUE OF COAL, AS FIRED, kB per hr	306,109	210,113	217,249	307,538	307,300	307,582	208,027	312,291	310,574	228,211	225,947	311,635	289,800	289,787	325,714	323,302	296,859	295,344
40	SENSIBLE HEAT ABOVE 80°F OF TOTAL AIR, kB per hr d/	25,939	16,730	16,347	25,290	28,584	25,997	15,983	28,561	30,002	16,419	19,226	24,675	26,537	27,589	25,581	26,597	24,138	25,904
41	SENSIBLE HEAT ABOVE 80°F OF REINJECTED DUST, kB per hr	222	437	562	184	370	528	660	0	0	0	0	335	1034	0	790	0	720	0
42	HEAT LOSS DUE TO UNBURNED CARBON, kB per hr	344	132	562	360	113	207	107	1,538	1,227	1292	829	344	66	855	143	2394	220	5763
43	HEAT AVAILABLE IN FURNACE, kB per hr	331,926	227,148	233,921	332,652	335,574	334,948	224,563	339,315	339,349	243,480	244,344	336,282	317,305	316,522	351,840	347,505	321,498	315,085
44	SENSIBLE HEAT IN WET GAS AT FURNACE OUTLET, kB per hr	151,533	97,670	95,664	149,510	158,090	156,452	92,159	163,853	173,644	105,268	118,702	149,801	136,798	136,908	147,181	140,597	131,960	130,667
45	SENSIBLE HEAT IN SLAG AND FLY ASH LEAVING FURNACE, kB per hr	3,361	3,744	4,697	3,026	2,728	3,861	4,257	2,278	1,959	1809	1355	2790	7636	1514	6962	1783	5831	1706
46	HEAT LOSS BY RADIATION FROM FURNACE, kB per hr f/	781	755	735	768	785	784	748	764	792	736	753	766	740	740	765	775	743	755
47	TOTAL SENSIBLE HEAT AND RADIATION LOSSES, kB per hr	155,675	102,169	101,096	153,304	161,595	161,097	97,165	166,895	176,397	108,383	120,811	153,336	145,174	141,361	154,908	143,155	138,533	133,128
48	HEAT ABSORBED IN FURNACE, kB per hr	176,251	124,979	132,825	179,348	173,979	173,871	127,398	172,420	162,952	135,035	123,533	182,945	172,131	175,160	197,032	204,351	182,964	181,957
49	SENSIBLE HEAT OF TOTAL AIR ENTERING UNIT, kB per hr	-336	-520	-1632	-2246	-1774	-1625	-138	-903	-1943	-1965	-1472	-2346	440	425	103	377	845	1105
50	TOTAL HEAT AVAILABLE IN UNIT, kB per hr	305,429	209,661	215,380	304,932	305,413	305,790	207,782	310,025	307,404	224,954	223,646	308,925	290,240	290,212	325,817	323,679	297,704	296,449
51	HEAT LOSS BY RADIATION FROM UNIT, kB per hr	1,562	1,669	1,470	1,536	1,564	1,568	1,496	1,528	1,587	1473	1506	1527	1480	1480	1529	1550	1486	1509
52	SENSIBLE HEAT IN WET GAS LEAVING UNIT, kB per hr	20,700	15,138	13,998	19,677	21,254	21,177	13,602	21,067	21,982	14,046	15,268	19,853	21,994	21,956	21,968	21,196	21,253	21,470
53	SENSIBLE HEAT IN SLAG AND FLY ASH LEAVING UNIT, kB per hr	1,792	1,112	1,201	1,781	1,942	1,953	1,368	1,163	1,126	889	848	1890	2785	1045	2759	1176	2453	1087
54	TOTAL HEAT LOSSES FROM UNIT, kB per hr	24,054	17,760	16,669	22,994	24,760	24,698	16,466	23,758	24,495	16,408	17,622	23,270	26,305	25,336	26,401	26,327	25,412	29,829
55	HEAT TRANSFERRED TO STEAM, kB per hr	281,375	191,901	198,711	281,938	280,090	281,051	191,315	286,493	282,708	208,547	206,023	285,655	263,847	264,876	299,416	297,362	272,293	266,620
56	NET HEAT AVAILABLE IN FURNACE, kB/(hr)(sq ft) f/	71.05	48.62	50.07	71.20	71.83	71.70	48.07	72.63	52.11	52.11	52.30	71.98	67.92	67.75	75.33	74.38	68.81	67.44
57	HEAT ABSORPTION IN FURNACE, kB/(hr)(sq ft) f/	37.72	26.75	28.43	38.39	37.24	37.22	27.27	36.90	34.88	28.90	26.44	39.16	36.84	37.49	42.17	43.74	39.16	38.95
58	FURNACE HEAT ABSORPTION EFFICIENCY, percent	53.10	55.02	56.78	53.91	51.85	51.91	56.73	50.81	48.02	55.46	50.56	54.40	54.25	55.34	55.98	58.81	56.91	57.75

a/ Calculated from relative dust loadings at furnace outlet and airheater inlet for all tests.
b/ Weighted average of 32 determinations and 8 extrapolated values at furnace outlet.
c/ Average of 32 determinations at furnace outlet.
d/ All enthalpy quantities referred to base of 80°F.
e/ One-half full load loss for entire unit as given by ABMA Standard Radiation Chart.
f/ Based on furnace water-cooled projected wall area of 4672 sq ft.
g/ No stack data - assumed same as test 12.
h/ Based on 10% loss up stack and 90% loss in slag pit.
i/ No flue-gas determination - estimated by comparison of overall averages for all tests.
j/ Based on 50% loss up stack and hoppers and 50% loss in slag pit.
k/ No stack data - assumed same as test 6.

* The number of significant figures given for derived data is not an indication of precision. The precise figures are given to preserve numerical relations.

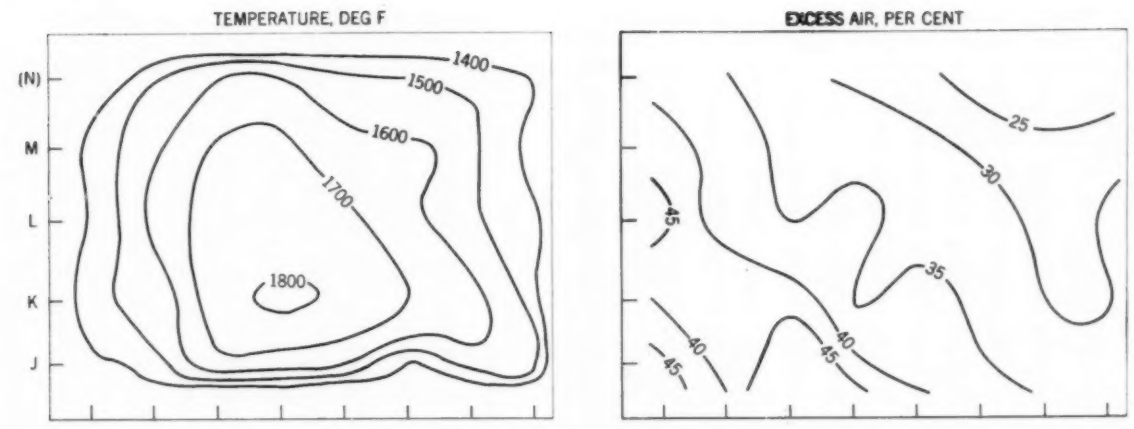

Test 2. Reinjection, load **196M**, 35.9% excess air

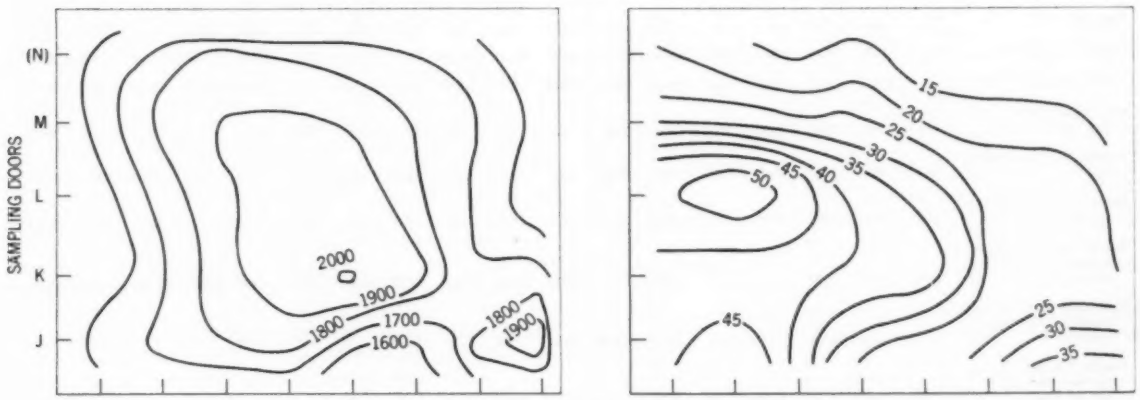

Test 6. Reinjection, load 285M, 30.4% excess air

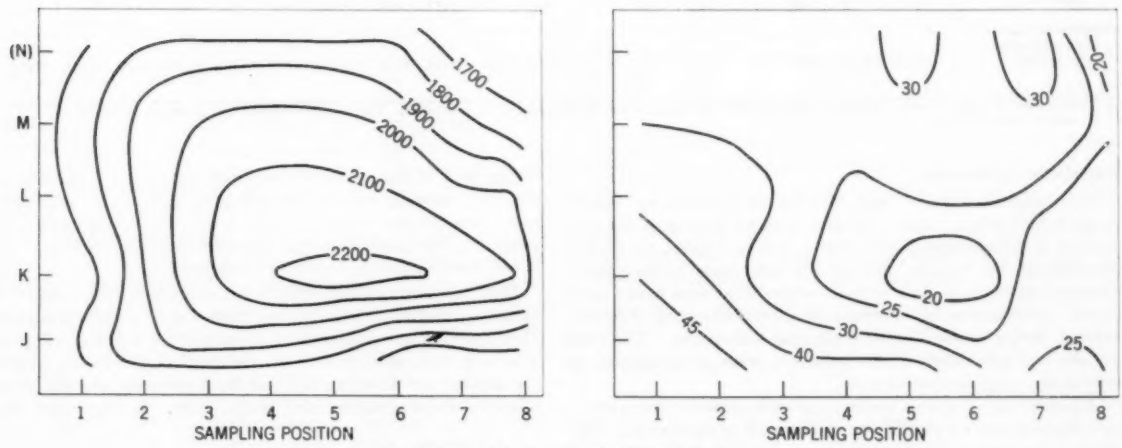

Test 9. Non-reinjection, load 283M, 28.1% excess air

Fig. 2 Distribution of temperature and excess air at furnace outlet

Table 2 Temperature of gas, deg F, at furnace outlet

Door	Heal-ing	Test No. 1	2	3	4	5	6	7	8	9	10	11	12
J	1	1590	1330	1520	1595	1630	1630	1620	1695	1720	1620	1710	1590
	2	1760	1470	1660	1760	1760	1720	1670	1900	1895	1670	1790	1650
	3	1850	1560	1780	1885	1860	1820	1780	1980	1950	1780	1850	1735
	4	1770	1640	1830	1895	1780	1840	1660	1890	1940	1820	1800	1690
	5	1710	1570	1530	1760	1650	1630	1620	1850	1920	1760	1695	1645
	6	1710	1420	1470	1720	1590	1590	1670	1695	1790	1880	1770	1830
	7	1680	1560	1710	1885	1880	1880	1795	1780	1780	1720	1840	1925
	8	1620	1510	1590	1820	1790	1930	1795	1880	1760	1640	1895	1920
K	1	1655	1470	1590	1620	1530	1590	1620	1570	1620	1630	1925	1500
	2	1815	1560	1660	1880	1760	1680	1705	1870	1885	1680	1880	1700
	3	1980	1750	1870	1980	1900	1850	1760	1980	2080	1760	1830	1830
	4	1905	1860	1710	2030	1950	1980	1720	2100	2195	1825	1965	1965
	5	1950	1780	1710	2015	1990	2000	1820	2150	2215	1925	1980	1970
	6	2080	1700	1660	1980	1850	1950	1850	2105	2215	1925	1990	1930
	7	1930	1630	1610	1890	1770	1920	1795	2005	2170	1925	1960	1860
	8	1820	1630	1660	1880	1780	1930	1880	2030	2075	1760	2040	1790
L	1	1630	1620	1660	1620	1580	1530	1630	1570	1760	1580	1660	1630
	2	1760	1680	1720	1770	1760	1750	1760	1820	1980	1760	1740	1730
	3	1875	1780	1650	1950	1925	1870	1650	1990	2080	1800	1890	1850
	4	1980	1960	1980	1998	2040	1990	1795	2090	2240	1960	2020	1980
	5	2020	1970	1790	2005	2030	1990	1880	2080	2130	1965	2000	1975
	6	2030	1830	1900	1980	1870	1960	1760	1970	2100	1930	1990	1870
	7	1860	1530	1660	1690	1800	1680	1790	1860	2020	1925	1960	1760
	8	1795	1620	1620	1500	1670	1530	1670	1800	1990	1965	1895	1695
M	1	1900	1660	1660	1830	1620	1830	1655	1690	1795	1535	1695	1690
	2	1925	1580	1800	1980	1790	1800	1560	1820	1980	1770	1775	1770
	3	1860	1710	1690	1890	1880	1900	1800	1960	2005	1825	1890	1875
	4	1900	1720	1780	1890	1920	1880	1685	2030	2030	1820	1980	1925
	5	1920	1660	1840	1900	1890	1885	1770	1990	2080	1790	1860	1985
	6	1980	1630	1820	1880	1860	1800	1795	1960	1990	1820	1900	1895
	7	1860	1580	1630	1860	1790	1900	1780	1850	1850	1815	1855	1780
	8	1900	1580	1580	1860	1840	1930	1860	1960	1930	1860	1890	1885

Table 3 Excess air, per cent, at furnace outlet[a]

Door	Heal-ing	Test No. 2	3	4	5	6	7	8	9	10	11	12
J	1	46.0	45.0	34.0	32.5	43.5	36.0	32.5	42.5	41.0	38.5	26.0
	2	41.5	38.0	37.0	34.0	46.5	38.0	29.0	38.5	34.0	34.5	26.5
	3	52.5	29.5	37.5	37.0	38.5	33.0	29.5	34.0	32.5	34.0	23.0
	4	41.5	29.5	33.0	32.5	28.5	29.0	23.5	32.5	19.0	32.5	21.0
	5	38.0	31.5	30.0	32.5	24.5	29.0	30.5	31.0	19.0	27.0	20.0
	6	36.0	27.5	27.5	28.0	24.5	21.5	21.0	26.0	13.5	25.0	20.5
	7	31.5	29.0	22.5	29.5	31.0	18.0	21.0	26.0	11.0	28.5	19.0
	8	31.5	29.0	26.0	29.5	31.0	19.0	18.0	25.5	11.5	28.0	23.0
K	1	40.5	46.0	27.5	36.0	43.0	36.5	49.0	39.0	33.5	46.5	29.5
	2	43.0	38.0	27.5	41.5	43.5	21.5	35.0	34.0	31.5	38.0	21.5
	3	43.5	38.0	26.0	35.0	42.0	23.0	28.5	26.5	26.0	30.5	22.0
	4	35.0	34.0	21.0	34.0	38.0	22.0	27.0	24.0	24.5	30.5	22.0
	5	38.0	32.0	27.5	29.5	36.5	19.0	24.0	18.0	28.5	29.5	20.0
	6	32.5	31.0	19.0	31.5	26.0	17.0	23.5	16.5	16.0	23.0	23.0
	7	30.0	31.5	19.0	27.0	28.5	22.0	23.0	27.5	16.5	21.0	20.5
	8	30.0	31.5	17.0	30.0	28.5	25.0	25.0	28.5	18.0	16.0	19.5
L	1	45.5	29.5	27.5	36.0	49.5	22.0	32.5	33.0	34.0	37.5	21.5
	2	37.0	26.5	26.0	36.0	52.5	23.0	27.5	33.0	27.5	29.5	21.0
	3	35.0	23.0	24.0	36.5	47.5	20.0	24.5	29.0	25.0	28.5	19.0
	4	36.0	24.5	22.0	31.0	35.0	20.0	24.5	24.5	27.0	28.5	18.0
	5	32.5	23.0	18.0	31.0	27.5	19.0	21.0	25.0	22.5	29.0	14.0
	6	32.5	20.0	17.5	41.0	23.5	32.0	21.0	25.5	22.0	27.5	10.0
	7	27.5	23.0	15.0	29.5	23.5	28.0	24.5	26.5	23.5	24.5	12.5
	8	31.0	19.0	18.5	24.5	18.0	28.5	21.5	28.5	24.5	22.0	18.0
M	1	42.5	24.5	26.0	40.0	30.0	23.0	25.5	30.0	20.0	32.5	23.0
	2	37.0	29.0	19.0	39.5	29.0	23.0	28.0	29.5	20.5	36.0	21.0
	3	33.5	29.0	19.5	36.5	29.5	22.0	28.0	28.5	19.0	28.0	19.5
	4	33.5	31.0	16.0	34.5	25.5	20.0	23.0	26.5	19.0	27.5	19.5
	5	30.5	30.5	13.5	31.5	19.0	18.0	19.5	29.0	20.5	27.5	18.0
	6	28.5	31.0	11.0	31.5	17.0	19.0	22.0	27.0	20.0	27.0	18.5
	7	27.5	33.0	14.0	28.5	18.5	19.0	17.5	28.5	18.5	23.0	18.0
	8	27.5	45.5	7.5	26.5	18.0	17.5	20.5	23.5	18.5	23.5	21.0

a/ Obtained from oxygen meter readings.

Table 4 Abridged summary of data[a]

Test No.	1	2	3	4	5	6	7	8	9	10	11	12	A1	A2	B1	B2	C1	C2
Excess air, percent	22.02	35.85	30.17	21.65	33.22	30.44	23.52	24.70	28.13	20.83	28.68	20.31	32.32	31.91	15.12	13.62	22.27	18.48
Steam flow, M lb/hr	285.6	196.1	204.5	287.0	284.3	285.4	197.0	290.4	283.3	213.0	207.9	291.0	251.4	252.1	285.8	283.8	261.2	254.8
Recirculation of fly ash	Yes	Yes	Yes	Yes	Yes	Yes	Yes	No	No	No	No	Yes	Yes	No	Yes	No	Yes	No
Adiabatic flame temp., T_a, °R	3905	3640	3700	3925	3760	3765	3780	3895	3850	3920	3825	3925	3690	3775	3945	4060	3825	3910
Furnace outlet temp., to, °F	1802	1580	1562	1797	1769	1770	1617	1875	1934	1727	1837	1787	1623	1647	1723	1706	1618	1645
Molar flow of gaseous combustion products, moles/hr	10691	8079	7983	10593	11479	11332	7374	11071	11342	7848	8233	10664	10949	10945	10875	10504	10527	10220
Residence time of hot gases in furnace, seconds	3.05	4.38	4.40	3.07	2.92	2.96	4.65	2.91	2.84	4.19	3.99	3.05	3.21	3.16	3.05	3.11	3.27	3.30
Pounds fly ash through furnace per pound ash in coal	3.06	8.00	5.37	2.37	3.57	5.22	4.17	1.23	0.90	0.43	0.66	4.76	-	-	-	-	-	-
Enthalpy to superheated steam, H_{sh}/M, Btu/mol of flue gas	3593	2998	3041	3571	3341	3350	3163	3591	3694	3439	3470	3594	3093	3140	3520	3513	3233	3337
(Adjusted to 25% excess air)	3548	3160	3118	3522	3463	3430	3141	3587	3740	3377	3525	3524	-	-	-	-	-	-
Furnace heat-absorption efficiency, E_f, percent	53.10	55.02	56.78	53.91	51.85	51.91	56.73	50.81	48.02	55.46	50.56	54.40	54.25	55.34	55.98	58.81	56.91	57.75

a/ The number of significant figures, given for derived data, is not an indication of precision. The precise numbers are given to preserve numerical relations.

Correlation of Results

An abridged summary of data used for correlation of test results is given in Table 4. This table also includes data on molar flow rates of gaseous combustion products, residence times, the flow of ash through the furnace, and the adiabatic flame temperatures. Correlations of these data were developed that were based upon linear combinations of functions of appropriate variables, permitting better application of statistical techniques. The data equally well may satisfy other theoretical or empirical expressions within the range of observation.

A partial survey of dust loading was made at mid-furnace elevation through ports F and G over the left half of the furnace. The ratio of the flow of fly ash to the total flow of ash from the coal fed is plotted against the adiabatic flame temperature in Fig. 3. Without recirculation, a portion of the ash is immediately carried to the slag bed, and the flow ratio should be less than 1. Possibly 90 per cent of the ash, with recirculation, should eventually be carried to the slag bed; but the necessary amount of recirculation, and hence the flow ratio, should fall with increasing flame temperature. The indicated ratios appear reasonable, provided tests 3 and 4 are classed as tests with recirculation.

Heat transferred to superheated steam was directly related to furnace-outlet conditions, because there was no superheat control. Heat transferred to superheated steam per mol of flue gas, H_{sh}/M, Btu/mol, was calculated on the assumption that steam entered the superheater at saturation and drum pressure, and left at the observed steam pressure and temperature. It was found that

$$\frac{H_{sh}}{M} = 787.4 + 1.7169\, t_o - 14.88\,(EA) \quad \ldots\ldots [1]$$

where t_o is the furnace-outlet temperature, deg F, and (EA) is

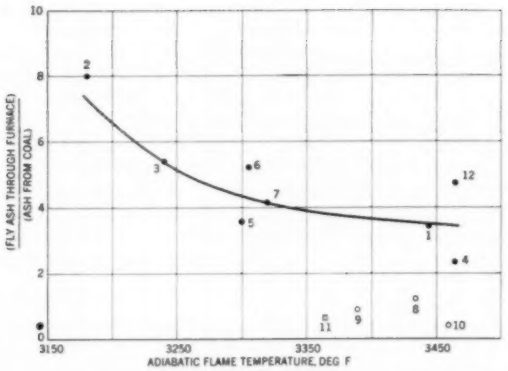

Fig. 3 Ratio of fly ash to ash from coal versus adiabatic flame temperature

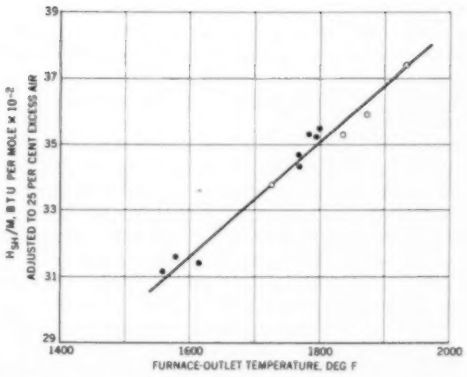

Fig. 4 Heat transferred to superheated steam per mol of flue gas versus furnace-outlet conditions

the per cent excess air. Heat transferred to steam per mol of flue gas, corrected to constant excess air, is plotted in Fig. 4 against furnace-outlet temperature. The probable error of estimate of furnace-outlet temperature, by inversion of Equation [1], was found to be 15 F. Since the temperature was obtained as an average of 32 measurements, this corresponded to a probable error, for a single observation, of 85 F. Heat transfer to superheat was independent of fly-ash recirculation. This correlation was used for estimating furnace-outlet temperatures for tests A1 through C2 and also showed that there were no extraneous values of furnace-outlet temperature among data for the first twelve tests.

The furnace heat-absorption efficiency is plotted against excess air as a function of steam flow in Fig. 5. The data were divided into groups, for each of which the efficiency decreased with increased excess air and with increased steam load. Data of the first series of tests may be divided into two groups, tests 1–7, tests 8–11. Data of test 12 would fit in either group. These groups corresponded to tests with or without fly-ash recirculation.

The furnace efficiencies for tests A1, A2, C1, and C2, alternately with and without fly-ash recirculation at medium load, were slightly lower but nearly equal to efficiencies for the earlier tests with fly-ash recirculation and at low load. Tests B1 and B2 were run under the normal operating conditions of high load and low excess air. The furnace efficiencies for these tests fell in line with earlier data at high load.

The correlation with excess air and boiler load, as measured by steam flow, is the correlation related most directly to operation, but it depends upon variables having complex relationship to the heat-transfer process. The excess air influences both the flame temperature and the volume-flow rate of gas. The steam flow is a result of the heat input and is involved with the furnace efficiency, the factor under study.

Variables of fundamental significance are the time of residence in the furnace of a given volume of combustion products and the intensity of radiation from the furnace contents. The residence time θ can be estimated, for this purpose, as the ratio of furnace volume to volume flow rate, using 20,600 cu ft as the furnace volume, and the average of adiabatic and furnace-outlet temperatures in estimating volume flow rate from molar flow rate. The flow of radiant energy depends upon temperatures, flame shape, furnace geometry, gas composition, dust loading, and fuel characteristics. For a given furnace, flame geometry, and fuel, variation of the adiabatic flame temperature T_a is primarily responsible for variation of the radiant intensity. The appropriate function of T_a, excepting a constant of proportionality, is $T_a{}^4$.

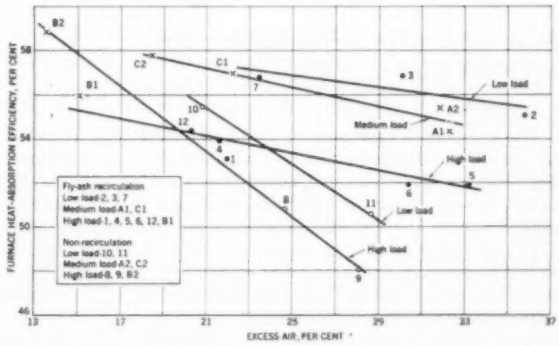

Fig. 5 Furnace heat-absorption efficiency as affected by steam load and excess air

Correlation of furnace heat-absorption efficiency E_f with these fundamental variables led to the following equation:

$$E_f = 35.5 + 2.98\theta + 3.88 \times 10^{-14}T_a{}^4 \quad [2]$$

for tests of the first group with fly-ash recirculation. For this equation, T_a must be measured on the Rankin scale. Furnace efficiencies for the second group of tests (8–11, run without fly-ash recirculation) satisfy a similar equation with the same coefficient of residence time:

$$E_f' = -5.2 + 2.98\theta + 20.48 \times 10^{-14}T_a{}^4 \quad [3]$$

Furnace efficiencies for the third group of tests were fitted with a similar equation with different coefficients:

$$E_f'' = 14.3 + 9.12\theta + 5.84 \times 10^{-14}T_a{}^4 \quad [4]$$

Graphic representations of Equations [2–4] require three-dimensional plots. Two-dimensional representations may be based upon transformations of these equations:

$$E_f + 2.98(\theta_0 - \theta) = (35.5 + 2.98\theta_0) + 3.88 \times 10^{-14}T_a{}^4 \quad [5]$$

$$E_f + 3.88 \times 10^{-14}(T_{a0}{}^4 - T_a{}^4) = (35.5 + 3.88 \times 10^{-14}T_{a0}) + 2.98\theta \quad [6]$$

$$E_f' + 2.98(\theta_0 - \theta) = (-5.2 + 2.98\theta_0) + 20.48 \times 10^{-14}T_a{}^4 \quad [7]$$

$$E_f' + 20.48 \times 10^{-14}(T_{a0}{}^4 - T_a{}^4) = (-5.2 + 20.48 \times 10^{-14}T_{a0}) + 2.98\theta \quad [8]$$

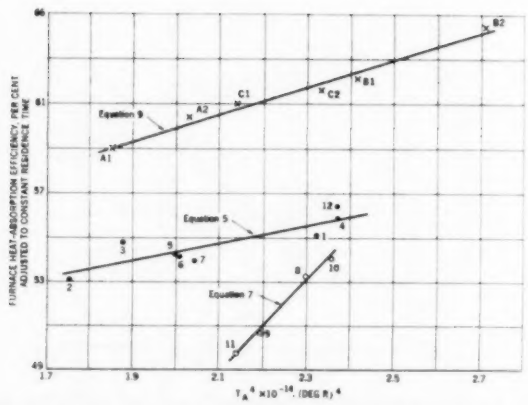

Fig. 6 Dependence of furnace heat-absorption efficiency upon adiabatic flame temperature

$$E_f'' + 9.12(\theta_0 - \theta) = (14.3 + 9.12\theta_0) + 5.84 \times 10^{-14} T_a^4 \ldots [9]$$

$$E_f'' + 5.84 \times 10^{-14}(T_{a0}^4 - T_a^4) = (14.3 + 5.84 \times 10^{-14} T_{a0}^4) + 9.12\theta \ldots [10]$$

The left sides of Equations [5–10] are the efficiencies corrected for variation of residence time or of adiabatic flame temperature. Fig. 6 shows the efficiencies, adjusted to an arbitrarily chosen value, $\theta_0 = 3.72$ sec, on the basis of Equations [5, 7, and 9] plotted against the indicated function of adiabatic temperature. Fig. 7 shows the efficiencies, adjusted to $T_{a0} = 3761\ R$ according to Equations [6, 8, and 10] plotted against residence time. Figs. 6 and 7 show that the test data may be divided into three groups with respect to furnace heat-absorption efficiency. Data from tests of the first series, as indicated in Fig. 5, comprise the first two groups, and data from tests of the second series, A1–C2, comprise the third group.

Discussion of Results

The correlations show the effect of operating conditions upon heat absorption in the boiler furnace. The correlations with excess air and steam load, Fig. 5, are useful for operating purposes. Interpretation is clearer when correlation is based upon residence time and flame temperature, Equations [2–4] and Figs. 6 and 7.

Flow patterns are ignored in estimating residence time. Much of the gas may flow through a fraction of the volume in less than the estimated time, and the converse may hold in other parts of the furnace volume. Since such effects are relatively constant or change regularly with flow rate, the result is a proportional change in the coefficient of residence time, which should be considered in comparisons of different furnaces but need not be considered for the given furnace with one fuel and burner arrangement.

Several variables are ignored in using the adiabatic flame temperature as a measure of intensity of radiation. An appropriate average temperature would be lower than the adiabatic. Use of some average between the adiabatic and furnace-outlet temperature is objectionable for statistical reasons, because the latter is a measure of furnace efficiency, the variable under study. As with residence time, the adiabatic flame temperature is an appropriate variable for study of furnace efficiency, although the coefficient may depend further upon the particular furnace design and the fuel.

The furnace heat-absorption efficiencies fell into three groups, each correlating with the same operating variables but with different coefficients. The first group resulted from tests with fly-ash

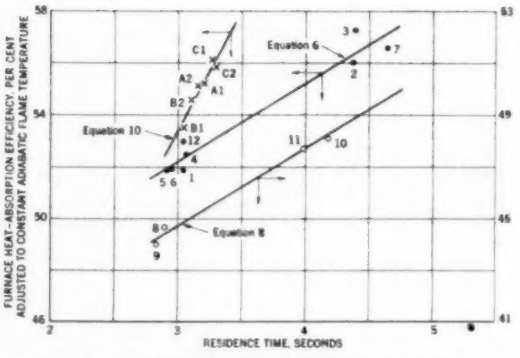

Fig. 7 Dependence of furnace heat-absorption efficiency upon residence time

recirculation, the second from tests without recirculation, and the third tests both with and without fly-ash recirculation. It must be concluded that some variable was changed between tests of different groups that was not changed within a given group of tests. The variable was not fly-ash recirculation, because this variable was changed within the last group of tests.

Different methods of stopping fly-ash reinjection were used. For the second group of tests ash feed lines were blocked, but airflow was maintained through the reinjection nozzles. Fly-ash reinjection was stopped for alternate tests of the third group by stopping the reinjection air fan. Visual observation of reinjection nozzles and stack effluents, and decreased density indication of a smoke recorder placed in a duct ahead of the induced draft fan showed that fly-ash recirculation was effectively stopped for these tests.

Stopping the reinjection air fan changed the air distribution to the flame. Optical pyrometer observations of the flame, through doors just above the burners, showed nearly a 300-F rise near the rear burners and a slight temperature fall near the front burners when the reinjection air fan was stopped. For tests B2 and C2, a compensation was made by a shift of secondary air from the front to the rear burners that was estimated to be equivalent to the reinjection air. Although this shift was not made for test A2, efficiencies of the third group of tests were all consistent, without regard to fly-ash recirculation. Methods of stopping fly-ash recirculation were different, but it does not seem reasonable that they could have caused the observed differences in heat absorption.

The furnace responded to burner adjustments. Visual observation showed that the flame position could be shifted by changing the relative mass flow through front and rear burners; the flame shape could be altered by directing one set of burners more toward the slag pool; and the temperature distribution could be changed by a shift of secondary air from front to rear burners. The response was such that the boiler operators had learned to use burner adjustments to move the flame for control of slag accumulations just above the melting zone.

Alternate tests of the third group, with and without fly-ash recirculation, were run on the same day, with complete control of burner adjustments and with removal of any accumulations of slag that might interfere with burner performance. Observations through the slag tap hole, during test C1, showed that impingement resulted in a sheet of flame directed downward and spreading toward the front and the rear over the slag pool. Observation through ports just over the burners indicated well-balanced flame throughout the last series of tests.

Higher furnace heat absorption, under otherwise similar conditions, indicated that the flame was well centered in the bottom

of the furnace during the last group of tests. The lower efficiency and stronger dependence upon flame temperature shown by coefficients of Equation [3], observed for the second group of tests, might be expected if the flame was off center and extended up either the front or rear wall. Under such conditions, the residence time for most of the gas would be less than the values given.

Responsiveness to burner controls, with lack of quantitative measures of resulting changes in the flame, introduced unexplained variability in furnace heat-absorption efficiency. Nevertheless, it may be concluded that variations in furnace heat absorption resulted from changes in flame distribution with no significant effect of fly-ash recirculation.

Acknowledgments

The authors gratefully acknowledge the contributions to this investigation made by the following:

The ASME Special Research Committee on Furnace Performance Factors, for the opportunity to participate in this project, and the individual committee members for helpful suggestions.

The officials of Carbide and Carbon Chemicals Company, D. C. Calhoun, assistant superintendent, and staff, for assistance in preparing and conducting the tests.

W. E. Archer and M. A. Yoder, Western Precipitation Corporation, who contributed data on dust loadings through the air heater and to the precipitator.

The service engineers and the research and design engineers, Riley Stoker Corporation, for their part in preparing for and conducting the tests, and particularly E. C. Miller, research engineer, for co-operation in conducting the last series of tests.

G. R. Kollar and J. Leff, Combustion Section, Bureau of Mines, for assistance in conducting tests.

J. W. Myers, Acting Chief of the Branch of Bituminous Coal, Pittsburgh Experiment Station, Bureau of Mines, for assistance in planning and conducting the tests.

References

1 J. W. Myers and R. C. Corey, "Furnace Heat Absorption in a Spreader-Stoker-Fired Steam Generator," TRANS. ASME, vol. 75, 1953, pp. 909–923.

2 A. R. Mumford and R. C. Corey, "Variation in Heat Absorption in a Natural-Gas-Fired, Water-Cooled Steam-Boiler Furnace," TRANS. ASME, vol. 74, 1952, pp. 1191–1215.

3 L. B. Schueler, W. T. Reid, Paul Cohen, R. C. Corey, A. R. Mumford, C. G. R. Humphreys, and G. W. Bice, "An Investigation of the Variation in Heat Absorption in a Pulverized-Coal-Fired Water-Cooled Steam-Boiler Furnace—Parts 1 to 4," TRANS. ASME, vol. 70, 1948, pp. 553–619.

R. I. Wheater, M. H. Howard, R. C. Corey, Paul Cohen, and H. H. Hemenway, "Furnace Heat Absorption in Paddy's Run Pulverized-Coal-Fired Steam Generator, Using Turbulent Burners, Louisville, Kentucky," Parts 1 to 3, TRANS. ASME, vol. 72, 1950, pp. 893–948.

J. W. Myers, R. C. Corey, F. G. Ely, and N. H. Twyman, "Furnace Heat Absorption in Pulverized-Coal-Fired Steam Generator, Willow Island Station," Parts 1 and 2, TRANS. ASME, vol. 73, 1951, pp. 419–459.

4 P. Cohen, R. C. Corey, and J. W. Myers, "Methods and Instrumentation for Furnace Heat-Absorption Studies: Temperature and Composition of Gases at Furnace Outlet," TRANS. ASME, vol. 71, 1949, pp. 965–978.

5 F. G. Feeley, Jr., "Fly-Ash Refiring," TRANS. ASME, vol. 78, 1956, pp. 1747–1755.

6 J. W. Myers, S. A. Goldberg, and R. W. Smith, Jr., "Calculation of Theoretical Flame Temperatures in Furnaces," TRANS. ASME, vol. 80, 1958, pp. 202–216.

7 R. C. H. Heck, "The New Specific Heats," *Mechanical Engineering*, vol. 62, 1940, pp. 9–12.

Discussion

F. G. Ely.[5] A word of appreciation should first be said to the authors, and to the several sponsors who are responsible for carrying out this test project. As many of us know, such data on furnace performance are difficult to obtain, and the labor does not end with test measurement, but continues through a maze of calculation and attempts to correlate results in a meaningful way.

The salient features of this unit, which initially led the ASME Committee to undertake tests, are that with the coal used at this plant it is a slag-tap furnace, which reinjects its own fly ash into the furnace and maintains clean heating surface without the need of soot blowers. The unusual features of the tests are that measurements were made of gas temperature at the furnace outlet and sufficient auxiliary data were acquired to calculate furnace heat-absorption efficiency, presented here as the ultimate criterion of performance.

Various correlations have been made to show the effects of load and excess air, of ash reinjection and nonreinjection, and to indicate relationships with the basic parameters of adiabatic flame temperature and residence time. The conclusions show a resulting over-all performance, but regrettably do not explain the how or why of this performance.

In general terms, one may look for such an explanation in gross factors such as: (*a*) The design parameters of heat available per sq ft of furnace surface, (*b*) the method of firing, (*c*) the geometry of the furnace, (*d*) the nature of the fuel, and (*e*) the influence of fly-ash reinjection.

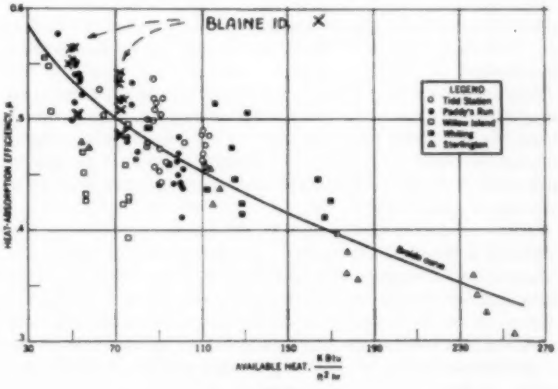

Fig. 8

With regard to the first of these, it seems appropriate to show a comparison with Fig. 8 from a previous paper by the author's associates.[6] Points for the Blaine Island tests have been superimposed on this plot of other tests run under the auspices of the ASME Committee.

(In this plot, the furnace heat absorption efficiency of all tests is plotted against heat-available rate per sq ft of water-wall surface, and the Broido curve is shown for reference.)

It is apparent that Blaine Island has a high value of furnace absorption efficiency, which is synonymous with low exit-gas temperature and indicative of clean furnace walls. In this respect it is similar to the points for Paddy's Run at the lower loads, which also was characterized by relatively clean furnace walls, but had front-wall firing. The low furnace temperature is compatible for a unit like Blaine Island, where steam at 620 psig and 680 F is required. These low steam and saturation temperatures may be of

[5] Consultant, Research and Development Department, The Babcock & Wilcox Company, Alliance, Ohio. Mem. ASME.

[6] Murray Greyson, G. P. Mazie, J. W. Myers, R. C. Corey, and E. G. Graf, "Evaluation of Factors Affecting Heat Transfer in Furnaces," TRANS. ASME, vol. 78, 1956, pp. 1741–1746.

some, perhaps minor, influence in maintaining ash-free conditions of the heat absorbing surfaces.

It is also apparent from the figure that the rate of furnace loading is conservative, tests at full load being at approximately 72,000 Btu/sq ft hr.

Furnace geometry and firing arrangement, with downward opposed burners, have been used in various forms for a number of years. Broadly speaking, this unit can be regarded as having a two-stage furnace which develops high turbulence and heat release in the lower portion, producing high temperatures obviously needed for fluid slag. The water walls below the throat are normally slag-covered, and the refractory bottom chamber is undoubtedly beneficial to tapping. Heat-release rate in the lower chamber, roughly calculated as 76,000 Btu/cu ft or 375,000 Btu/sq ft of water-cooled surface, is somewhat severe for a refractory structure, but to facilitate tapping this section might be regarded as expendable. In many cases this would be an objectionable limitation.

It is conceivable that the sloping arches of the throat section tend to divert the gas stream away from the front and rear walls of the upper furnace, also that an eddy or downward flow of cooled gas along these walls may act as a deterrent to deposit of ash. It would have been interesting to include, as part of the test observation, a study of the gas flow pattern, augmented by additional temperature traverses at lower elevations of the upper furnace.

The arch configuration is present only in the front and rear walls, and there would seem to be no corresponding logic to explain the absence of slag on the vertical side walls as far as gas-flow pattern is concerned. This feature may then be of secondary importance.

The next item of fuel characteristics is one of the hardest to evaluate. The coal is described as Pittsburgh No. 8 seam, mined locally in West Virginia. Conventional analyses are given, showing ash-softening temperature from 2160 to 2280 F for the principal series of tests, and about 200 deg higher (2450 to 2520 F) in the supplementary tests.

These values are consistent with determinations made at The Babcock & Wilcox Company's Alliance laboratory on preliminary samples from this unit taken in 1955, which show 2340 and 2280 softening temperature of the coal-ash and tap-slag respectively. When run under oxidizing conditions, these samples showed an increase of about 200 deg to 2540 and 2490 F softening temperature.

Additional tests of the sintering strength of precipitator fly ash, taken in 1955, showed a moderately friable structure, having crushing strength of 4450 psi as compared to 45,000 psi for a Central Illinois coal when treated at 1700 F by the method of Barnhart and Williams, TRANS. ASME, vol. 78, 1956, pp. 1229–1236. Fly ash from the mechanical collector was too coarse to form a pellet for making the sintering test.

Another set of coal samples, sent to Germany, and reported by Dr. Gumz in a letter which was later distributed to the Committee, contains the findings of a differential thermal analysis used for identification of mineral constituents of the ash. Kaolinite and montmorillonite were found to be the predominant minerals, with "only a small amount of illite present, which is usually the principal source of alkalies." It is stated that, "in our experience, alkali content of the coal minerals are especially contributory to deposit formation, because they produce low-melting compounds on the tube walls which lead to deposit build-up because of their stickiness." The further comment is made: "according to our opinion, the reason for the excellent results is twofold; a moderate heat release in the combustion chamber, and a very good-natured coal . . . the coal sample which we have examined is a type which should not give any trouble in most types of boiler furnaces."

Fly-ash reinjection provides a useful means of disposing of this unwanted product. Some theories have been expressed that the addition of cool fly ash is instrumental in removing troublesome alkali constituents from the gas stream; others that the high population of recirculated fly ash might increase heat transfer by the mechanism of particle radiation.

The data of Fig. 3 show comparatively high dust loading of gases in the furnace. If the extreme point for test 2 were disregarded, the trend with adiabatic flame temperature would be less apparent; however, an average ratio of about four times the ash in the coal is indicated. This is equivalent to a dust loading of approximately 40 lb/1000 lb of gas.

At these concentrations there is a good possibility that particle cleaning of tube surfaces is obtained, as we know it to happen in units fired by spreader stokers. The effect would not be noticeable in short-time consecutive tests. Although not an extremely coarse dust, experience has shown that there is a precarious balance between realizing the beneficial effects of cleaning and the undesirable consequences of tube erosion, which makes this situation of debatable advantage.

In other units, such as those reported by Maull and McMahon at Marion and Seawaren Stations in New Jersey, fly-ash refiring apparently increased the dust loading about 50 per cent in the furnace gases. With refiring of fly ash to the vortex of a cyclone furnace, now being practiced in several plants, it has been found that 85 per cent of the ash is captured in the first cycle, and dust loading through the unit is increased about 15 per cent.

In conclusion, it is the writer's opinion that test data of this nature are of great value in the analysis of furnace performance and should be extended to include more complete surveys of operating conditions in the units tested. The effort to resolve such observations to basic correlations is applauded, and the investigations should be strongly supplemented by scientific principles and knowledge already available from other fields.

In view of the many simultaneous and complex variables involved, the design of boiler units, for the time being, may have to remain something of an art, with which breakthroughs can occur occasionally, but these should be looked at with some wholesome degree of skepticism.

F. G. Feeley, Jr.[7] Only the highest of praise can be given this paper and the persons who have contributed to its contents. The major conclusion to be drawn from it is that the testing of large boiler furnaces is an inexact science which is perhaps affected at least as much by variables beyond our control as by those within our control.

It should be pointed out that the 250,000-lb-per-hr rating of this boiler is at a feed-water temperature of 240 F. At the prevailing feed-water temperature, 385 F, the boiler is rated at 289,000. Accordingly, none of the data for this study were obtained under conditions exceeding the nominal full rating. One or more tests at overload conditions might have been very interesting inasmuch as this discusser's observations of the unit have been that it is almost too conservatively rated and is undoubtedly capable of continuous operation—at least in so far as heat absorption and slagging are concerned—at ratings 15 to 20 per cent above design.

Data presented in other furnace studies have shown that furnace gas temperatures drop precipitously as the flowing stream approaches the slag screen. This being the case, it is unfortunate that the furnace-outlet temperatures on these tests were obtained so close to the slag screen since much of the erratic temperature data might well be due to differences of only a few inches between the probe tip and the slag screen on different readings at supposedly the same station.

It is gratifying to those of us who selected a pressure-type cas-

[7] Development Engineer, Olin Mathison Chemical Corporation, New York, N. Y. Mem. ASME.

ing for this boiler, even though it is a balance-draft job, that the oxygen concentration in flue gas at the furnace outlet and the induced-draft fan discharge were shown to be identical. Such freedom from setting leakage should assuredly have paid out before now the increased cost of the tighter setting.

This discusser would like very much to have seen a repeat run of test 8 after test 11 during which the boiler had run for five days without fly-ash reinjection. While not shown by the furnace absorption efficiency, there is a trend in steam temperature which would indicate that some fouling of furnace waterwalls had occurred in this time that would have showed up in higher steam temperature under identical operating conditions at the conclusion of the five-day run. Could the author inform us as to any visual observations regarding wall cleanliness made at the end of the five days?

The substantial variation in dust reinjected to the furnace per lb of coal fed needs some explanation. Examination of the data indicates a trend toward increased reinjection with decrease in boiler loading. Assuming that this means the energy content of returning dust particles is sufficient to cause their entrapment in the slag bed, it would dictate the design of this type of furnace for higher than normal burner velocities as a means of decreasing the admittedly high furnace dust loading.

Earle C. Miller.[8] It has been very interesting to follow the test work which led up to this presentation. The authors are to be congratulated on the paper, the testing, and upon the analysis of the test work. The study has been followed with interest by many throughout the world for there has been much discussion as to the reasons for the unusual behavior of this particular furnace and other furnaces of this design; for it was known that this particular unit remained slag free without the need for lancing and soot blowers while in the same plant units with comparable heat-release rates required hand lancing and soot blowers as normal procedure. In addition, other units of the same design were operating on coals having much lower ash-fusion temperatures and were remaining clean with neither hand lancing nor blowers. It was thought that a study of the furnace heat absorption would shed light on the reason for the clean furnace walls and it would appear as though it has.

The very excellent correlation in the three families of curves illustrating the dependence of furnace heat absorption upon adiabatic flame temperature, Fig. 6, and upon resident time, Fig. 7, shows very conclusively that the furnace heat absorption is also dependent upon the flame placement. Certainly the flame placement within the furnace would influence the actual resident time. A study of flame placements in the furnaces previously studied by this research committee, with an analysis of these data on the basis of resident time, might eliminate some of the apparent differences that were evident in the prior tests. Comments by the authors on this would be appreciated.

The influence of burner adjustment upon the placement of flame within the furnace and upon superheat had been noticed on this and similar units on oil, gas, coal, and fluid coke. This had been reduced to a comparison between the furnace-exit gas temperatures of this type of unit as compared to conventional units and reported in previous discussions.[9] However, the spread of approximately 200 deg in the furnace-outlet temperatures for a given load point was greater than had previously been detected but none of these furnaces had been operated at their maximum outlet temperatures at full load nor had they operated at their minimum temperatures at low loads.

It is noted that the range of ash-fusion temperature for the tests reported is 2360 to 2640 F. This design has now operated with ash-fusion temperature range of 1900 to 2748 F. As the authors have pointed out the placement of the flame within the furnace and with relation to the slag pool can be controlled. Control of the flame position with respect to the wet bottom permits the use of higher-fusion-temperature ashes in this furnace than is normally considered practical for slag-tap units. It should be pointed out that in the test furnace slag is tapped from along the side where the temperatures are known to be lower than they are in the center of the furnace where the slag-tap holes of the units of later design are located.

William T. Reid.[10] What may appear at first glance in this paper to be an exercise in rhetoric and bookkeeping is actually an ambitious attempt to settle once and for all why this boiler furnace remains so remarkably free of slag deposits. It burns a fuel and is of a general design that invariably causes the usual troubles from slagging. Dr. Orning and his associates at the Bureau of Mines have done their traditionally excellent job of furnace testing and later correlation of data. One might well expect, however, that they could also have answered the basic question behind this study: "Why does this furnace remain clean?"

That they ignore this point is not difficult to explain. The facts seemingly are that the tests turned up no unusual furnace conditions showing why slagging did not occur. The data show nicely the correlations between operating conditions and heat absorption in the furnace—correlations that should be helpful both to the manufacturer and the customer—but they do not add measurably to our knowledge of wall slagging. The authors recount in convincing fashion that the furnace responded well to burner adjustments, and that the temperature distribution and the shape of the flame could be modified at will. But they do not answer the important question as to the effect of flame adjustment on slagging.

The point here is not that a poor job of furnace testing had been done, for in reality the tests were thoroughly and intelligently carried out. Rather, it is that the problem of slagging is so incompletely understood and so perplexingly complex that the tests made here are apparently incapable of defining the conditions responsible for a clean furnace. The one sure fact seems to be that reinjection of fly ash is not the responsible factor, as had appeared likely earlier.

Wisely, the original data and calculations have been listed in tabular form, that others can search too for correlations that might have been overlooked here. But the chance is indeed slim. Slagging remains largely unexplainable, and a great deal of tedious work in the laboratory and in operating boiler furnaces remains to be done before the slagging problem can be brought under control at last.

Authors' Closure

The authors wish to thank the discussers for their interest in the investigation and their contributions to the discussion. As stated by Mr. Ely and emphasized by Mr. Reid's discussion, the cleanliness of the furnace without the need of soot blowers and the possibility that this may have been the result of special design features were reasons which led the ASME committee to undertake the tests. The present paper, however, was written primarily to present data on heat absorption and to relate variation in heat absorption to operating variables. This was true of similar papers reporting on variation of heat absorption in five furnaces previously tested in co-operation with the ASME committee. There was no intent to infer, as Mr. Ely has stated,

[8] Research Engineer, Riley Stoker Corporation, Worcester, Mass. Mem. ASME.

[9] C. F. Hawley discussion, TRANS. ASME, vol. 78, 1956, p. 1753.

[10] Assistant Technical Director, Battelle Memorial Institute, Columbus, Ohio. Mem. ASME.

that heat absorption was the "ultimate criterion of performance." Other aspects of performance have, for the previous tests of the series, been considered in companion papers by other authors.

The various discussers have given the obvious explanation for the lack of troublesome deposits in the present furnace. The furnace heat-release rates are moderate. The furnace shape and the burner arrangement are designed to hold the flame close to surfaces where slagging is desired and away from other surfaces where deposits would be troublesome. It might be debated whether the coal was "very good-natured" with respect to ash characteristics. The more important contributor to clean furnace operation was probably the moderate heat-release rate and the management of the flame.

Reference to the Broido curve, given by Ely in Fig. 8, shows that the present data scatter about the curve, with a bias toward high values. The data are more precisely correlated in Equations [2] to [4]. The coefficients of these equations must bear some relation to the Broido curve. A study is in progress using methods of the present paper applied to data for furnaces previously tested. It has appeared that the significant deviation from the Broido curve, shown for various furnaces, is due in part to differences in such things as furnace shape and flame size. These differences cannot be given representation in the Broido curve which depends only on the rate of heat release per unit of wall area.

Mr. Feeley noted the possibility of large errors in furnace outlet temperatures due to proximity of sampling points to the furnace outlet tubes. The large temperature drops mentioned in relation to other furnace studies may have been due in part to the use of poorly shielded thermocouples. Large temperature drops may also appear when gas flows parallel to a wall. Temperature drop as a result of convective heat transfer should be negligible for gas entering the furnace outlet unless gas entering the thermocouple shield is drawn from the stream passing directly over a screen tube. Observations in other furnaces with the shielded high velocity thermocouple have shown drops in gas temperature on passing completely through the screen on the order of 100 to 200 F. The probable error of the average temperature at the entrance to the furnace outlet, as indicated by correlation with the heat absorption by the superheater, was about 15 F for the present data. The precision was quite satisfactory for the purpose, which was to estimate heat absorption within the furnace including heat transfer by radiation to the outlet but not including heat transfer by convection to the furnace outlet screen tubes.

The steam temperatures for tests 8 through 11 were 683, 701, 666, and 684 F, respectively. There is no consistent trend with time during the period of nonreinjection of fly ash. As shown in Fig. 4, heat transferred to superheated steam was related to furnace-outlet conditions in the same way as found for the tests with fly-ash reinjection. There was some deposit of ash on the furnace side of the first screen tubes during tests 8 to 11. This deposit was adherent and was present throughout later tests. Dust was observed on other surfaces, but no quantitative estimates of the amount or thickness of the dust layer are available. There were no obvious differences in the amount of dust present on the heat-transfer surfaces in the furnace with or without fly-ash reinjection.

Entrapment of reinjected fly ash in the slag depends upon the flame intensity, as measured by the adiabatic temperature, Fig. 3, rather than reinjection velocity as suggested by Feeley. The reinjection velocity probably decreased with ash loading since the reinjection air fan was operated directly off the power line with on-off control only. Some effect of boiler loading might be expected through resultant variation of turbulence and flame volume. This does not appear to be significant when judged by the scatter of data points about the curve shown in Fig. 3.

A study of flame placements in furnaces previously studied, as mentioned by Miller, would be desirable. Studies in progress show an effect of flame size and shape which might be given quantitative treatment if measurements of flame placement were available.

Effect of Temperature Variation on Composition, Fouling Tendency, and Corrosiveness of Combustion Gas From a Pulverized-Fuel-Fired Steam Generator

By JOHN D. PIPER[1] and HAZEN VAN VLIET,[2] DETROIT, MICH.[3]

Metal condensers, cooled to selected temperatures between 87 and 242 F, were placed in stack gas of a pulverized-fuel-fired steam generator. The amount and nature of substances depositing upon the condensers were determined as well as the corrosion resistances of many materials. Chlorides were found to deposit at unsuspectedly high temperatures and concentrations. Corrosion rates increased markedly as the water dew point was reached.

Introduction

Recently, Wingert and Stanley [1][4] described the design of a large coal-fired steam generator for a 200-F stack-gas temperature. A unique feature of the design is the use in series of two air preheaters, called the hot-air heater and the cold-air heater. Gases leaving the hot-air heaters at slightly over 300 F pass in turn through the dust collectors, the induced-draft fans, and the cold-air heaters, to the stack.

As Wingert and Stanley pointed out, the principal unknowns connected with the design concerned corrosion and blockage of the cold heater. Initially they presumed that "flue gas at a temperature approximating 235 F is probably the most highly corrosive," and "that corrosion action should not increase appreciably with decreasing temperature from this point." The quoted conclusion was based principally upon the experimental work of Hodson [2] who passed stack gas through a series of glass condensers cooled to desired temperatures in the range between 200 and 300 F.

In order to obtain performance data for the operation of the cold-air heater two separate experiments were carried out simultaneously. One of these experiments consisted of the operation of a pilot-plant air preheater using stack gas from no. 17 steam generator at the Conners Creek Power Plant. The pilot plant and the early experimental results obtained with it were described by Wingert and Stanley [1]. The second experiment consisted of determining the composition, corrosiveness, and fouling tendencies of the materials that condensed or otherwise deposited from the stack gas upon surfaces cooled to selected temperatures. The present paper deals with that second experiment, which was carried out in three parts.

Properties of the Stack Effluent

Properties of the effluent from no. 17 steam generator, significant to the corrosion and blockage of the cold-air heater, are summarized in Table 1. The minimum of 38 and maximum of 56 mm for the partial pressure of water vapor represent winter and summer conditions, respectively, averaged over 1-month periods, rather than the extremes that exist for short periods. These values were computed from the composition of the coal, the proportion of excess air, and the moisture content of the air. The range adequately covers the period during which the experiments were carried out. The average partial pressures of SO_3 and HCl shown were essentially the same whether computed from the analyses of the stack gases or from the composition of the coal and the proportion of air used.

The partial pressures of SO_3 given in the table are computed values based upon the analyses shown at the top of the table. As discussed later, the partial pressures of SO_3, as such, must be extremely low at the temperatures dealt with in this study, the gas being converted to H_2SO_4 vapor and then to sulfuric-acid condensate.

Table 1 Properties of stack-gas effluent used for experiments

	Nominal or average	Range
Gas temp, deg F	300	280 to 320
Dust loading, grains/cu ft	....	0.03 to 0.05
Corrodents, per cent by volume		
SO_2	0.18	0.15 to 0.20
SO_3	0.0029	0.0014 to 0.0039
HCl	0.0049	0.0017 to 0.0082
Composition of coal as burned, per cent by weight		
Moisture	7.70	
C	69.13	
H	3.97	
N	1.38	
O	5.63	
S	2.67	
Cl	0.066	
Ash	9.45	
Air, per cent of theoretical	135	
Mean humidity of air for 1-month period, lb water/lb dry air[a]	....	0.0023 to 0.0144
Partial pressures of corrodents, mm Hg, based on total pressure of 750 mm	....	
Water	....	38 to 56
SO_2	1.4	1.1 to 1.5
SO_3	0.022	0.01 to 0.03
HCl	0.037	0.013 to 0.062

[a] From U. S. Weather Bureau Data for Detroit, Mich., 1955.

---

[1] Supervisor, Chemical and Metallurgical Division.

[2] Engineer, Chemical and Metallurgical Division.

[3] Engineering Laboratory and Research Department, The Detroit Edison Company.

[4] Numbers in brackets designate References at end of paper.

Contributed by the Research Committee on Corrosion and Deposits from Combustion Gases and presented at a joint session of the Research Committee on Furnace Performance Factors, Research Committee on Corrosion and Deposits from Combustion Gases, and Fuels Division, at the Annual Meeting, New York, N. Y., December 1–6, 1957, of The American Society of Mechanical Engineers.

Note: Statements and opinions advanced in papers are to be understood as individual expressions of their authors and not those of the Society. Manuscript received at ASME Headquarters, November 6, 1957. Paper No. 57—A-281.

Just what happens when cooled surfaces, such as the plates of an air preheater, come into contact with stack effluent is a complicated problem. The phenomenon most discussed concerns the conversion of sulfur trioxide to sulfuric acid with attendant increase in what Rylands and Jenkinson [3] aptly termed the "acid dew point." The effect of hydrogen-chloride vapors and dusts has also been considered, but little information exists concerning what happens when cooled surfaces contact the complicated mixture of dust, sulfur trioxide, sulfur dioxide, and hydrogen chloride as they exist in stack effluent. Before the experimental work is described, prior knowledge of the nature of condensate from systems having the vapor components of stack gas will be reviewed briefly.

Equilibria Between Acid Vapors and Water Vapor

Nearly 30 years ago Barkley [4] pointed out that, as the flue-gas temperature drops, the sulfur-trioxide gas begins to unite with the water vapor forming sulfuric-acid vapor, until at the boiling point of concentrated acid, practically all of it is united. He calculated the temperatures at which liquid acid would form on a cooled surface, using the composition of the gases and the partial pressure data of Thomas and Barker [5]. Johnstone [6], believing that, "in all probability the rate of corrosion would be greatest at the temperature of the dew point," devised an electrical method for the determination of the dew point of flue gases.

Since Johnstone's paper was published in 1929 many investigations concerning the dew point of flue gases have been carried out, most of them using equipment similar to Johnstone's. Many of these investigations have been reviewed by Rylands and Jenkinson [3]. The following estimation of the acid dew points in stack effluent is based upon Abel's thermodynamic data [7].

Fig. 1 shows the sulfuric-acid water equilibrium for a system having the partial pressures of water and sulfur trioxide that existed in the stack gas from no. 17 Conners Creek, but without the other acid gases and dust. The curves were derived by plotting the logarithms of the respective partial pressures of sulfur trioxide, sulfuric acid, and water in the gas phase, for given concentrations of sulfuric acid in the liquid phase, against the reciprocals of the absolute temperatures and graphically solving for the partial pressures listed in Table 1.

The crescent-shaped pair of curves in Fig. 1 show the equilibrium between the water vapor in the gas phase and sulfuric acid in concentrations to 99 per cent in the liquid phase. A liquid phase having the compositions indicated is possible for the conditions represented on the convex side of the two curves constituting the crescent, provided adequate sulfuric-acid vapor is present. However, the sulfuric acid to form the liquid phase can come only from the sulfur trioxide in the gas phase. The partial pressures of sulfur trioxide are shown by the broken curves intersecting the crescent. For the highest measured concentration of sulfur trioxide, corresponding to 0.03 mm, the broken curve intersects the 56-mm curve for water at 390 F. Condensation cannot take place, however, because the corresponding vapor pressure of sulfuric acid is many-fold greater than the available partial pressure of sulfur trioxide. Before condensation can take place the temperature must drop approximately 100 deg F, with the result that when condensation starts practically all of the sulfur trioxide has been converted to sulfuric-acid vapor.

The vapor pressures of sulfuric acid corresponding to the original partial pressures of sulfur trioxide are shown, also in Fig. 1, by the solid lines, marked 0.03 mm and 0.01 mm, intersecting the crescent. For example, the 0.03-mm curve for sulfuric-acid vapor, corresponding to the highest measured concentration of sulfur trioxide, intersects the 56-mm curve for water at 288 F; the 0.01-mm curve, corresponding to the lowest measured concentration, intersects the 38-mm curve for water at 259 F. The striated area including those two points represents the acid dew points of systems having the moisture and sulfur trioxide content of the Conners Creek stack gas. The dotted curve marked 0.00001 mm intersects the crescent above the striated area showing that the partial pressure of SO_3 as such is less than 0.00001 mm before condensation takes place.

Fig. 1 further shows that before the equilibrium concentration of sulfuric acid in the liquid state reaches 70 per cent on cooling, its concentration in the vapor state is less than 0.0001 mm. In condensing, the sulfuric acid removes some water from the vapor phase but the amount removed is too small to change the partial pressure of water significantly. Hence further cooling of an equilibrated system below approximately 200 F results primarily in dilution of the sulfuric acid already condensed. From the figure it is obvious that the cold-air heater, receiving gas at approximately 300 F, discharging it at 200 F, and receiving air at a temperature as low as 60 F, is operating in a range where the condensation of sulfuric-acid vapors could be most significant.

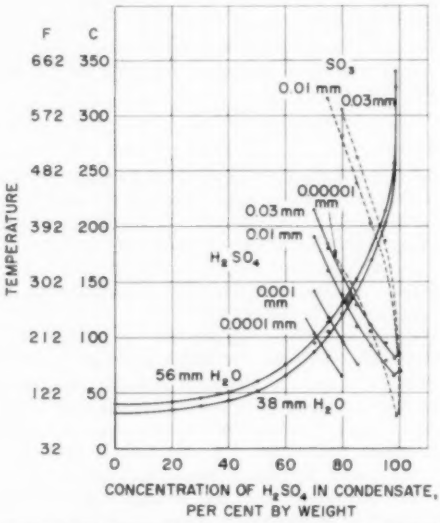

Fig. 1 Equilibrium between liquid sulfuric acid and the vapors SO_3, H_2SO_4, and H_2O, for the SO_3 and H_2O concentrations in Conners Creek stack gas. Initial equilibrium on cooling shown by striated area.

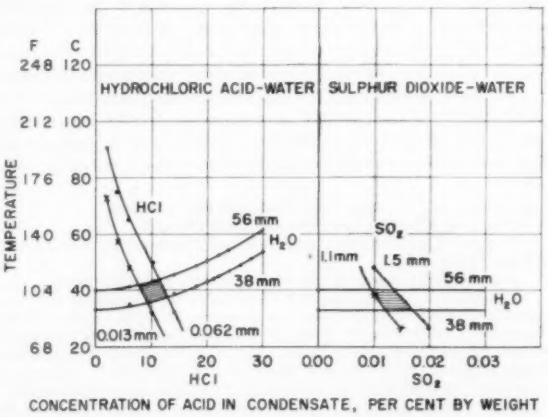

Fig. 2 Equilibrium between acid liquids and their vapors for the SO_2, HCl, and water concentrations in Conners Creek stack gas. Initial equilibrium on cooling shown by striated areas.

Fig. 2 was constructed according to the method described for Fig. 1, using instead of data for the sulfuric-acid system, data [8] for the hydrochloric and sulfurous-acid systems, the latter extrapolated toward zero. The striated area in the left-hand part of the figure shows that if the hydrogen-chloride and moisture content of the stack gas behaved as though the other acid vapors and dust were not there, the acid dew point would be within 7 deg F of the water dew point and the maximum concentration of hydrochloric acid would be 13 per cent. Similarly, the right-hand part of the figure shows that the acid dew points of a water-sulfur-dioxide system containing the proportions of moisture and sulfur dioxide that were in the stack gas are the same as the water dew points. It further shows that the condensate should contain not over 0.016 per cent sulfurous acid, computed as SO_2.

Few data are available on the equilibria of the mixed systems of the acids possible in stack gases, especially in the ranges of partial pressures in which the gases exist. Luchinskii has studied the system H_2SO_4–HCl–H_2O at 25 C [9] and at the boiling point [10]. Although the data are insufficient to describe adequately systems having the low partial pressures of HCl found in stack gases, they do show that for all systems containing sulfuric acid, the concentrations of HCl in the liquid phase must be less, for a given temperature and partial pressure of HCl, than for systems containing HCl and water alone. The maximum concentration of HCl that would be expected in the condensate from the stack gas under discussion would, therefore, be much less than 13 per cent. Available data are not sufficiently complete to predict the maximum temperature at which HCl would be expected to occur in the condensate.

The Condenser Test

The first of the three experimental parts of the present program consisted of inserting a condenser into the breeching of the stack of no. 17 steam generator, controlling the temperature of the condenser surface to desired levels, and determining the amount and composition of materials that deposited upon it during a selected time interval. Fig. 3 shows the location of the condenser within the breeching, approximately 12 ft below the point from which gases were led to the test air preheater described by Wingert and Stanley [1]. Fig. 4 is a sketch of the condenser and auxiliary equipment. Two materials were used in constructing the condensers. One of these was Inconel, selected as a highly corrosion-resistant metal and the other was aluminum selected for minimum catalytic effect in oxidizing sulfur dioxide to sulfuric acid.

Before each test the condenser proper was polished to bright metal and wiped clean. Premixed steam and water were then introduced to bring the condenser approximately to the desired temperature; the assembly was inserted into the breeching, and the temperature was adjusted, if necessary. Usually the condenser was left in the breeching exactly 1 hr while the load on the steam generator and the temperature of the condenser were held reasonably constant. The condenser was then removed.

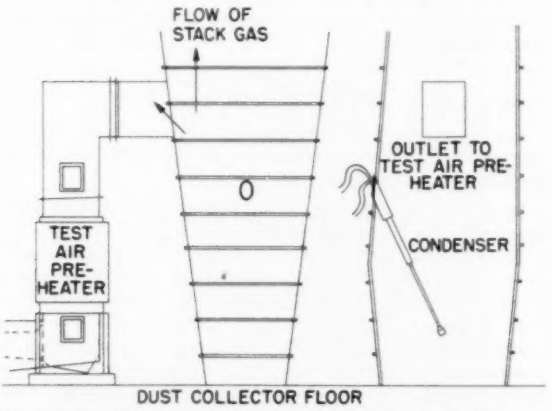

Fig. 3 Location of steam-water-cooled condenser in breeching of stack of no. 17 steam generator

The material collected was removed in three parts: (*a*) The condensate, if any, in the receiver was transferred to a preweighed sample bottle and tightly stoppered. (*b*) As much deposit as could be scraped from the condenser proper was quickly removed, while the condenser temperature was maintained; the scrapings were transferred to another preweighed sample bottle which was then tightly stoppered. (*c*) Both the receiver and the condenser were scrubbed with bristle brushes wet with distilled water to remove any remaining deposits. The wash water containing the residues thus removed constituted the third sample.

The samples were analyzed for total water, acid, sulfate, and chloride content; for components of the dust; and for corrosion products from the condensers. The water content of the scrapings was determined on an aliquot by using a microcombustion train. Carbon was determined simultaneously on some of the samples. The original water content of the material scrubbed off and collected as sample 3 was estimated by proportion using the sulfate contents of the washings and the water-to-sulfate ratios for the condensate and the scrapings. For the cases where the Inconel condenser was used the total corrosion was estimated to be the sum of the nickel and the chromium, which constitute nearly all the Inconel. For the cases involving the aluminum condenser, the corrosion was estimated by subtracting from the total aluminum a correction for the alumina in the fly-ash deposits. The amount of the correction was computed from the amount of iron in the deposits collected on the aluminum condenser and the average aluminum-to-iron ratio found for the deposits collected on the Inconel condenser.

Fig. 5 shows the variation with temperature in the total liquids collected on the condenser, including any that ran off into the receiver, and the total solids that were retained on the condenser. The liquids were computed as the sum of the water plus the H_2SO_4 and HCl corresponding to the sulfate and chloride contents. Both are expressed as amounts per square foot per hour. At temperatures above 150 F the total deposit was dry in appearance and was easily removable from the condenser. As the temperature was reduced below 150 F the deposits became progressively more sticky and moist. At approximately 105 F the deposit consisted of nearly equal parts by weight of solid and liquid, as shown, and was sufficiently fluid to flow. At a slightly lower temperature the amount of condensate was sufficient to wash nearly all the solid deposits off the condenser and into the

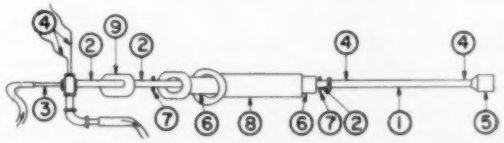

Fig. 4 Steam-water-cooled condenser used for collection of solids and liquids that collect on metal surfaces of an air preheater: ① Condenser proper, Inconel or aluminum 5 ft long, OD of std 3/4-in. pipe. Area of active length, 198 sq in. ② Extension pipe. ③ Tubing within ① and ② to provide inlet for water and steam coolant which escapes through concentric space. ④ Two thermocouples in concentric space between ③ and top and bottom, respectively, of ①. ⑤ Receiver for condensate. ⑥ Sleeve into which condenser slides before apparatus is removed from breeching, to prevent deposit from being blown off during removal. ⑦ Guides to prevent walls of condenser from touching sleeve—receiver also acts as terminal guide. ⑧ Mount in wall of breeching through which ⑥ slides to sleeve flange. ⑨ Stop, welded to ②.

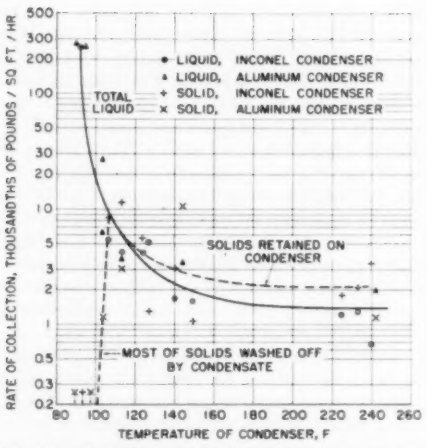

Fig. 5 Liquids collected at various temperatures on condenser or in receiver, and solids retained on condenser

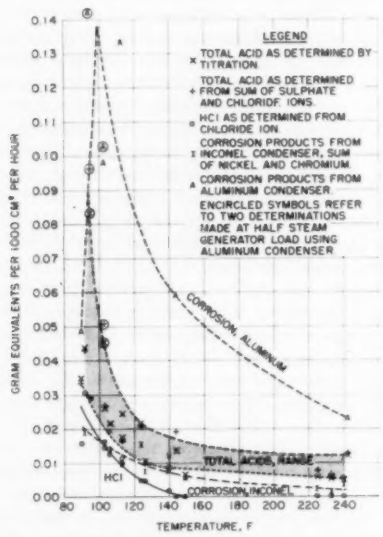

Fig. 6 Variation with temperature change in acids collected and corrosion products formed

receiver. Most of the solid was fly ash; carbon content was usually less than 1 per cent by weight.

Fig. 6 shows the variation with temperature change in the amounts of acids collected on the condensers and the amount of corrosion products formed from them. As the temperature of the condensers was lowered, the first chloride was found at surprisingly high 140 F. Further lowering caused a marked increase in the amount collected, as shown. The amount collected was independent of whether the condenser was Inconel or aluminum.

When the Inconel condenser was used the total sulfate collected (not shown separately in the figure) was nearly independent of the temperature, averaging 0.008 gram equivalents per 1000 sq cm per hr. With that condenser the equivalent weights of chloride exceeded those of the sulfate at temperatures below 116 F. Contrary to expectations, the quantity of sulfate collected with the aluminum condenser was considerably higher than for the Inconel condenser in four of seven determinations. The other three followed the curve for the Inconel condenser. The total acids are

Table 2 Apparent concentrations of acids collected on condenser

Temp, deg F	Condenser material	Steam generator load	Weight, per cent H_2O	H_2SO_4	HCl
90	Aluminum	Full	98.9	0.65	0.43
92	Inconel	2/3	98.6	0.52	0.91
95	Aluminum	1/2	96.4	2.7	0.87
103	Aluminum	Full	63.8	16.7	19.5
103	Aluminum	1/2	82.0	13.9	4.1
106	Inconel	Full	70.0	12.8	17.2
113	Inconel	2/3	62.9	17.9	19.2
113	Aluminum	Full	55.8	17.6	26.6
124	Inconel	Full	52.4	38.8	8.8
126	Inconel	1/2	82.2	10.8	7.0
140	Inconel	1/2	49.4	42.4	8.2
144	Aluminum	Full	56.2	43.8	...
149	Inconel	1/2	59.3	40.7	...
225	Inconel	2/3	35.9	64.1	...
233	Inconel	Full	51.2	48.8	...
240	Inconel	1/2	37.0	63.0	...
242	Aluminum	Full	35.4	64.6	...

Table 3 Initial corrosion rate of condenser materials in stack gas

Temp, deg F	Average rate of penetration, mils per hr for first hour: Inconel	Aluminum
240	0.002	0.027
140	0.007	0.08
90	0.025	0.23

presented as a range in Fig. 6, the minimum being formed by a curve representing nine of the ten determinations for which the Inconel condenser was used, together with three of the seven for aluminum. The maximum represents the other four determinations with the aluminum condenser. Two of those, separately coded in the figure, were for half load on the steam generator.

The acids, as recovered, existed principally as the salts of the metals constituting the condenser. This is shown by the fact that when the Inconel condenser was used nickel and chromium corrosion products averaged over 60 per cent of the total equivalents of acids. The total aluminum corrosion product exceeded the total equivalents of acids many times, as shown. No clear-cut effect of load changes between half and full load was evident.

Table 2 shows the variation with temperature change in the "apparent" concentrations of the acids collected. These apparent concentrations include the salts, as previously stated. Table 3 shows the average rate of corrosion of the two condenser materials during a 1-hour exposure. As shown, the initial corrosion rate was very high. Inasmuch as the condenser test was not designed as a corrosion test but as a test of the severity of operating conditions, further discussion of the corrosive effect of the acids condensed is deferred to later sections.

Stress-Corrosion Test

The second experimental part of the program was a stress-corrosion test. A corrosion test was desirable in conjunction with the pilot-plant air-preheater test [1] in order to:

(*a*) Examine a much wider variety of materials than would be practical on the pilot plant.

(*b*) Determine the corrosion rates on these materials at selected temperatures rather than over the range of cyclic temperatures to which the plates of the pilot air preheater were subjected.

At the time the test was designed, stainless steels were under consideration and some of these were known to be susceptible to stress corrosion by chlorides, which had been shown by the condenser test to be in the condensate in surprisingly high concentrations. Accordingly, a stress-corrosion test was devised to operate at selected temperatures within the range of temperatures to

which air-preheater plates are subjected. This test was patterned after the condenser test.

Fig. 7 shows one of the four assemblies used, three being nearly identical. Each consisted of five cylindrical water-cooled condensers connected in parallel. The cylinders were welded together, one from each of five different kinds of 50-mil flat stock under test. Hence each cylinder constituted a corrosion specimen. The stress-corrosion specimens were made from the same flat stock, bent to fit snugly around approximately 80 per cent of the circumference of the cylinders, with the legs of the hairpin-shaped specimens extending away from the cylinders, as shown. These specimens were slipped to their places over the cylinders of the same composition, to avoid galvanic action. The ends of the specimens were then clamped together, as shown, subjecting the legs to a determinable stress.

One "hairpin" on each assembly was fitted with two thermocouples, the one at the approximate point of maximum stress, just beyond the line of contact with the cylinder, and the other approximately midway down the length of the 4-in. legs. Thermocouples were also placed in the inlet and the outlet water headers and at the surface of the outlet ends of the cylinders, as shown in the figure.

Three stress-corrosion samples of each of the five materials comprising the cylinders were placed at given distances from the ends of their respective cylinders. The 15 stress-corrosion specimens and the thermocouple specimen occupied 16 of the 60 places designated in Fig. 7. Most of the remaining places were occupied by protective coatings, some applied to metal specimens having the same shape as the stress-corrosion specimens, and others applied directly on the cylinders.

The fourth assembly was similar to the other three except that it was constructed of aluminum. Four of the spaces were occupied by bare-aluminum hairpins, one of them equipped with thermocouples installed as previously described. Most of the remaining spaces were used for protective coatings; other spaces were bare.

Fig. 8 shows the positions in the ductwork where two of the four assemblies were installed immediately ahead of the induced-draft fan. The other two were installed on the opposite face of the duct with their backs nearly touching at the center of the duct. The side of the assembly shown open in Fig. 7 was placed on top, toward the gas stream in all installations. As soon as the assemblies were introduced, prefitted plumbing connections to general-service water were made in series, as follows: Water heater, assembly 1, assembly 2 (aluminum), water heater, assembly 3, water heater, assembly 4, waste. Water temperatures and flow rates were adjusted to keep the condenser temperatures at approximately the desired levels of 92, 125, and 160 F. During the first half of the test the daily variation from minimum to maximum temperature averaged approximately 30 F; later the variation averaged less than 20 F. Inlet and outlet water and condenser temperatures were the same within approximately 2 F.

The original plan was to examine the assemblies at the end of 30, 60, and 90 days, removing one set of the stress-corrosion specimens each time. The test had to be discontinued on the 25th day, however, because one cylinder on each of the two 92-F assemblies corroded through, allowing the cooling water to escape.

Fig. 9 shows the appearance of test assembly No. 1, which had been constructed of ferrous materials and operated at 92 F. In contrast to the 1-hr condenser test previously described, in which the deposits were washed from the condenser by the condensate formed, the surfaces of the cylinders and hairpins became fouled over the 25-day period. The cylinder shown on the left is the one that failed. Escaping water struck only the expanded-metal cover and thus did not damage adjacent corrosion specimens. Test assemblies 2, 3, and 4 were also fouled but the deposits on 3 and 4, which operated at average temperatures of 125 and 160 F, respectively, were caked less than those on 1 and 2.

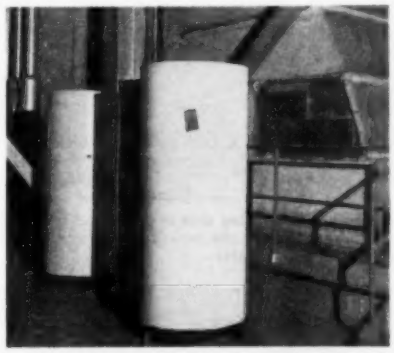

Fig. 8 Location where corrosion test assemblies were installed in ductwork on suction side of induced-draft fan. Two of the water heaters used to heat assemblies to desired temperature are shown.

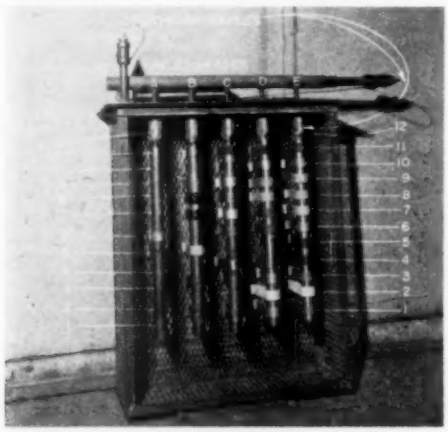

Fig. 7 Assembly for stress-corrosion test (shown without protective screen on top side), figures in margin and letters on inlet header refer to various locations where specimens were placed

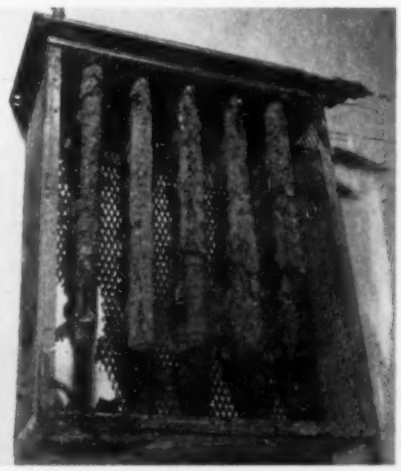

Fig. 9 Test assembly after 25 days of exposure to stack gas at average cylinder temperature of 92 F. Some loose deposit brushed off.

Fig. 10 identifies the five uncoated steels tested and shows the degree to which the cylinders constructed of each resisted chemical attack at 92 F. The figure shows the upper side of the cylinders; that is, the side toward the gas stream. The more-or-less unattacked bands shown had been covered during the test by the hairpin-shaped stress-corrosion specimens. Some of the spaces between those bands originally had been bare whereas others had been covered by protective coatings.

The undersides of all the cylinders were corroded more extensively and more intensively than the respective upper sides shown in Fig. 10. Fig. 11 shows the severely pitted condition of the underside of a short length of the cylinder made of 302 steel. The more extensive corrosion resulted because only a small part of the underside was protected by the stress-corrosion specimens, as is plainly evident. Presumably the more intensive corrosion

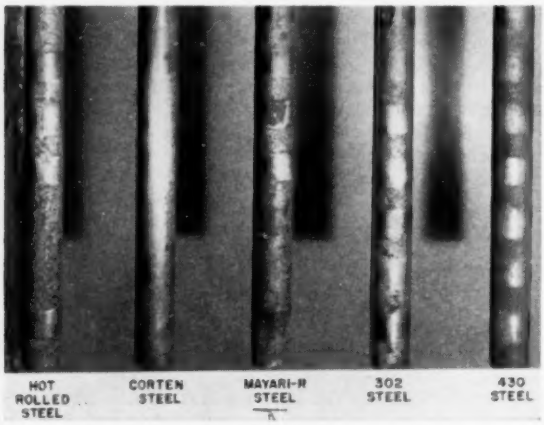

Fig. 10 Close-up view of top side of cylindrical test specimens after 25 days of exposure to stack gas, average temperature 92 F. Cylinders thoroughly cleaned with water.

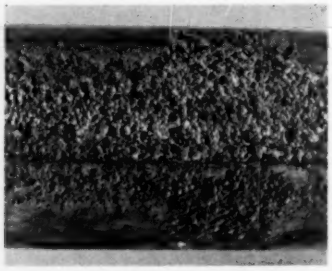

Fig. 11 Close-up view of pitting on underside of 302-steel test cylinder after 25 days of exposure to stack gas, average temperature 92 F, cylinder cleaned thoroughly with water

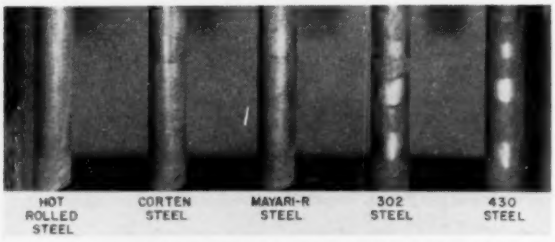

Fig. 12 Close-up view of cylindrical test specimen after 25 days of exposure to stack gas; average temperature 125 F. Cylinder thoroughly cleaned with water.

was caused by flow of condensate toward the underside. The corroded-through part of the hot-rolled steel cylinder that failed was on the underside near the blind end. Two of the four aluminum cylinders on assembly 2 likewise failed on the underside. Thus for hot-rolled steel and aluminum the penetration rate was 50 mils in 25 days.

Fig. 12 shows the cylinders composed of the same five steels subjected to the same test except at 125 F instead of 92 F. Corrosion was much less at 125 than at 92 but the stainless steels, particularly the 302 steel, were considerably pitted as shown. At 160 F corrosion was still less severe; the cylinders, however, had an etched appearance in the unprotected regions.

Fig. 13 shows two sets of the stress-corrosion specimens after test. The average temperatures at various points on the specimens are shown in the margin. The gas temperature averaged 295 F. The figure shows that the most severe corrosion took place on the arc part of the specimens; that is, the coolest part. No evidence of stress-cracking was found. Marks on the specimens, some visible in the figure, showed that condensation had taken place on the arc-shaped parts and that the condensate had run past the maximum-stress zones, to part way down the legs, where much of it evaporated.

Fig. 14 shows the average reduction of thickness of the arc-shaped part of the stress-corrosion specimens. The average reduction of thickness of the hot-rolled steel at 92 F was $6^1/_2$ mils and the aluminum was $3^1/_2$ mils. As previously stated, however, the cylinders made of the same materials corroded completely through at a spot in their 50-mil walls within the same period

Fig. 15 shows the average weight losses not only for the specimens described in Fig. 14, but also, for similar sets of specimens made on a Cor-Ten base but coated with vitreous enamel; lead, sprayed-on; and aluminum, sprayed-on. Sprayed lead is shown to be ineffective for protecting low-temperature elements in stack gas. The sprayed aluminum samples were considerably more resistant than aluminum itself. The markedly greater corrosion of the 92 F samples over the 125 F samples is evident in both Figs. 14 and 15, the Cor-Ten samples being an apparent exception that will be discussed later.

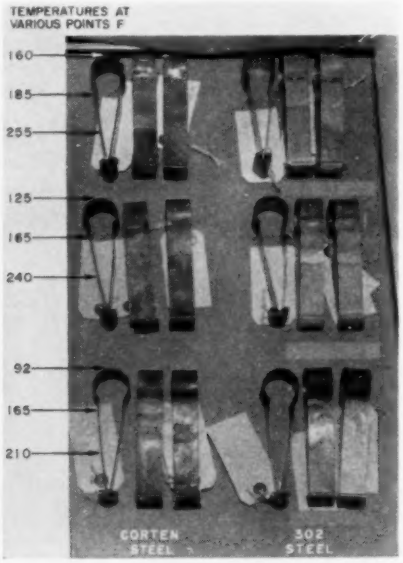

Fig. 13 Two sets of stress-corrosion specimens after 25 days of exposure to stack gas at condenser temperatures of 160, 125, and 92 F

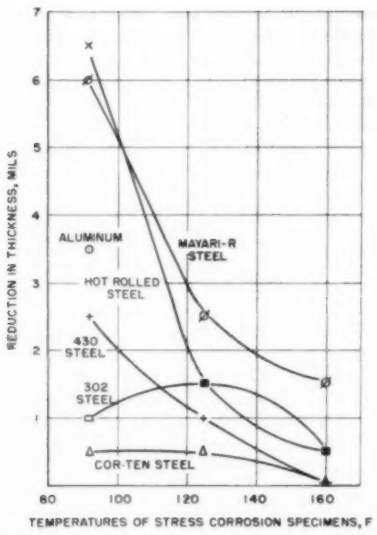

Fig. 14 Average reduction in thickness of arc-shaped part of stress-corrosion specimens

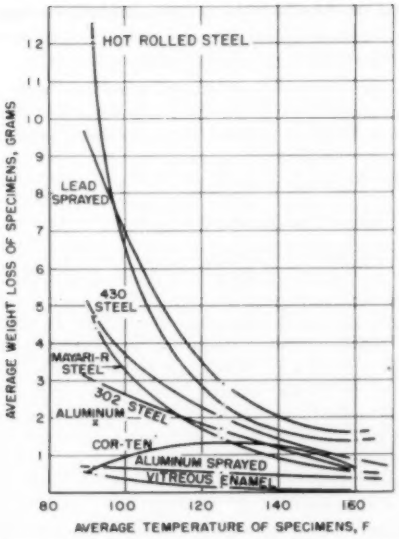

Fig. 15 Average weight loss of stress-corrosion specimens after 25 days of exposure to stack gas

Protective Coatings

None of the many organic protective coatings tried showed any promise of protecting metal surfaces subjected to stack gas at the temperatures to which the several parts of the stress-corrosion specimens were tested. The following were tried:

Type 4 red lead, one to three coats; bituminous coatings; epoxy thiokol, epoxy rubber, and baked epoxy enamel; neoprene; silicones and silicone alkyds of various formulations and bakings both unfilled and filled with graphite, aluminum, and mica, also many proprietary lacquers.

A thiokol vinyl and a graphite-filled silicone furnished fair protection at temperatures up to 210 F but failed at higher temperatures. Of the organics, only fiberglas-reinforced polyester remained in fair condition. The surface of the resin had been destroyed on many of the samples, however, exposing the glass fibers.

General Corrosion Test

The third and final experimental part of the program was a general corrosion test patterned after the stress-corrosion test. Essential differences in the two tests, some of them made clear by Fig. 16 when used in comparison with Fig. 7, were as follows:

(*a*) Means for applying external stress to the specimens were eliminated. The samples were in the form of 325-deg arcs contacting the cylindrical condensers as shown; that is, the general-corrosion specimens looked much like the stress-corrosion specimens with their legs cut off. The entire general-corrosion specimen presumably acquired essentially the same temperature as the cylinder over which it was placed and hence was suitable for weight-loss tests.

(*b*) The tests were conducted at four temperatures instead of three in order better to evaluate the significance of abnormally low metal temperatures on rate of corrosion.

(*c*) Many more solid-metal, metal-coated, and vitreous-enameled specimens were tested in the general corrosion test than in the stress-corrosion test. Organic coatings were eliminated.

(*d*) Because of the many kinds of metals and metallic coatings tested it was impractical to avoid placing the general-corrosion specimens over cylinders of different composition. The four cylindrical metal condensers used on each of the two lower-temperature assemblies during the first period of the test were constructed, one each, of Cor-Ten steel, 50 mils, and NAX-A, B, and C steels, 36 mils thick. During the remainder of the test all four were composed of Cor-Ten, 50 mils thick. For the two higher-temperature assemblies four of the five original cylinders were retained; that is, the ones composed of Cor-Ten, Mayari-R, 302, and 430 steels. The carbon-steel cylinders on each assembly were converted to test nonmetallic materials as shown.

(*e*) To minimize the effect of a considerable difference in corrosivity found at different parts of the assemblies during the stress-corrosion test, each assembly was divided into zones; the specimens were rotated from zone to zone, and their relative positions in the several zones were changed after each inspection. It was

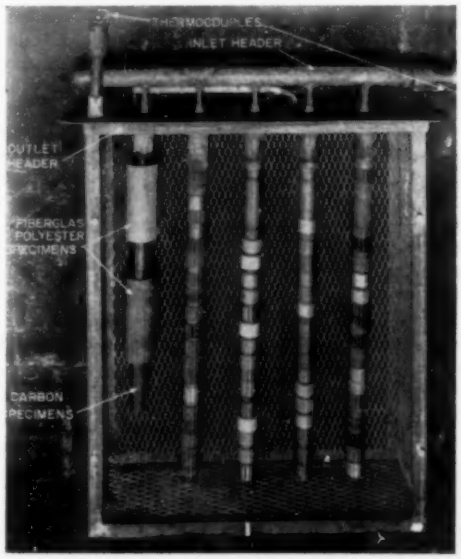

Fig. 16 One of four assemblies for general-corrosion test

intended that one set of specimens be removed, cleaned, weighed, and replaced after 1 month, the second after 2 months, and the third removed, cleaned, and weighed after 3 months.

Control of the temperature of the cylinders was within ±5 deg for the 87, 115, and 141-F assemblies nearly everyday. The range of the daily fluctuations between maximum and minimum temperatures was considerably greater for the 161-F assembly, averaging from −7 to +20 F.

Pitting Corrosion of Steel Cylinders

After the test had been in progress 28 days with the cylinders of the four assemblies operating at average temperatures of 87, 115, 141, and 161 F, respectively, one of the 36-mil cylinders on the 87-F assembly corroded through terminating the first month of the test. The four metal cylinders on both the 87 and the 115-F assemblies were then replaced using 50-mil Cor-Ten, as previously stated, and the test was run for a second period of 27 days without interruption. Inspection of the cylinders indicated that they would last the final month without replacement. After 6 days of the final month, however, one of them on the 115-F assembly pitted through beside the seam weld. The next day one on the 87-F assembly failed. The two assemblies having the failed cylinders were removed from test and the other two were continued for the remainder of the third period of 27 days.

Uncoated Specimens

Table 4 shows the composition of the low-alloy steel specimens used on the general-corrosion test as well as of some of the specimens used on the stress-corrosion test previously described. Fig. 17 shows the reduction in average thickness of the general-corrosion specimens made from four of those low-alloy steels and three stainless steels, as computed from the weight losses. In order to simplify the figure, some of the coded points that practically coincided with others, have been omitted. For example, in the curves representing 141-F conditions the points for the three NAX steels and the Cor-Ten nearly coincided. Points are shown only for the NAX-A and the Cor-Ten; the curve, however, represents the NAX-B and NAX-C steels as well.

Fig. 17 shows that the four low-alloy steels all corroded less than the three stainless steels in the range between 115 and 161 F. This observation is in agreement with the observations of Barkley, Karlsson, Berk, Stark, and Burdick [11] for air-preheater plates operating in the range from 220 to 260 F mean temperature, minimum temperature not stated. The order of merit of the several steels differs somewhat between the two investigations. Barkley, et el., showed NAX steel to be significantly inferior to Cor-Ten; Fig. 17 shows all three NAX steels to be at least the equivalent of Cor-Ten in the range 115 to 161 F. At 87 F the Cor-Ten showed a somewhat lower corrosion rate than any of the NAX steels. Variation from specimen to specimen of the same material was greater, however, than the average variation between the several low-alloy steels tested at each of the four temperatures selected.

Table 4 Composition of uncoated samples tested in stress-corrosion and general-corrosion tests

	Composition, per cent by weight—spectrographic analysis of specimens tested					
Name	Mn	Si	Cu	Ni	Cr	Zr
Hot-rolled	0.28	...	0.05	...	...	...
Mayari-R	0.61	0.15	0.40	0.76	0.38	...
Cor-Ten	0.40	0.38	0.23	0.29	0.61	...
NAX-A	0.85	0.90	0.07	<0.1	0.59	Present
NAX-B	0.82	0.79	0.29	<0.1	0.60	Present
NAX-C	0.53	0.54	0.07	<0.1	<0.1	Present

All the steels appear to have corroded first through pores in their smooth-finished surfaces. Thereafter the corrosion spread laterally. This phenomenon was most apparent on the 115 F specimens inspected after 61 days. Plateaus having nearly their original brightness remained on these specimens surrounding roughened and depressed areas. The 302 and 316 steels had remained bright over most of their surfaces but were pitted. Retention of the bright plateaus was somewhat more evident in the Cor-Ten specimens than in the NAX specimens.

The 87-F test was so severe that the surface finish had disappeared entirely from all the low-alloy specimens by the time of the first inspection at 28 days. The 302 and 316 steels maintained much of their original surfaces even after 61 days. Their average reduction in thickness was much less than for the low-alloy steels as Fig. 17 further shows. Both, however, were deeply pitted, some of the pits extending halfway through the specimens.

The most significant point brought out by Fig. 17 is that the low-alloy steels corroded 50 to 75 times more rapidly at 87 F than at 141 F. The indicated values of 11 to 15 mils for a 60-day period of exposure on one side represent, moreover, average reduction in thickness rather than reduction relative to useful life. Useful life for air-preheater plates would be somewhat shorter than could be derived from those values even after allowing for corrosion on both sides of the plates. As previously pointed out, the corrosion was much more severe where the condensate flowed toward the bottom of the cylinders, five of which corroded through at a point in their wall thicknesses, three during the general corrosion test, and two during the stress-corrosion test previously described, as follows:

Temp, deg F	Material	mils	Days
87 F	NAX-A	36	27
87 F	Cor-Ten	50	34
92 F	Hot-rolled steel	50	25
92 F	Aluminum	50	25
115 F	Cor-Ten	50	33

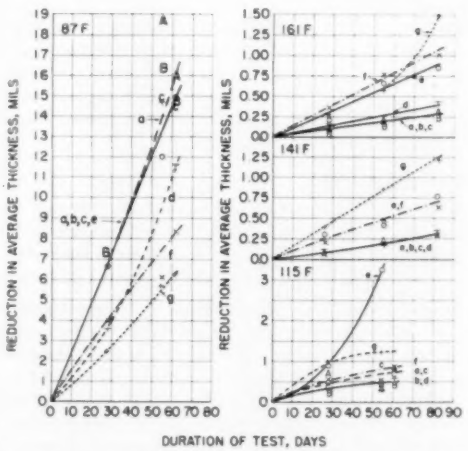

Fig. 17 Reduction in average thickness of uncoated steel specimens subjected at various temperatures, to stack gas

Curve designation	Kind of steel	Code
a	NAX—A	A
b	NAX—B	B
c	NAX—C	C
d	Cor-Ten	T
e	430	⊙
f	302	X
g	316	+

Coated Steels

Figs. 18 and 19 show the same information for the coated specimens as Fig. 17 showed for the uncoated ones including identification; that is, the weight losses were converted to average reduction in thickness, computed as steel. For the coated specimens part of the weight loss was coating and part steel.

Fig. 18 shows the reduction in thickness for metal-coated and metal-oxide-coated specimens, all of which had been prepared over Cor-Ten steel. All specimens except those sprayed with aluminum and aluminum oxide were subjected to the conditions previously described for the bare steels. The aluminum and aluminum-oxide coated specimens were on test only during the latter two periods.

The aluminum oxide on the specimens tested did not adhere well and consequently offered little protection to the steel. On all but two specimens, one at 141 and the other at 161 F, rust was found, at least on patches. The aluminum oxide was tried because it was thought that possibly the better behavior of sprayed aluminum over sheet aluminum on the stress-corrosion test might have been caused by aluminum oxide over the aluminum.

The sprayed aluminum prevented rusting on the 161, 141, and 115-F specimens. At 161 F the weight loss was comparable with that of Cor-Ten. At 115 and 141 F the specimens gained weight during the first month, as shown, which simply means that some corrosion product remained on the rough surfaces.

The specimens coated with the four nickel-phosphorus treatments and crack-free chrome were protected completely from rusting for the entire 82 days of the tests at 161 and 141 F. The average reductions in thickness were approximately one third those of the bare Cor-Ten, as shown. At 115 F the specimens coated with the nickel-phosphorus, fire-reduced, and the crack-free chrome were still free of iron rust at the end of 61 days. Reductions in thickness were a third to a half those for Cor-Ten. The nickel-phosphorus coatings applied by the wet process had all corroded through to the steel within the 61 days; the two that were examined after 28 days, one heat-treated, the other not, were also found to be corroded through. The behavior of individual specimens varied markedly.

All specimens subjected to the 87-F test corroded through to the steel within 62 days. As Fig. 18 shows, the resulting total reductions in thickness were greater than the original thicknesses of the respective coatings. The crack-free chrome; the one and the two-coat, heat-reduced, nickel-phosphorus; and the not-heat-treated, wet-reduced, nickel-phosphorus coatings all furnished considerable protection to the steel initially. All but one of the specimens examined after 28 days had corroded through at least a part of the coating, however. The exception was the specimen having the single coat of nickel-phosphorus, reduced by firing.

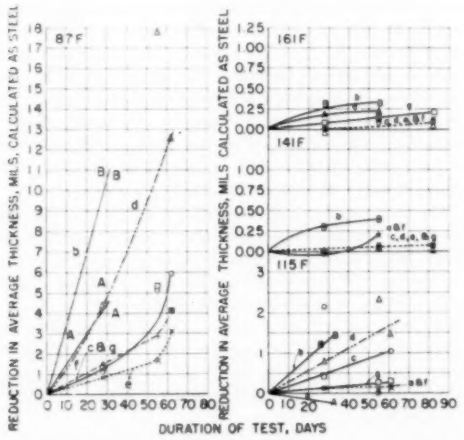

Fig. 18 Reduction in average thickness of metal-coated and metal-oxide-coated Cor-Ten specimens subjected at various temperatures to stack gas

Curve designation	Coating	Average thickness each side, mils	Code
a	Sprayed aluminum	8.77[a]	A
b	Sprayed aluminum oxide	5.89[a]	B
c	Nickel-phosphorus, coating, wet reduction process [12]	0.94	⊙
d	Same as (c) but subsequently heat-treated 4 hr at 1400 F	0.94	Δ
e	Nickel-phosphorus coating, reduced by firing [13]	1.06	X
f	Same as (e) but two coats	3.03	+
g	Crack-free chrome [14]	1.47	□

[a] Thickness of coating was to be 10 mils on outside of sample and 4 mils on inside of sample.

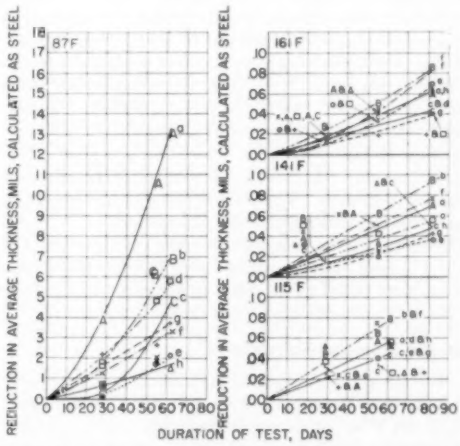

Fig. 19 Reduction in average thickness of vitreous-enameled metal specimens subjected at various temperatures to stack gas

Curve designation	Kind of steel and coating	Avg. thickness of coating per side, mils	Code
a	Appliance grade of enamel, single coat on Armco enameling iron	7.24	A
b	Same on Cor-Ten	6.16	B
c	Reference enamel, one coat Pyroenamel on Cor-Ten; reference combination used on pilot air preheater test	4.30	C
d	Same except on Armco enameling iron	4.31	Δ
e	Borosilicate glass, two coats individually fired on Armco enameling iron	5.56	⊙
	Ground coat and borosilicate glass coat, individually fired on Armco enameling iron	6.27	X
g	One coat borosilicate glass on Armco enameling iron	2.98	+
h	One coat borosilicate glass on Cor-Ten steel	4.10	□

Fig. 19 identifies the vitreous enamels tested and shows the reduction in average thickness for the enameled specimens, some having a base of Cor-Ten and others Armco enameling iron. The data for the 87-F assembly are plotted on the same scale as was used in Figs. 17 and 18; a more expanded scale than that on those figures was used for the 161, 141, and 115-F assemblies.

Outstanding in Fig. 19 is the evidence that at 87 F even vitreous enamels were considerably attacked. All three specimens of the reference single-coated enamel ("C," Fig. 19) on Cor-Ten were devoid of enamel on over half the outside surfaces of the specimens after 62 days. The enamel that remained was deeply etched. The same was true of the reference enamel on enameling iron. Most of the residual enamel was on the top side of the specimens where they had been subjected to a minimum of washing action. Practically none of the enamel remained on the outside surfaces of either the Cor-Ten or the enameling-iron specimens that had been given a single coat of appliance-grade enamel. Specimens given two coats over enameling iron showed only surface etching where the enamel adhered. These specimens chipped so badly, however, and corroded particularly at the edges, that the data are not included in the figure.

Two of the four three-membered sets of specimens having the borosilicate-glass enamels withstood the severe conditions of the 87-F test fairly well, namely those identified as *e* and *h* in Fig. 19. The enamel on the outside surfaces of the specimens was etched slightly but the underlying steel was well protected except at the edges of the specimens. Even there the corrosion had not spread beneath the enamel. One of the three specimens identified as *f* was badly etched and had corroded through to the steel over approximately 10 per cent of the outside surface area. The other two specimens showed considerably more edge corrosion than did the *e* and *h* specimens. The three specimens identified as *g* were similar to the most corroded of the *f* specimens.

All the vitreous enamels protected the steels well at 115, 141, and 161 F. Some of the enamels were lightly etched and a few rust spots were noted at the edges of the specimens but all withstood the test for the time intervals shown.

Carbon and Fiberglas-Polyester

The carbon and the fiberglas-polyester cylindrical specimens, shown before installation in Fig. 16, withstood the tests at 87, 115, 141, and 161 F so far as visual observation could detect. The carbon cylinders had been slipped over a closely fitting steel tube to be removable for weighing. The one on the 87-F assembly broke as it was being removed after 28 days and therefore was not weighed or tested further. The other three samples chipped slightly in being handled and hence the weighings are of no significance. The fiberglas-polyester samples were cemented over steel stubs so that the cooling water was on the inside of the cylindrical specimens. They were not weighed. Inasmuch as the thickness of the carbon specimens was $^3/_{16}$ in. and the polyester specimens $^1/_8$ in., it is probable that their surface temperatures were somewhat higher than those of the metal specimens. In addition to the two cylindrical fiberglas-polyester specimens, the fiberglas-polyester coverings over the thermocouples on each of the steel condensers also may be considered to be test specimens. The same coverings were used throughout both the stress-corrosion and the general-corrosion tests without apparent deterioration. A piece of corrugated fiberglas-polyester awning material suspended in the gas stream without cooling darkened and bared the first layer of glass fibers, thus showing that the material has a temperature limitation for use in stack gas. That limitation, somewhere over 160 F, was not determined by these experiments.

Summary and Interpretation

The following summary and interpretation of the results of the condenser tests and the two corrosion tests is offered for air preheaters or other equipment operating in stack gas having the approximate composition given in Table 1:

(*a*) The deposit on any metal surface that remains above 150 F will be sufficiently dry for the surface either to remain clean or be cleanable by air blowing.

(*b*) Condensate will drip from cooled-metal surfaces in stack gases, even "cleaned" gases, only if the metal temperature falls below 105 F and remains below that temperature for sufficient time for drops to accumulate. Such condensate is extremely corrosive.

(*c*) The lowest temperature reached by the metal of a regenerative air preheater as the metal passes into the stack gas is the significant temperature so far as collection of acids is concerned. Any sulfuric acid that condenses in the cooler part of the cycle will not evaporate on the hot part of the cycle below approximately 260 F, Fig. 1. Chlorides appear at a much higher temperature than could be predicted from any known vapor-equilibrium data for hydrochloric acid. Both sulfuric acid and hydrochloric acid react with metal, and possibly with fly ash also to form salts having lower vapor pressures than the acids. Thus once the acid deposits during the cool part of the cycle, the hot part cannot be relied upon to drive all of it off.

(*d*) Deposits that form between 105 and 125 F are sticky in character; the most severe conditions for blockage of air preheaters will probably be on plates that pass through that temperature range Such deposits cannot be removed effectively by air blowing but are easily removed by water washing when fresh. Unless they are completely removed by water washing, however, such deposits may be partially hydrolyzed by a little water to a point where they bake to an insoluble mass when again heated.

(*e*) Sorption of acids on the residual fly ash in the stack gas appears to be the principal mechanism by which acids that otherwise would deposit on air-preheater plates are cleaned from or carried past them. Complete removal of dust ahead of a cold-air preheater probably would increase corrosion.

(*f*) The amount of sulfuric acid that collects on cooled surfaces in stack gas is nearly independent of the temperature of the surface from 240 F down nearly to the water dew point of the gas. The conclusion of Rylands and Jenkinson [3] that the "acid dew point" has little practical significance is supported.

(*g*) Chlorides appear in the condensate at approximately 140 F. The amount of chloride increases rapidly as the temperature is lowered. At the water dew point the chemical equivalents of chloride exceeded those of sulfate even though the coal had a low chloride content.

(*h*) The chloride-to-water ratio was a maximum at approximately 113 F, at which temperature the apparent concentrations of both hydrochloric and sulfuric acids were between 20 and 30 per cent, concentrations usually considered to have maximum corrosivity. Corrosion, however, was much more severe at the water dew point. For the low-alloy steels the relative corrosion rates at 161, 141, 115, and 87 F were 1, 1, 3, and 66 respectively for 2-month exposures. Stress corrosion was negligible as compared with general corrosion.

(*i*) The low-alloy steels have corrosion resistances superior to the stainless steels, hot-rolled steel, and aluminum in the range of temperatures between 115 and 161 F, in agreement with the previous conclusion of Barkley, et al., [11] for higher temperatures. At the water dew point, the stainless steels thin more slowly than the low-alloy steels but pit much more. Choice of the best of the low-alloy steels is not warranted from the limited number of specimens used in the study. Differences in the behavior of individual specimens are so great that many samples of the several kinds of low-alloy steels would have to be tested before a reliable choice could be made.

(*j*) Certain metallic coatings over low-alloy steels provide corrosion resistance up to three times as great as that of the low-alloy steels themselves. Arranged in order of apparent merit the coatings are: Nickel-phosphorus fired under reducing conditions [13], crack-free chrome plate [14], nickel-phosphorus applied by a wet-reduction process [12], and sprayed aluminum. Sprayed aluminum oxide, as applied to the specimens tested, was ineffective because of poor adherence. Sprayed lead corroded through quickly.

(*k*) Vitreous enamels provide good protection for steels at temperatures of 115 F and above. The condensate formed at temperatures below the water dew point, possibly in combination with residual stack dust, attack even these enamels more or less, depending upon the enamel or its porosity. The most resistant of the vitreous enamels furnished the best protection for steel, at temperatures below the water dew point, of any of the materials tested. Others gave protection comparable to the best metal coatings tried.

(*l*) Carbon has ample corrosion resistance for use in stack gas if problems of strength and brittleness can be overcome.

(*m*) Fiberglas-polyester appears to have promise as a material to be used in stack gas at temperatures up to at least 160 F but below 300 F.

(*n*) Corrosion in air preheaters could be greatly minimized if: 1) They are designed and operated in such a way that the temperature of surfaces while contacting flue gas never drops below 105 F. 2) Routine removal of the acid-laden dust from surfaces is carried out as far as possible by some dry process such as air blowing. Water or steam washing should be kept to the minimum frequency necessary to keep the plates clean. 3) When washing becomes necessary it should be sufficiently complete to remove all deposits. 4) Upon being removed from service, units of a "cold" air preheater should be washed free of acid and deposits and allowed to dry. Otherwise the residual acids and metal salts, which are hygroscopic, will pick up moisture and subject underlying metals to corrosion during idle periods.

(*o*) There appear to be design opportunities for combined heat exchangers and by-product reclaimers to operate in the condensation zone, discharging air, heated to approximately 140 F, to conventional regenerative air preheaters.

Acknowledgments

The authors gratefully acknowledge the contributions of many colleagues, particularly those of W. C. McMurray and R. J. Stanley. They express their appreciation also to representatives of the following corporations for their co-operation in furnishing test materials or in applying coatings used in the corrosion tests: Great Lakes Steel Corporation, The Dix Engineering Company, Metal and Thermit Corporation, The Wolverine Porcelain Enameling Company, NiPhos Process Sales Corporation, General American Transportation Corporation, The Pfaudler Company, The Air Preheater Corporation, and National Carbon Company.

References

1 W. L. Wingert and R. J. Stanley, "Design of a Large Coal-Fired Steam Generator for 200 F Exit-Gas Temperature and Operating Experience With Pilot Plant," TRANS. ASME, vol. 78, 1956, pp. 1393–1402.

2 Peter Hodson, "Influence of Fine Particles on Corrosion of Economizer and Air-Preheater Surfaces by Flue Gases," TRANS. ASME, vol. 77, 1955, pp. 279–286.

3 J. R. Rylands and J. R. Jenkinson, "The Acid Dew Point," *Journal of the Institute of Fuel*, vol. 27, 1954, pp. 299–318.

4 J. F. Barkley, "The Sulfur Problem in Burning Coal," Bureau of Mines Technical Paper No. 436, 1928, pp. 1–7.

5 J. S. Thomas and W. F. Barker, "The Partial Pressures of Water Vapor and of Sulphuric Acid Vapor Over Concentrated Solutions of Sulphuric Acid at High Temperatures," *Journal of the Chemical Society* (London), vol. 127, 1925, p. 2820.

6 H. F. Johnstone, "An Electrical Method for the Determination of the Dew Point of Flue Gases," University of Illinois Engineering Experiment Station Circular no. 20, 1929, pp. 5–22.

7 E. Abel, "The Vapor Phase Above the System Sulphuric-Acid Water," *Journal of Physical Chemistry*, vol. 50, 1946, p. 260.

8 E. W. Washburn, editor in chief, "International Critical Tables," McGraw-Hill Book Company, Inc., New York, N. Y., first edition, 1928, vol. 3, pp. 301–302.

9 G. P. Luchinskii and A. I. Likhacheva, "Phase Equilibria in Systems Containing Sulphuric and Hydrochloric Acids. (I) Tensimetric Investigation of the System H_2O–HCl–H_2SO_4," *Journal of Physical Chemistry* (USSR), vol. 9, 1937, pp. 199–212.

10 G. P. Luchinskii, "Phase Equilibrium Conditions in Systems Containing Hydrochloric and Sulphuric Acids (III) Ebulliometric Investigations of the System H_2O–HCl–H_2SO_4," *Journal of Physical Chemistry* (USSR), vol. 13, 1939, pp. 1340–1345.

11 J. F. Barkley, Hilmer Karlsson, A. A. Berk, C. F. Stark, and L. R. Burdick, "Corrosion and Deposits in Regenerative Air Preheaters," Bureau of Mines, Report of Investigations 4996, United States Department of the Interior, August, 1953, 23 pages.

12 Gregoire Gutzeit, "Kanigen Nickel Plating," Metal Progress, vol. 66, July, 1954, pp. 113–120.

13 G. J. Harvey, "New Low-Cost Coating Gives Mild Steel Good Corrosion Resistance," *Iron Age*, vol. 173, no. 15, 1954, pp. 125–127.

14 J. E. Stareck and Ronald Dow, "Crack-Free Chrome Plating," U. S. Patent 2,686,756, August 17, 1954.

Discussion

G. D. Braddon.[5] This paper contains much valuable information pertinent to the problems associated with fouling and corrosion of air-heater cold-layer surfaces. It is particularly significant when evaluated in conjunction with Wingert and Stanley's paper, "Design of a Large Coal-Fired Steam Generator for 200 F Exit-Gas Temperature and Operating Experience With Pilot Plant," TRANS. ASME, vol. 78, 1956, pp. 1393–1402.

Under the authors' Summary and Interpretation paragraphs some significant statements appear:

Under (*a*) the statement is made that for fuel and firing conditions of the test any metal temperature remaining above 150 F will not collect an unyielding deposit. In a regenerative air preheater this would correspond to a mean cold-end metal temperature of about 165 F. Many installations under similar fuel and firing conditions collect stubborn deposits when cold-end temperature averaged well above 165 F at normal load. But, of course, the vicissitude of normal operation would incur cold-end average temperatures below this level, so it may well be that the authors' minimum metal temperature of 150 F for avoiding stubborn deposits under test conditions is not in conflict with operating experience, taking into account their warning that deposits once collected at lower temperatures will not subsequently dry out and yield to soot blowing at temperatures likely to prevail at the cold end. It should be pointed out, however, that the tests were carried out in flue gas from which most of the fly ash had been removed and that to date nearly all regenerative preheaters handle flue gas with the full burden of fly ash. The minimum metal temperature at which unyielding deposits will begin to collect may be a function of the dust loading, other factors being the same.

The authors' findings that some of the stainless steels offer higher resistance to corrosion than low alloy steels in the metal temperature range below 115 F constitute very useful new information. In this connection the statement under (*i*) of the Summary seems to be contradictory to the findings of the general-corrosion test (see Fig. 17).

The finding that nickel-phosphorous coating gives protection comparable with vitreous enamel is also a contribution indicating that the economics of its use should be investigated. Meanwhile,

[5] Assistant Chief Engineer, The Air Preheater Corporation, Wellsville, N. Y. Mem. ASME.

it appears that suitable grades of vitreous enamel constitute the most effective protection.

The warning expressed by the authors under (*d*) cannot be overstressed. This discusser emphasizes the importance of thoroughly carrying out the washing operation whenever resort to washing is necessary in order to avoid the cementing of residual deposits impossible to remove by other than mechanical means.

Under (*e*) the authors expressed the supposition that complete removal of dust ahead of the air heater probably would increase corrosion. Experiments are now being carried out in actual boiler-plant operation aimed at establishing the role of dust in either accelerating or inhibiting the corrosion rate of air-heater elements. It is hoped these experiments will yield some results this year.

This discusser's company has recognized the opportunity pointed out by the authors under (*o*). The company has initiated investigations into the design of equipment to effect higher heat recovery from flue gas than is now practicable and at the same time effect the reclamation of constituents from the flue gas having a commercial value.

C. F. Stark.[4] The authors have given an excellent presentation of a complex series of experiments. Considerable study is needed to fully appreciate its contents. This is particularly true of the equilibrium curves in Fig. 1.

The authors assume that the pitting condition shown in Fig. 11 is caused by flow of condensate toward the underside of the test cylinders.

Pitting has been noted on cold-end air-preheater plates of regenerative heaters operating at much higher temperatures than those given in the authors' paper. The pitted zone was located beyond a smooth-surface area, extending some distance in from the cold-end edges of the plates. If acid formation is assumed to be the cause of pitting at a given temperature, would not this smooth area also be affected, since its temperature level is below that of the pitted zone?

It is further reported in the section, Stress-Corrosion Test, that useful life of preheater plates would be somewhat shorter than the average values given. Plate life would depend more on the zone, or depth at which maximum corrosion occurs. In addition, the contact protection offered by the test clamps is similar to that existing between the contacting planes of adjacent plates in regenerative air heaters. Provided the edges of the cold-end plates are still intact, they may be reversed for continued useful life.

For comparative purposes, the corrosion rate of a pair of Cor-Ten test plates from the Conners Creek Station test heater was measured against the corrosion-rate curve shown in Fig. 17. The test plates had been in service for 87 days with a cold-end metal temperature of approximately 141 F. The authors' curve for Cor-Ten at this temperature indicated a loss of about 0.3 mil for 82 days' service with one face exposed. Measurements of the Cor-Ten test plates, however, showed a loss of 10 mils or approximately 16 times greater per side.

Authors' Closure

The authors appreciate the comments by Mr. Braddon and Mr. Stark. Only a few of the comments require further discussion.

In reference to Mr. Braddon's third paragraph, it is the authors' contention that the important temperature in avoiding stubborn deposits is not the mean cold-end metal temperature but the minimum metal temperature. In normal air-preheater installations employing a single air preheater, operating at a mean cold-end metal temperature of 165 F and an inlet air temperature of 60 to 80 F, the minimum metal temperature will be considerably below 150 F as judged by data obtained by R. J. Stanley. The authors agree that even if the minimum metal temperature is kept above 150 F during operation, stubborn deposits may form if the equipment is shut down without being washed because the deposits, being hygroscopic, will absorb moisture and partially hydrolyze. When the equipment is started up again, these deposits will bake into an insoluble mass that will not yield readily to soot blowing or water washing.

The authors further agree with Mr. Braddon's inference that a similar investigation should be carried out on gas as it enters the precipitators. The Company with which the authors are associated has no plans for carrying out such an investigation in the immediate future.

Mr. Braddon is right that conclusion (*i*) was too broad. It might better have been stated ". . . . . in the range of temperatures between 115 and 161 F in agreement with . . . . ." For air-preheater plates the stainless steels would probably be superior to low alloy steels below 115 F. However, for other applications of steels in contact with flue gas, where penetration is of major importance, the authors believe the stainless steels would offer little if any advantage over the low alloy steels.

Pitting corrosion in a zone some distance in from a relatively uncorroded cold-end edge of regenerative air preheaters, such as Mr. Stark refers to, has also been observed by our colleague, R. J. Stanley. The authors are of the opinion that such pitting is caused by acid-laden deposits. Such deposits are usually swept clean from the top and bottom edges but are less effectively removed from intermediate regions by conventional soot-blowing equipment. As Fig. 1 shows, sulfuric acid can condense continuously on the entire surface of air-preheater plates operating under conventional conditions. For example, in a test conducted by Stanley during the summer season with the average temperature of the inlet air 113 F and the exit gas 288 F, the average metal temperatures of the cold-end edges were, minimum 174 F, maximum 201 F. Those of the hot-end edges were 249 F minimum and 274 F maximum. The corresponding equilibrium concentrations of sulfuric acid for stack gas containing 56 mm water are: Cold-end edge, 63.5 to 69.5 per cent; hot-end edge, 77.5 to 81 per cent, all values falling at vapor pressures of sulfuric acid less than that of stack gas such as is described in Table 1. Thus condensation can take place continuously, even neglecting the effects of stack dirt. Most of the acid is probably absorbed in the stack dirt. What little actually condenses on the metal surfaces is of such high concentration as to be only mildly corrosive. Corrosion will, therefore, be mild on any metal surface that is kept dry and free from deposits such as the edges. At any locations where deposits accumulate, however, much acid is present, ready to cause corrosion whenever the hygroscopic sulfuric acid is allowed to pick up moisture, either from the air during shutdown, from wash water left from incomplete washings, or from steam from soot blowers. Thus the presence of severe corrosion at some intermediate zone between the hot and the cold edge of a regenerative air preheater does not necessarily indicate preferential deposition of sulfuric acid in that zone.

The comment that "useful life of air-preheater plates would be somewhat shorter than could be derived from" the values cited was intended to warn the reader not to try to make an estimate of plate life from those values. As stated in connection with the tests, the corrosion tests had two functions:

(1) To compare the relative corrosion rates of different materials subjected to the same conditions.

(2) To determine the effect of specimen temperature on corrosion rate.

[4] Mechanical Engineer, The Air Preheater Corporation, Wellsville, N. Y. Mem. ASME.

The corrosion specimens were 325-degree arcs, open at the bottom. Corrosion on those specimens was mildest at the tops and increased in severity toward the bottoms. The same was true for the cylinders on which the specimens hung. The paper shows, for example, that at 87 F the average corrosion rate for the Cor-Ten specimens was 0.25 mil per day. The bottom of a Cor-Ten cylinder actually corroded through in a spot in 34 days, a rate of nearly 1.5 mil per day at that particular spot, but probably less than 1 mil per day over the entire bottom consisting of the 35 degrees of arc not covered by the open-bottomed specimens. The actual corrosion rate at any spot was a function of the extent to which the spot was swept by the condensate.

The sixteen to one ratio between the corrosion rates of the Cor-Ten test plates cited in Mr. Stark's last paragraph and the Cor-Ten test specimens reported upon in the paper is less surprising when the conditions are examined. In addition to the factor discussed in the preceding paragraph, two other known factors entered:

(1) The test plates referred to were in the pilot-air preheater during a period when wet steam was being used as the cleaning medium. After air blowing was substituted as the primary cleaning medium the corrosion rate of Cor-Ten test plates was 40 per cent of what it had been with wet steam washing. During the period when air was being used, occasional water washing was necessary, with consequent corrosion not chargeable to stack gas corrosion.

(2) Although the average of the air-in, gas-out temperatures in the pilot heater was the same as the average metal temperature of our 141-F specimens, the cold-end edges of the test plates were subjected to much more severe corrosion conditions than our samples because they dipped to low temperatures each cycle. A thermocouple 1 inch from the cold-end edge showed temperature variations from 89 to 156 F.[7] Graphical solution, based upon (*a*) the proportion of time a spot in that region was at given temperature ranges, and (*b*) the changes in relative corrosion rates caused by temperature change, established in the authors' paper, shows that the corrosion rate for the zone involved should be approximately $8^1/_2$ times the rate at 141 F. This zone covered approximately 2 inches of the 12-in. test plates, as judged from the corrosion pattern.

Many test data were obtained on the pilot air preheater other than the preliminary data reported by Wingert and Stanley. When and if the additional data are published further comparison between the data from the pilot air preheater and those from the companion studies given in this paper may be advantageous.

[7] Data obtained by R. J. Stanley.

A Simple Method of Estimating the Reynolds Number Effects on Aircraft Gas-Turbine Engines Operating at High Altitudes

By ROBERT W. PINNES,[1] WASHINGTON, D. C.

At present, the altitude performance of an aircraft gas-turbine engine is usually estimated by generalizing sea level data. Sufficient altitude test data have now been obtained to demonstrate that this method is not entirely valid. One of the primary reasons for the deviations from the generalized data is the Reynolds-number effect.

In this paper, an attempt is made to establish a simple method for estimating correction factors for these Reynolds-number effects, for both turbojet and turboprop engines. These correction factors are based on an empirical correlation of some available test data by means of an "effective Reynolds-number diameter" parameter.

The paper (*a*) discusses the general problem, (*b*) reviews the available test data, and (*c*) recommends correction factors for each of the cases considered. In the last analysis, an altitude calibration of each specific engine is still required to establish accurate altitude data. However, in the absence of any better information, the curves established herein may be used to provide some preliminary estimates.

Nomenclature

THE following nomenclature is used in this paper:

A_N = exhaust nozzle area
D = diameter
D_C = compressor-inlet-tip diameter
ERND = effective Reynolds-number diameter
F_N = actual net thrust
$(F_N)_0$ = net thrust based on generalized data
K_{RN} = Reynolds-number correction factor (applied to subscript indicated)
N = engine rotor speed
N_{mil} = reference rotor speed for military rating
N^* = ratio: $[N/\sqrt{(\theta)}]/N_{mil}$
P = pressure
RN = Reynolds number
ReI = Reynolds-number index ($= \delta/\varphi\sqrt{\theta}$)
SFC = actual specific fuel consumption
$(SFC)_0$ = specific fuel consumption based on generalized data
SHP = actual shaft horsepower
$(SHP)_0$ = shaft horsepower based on generalized data
ESHP, $(ESHP)_0$, ESFC, $(ESFC)_0$ = equivalent values
T = temperature
T_{T1} = turbine-inlet total temperature
T_{T2} = turbine-outlet total temperature
V = flow velocity
W_a = engine air flow rate
W_f = engine fuel flow rate
$(\Sigma_P)_R$ = ram pressure ratio
ρ = density
μ = absolute viscosity
δ = ratio of engine-inlet total pressure to NACA standard sea-level pressure
θ = ratio of engine-inlet total temperature to NACA standard sea-level temperature
φ = ratio of coefficient of viscosity corresponding to engine-inlet total temperature to coefficient of viscosity corresponding to NACA standard sea-level temperature
$(\ )_0$ = values based on generalized data

Introduction

One of the continuing difficulties in the engine development business is that, because of the shortage of suitable test facilities, the altitude calibration of an engine is usually obtained relatively late in the program. Consequently, early estimates of altitude characteristics are usually based on a generalization of sea-level data. For a turbojet engine, for example, this assumes that if referred rotor speed $(N/\sqrt{\theta})$, referred turbine inlet temperature (T_{T1}/θ), and ram pressure ratio $(\Sigma_P)_R$ are the same, then referred net thrust (F_N/δ), referred fuel flow rate $(W_f/\delta\sqrt{\theta})$, and referred specific fuel consumption $(SFC/\sqrt{\theta})$ will be the same.

Sufficient altitude test data have now been obtained to demonstrate that these generalizations are not entirely valid. Deviations from the generalized data are currently attributed primarily to two causes: (*a*) Reynolds-number effects and (*b*) combustion efficiency effects. It should be noted that these effects are quite independent of any altitude difficulties which may be encountered because of poor matching of components at high referred speeds.

In this paper, primary consideration is given to the Reynolds-number effects. The concept of an "effective Reynolds-number diameter" is introduced and an attempt is made to correlate some available test data through this parameter. Only engines with axial-flow compressor units are considered herein. The primary objective of the paper is to establish some approximate correction factors for these Reynolds-number effects, which may be applied to any size engine for any operating condition.

Discussion of Altitude Effects

As indicated previously, deviations from the generalized data at altitude are currently attributed to two primary causes: (*a*) Reynolds-number effects and (*b*) combustion efficiency effects. These effects are essentially independent of each other and are discussed separately in the following sections.

Reynolds-Number Effects. As the Reynolds-number level through a gas turbine is lowered, the primary effect is some combination of decreased compressor efficiency, decreased turbine

[1] Research Division, Bureau of Aeronautics, Department of the Navy.

Contributed by the Gas Turbine Power Division and presented at a joint session with the Aviation and Hydraulic Divisions at the Annual Meeting, New York, N. Y., December 1–6, 1957, of THE AMERICAN SOCIETY OF MECHANICAL ENGINEERS.

NOTE: Statements and opinions advanced in papers are to be understood as individual expressions of their authors and not those of the Society. Manuscript received at ASME Headquarters, August 15, 1957. Paper No. 57—A-157.

efficiency, and/or decreased air flow rate. In addition, the compressor surge characteristics can be affected, thus possibly causing difficulties on this score. The essentially fixed mechanical losses (bearing losses, gear losses, and so forth) tend to become a greater proportion of the engine output, as Reynolds number decreases, but this effect, especially for turbojet engines, is generally relatively small.

These Reynolds-number effects are not completely understood. There are some data, for example, which indicate that these losses are not strictly a function of Reynolds number, but of additional parameters as well. The actual effect is rather complicated, and a detailed investigation of the many different flow passages through an engine would have to be made to attempt to get a specific correlation.

However, sufficient test data have been obtained—primarily by the National Advisory Committee for Aeronautics—to demonstrate that the "Reynolds-number index" ($\delta/\varphi\sqrt{\theta}$) is a relatively good basis for correlating the altitude performance of a given engine. This is the method which is primarily in use at this time. However, it is limited only to the engine for which the data are available. As far as is known, no attempt has been made to obtain a set of generalized corrections which could be applied to any engine, at any operating condition.

Combustion Efficiency Effects. A decrease in combustion efficiency would void the generalized data by increasing the fuel flow rate, and consequently, the specific fuel consumption. However, if the same final combustion chamber temperature is obtained and the additional mass of the fuel is neglected, the thrust or horsepower output would remain the same.

It has been demonstrated that combustion efficiency for conventional fuels may be expressed as a function of a combustion parameter (PT/V). For the purposes of this investigation, it may be considered that the pressure term is the significant variable. Further, as a general guide, it may be assumed that the combustion efficiency will not decrease significantly as long as the total pressure in the combustor is above approximately one standard atmosphere (14.7 psia). Obviously, this is a rather rough approach to the combustion efficiency problem, but it is considered reasonably adequate for the purposes of this investigation.

Primary Combustion Chamber. Fig. 1 shows the pressure level existing in the primary combustion chamber of a turbojet engine as a function of altitude and compressor pressure ratio. The basic pressure scale shown is for a Mach number of zero and a ram recovery ratio of 1.0. In addition, lines are shown, for reasonable combinations of Mach number and ram recovery ratio, which will give one standard atmosphere in the combustion chamber for the altitude and the compressor pressure ratio indicated. It should be noted that the "compressor pressure ratio" is at the actual operating point under consideration, not the static sea-level value. It may be seen from Fig. 1 that the range of interest of the subject investigation is essentially within the region where the total pressure in the combustion chamber will remain above one standard atmosphere. On this basis, it was assumed that the combustion efficiency effects in the primary burner could be neglected for the purposes of this investigation. For those regions where combustion efficiency effects may be important, these effects will have to be evaluated separately.

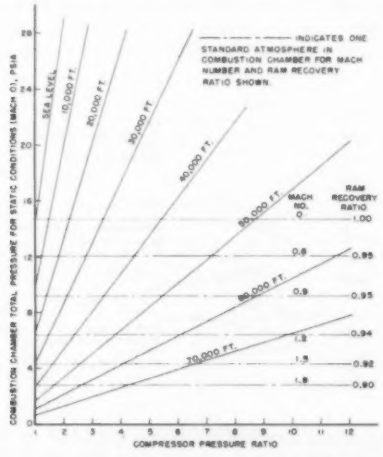

Fig. 1 Factors relating to combustion chamber pressure

Afterburner. The operation of an afterburning turbojet engine is, of course, of interest. For the range of operation being considered herein, combustion efficiency effects in the afterburner could be very significant. However, to date, relatively few actual test data on afterburning engines at altitude are available. Consequently, only the nonafterburning case is considered herein. Consideration of the afterburning case will have to await the availability of more actual test data.

Effective Reynolds-Number Diameter

For the purposes of this investigation, it is assumed that the altitude losses are some function of Reynolds number. The basic Reynolds number equation is

$$\mathrm{RN} = \frac{DV\rho}{\mu}$$

For simple cylindrical pipe flow, D is the pipe diameter, V is the average velocity over the entire cross section, ρ is the density of the fluid, and μ is the absolute viscosity.

Obviously, in considering a gas turbine engine, the Reynolds-number concept is considerably more complicated. All the factors affecting Reynolds number are varying continuously throughout the engine, so that, consequently, any single number is, at best, only a rough approximation. However, for the purposes of this investigation, it is desired to establish some Reynolds-number function which would be applicable to any size engine, at any operating condition. In an attempt to accomplish this, the following approach was taken for each of the variables affecting Reynolds number:

(*a*) *Characteristic Dimension.* For the characteristic dimension D, the compressor-inlet tip diameter D_C will be used. This has the shortcoming of not necessarily being a representative dimension. For example, two units with the same compressor tip diameter can still have different chord-length blades, different flow passage proportions, and so forth. However, as a rough indication of engine size, the compressor-inlet tip diameter appears to be a reasonable choice.

(*b*) *Characteristic Velocity.* It is assumed that the characteristic velocity V is proportional to the ratio N/N_{mil}, where N is the actual rotor rpm at the operating condition under consideration and N_{mil} is the rotor rpm for military rating at standard sea-level static conditions. This assumes, in effect, first, that all engines at military rating have approximately the same velocity levels (tip speeds, relative gas velocities, and the like); and second, the velocity triangles for all operating points of the engine are similar, and consequently, all velocities are proportional to the rotor rpm. This assumption is not valid; first, because different engines at military rating will have somewhat different velocity levels; and second, different parts of the engine (for example, compressor-inlet stage, middle stage, and outlet stage) will react differently to part loads. However, here again, it appears that a

representative velocity, for the purposes of this investigation, may be expressed as a percentage of the rotor speed at military rating.

(*c*) *Density and Viscosity.* Density and viscosity are varying throughout the engine. For the purposes of this investigation, density and viscosity will be based on total conditions at the compressor inlet. Engines with different compressor pressure ratios and different turbine-inlet temperatures will consequently have different density and viscosity levels throughout the engine. However, here again, compressor-inlet conditions appear to be a reasonable choice.

In an attempt to establish a generalized Reynolds-number function, applicable to any size engine at any operating condition, the concept of an effective Reynolds-number diameter (ERND) is introduced. On the basis of this discussion, the ERND is established as follows:

The basic Reynolds number is

$$\mathrm{RN} = \frac{DV\rho}{\mu}$$

For D, the compressor-inlet diameter D_C, in inches, is used.

For V, the dimensionless ratio N/N_{mil} is used.

For ρ/μ, the dimensionless ratios of these values at the operating condition under consideration, to the standard reference values at static sea-level conditions, are used; that is, $\delta/\varphi\theta$.

This gives

$$\mathrm{ERND} = D_C\left(\frac{N}{N_{\mathrm{mil}}}\right)\left(\frac{\delta}{\varphi\theta}\right), \text{ in.}$$

Introducing the Reynolds-number index (ReI) currently in use

$$\mathrm{ReI} = \frac{\delta}{\varphi\sqrt{\theta}}$$

and defining N^*

$$N^* = \frac{N/\sqrt{\theta}}{N_{\mathrm{mil}}}$$

gives

$$\mathrm{ERND} = D_C(N^*)(\mathrm{ReI}), \text{ in.}$$

For convenience, curves of (ReI), as a function of altitude and forward speed, are reproduced herein, from NACA data, in Fig. 2.

The physical significance of the ERND is that it represents the size of an engine operating at standard static sea-level conditions which will have the same Reynolds-number effects as a larger engine operating at altitude. Specifically, the Reynolds number of an engine can be decreased by (*a*) operating the engine at altitude, or (*b*) physically scaling the engine down at sea level. For example, if an engine with a compressor tip diameter of 30 in. is operated at altitude and flight speed, so as to give an ERND of 4 in., the losses will be the same as if the engine had been scaled down to 4 in. at sea level.

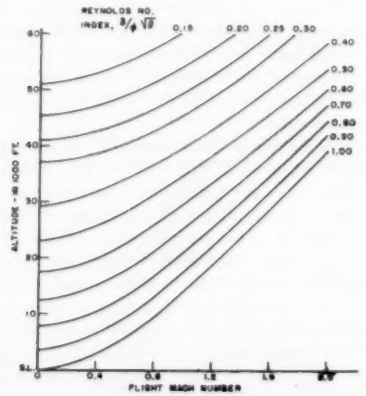

Fig. 2 Reynolds-number index as a function of Mach number and altitude; 100-per-cent ram-pressure recovery, NACA standard day

Effects of Various Losses

In considering the effects of the various loss possibilities being considered herein on over-all performance, it is very important to consider exactly how the engine's control system reacts to these losses. Merely for illustration, a control system which schedules fuel flow as a function of engine inlet conditions and throttle setting might be considered. If such an engine suffered an air flow loss due to altitude effects, the turbine-inlet temperature would tend to increase. For a combustion efficiency loss, the turbine-inlet temperature would tend to decrease.

In order to isolate the Reynolds-number effects, it is assumed that, for any desired engine rating, the engine control system will give the same rotor speed and turbine-inlet temperature, regardless of what losses are encountered. This can be readily accomplished in a turbojet engine with a variable area exhaust nozzle, and in a turboprop engine. However, it is not possible in a fixed geometry turbojet engine. Consequently, for the latter case, it is very important to distinguish between the losses which may be attributed to Reynolds-number effects (with the engine staying at the same $N/\sqrt{\theta}$, T/θ, and $(\Sigma_P)_R$, as altitude is increased) and any additional altitude effects which may be caused by the engine moving to a different operating point.

In Fig. 3(*a*), the various loss possibilities discussed herein [assuming that the engine stays at the same $N/\sqrt{\theta}$, T/θ, and $(\Sigma_P)_R$] are considered separately, and the effects of each on over-all performance are indicated. The data shown in Fig. 3(*a*) are intended to be general in nature and do not apply to any specific engine. The effects of the losses are shown as $F_N/(F_N)_0$ and $(\mathrm{SFC})_0/\mathrm{SFC}$, where F_N and SFC indicate actual altitude values, and the subscript "0" indicates the altitude values obtained from a generalization of sea-level data. The data are equally applicable to a turboprop engine by substituting SHP for F_N in the following discussion.

(*a*) *Air Flow Loss.* A reduction in air flow rate will reduce F_N. However, if there are no reductions in the compressor, turbine, or combustion efficiencies, the fuel flow rate will be correspondingly reduced, and there will be no change in SFC.

(*b*) *Compressor and/or Turbine Efficiency Loss.* Reductions in compressor and/or turbine efficiency will decrease F_N and increase SFC. If there are no air flow or combustion efficiency losses, the ratios $F_N/(F_N)_0$ and $(\mathrm{SFC})_0/\mathrm{SFC}$ will tend to be equal.

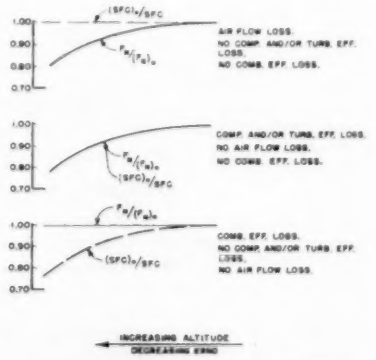

Fig. 3(*a*) Effects of various losses on turbojet engine performance

(*c*) *Combustion Efficiency Loss.* A reduction in combustion efficiency will increase SFC. However, if there are no reductions in air flow, or compressor and turbine efficiency, there will be no change in F_N.

(*d*) *Combined Losses.* In an actual engine, the over-all loss will tend to be some complicated combination of the above. However, consideration of the relative positions of the $F_N/(F_N)_0$ and $(SFC)_0/SFC$ curves will tend to give some indication of which loss is predominant. It should be noted that if the $F_N/(F_N)_0$ and $(SFC)_0/SFC$ curves coincide, it may be due to either compressor and/or turbine efficiency loss alone [as in (*b*)]; or a combination of air flow loss and combustion efficiency loss [as in (*a*) and (*c*)].

Method of Analysis

Before getting into a detailed analysis of available data, it is important to establish clearly the approach to the problem. As discussed previously, one of the most important points is to consider exactly how the engine's control system reacts to Reynolds-number effects, and to distinguish between the losses which may be attributed to Reynolds-number effects, and any additional effects caused by the engine moving to a different operating point.

For the turbojet phases of this investigation, the following three cases were considered.

(*a*) *Case I, Variable Area Exhaust Nozzle.* For this case, it was assumed that the engine control system will give the same rotor speed and turbine-out temperature, regardless of what losses are encountered. It is further assumed that turbine-inlet temperature will remain essentially constant with constant turbine-out temperature, for the same rotor speed. The available data were investigated for conditions of constant $N/\sqrt{\theta}$, T/θ, and $(\Sigma_P)_R$, and for conditions of constant N, T, and $(\Sigma_P)_R$. The general relationship between the generalized data and the actual test data are shown in Fig. 3(*b*). The Reynolds-number correction factor, K_{RN}, is defined as $F_N/(F_N)_0$ or $(SFC)_0/SFC$.

(*b*) *Case II, Fixed Area Exhaust Nozzle, Constant Rotor Speed Control.* For this case, it was assumed that the engine control system will maintain constant rotor speed. This means that the engine will tend to over-temperature as losses are encountered.

(*c*) *Case III, Fixed Area Exhaust Nozzle, Maximum Temperature Override.* This is the same as Case II, except that the engine is prevented from going over rated temperature for the desired engine setting. This may be done by pilot or automatic control. This means that the engine rotor speed will have to be reduced as losses are encountered, to stay within permissible temperature limits.

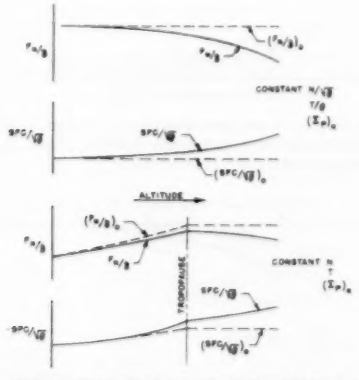

Fig. 3(*b*) Relationship between generalized data and actual test data; Case I, variable area exhaust nozzle, constant rotor speed control, constant temperature control

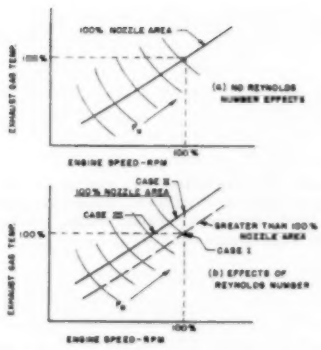

Fig. 4 Modes of engine operation for Cases I, II, and III

In Fig. 4, the three modes of turbojet engine operation discussed are illustrated graphically on an exhaust gas temperature versus engine speed plot.

For the turboprop engine, it is assumed that the same rotor speed and turbine-inlet temperature are maintained. This can be readily accomplished by means of suitable propeller control. Consequently, the turboprop case is essentially similar to the Case I turbojet.

Turbojet Engine (Case I)—(Variable Area Exhaust Nozzle)

Thrust and Specific Fuel Consumption Correction Curves. In this section, data are considered for engines with variable area exhaust nozzles. In addition, some fixed area engines, where data are available for a range of exhaust nozzle sizes, have also been included.

The data are presented in the form established herein; that is, K_{RN} versus ERND; in Figs. 5(*a* and *b*). It may be seen that a reasonably good correlation is obtained among the data available.

In general, the $F_N/(F_N)_0$ and the $(SFC)_0/SFC$ curves tend to cover about the same range. Since the detailed engine data show that combustion efficiency losses and air flow losses tend to be relatively small over the range being considered, it would appear that the losses are due primarily to compressor and/or turbine efficiency losses.

On the basis of these data, a single correction curve was established. This final curve is shown in Fig. 6. Most of the data

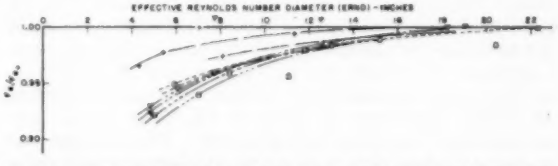

Fig. 5(*a*) Test results of altitude effect on net thrust as a function of effective Reynolds-number diameter, ERND; Case I, variable area exhaust nozzle, constant temperature plus rotor speed control

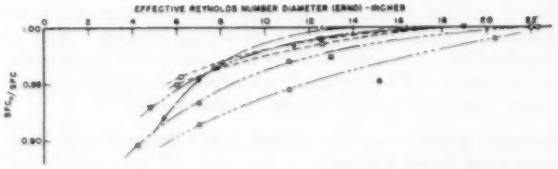

Fig. 5(*b*) Test results of altitude effect on specific fuel consumption as a function of effective Reynolds-number diameter, ERND; Case I, variable-area exhaust nozzle, constant temperature plus rotor speed control

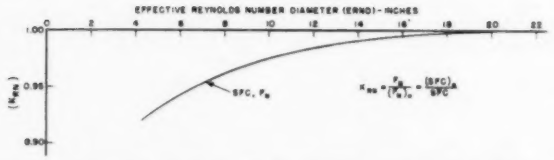

Fig. 6 Estimated effect of altitude on net thrust and specific fuel consumption as a function of effective Reynolds-number diameter, ERND; Case I, variable area exhaust nozzle, constant rotor speed control, constant temperature control

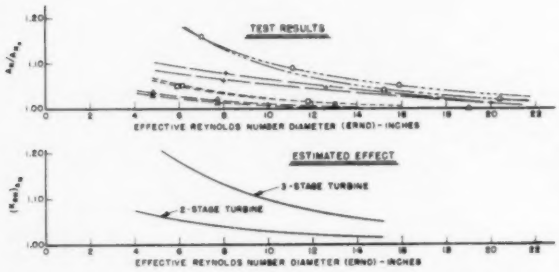

Fig. 7 Altitude effect on exhaust nozzle area as a function of effective Reynolds-number diameter, ERND; Case I, variable area exhaust nozzle, constant rotor speed control, constant temperature control

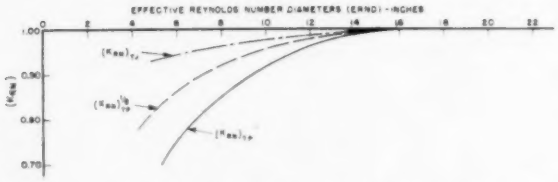

Fig. 8 Comparison of altitude effects on the performance of turboprop engines and turbojet engines equipped with variable area exhaust nozzle

considered herein are within about 3 per cent of the final curve established.

Exhaust Nozzle Area Correction Curve. As compressor and/or turbine efficiency losses are encountered, the engine exhaust nozzle area must be increased in order to maintain rotor speed and turbine-out temperature. An attempt was made to obtain a correlation of the ratio $A_N/(A_N)_0$ (where A_N is the actual area and $(A_N)_0$ is the generalized, or constant, area) as a function of the ERND. These data are shown in Fig. 7, and include both two-stage and three-stage turbine engines. The two-stage turbine data correlate fairly well, but the three-stage turbine shows higher values. This is reasonable, since the larger the number of turbine stages, the larger the increase in the exhaust-nozzle area would have to be to obtain the same effect. Consequently, in Fig. 7, exhaust nozzle area correction curves are shown separately for two-stage turbines and three-stage turbines. The two stage turbine curve is within about 3 per cent of all the data considered herein. The three-stage turbine curve is based on a single engine, and consequently, requires further verification.

Turbojet Engine (Case II)—(Fixed Area Exhaust Nozzle, Constant Rotor Speed Control)

Thrust and Specific Fuel Consumption Correction Curves. In this section, data are considered for engines with fixed area exhaust nozzles. In addition, data for the variable area exhaust nozzle engines, considered under Case I, are presented herein as fixed nozzle engines. Data for these engines are presented for the exhaust nozzle area which, in general, tends to give the best specific fuel consumption characteristics over the whole operating range.

It should be noted that Case II introduces an additional complication as compared with Case I. In Case I, the exhaust nozzle area was increased as component-efficiency losses were encountered in order to keep the compressor and turbine at essentially the same "matching point"; that is, same N and T. However, for Case II as component efficiency losses are encountered, the fixed exhaust nozzle area forces the engine to operate at higher turbine-inlet temperatures in order to maintain rotor speed. This means, in effect, that the engine has moved to a different operating point. Consequently, the data for Case II are actually the result of a combination of two effects: (*a*) The Reynolds-number effects, similar to those for Case I, and (*b*) the effects caused by changing the engine matching point. Changing the engine matching point introduces the specific characteristics of each engine and, therefore, could be expected to introduce additional scatter in the data.

The available data are presented in the form established herein in Figs. 9 and 10.

It will be noted that the thrust corrections are greater than 1.0; that is, the actual thrust values are higher than the generalized values would indicate, as ERND is decreased. This means that the effect of increasing turbine-inlet temperature is greater than the effect of decreasing Reynolds number, and a greater thrust actually results. It should be noted that there is a significant scatter among the data. For some cases, the thrust is essentially constant as ERND is decreased; and for certain exhaust nozzle areas (significantly different from the optimum values) a decreasing thrust was noted, although these data have not been shown in Fig. 9. However, in general, an increasing thrust correction is reasonably typical for the rated value of exhaust nozzle area.

The specific fuel consumption corrections are shown in Fig. 10. The correlation is somewhat better for the specific fuel consumption data than for the thrust data.

On the basis of these data, recommended correction curves were established for thrust and specific fuel consumption. These final curves are shown in Fig. 11. Most of the data considered herein are within about 5 per cent of the final curve established for specific fuel consumption; within about 8 per cent for thrust.

Fig. 9 Test results of altitude effect on net thrust as a function of effective Reynolds-number diameter, ERND; Case II, fixed area exhaust nozzle, constant rotor speed control

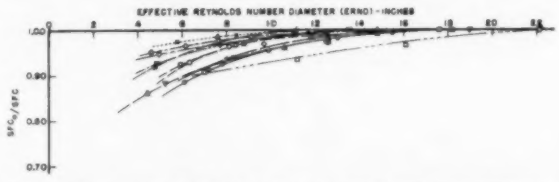

Fig. 10 Test results of altitude effect on specific fuel consumption as a function of effective Reynolds-number diameter, ERND; Case II, fixed area exhaust nozzle, constant rotor speed control

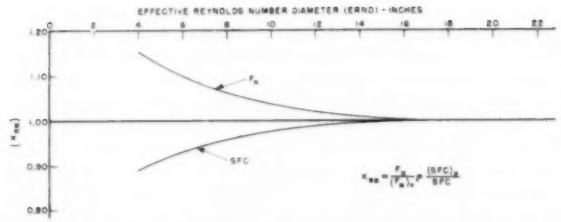

Fig. 11 Estimated altitude effect on net thrust and specific fuel consumption as a function of effective Reynolds-number diameter, ERND; Case II, fixed area exhaust nozzle, constant rotor speed control

Turbine-Out Temperature Correction Curve. As discussed previously, for Case II the engine tends to over-temperature as losses due to Reynolds-number effects are encountered. In general, this makes this method of operation impractical.

To indicate the magnitude of this effect, $T_{T2}/(T_{T2})_0$ versus ERND data are shown in Fig. 12. On the basis of these data, the recommended curve shown in Fig. 12 was established. Most of the data considered herein are within about 6 per cent of the final curve established.

Air Flow Rate Correction Curve. As discussed previously, the losses in air flow rate tend to be relatively small over the range being considered herein. To demonstrate this, $W_a/(W_a)_0$ versus ERND data are shown in Fig. 13.

For Case II, the fact that turbine-inlet temperature is increasing as ERND is decreased, tends to introduce an additional effect on air flow rate. However, since the compressor characteristics are very steep in the regions being considered, the temperature effect is considered relatively unimportant.

It will be noted that the corrections in air flow rate are relatively small over the entire range being considered. The recommended curve shown in Fig. 13, shows a maximum correction of only about 2 per cent, and is within about 2 per cent of most of the data considered herein.

As compressor state-of-the-art improves, the losses in air flow rate may become more important. Specifically, as relative Mach numbers increase, the increasing boundary layer thicknesses with decreasing ERND, may introduce greater reductions in air flow rate.

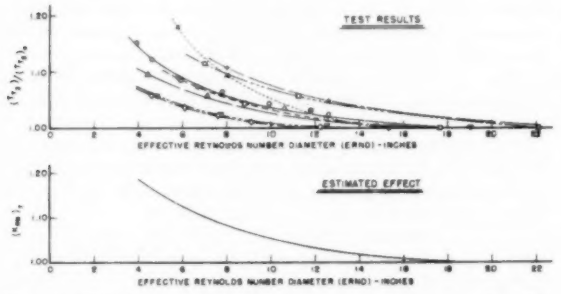

Fig. 12 Altitude effect on turbine-outlet temperature as a function of effective Reynolds-number diameter, ERND; Case II, fixed area exhaust nozzle, constant rotor speed control

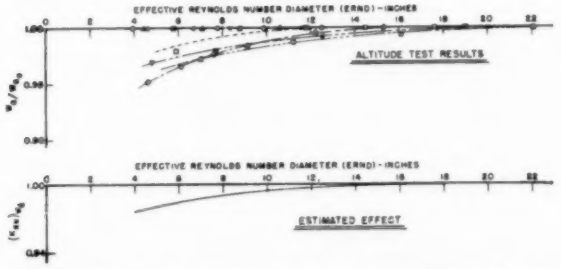

Fig. 13 Altitude effect on engine air-flow rate as a function of effective Reynolds-number diameter, ERND; Case II, fixed area exhaust nozzle, constant rotor speed control

Turbojet Engine (Case III)—(Fixed Area Exhaust Nozzle, Maximum Temperature Over-Ride)

Thrust and Specific Fuel Consumption Correction Curves. As discussed previously, Case II is an impractical way, in most cases, of controlling an engine. Consequently, for an engine with a fixed exhaust nozzle area, the rotor speed must be reduced, as losses are encountered, to stay within permissible turbine-inlet temperature limits.

In this section, the same engines as for Case II are considered on the basis of reducing rotor speed to stay within temperature limits. This introduces the same additional complication discussed under Case II; that is, the effects of the engine moving to a different operating point are superimposed on the effects of Reynolds number. However, since a turbojet engine is probably more sensitive to rotor speed than to any other single parameter, and since different engines will react differently to the same change in rotor speed, it is reasonable to anticipate that Case III will provide a poorer correlation than Case II. The available data are presented in the form established herein in Figs. 14 and 15.

As anticipated, there is considerable scatter among the thrust correction data. The correlation is significantly better for the specific fuel consumption data than for the thrust data.

On the basis of these data, recommended correction curves were established for thrust and specific fuel consumption. These final curves are shown in Fig. 16. Most of the data considered herein are within about 5 per cent of the final curve established for specific fuel consumption, and within about 14 per cent for thrust.

Rotor Speed Correction Curve. To demonstrate the magnitude of the reductions in rotor speed required to stay within temperature limits, $N/(N)_0$ versus ERND data are shown in Fig. 17. On the basis of these data, the recommended curve shown in Fig.

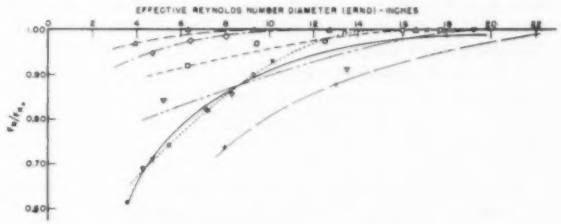

Fig. 14 Test results of altitude effect on net thrust as a function of effective Reynolds-number diameter, ERND; Case III, fixed area exhaust nozzle, constant temperature control

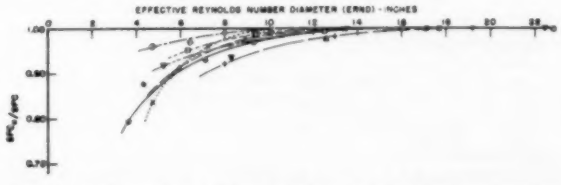

Fig. 15 Test results of altitude effect on specific fuel consumption as a function of effective Reynolds-number diameter, ERND; Case III, fixed area exhaust nozzle, constant temperature control

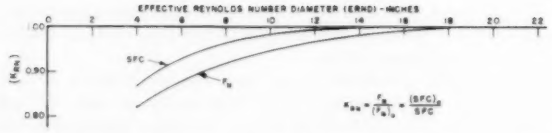

Fig. 16 Estimated effect of altitude on net thrust and specific fuel consumption as a function of effective Reynolds-number diameter, ERND; Case III, fixed area exhaust nozzle, constant temperature control

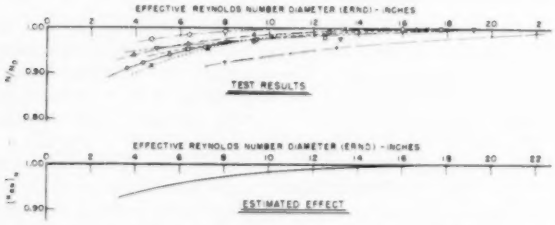

Fig. 17 Altitude effect on rotor speed as a function of effective Reynolds-number diameter, ERND; Case III, fixed area exhaust nozzle, constant temperature control

17 was established. Most of the data considered herein are within about 2 per cent of the final curve established.

Comparison of Data for Cases I, II, and III

In the previous sections, correction data have been established independently for each turbojet case considered. In this section, it is desired to compare these various sets of data.

The correction curves established for Cases I, II, and III—for both thrust and specific fuel consumption—are shown in Figs. 18 and 19.

The relationship among the thrust data is quite logical. The Case I curve represents the actual Reynolds-number effect for all three cases. The increase in thrust from Case I to Case II is caused by the increase in turbine-inlet temperature. The decrease in thrust from Case II to Case III is caused by the decrease in rotor speed.

The correction curves for specific fuel consumption fall very close to each other for all three cases. Within the accuracy of the data, the three curves are essentially equal. This would indicate that the primary reason for the increase in specific fuel consumption is the Reynolds-number effect, rather than the effect of

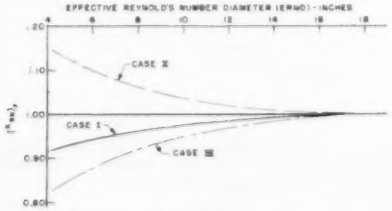

Fig. 18 Estimated altitude effects on net thrust; comparison of Cases I, II, and III

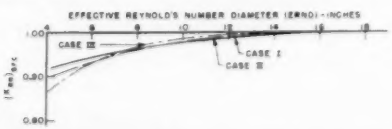

Fig. 19 Estimated altitude effects on specific fuel consumption; comparison of Cases I, II, and III

changing the engine matching point. This means that the various operating points shown in Fig. 4(*b*), for Cases I, II, and III, are in a relatively flat portion of the specific fuel consumption islands. Since most of the data considered herein are in the region of about normal to military rating, this is quite reasonable.

The relative accuracy of the data established for the three cases is summarized below. The per cents indicated represent the maximum deviations at the minimum values of ERND considered; that is, about 4 in. For larger values of ERND, the accuracy would be better.

	Thrust	Specific fuel consumption
Case I	3 per cent	3 per cent
Case II	8 per cent	5 per cent
Case III	14 per cent	5 per cent

This tabulation would indicate that specific fuel consumption data are fairly good for all three cases. However, the thrust data become significantly less reliable as the additional complications of Cases II and III are introduced.

It should be noted that approximately twice as many engines have been considered for Cases II and III, as compared with Case I. Consequently, it is possible that the apparent better accuracy of Case I might merely be the result of fewer data.

Turboprop Engine

There are still relatively few actual altitude test data available on turboprop engines. Consequently, any attempt to generalize the Reynolds-number effects must be considered as preliminary.

The available data are presented in the form established herein in Fig. 20. It may be seen that a reasonably good correlation of the available data is obtained.

An attempt was made to distinguish the effects of the various losses, as discussed in Fig. 3(*a*). The data available show that the effects of air flow loss and combustion efficiency loss are essentially negligible over the operating range being considered herein. This is similar to the turbojet data discussed previously. Here again, this means that the altitude losses are primarily due to component efficiency losses, and consequently, the SHP/$(SHP)_0$ and the $(SFC)_0/SFC$ curves should tend to coincide. Considering the general accuracy of the data shown in Fig. 20, this is generally true.

On the basis of all the foregoing, a single correction curve was established. This final curve is shown in Fig. 21. Over most of the operating range, all the data considered herein are within about 3 per cent of the final curve established.

Since the difference between SHP and ESHP, for any given engine, tends to be relatively small, the correction factors shown in Fig. 21 may be applied to either SHP and SFC, or ESHP and ESFC, whichever is more convenient. It is believed that this is within the accuracy of the correction data.

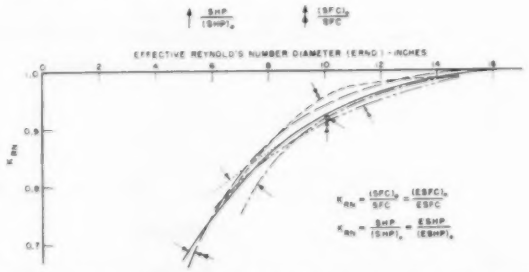

Fig. 20 Test results of altitude effects on horsepower and specific fuel consumption as a function of effective Reynolds-number diameter, ERND

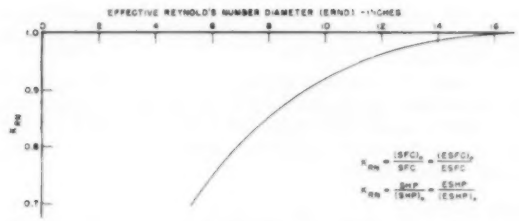

Fig. 21 Estimated effect of altitude on horsepower and specific fuel consumption as a function of effective Reynolds-number diameter

Comparison of Turbojet and Turboprop Data

As discussed previously, the case of the turbojet engine with variable area exhaust nozzle (Case I) is generally similar to the case of the turboprop engine. Consequently, it is of interest to compare the correction curves established independently for each of the two cases.

This comparison was made roughly as follows: For the turboprop case, the shaft horsepower is proportional to the net enthalpy (ΔH) available to the output turbine. For the turbojet case, the gross thrust is proportional to the exhaust jet velocity, which is proportional to $(\Delta H)^{1/2}$. If it is assumed that the exhaust jet velocity is large compared to the forward speed of the airplane, the net thrust would also tend to be roughly proportional to $(\Delta H)^{1/2}$. Consequently, in Fig. 8, the relationship between $(K_{RN})_{TJ}$ and $(K_{RN})_{TP}{}^{1/2}$ is shown.

It will be noted that the turboprop corrections are more severe. Although there may be some question about the quantitative values shown, the general relationship between the turboprop and turbojet appears to be valid. Specifically, the turboprop would appear to be the more severe case for two reasons: (*a*) The effective Reynolds number decreases as the gas flows through the turbine. Consequently, the major Reynolds-number effects are felt in the later stages of the turbine. Since the turbojet has fewer turbine stages, the turbine efficiency losses should be less severe for the turbojet. (*b*) The reduction-gear losses of the turboprop tend to become a larger percentage of the output as altitude is increased. This tends to make the altitude corrections more severe for the turboprop.

It should be noted that there is relatively good agreement between the turbojet and turboprop as far as the critical ERND is concerned. Losses for both cases start to appear at an ERND value of about 16 in.

Effect of Engine Size

Obviously, the physical size of an engine is very important in determining the susceptibility of an engine to Reynolds-number effects. In Fig. 22, quantitative estimates of the effect of engine size are shown on the basis of the data established herein.

Fig. 22 shows data for engines with a range of compressor inlet diameters from 10 to 50 in. Data are shown for turbojet engines (Case 1) at a flight Mach number of 0.9, and for turboprop engines at a flight Mach number of 0.7. Fig. 22 shows the loss, $(1 - K_{RN})$, in F_N and SFC for turbojet engines, and in SHP and SFC (or ESHP and ESFC) for turboprop engines, as a function of altitude.

When the actual engine size is less than the critical ERND of about 16 in., a value of K_{RN} less than 1.0 would be indicated for static sea-level operation. This may be interpreted to mean that the engine is experiencing "size" losses even at static sea level. For these cases, the K_{RN}, indicated by the correction curve for the operating point being investigated, is divided by the reference value of K_{RN} for the static sea-level point, to give altitude corrections for smaller engines. This explains the sharper increase in $(1 - K_{RN})$ with altitude for the 10-in-diam data in Fig. 22.

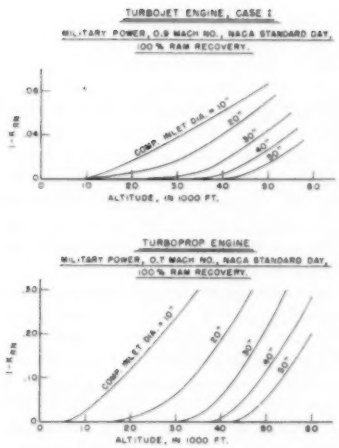

Fig. 22 Estimated effect of engine size on altitude losses of turbojet and turboprop engines

Concluding Remarks

The primary objective of this study was to establish a simple method for making preliminary estimates of the Reynolds-number effects. Throughout the investigation, simplicity has been stressed, perhaps at the expense of accuracy. As set up at present, the only engine datum which must be known is the compressor tip diameter. Considering the many differences in the engines considered herein—for example, differences in size, compressor pressure ratio, turbine-inlet temperature, number of compressor and turbine stages—it is believed that a reasonably good correlation has been obtained.

Undoubtedly, many methods of improving accuracy could have been attempted, however, all at the expense of complexity. In view of the general accuracy of the test data relative to the magnitude of the correction factors, and the general uncertainties involved in the entire Reynolds-number problem, it is perhaps doubtful that any additional refinement would be warranted, for making preliminary estimates.

Considerably more altitude test data will be required to establish more specifically the range of operating conditions for which the data established herein may be applied with reasonable accuracy. However, on the basis of the data used to establish the correction curves, it is reasonable to assume that the data are most directly applicable to (*a*) moderate to high subsonic flight speeds for turbojet engines, (*b*) low to moderate flight speeds for turboprop engines, and (*c*) approximately normal or military rating for both engine types. In general, these tend to be the ranges of primary interest, for current operating conditions, as far as Reynolds-number effects are concerned.

Acknowledgments

This paper was originally published as NAVAER Unclassified Report No. DR-1794 of April, 1956. The engine altitude tests, which form the basis for the subject investigation, were done by the Lewis Flight Propulsion Laboratory of the National Advisory Committee for Aeronautics, in Cleveland, Ohio, and the Aeronautical Engine Laboratory of the Naval Air Material Center, in Philadelphia, Pa. The co-operation of Mr. C. A. DeCrescente, of the Naval Air Development Center, in Johnsville, Pa., is gratefully acknowledged.

Discussion

J. Austin King.[2] The proposal to correlate engine performance with an "effective Reynolds-number diameter," presents a useful approach to the problem of estimating altitude effects on a number of different engines. The difficulty, as pointed out by the author, in the use of the "Reynolds-number index" is that the correlation applies only to the specific engine from which the data were obtained. To a significantly smaller degree this difficulty probably still applies to the parameter suggested in the paper. In particular, the parameter is probably a little too severe on the small "state-of-the-art" engine.

The small, modern engine operates at axial Mach numbers into the compressor as high as 0.8. Compared with more conservative engines whose axial Mach numbers may be as low as 0.4 there could be a difference of almost 2 to 1 in Reynolds number because of the velocity term in the numerator. In this case, it would seem that a correction factor should be applied to the N/N_{mil} term, in the effective-Reynolds-number diameter. However, the presentation of a particular parameter implies that several others have been tried and found inferior. Perhaps the author has tried such a correction and rejected it.

Another possible source of error is the selection of compressor-tip diameter as the characteristic length. This would be an excellent choice for scaling up or down a specific engine, but in comparing engines of approximately the same size the choice neglects the chord lengths of the compressor and turbine, and the chord is generally recognized as the controlling length that influences Reynolds number.

The author's approach does provide a quick means of evaluating altitude effects on any engine within the limits of accuracy as stated by the author. The method eliminates the necessity for estimating the Reynolds number and other altitude effects on each of the individual components prior to deriving estimated performance curves. As we all know, this is a rather long and involved procedure.

The paper also presents additional data on the subject of Reynolds-number effects, a subject on which more of this type of information is needed before the last word can be said.

In closing, the author should be congratulated on a fine and valuable presentation.

[2] Project Engineer, Fairchild Engine Division, Deer Park, N. Y.

Author's Closure

Mr. King's points are well taken. The limitations in the ERND parameter, as pointed out in his discussion, should be appreciated when using the data. The refinements proposed by Mr. King were given consideration, but were not investigated in detail. The primary purpose of the paper was to investigate the degree of correlation that could be obtained with a basically simple parameter. As indicated in the paper, it is doubtful that any additional refinement would be warranted for the purpose of making preliminary estimates.

In connection with the axial Mach numbers of modern compressors, it is true that the higher velocities are beneficial as far as Reynolds number is concerned. However, the higher velocities are not an unmixed blessing. As pointed out in the paper, these higher velocities may introduce greater reductions in the air-flow rate with decreasing Reynolds number. Consequently, the over-all thrust losses may be just as great as with the lower velocity levels. Further test data will be required to definitely establish this point.

As pointed out in the abstract, an altitude calibration of each specific engine is still required to establish accurate altitude data. If any actual test data are available, they should be used by all means. However, in the absence of any other information, the data in the paper are offered to help make some preliminary estimates. It should be fully appreciated that this offer is made on a no-guarantee, no-money-back basis.

Effects of Stage Characteristics and Matching on Axial-Flow-Compressor Performance

By AUBREY STONE,[1] SAN DIEGO, CALIF.

The use of stage characteristics obtained from test data in the performance analysis and development of an axial-flow compressor is described. The discussion is illustrated by an analysis of the general trends in relative stage matching as shown by an idealized example and also by test experience. Factors governing major performance parameters are discussed and certain development problems and possible solutions are reviewed.

Introduction

THE performance of an axial-flow compressor is a function of the characteristics of the individual stages and their relative matching. Although numerous papers discussing single-stage performance are available, relatively few have been published dealing with performance analysis and development of the complete compressor.

After considering the basic stage characteristics, this paper analyzes the operation of an actual compressor by first considering the general trends in relative stage matching as shown by an idealized procedure. The results of the idealized case are examined in the light of the effects of Mach number and stage interaction existing in an actual compressor as indicated by test experience. The factors governing major performance parameters are discussed.

The use of measured stage-performance data in analyzing compressor performance is next considered, followed by a review of development problems and some possible solutions.

The Stage Characteristic

The velocity diagram for any radial section of the stage of an axial-flow compressor may be represented as shown in Fig. 1. It may be seen that this diagram is partly a function of the velocity vector leaving the previous stator row. The temperature rise produced by the section is given by

$$\Delta T = \frac{U \Delta V_w}{g J C_p} \quad \ldots\ldots [1]$$

where

U = blade speed
ΔV_w = change in tangential velocity imparted to air by rotor
g = acceleration due to gravity
J = mechanical equivalent of heat
C_p = specific heat at constant pressure

This may be expressed nondimensionally as a fraction of the temperature equivalent of blade speed, $U^2/(2gJC_p)$, to obtain temperature coefficient, ϵ. The number 2 is usually omitted.

Thus $$\epsilon = \frac{gJC_p\Delta T}{U^2} \quad \ldots\ldots [2]$$

Combining Equations [1] and [2] shows that

$$\epsilon = \frac{\Delta V_w}{U} = \frac{\text{change in tangential velocity}}{\text{blade speed}} \quad \ldots\ldots [3]$$

If η_{st} = adiabatic efficiency of stage, then

$$\Delta T' = \eta_{st}\Delta T$$

where $\Delta T'$ = isentropic temperature rise.

A pressure coefficient is defined as

$$\psi = \frac{gJC_p\Delta T'}{U^2} = \frac{gJC_pT_1}{U^2}\left[P_2/P_1^{\frac{\gamma-1}{\gamma}} - 1\right] = \eta_{st}\epsilon \ldots [4]$$

where

T_1 = total temperature at stage inlet
P_2/P_1 = total pressure ratio over stage
γ = ratio of specific heats

Temperature and pressure coefficients and stage efficiency for a given stage are, to the first order, functions of rotor incidence angle. For a given absolute air-inlet angle, rotor incidence is a function of the ratio of inlet axial velocity to blade speed, defined as the flow coefficient ϕ. The usual method of presentation is to express mean stage performance on the basis of the average axial velocity into the stage and the blade speed at some convenient radius, such as that for the rotor tip.

Assuming no variation in absolute air-inlet angle and relative air angle leaving the rotor, and no change in the axial velocity ratio across the rotor, then the change in tangential velocity would

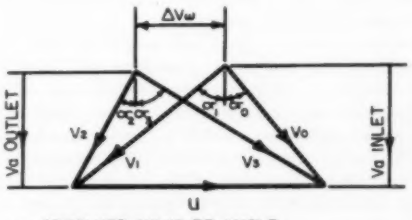

α_0 = ABSOLUTE AIR INLET ANGLE
α_1 = RELATIVE AIR INLET ANGLE
α_2 = RELATIVE AIR OUTLET ANGLE
α_3 = ABSOLUTE AIR OUTLET ANGLE
V_0 = ABSOLUTE AIR INLET VELOCITY
V_1 = RELATIVE AIR INLET VELOCITY
V_2 = RELATIVE AIR OUTLET VELOCITY
V_3 = ABSOLUTE AIR OUTLET VELOCITY
U = BLADE SPEED
V_a = AXIAL VELOCITY
ΔV_ω = CHANGE IN TANGENTIAL VELOCITY

Fig. 1 Velocity diagram for a compressor stage

---

[1] Engineer in Charge, Aero-Thermodynamics Group, Engineering Analysis Department, Solar Aircraft Company.

Contributed by the Gas Turbine Power Division and presented at a joint session with the Aviation and Hydraulic Divisions at the Annual Meeting, New York, N. Y., December 1–6, 1957, of THE AMERICAN SOCIETY OF MECHANICAL ENGINEERS.

NOTE: Statements and opinions advanced in papers are to be understood as individual expressions of their authors and not those of the Society. Manuscript received at ASME Headquarters, August 5, 1957. Paper No. 57—A-139.

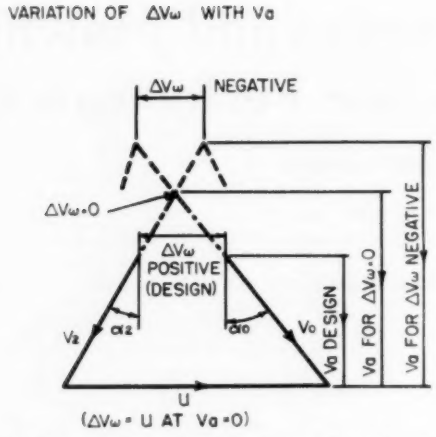

Fig. 2 Effect on velocity diagram of varying axial component

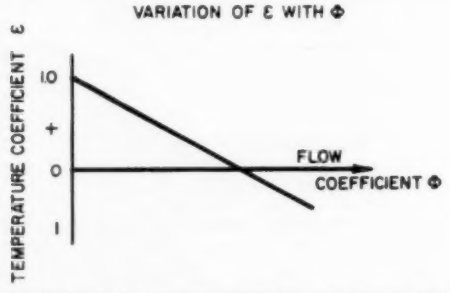

Fig. 3 Variation of temperature coefficient with flow coefficient for constant flow angles

vary linearly with V_a. This is illustrated in Fig. 2. Thus, when $V_a/U = 0$, $\Delta V_\omega = U$, and the temperature coefficient reaches a maximum value of unity. When V_a/U becomes sufficiently high, the temperature coefficient becomes zero. At still higher flow coefficients, ΔV_ω becomes negative and the stage then operates as a turbine rather than a compressor. Fig. 3 shows the resulting characteristic of these coefficients.

In practice, it is found that, although over a certain range of flow coefficients the changes in absolute air-inlet angle and relative air-outlet angle leaving the rotor are fairly small, they change considerably at extreme blade incidences. A typical stage characteristic for constant Mach number is shown in Fig. 4. As the flow coefficient is reduced, rotor incidence increases and eventually positive stall occurs. Conversely, as the flow coefficient is increased, negative incidence stall, or perhaps choke—depending on the Mach number—is eventually reached. It is interesting to note from Fig. 4 that, after an initial fall-off as the stage passes through its positive incidence stall point, the temperature coefficient recovers and continues to increase upon further reduction in flow coefficient. What happens is that as the rotor stalls its relative air-outlet angle changes from a regime where it is of about design value to a regime where it is much greater because of flow separation.

Examination of stationary cascade results shows the effect of Mach number on stage performance. Fig. 5 illustrates a typical polar diagram showing the envelope of Mach number and air-inlet angle bounding the region of efficient cascade operation. Such an envelope could be plotted to indicate the operating limits beyond which the cascade losses exceed a given multiple of the

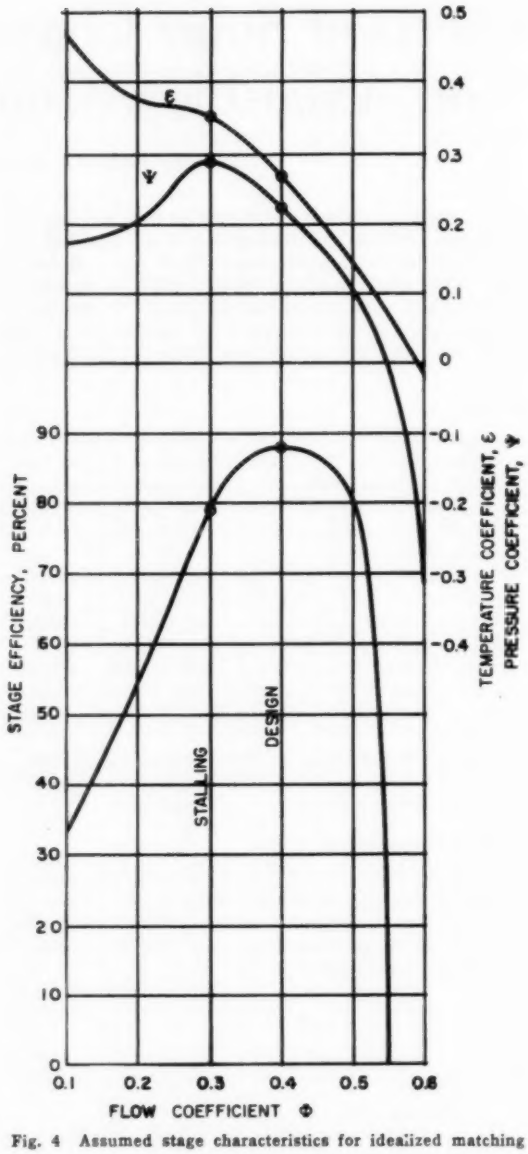

Fig. 4 Assumed stage characteristics for idealized matching

minimum loss. Twice-minimum loss is usually shown. A similar diagram can be derived for a compressor rotor based on pitch line conditions, Fig. 6. Assuming an absolute air angle from the previous stator and a Mach-number equivalent of pitch-line blade speed, based on static temperature, it is possible to show the relative Mach number and air-inlet angle and thus the operating limits of axial Mach number (and hence flow coefficient) for stall and choke. Fig. 6 illustrates how the efficient range of flow coefficient narrows at Mach numbers above 0.4. Fig. 7 shows how this affects the stage characteristic.

Idealized Stage Matching in Compressor

To illustrate broadly how the individual stages operate over a wide range of conditions, an over-all performance map was calculated for a hypothetical ten-stage compressor assuming, for

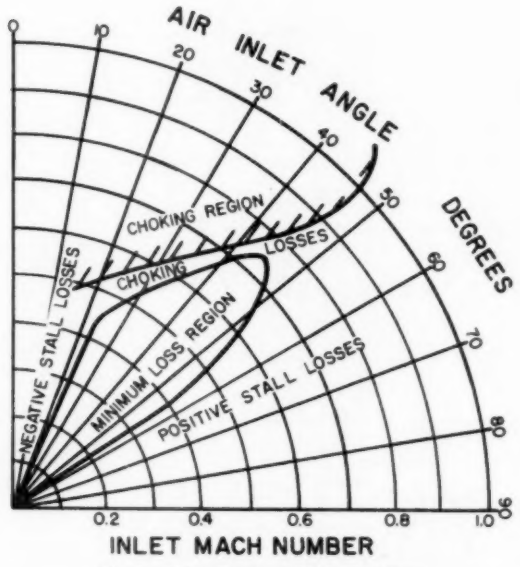

Fig. 5 Polar diagram of cascade losses

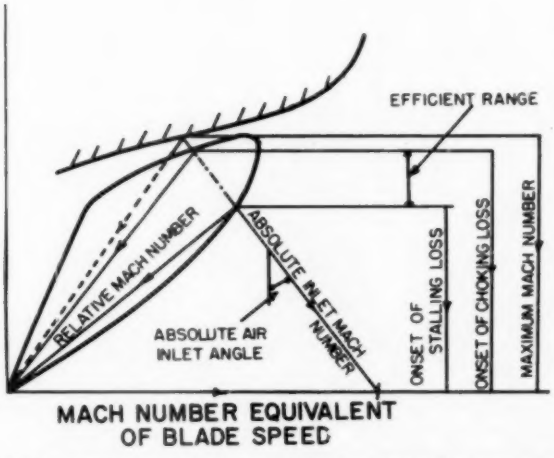

Fig. 6 Range of operation of rotor for different blade Mach numbers

simplicity, ten identical stage characteristics as shown in Fig. 4. Stage pressure ratio and temperature rise were computed from Equations [2] and [4], the flow coefficient at each stage being obtained from the equation of continuity. The area schedule was chosen to give constant axial velocity through the compressor at the design point, with each stage operating at a flow coefficient of 0.4, corresponding to a pressure coefficient of 0.8 of the maximum. In order that the matching could be illustrated as simply as possible, no allowance was made for Mach number and interaction effects on stage performance. Consequently, the results shown are only qualitative in value. How they differ from those appertaining to the behavior of an actual compressor is discussed later.

The computed over-all performance map is shown in Fig. 8(*a*) as a plot of total pressure ratio against percentage of design weight flow, and includes the contours of constant adiabatic efficiency.

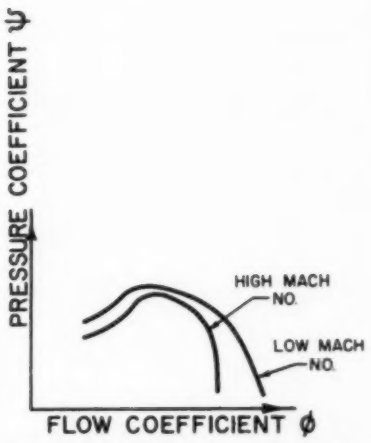

Fig. 7 Effect of Mach number on operating range of a stage

Fig. 8(*b*) provides a further illustration which includes those regions normally cut off by compressor surge, in order to show where (for this idealized case) each stage reaches its stalling point. Stage stall was assumed to occur at maximum stage-pressure coefficient; i.e., at a flow coefficient of 0.30.

Since the area schedule was chosen so that all stages operate at the same value of flow coefficient at the design point, any variation in mass flow or speed from the design condition generally means that the stage density ratios across the blading, and hence axial-velocity ratios, differ from design. Fig. 9 illustrates the variation in stage-flow coefficient through the compressor for various speeds and mass flows. The pressure coefficient at which each stage operates may be seen by referring to the stage characteristic, also included in Fig. 9.

As Fig. 9 indicates, when the first stage operates at above design density ratio—due to working at a higher pressure coefficient and/or higher speed than design—the second stage operates at a lower flow coefficient and hence higher pressure coefficient than stage 1. The second-stage density ratio is thus even farther above design than that of stage 1. This effect is cumulative through the compressor until the flow coefficients become sufficiently low to cause stage stall, whence the rate of decrease of flow coefficient diminishes. The converse is of course true when the first stage operates at below its design density ratio.

It is interesting to note that approximately constant flow coefficient can be maintained below design speed, providing the pressure coefficients, and hence density ratios, are sufficiently high. Fig. 9(*d*) shows that at 95 per cent speed, a constant flow coefficient of about 0.37, corresponding to a pressure coefficient of 0.25, can be maintained throughout the compressor. (At design speed, the constant flow coefficient condition is achieved with a pressure coefficient of 0.225.)

For the peak pressure coefficients assumed in this example, 92 per cent is the lowest speed at which a schedule of approximately constant ϕ can be maintained. This is represented on the compressor map, Fig. 8(*b*), as the intersection of the stall lines of all the stages. Above this speed, as may be seen from Fig. 8(*b*) and also Fig. 9, stage 10 is always the first stage to reach stall, since the density ratios for the corresponding matching are above design. As mass flow is reduced, the other stages reach stall in the order 9, 8, 7, and so on. Below 92 per cent speed, the density ratios are always below design, and the order of stalling reverses; i.e., stage 1, 2, 3, and so forth.

Fig. 9 indicates that the maximum mass flow at any constant speed is governed by stage 10 reaching maximum flow coefficient.

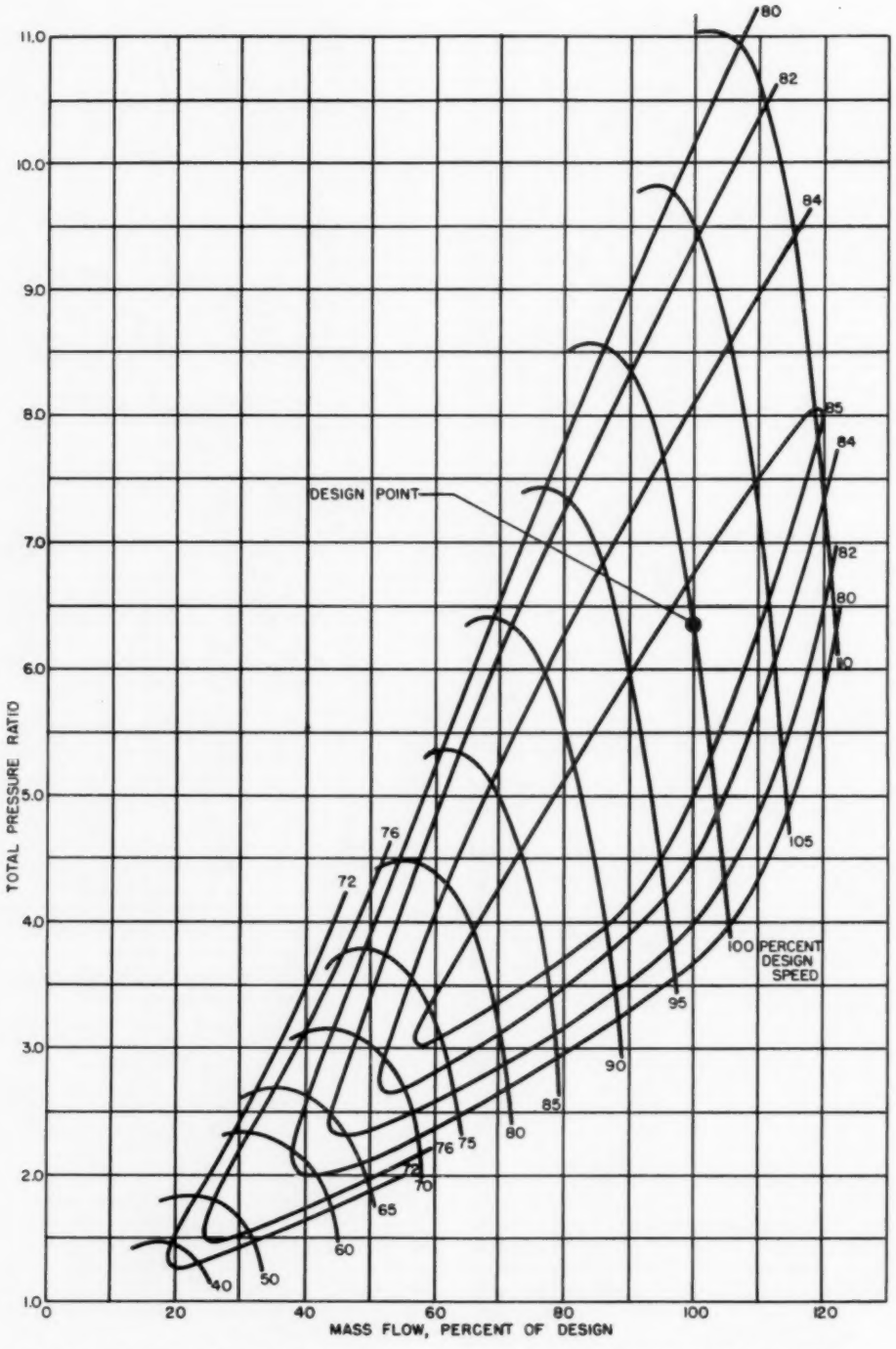

Fig. 8(*a*) Over-all performance of idealized compressor with contours of constant adiabatic efficiency

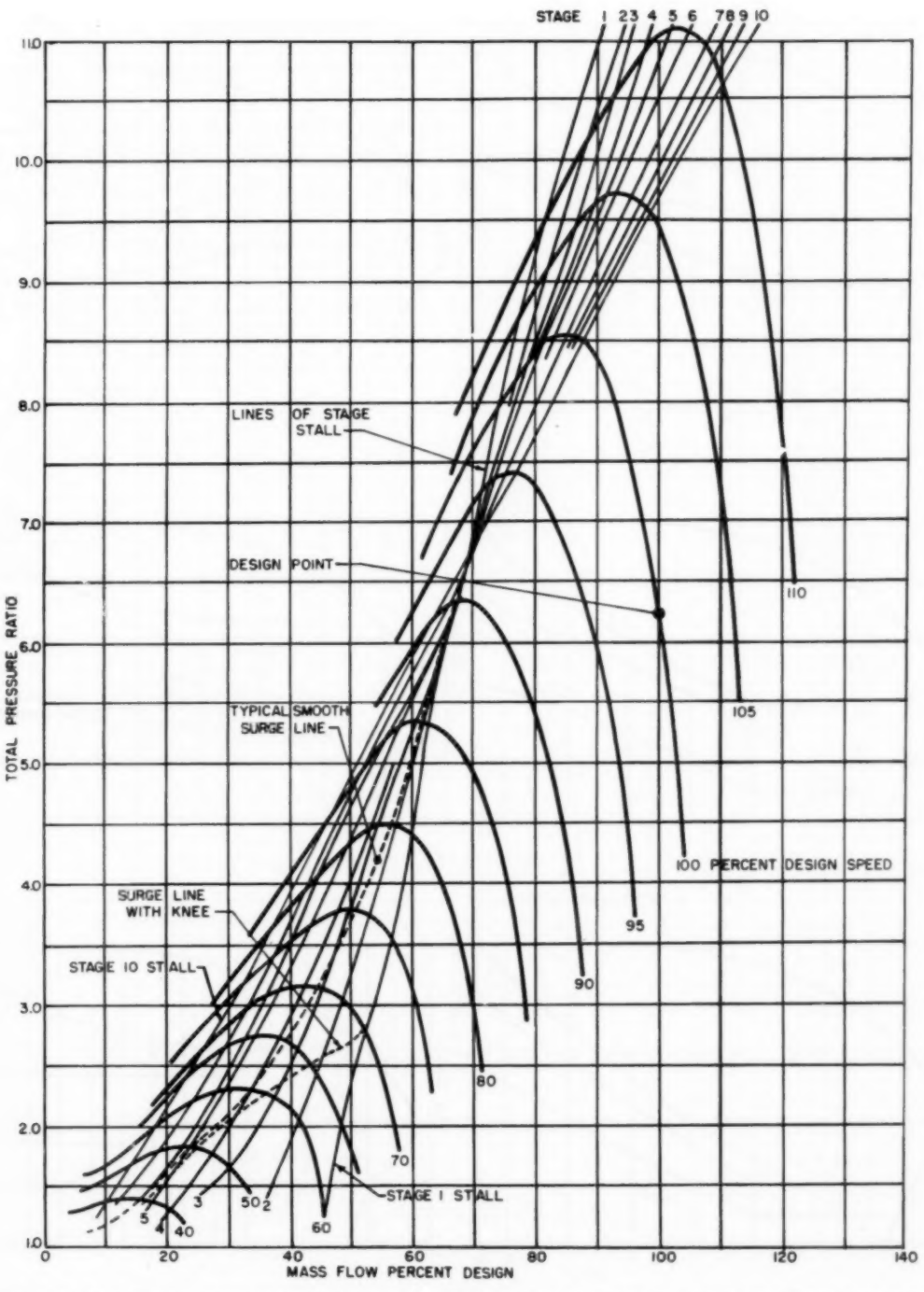

Fig. 8(*b*) Over-all performance of idealized compressor showing where each stage reaches stall and typical surge lines

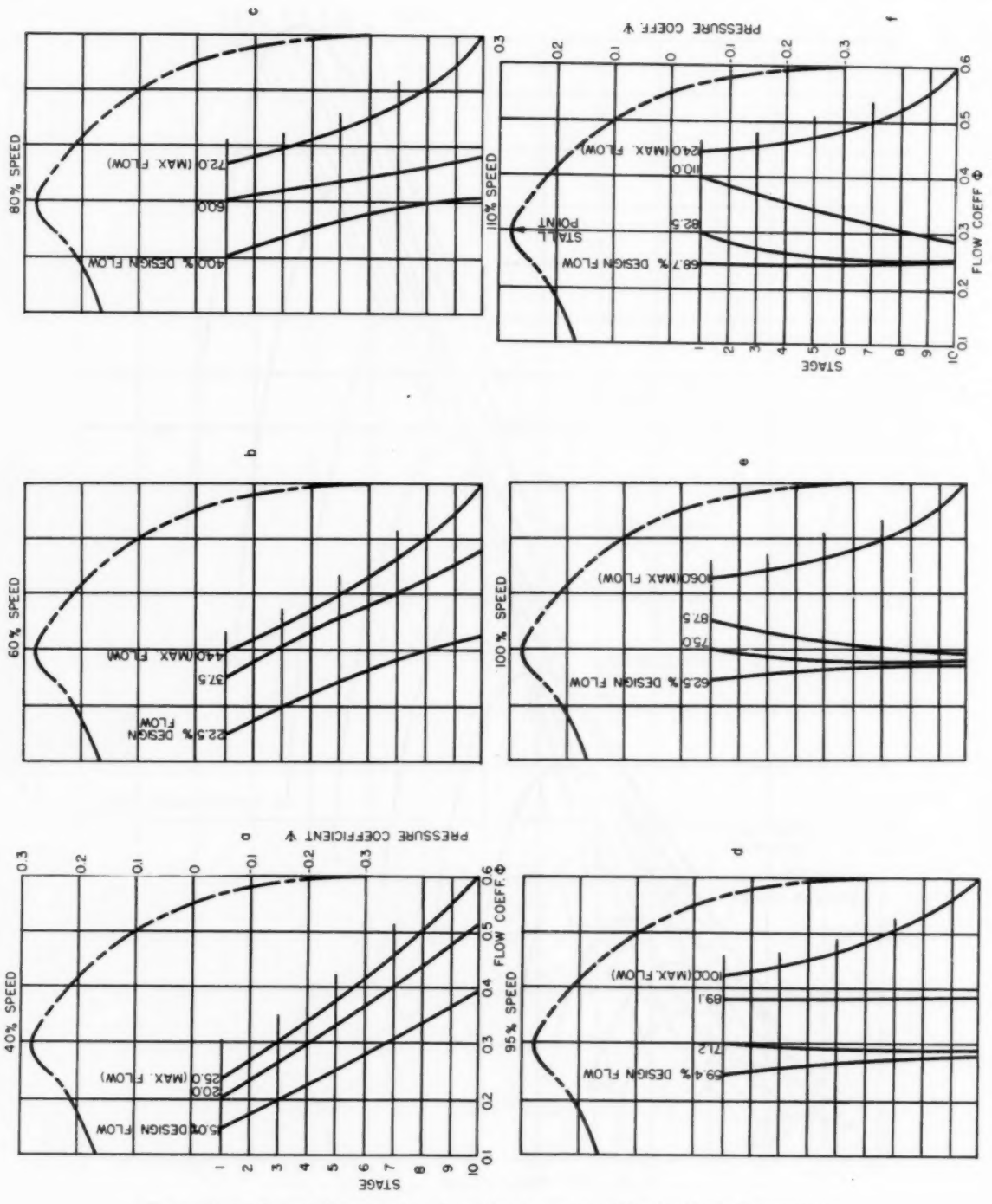

Fig. 9 Assumed stage characteristic and variation in stage matching for idealized compressor

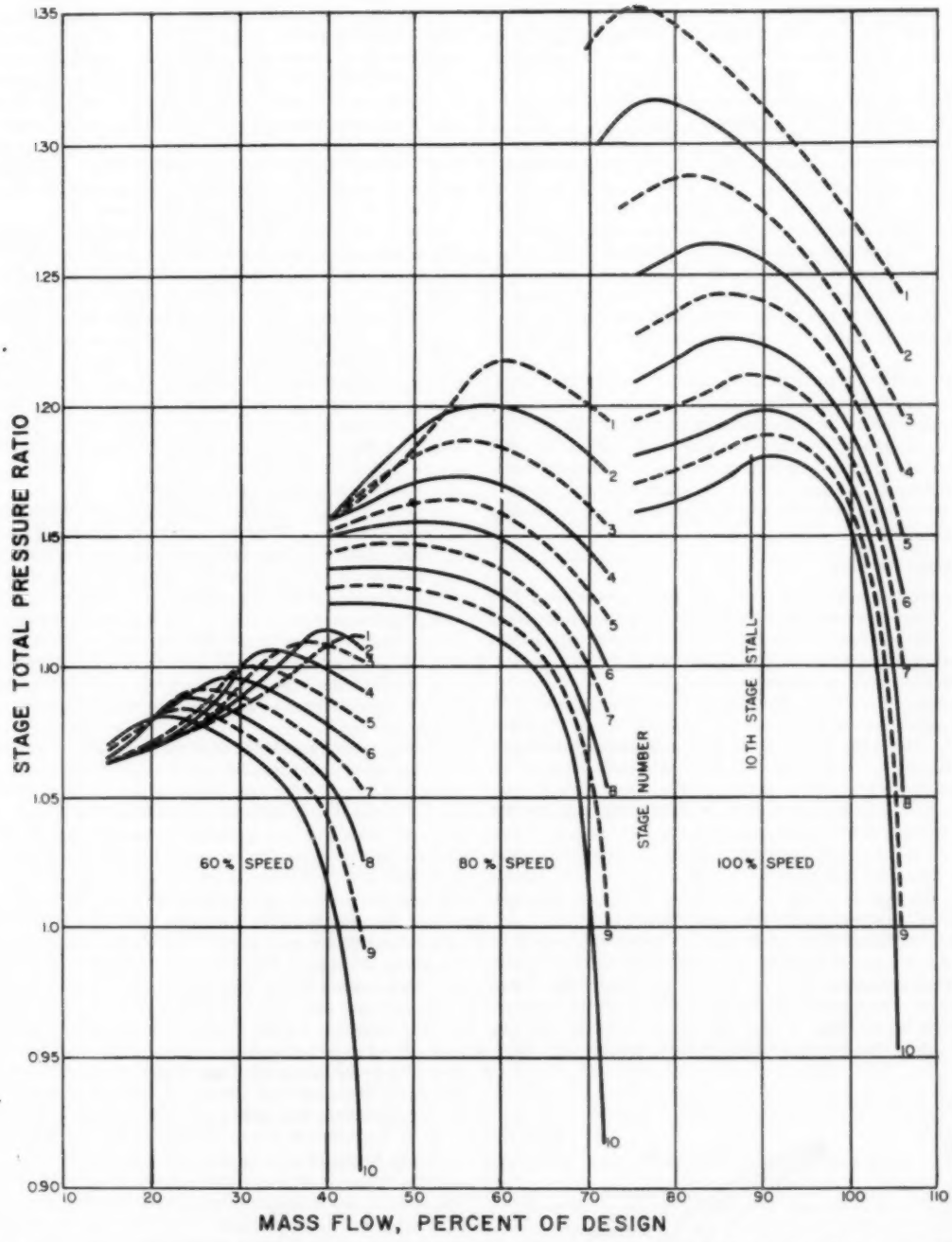

Fig. 10 Stage pressure ratio versus mass flow for idealized compressor at 60, 80, and 100 per cent of design speed

In other words, increasing mass flow at constant speed will always result in the ratio of stage-inlet density to the corresponding design density being lower for the last stage than for any other stage in the compressor. However, as described later in the paper, the stage matching in an actual unit differs at the higher speeds from that shown by this idealized case.

Fig. 9 also shows how the maximum flow coefficients reached by the early stages, as determined by stage 10 choking, decrease continuously as the speed falls. Thus, although at above 60 per cent speed the over-all characteristic, Fig. 8(*b*), includes the stall points of all the stages, at lower speeds the tenth stage chokes before the over-all characteristic can include the stall points of certain early stages. For example, at 40 per cent speed, stages 1, 2, and 3 are forced to operate fully stalled even up to maximum mass flow. This combination of the early stages stalling and later stages tending to choke is reflected by poor over-all efficiency at low speeds.

Fig. 10 shows the total pressure-ratio characteristic of each stage on a basis of compressor mass flow. It may be noted how the characteristics of the successive stages appear at higher flows relative to the characteristics of the preceding stages as speed is increased, due to increasing stage-density ratio. Because stage-inlet temperature increases through the compressor (at constant speed), the level of pressure ratio diminishes through succeeding stages, Equation [4].

Actual Stage Matching

The foregoing analysis is obviously highly idealized. The effects of Mach-number variation with speed and stage interaction have to be taken into account when considering the actual case. A typical matching analysis for a unit designed with stages near optimum incidence is presented below.

Maximum Mass Flows. The idealized matching analysis indicated that, at least up to 110 per cent of design speed, the tenth stage was always the first to choke and so determined the maximum mass flow. In practice, however, as speed increases, the Mach number relative to the early blade rows increases at a faster rate than at the later stages, which means that the stage choking flow coefficients reduce more rapidly in the early stages. Thus, usually at about design speed and higher, the maximum mass flow is governed by choking somewhere in the early stages. Consequently, the rate of increase of maximum mass flow with rpm generally falls as speed is increased above design value.

Typical matching of the maximum flow point with respect to stage 1 is illustrated in Fig. 11. As speed, and hence Mach number, increases, the first-stage choking flow coefficient falls. Up to about 90 per cent speed the maximum flow through the compressor is governed by stage 10 reaching choke, the matching being very similar to that shown for the idealized compressor. However, the narrowing of the early stages flow coefficient range due to Mach number generally means that at about design speed some stage between the front and middle of the compressor determines the maximum flow, in contradistinction to the idealized case. At about 105 per cent speed, stage 1 generally becomes the first to reach maximum flow coefficient, and hence the compressor-inlet flow coefficient reaches its maximum value. At higher speeds the inlet flow coefficient decreases because of the reducing first stage choking flow coefficient, resulting in a sharp reduction in the rate of increase of maximum mass flow with speed.

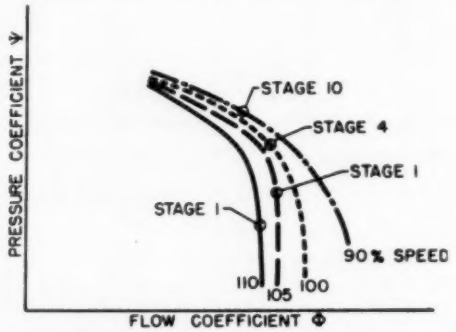

Fig. 11 Typical matching at maximum mass flow showing operating point of choking stage relative to first-stage characteristic

Over-all Efficiency. The idealized compressor showed little drop in over-all efficiency with overspeed, Fig. 8(*a*), whereas in actual fact it is usual to find that the efficiency reaches a maximum at about 90 per cent speed, falls off fairly gradually (by 1 or 2 per cent) to design speed, then drops quite rapidly with overspeed. At 90 per cent speed, all stages usually can match at flow coefficients fairly close to design. At design speed, although the stages may match at the design flow coefficients, the Mach-number level through the early stages is higher, so that they suffer somewhat higher losses than at 90 per cent speed. At overspeed the change in matching and narrowing of the early stage ranges due to Mach number forces the early stages toward the choke, whence their losses increase rapidly.

Surge Line. The surge limit is generally associated with one or more stages stalling. Thus the stall points indicated on the over-all performance map, Fig. 8(*b*), of the idealized compressor provide an indication of the cause of surge at different speeds.

Experience has shown that stable operation at the higher speeds with a stage operating in the stalled regime is unusual. A line drawn through the points corresponding to stage 10 stall at and above 92 per cent speed would therefore probably represent the surge limit of the hypothetical unit. It may be seen why the over-all characteristics at high speed remain quite steep even up to the surge point.

At 90 per cent speed, the fact that stages 1 to 5 reach stall simultaneously would probably cause surge at that point. As the speed is reduced further, the probable position of the surge line on the idealized unit becomes more difficult to define. As the stage-matching analysis indicated, when the speeds are sufficiently low, the mass-flow ranges of stable operation are bound to include stalling sections of several early stage characteristics. On some compressors it is found that the surge line passes through or near the peaks of all the over-all constant speed characteristics up to about 90 per cent speed. This yields a relatively smooth surge line, as shown in Fig. 8(*b*). Such a surge line generally implies that several of the early stages can operate through the transition from unstalled to stalled without causing compressor surge. Otherwise, a discontinuous surge line would probably result. If surge is triggered by the first stage reaching stall, the surge line would fall steeply from 92 per cent speed, following the line of the first-stage stall. However, this cannot continue since at lower speeds the first-stage stalling point does not appear on the over-all characteristic due to choking of the later stages. Since the surge line must pass through the origin of the map, it must suffer a change in slope (or knee) at the speed where stage 1 no longer continues to trigger surge. It may be seen from Fig. 8(*b*) that the lower the speed at which stage 1 persists in triggering surge, the more acute becomes the knee. This critical speed depends both on the severity with which stage 1 stalls, and on the degree of stabilizing influence associated with the unstalled later stages. As the speed is reduced, these later stages operate at increasingly higher flow coefficients at the mass flows corresponding to the first-stage stall point, Fig. 9. Consequently they operate on regions of their characteristics possessing high negative slope, providing a stabilizing influence which increases with reducing speed, and eventually offsetting the effects of the steep initial

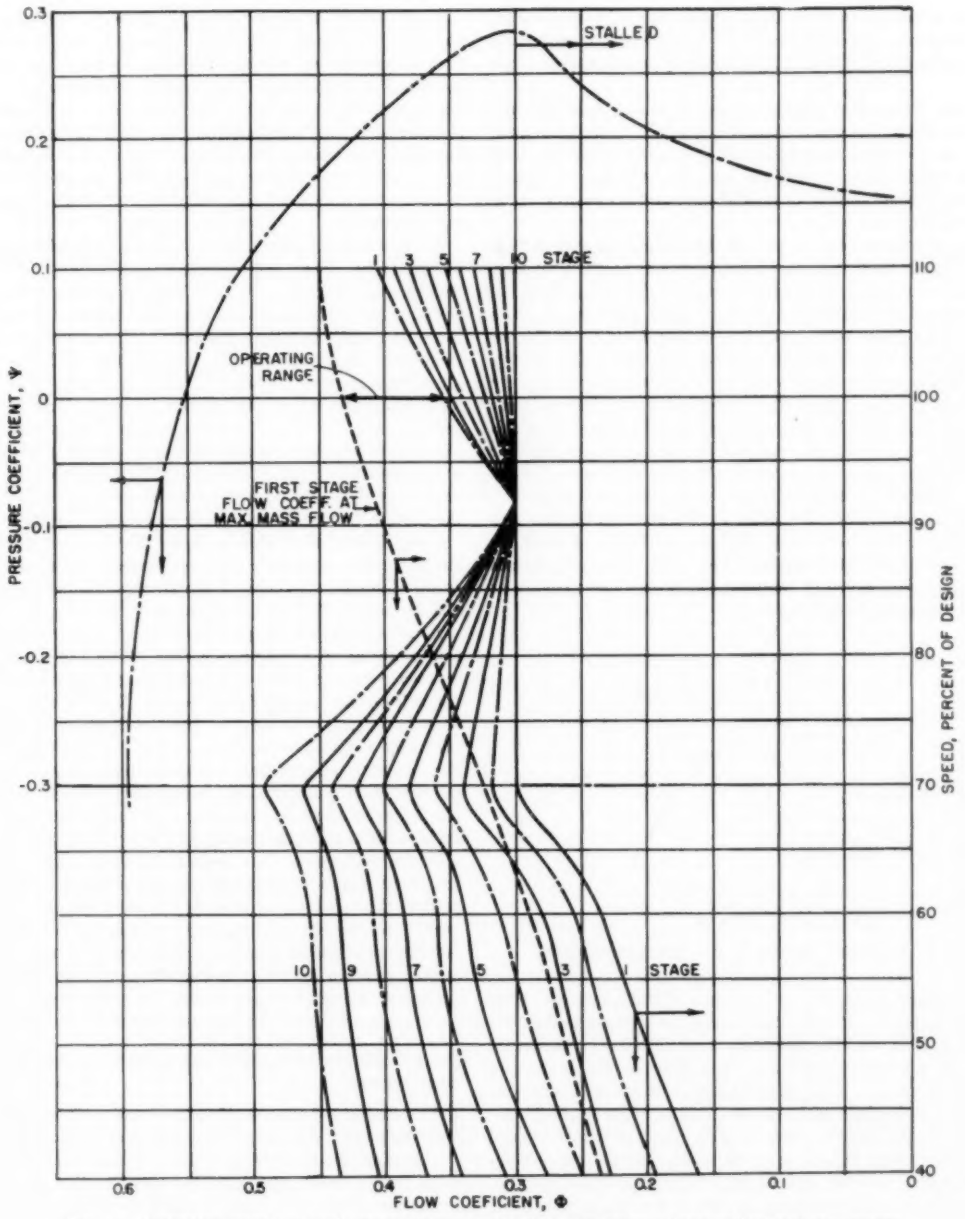

Fig. 12 Operating points of each stage along a surge line possessing a knee—idealized compressor

positive stalling slope of the first-stage characteristic. Also, the severity of the first-stage stall diminishes as the speed is lowered.

It may be that some early stage other than the first is the cause of the knee; stage 1 may possess a relatively "soft" stall which in itself might not persist in triggering surge as the speed is lowered. Stage 1 would then operate some way into stall without triggering surge and the mass flow might be reduced until some following stage reaches stall. At this point the compressor may surge, partly because stage 1 is already stalled, and also because the stabilizing influence of the later stages has diminished due to the lower mass flow.

Below the knee, the speeds, and hence pressure differences due to stage stall, are relatively low, and the surge line tends to follow a relatively smooth path to the origin of the map. However, it is still possible that some stage near the middle of the compressor persists in triggering stall for some range of speed below that at which the knee occurs. This may be reflected by a further, but slight, discontinuity in the surge line.

In the analysis so far, it has been assumed that the stalling flow coefficient of each stage is unaffected by the performance of the other stages. However, when a stage stalls, it sets up disturbances, such as rotating zones of low flow, which can affect the

stability of adjacent stages and cause them to stall prematurely. This is, of course, especially possible when the matching is such that the stall points of these stages normally would appear close together.

When this interaction effect persists in causing simultaneous stalling of several stages as the speed is lowered, a surge-line knee of a very severe nature may be induced, since the high degree of stabilizing influence required of the later stages in order to counteract the combined stalling of several early stages can only occur at a relatively low speed.

Employing results obtained from the theoretical stage-matching process, Fig. 12 illustrates the operating points reached by each stage along a surge line possessing a knee as shown in Fig. 8(*b*). It was assumed that above 92 per cent speed, surge occurred as stage 10 reached its stalling point, and that from 92 to 70 per cent speed surge was triggered as stage 1 reached stall. It may be seen that so long as stage 1 triggers surge the rear stages are forced to operate at higher flow coefficients and hence lower pressure coefficients. At 70 per cent speed, the lowest at which the stalling point of stage 1 persists in causing surge, the rear stages reach their maximum flow coefficients and hence lowest pressure coefficients. Below 70 per cent speed, the surge-line slope was reduced in order that it could pass through the origin of the map. Also included in Fig. 12 is the variation of the first-stage flow coefficient at maximum mass flow. This emphasizes how the minimum range of first-stage flow coefficient occurs at the speed where the knee is apparent.

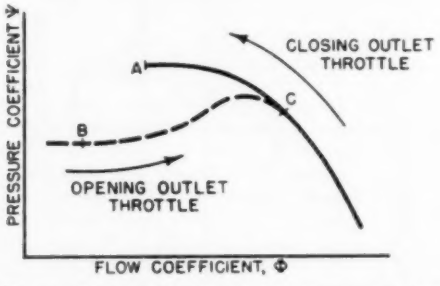

Fig. 13 Unstalling hysteresis of a compressor stage

Double-Valued Performance Curves. Compressor-rig tests sometimes indicate that over certain regions in the intermediate speed range it is possible to obtain two different performance curves at each speed, depending on the order at which the test points are obtained. This phenomenon is associated with unstalling hysteresis of the early stages; that is, when the incidence at stall is greater than at unstall. Fig. 13 illustrates a typical unstalling hysteresis of a compressor stage. As the flow coefficient is reduced from the choking side of the stage characteristic, operation occurs on the solid line and the stall point appears at *A*. Further throttling forces the stage over the stall and through point *B* to a high loss, but relatively stable region. When the throttling is then reduced, the operating point passes back through point *B* and then along a further shallow sloped stable region (although still of high loss) to unstall at point *C*.

Fig. 14 illustrates diagrammatically how this affects the over-all characteristics. The group characteristic of the inlet stages, the succeeding stages, and the resulting over-all characteristics are shown plotted against compressor-inlet mass flow for three speeds. The characteristic of the early stage group was assumed to possess unstalling hysteresis as indicated by the broken line. For each speed shown, the maximum mass flow is governed by choking in the later stage group.

At the higher speed indicated, Fig. 14(*a*), the maximum mass flow, i.e., that for choking of the succeeding stages, is higher than that corresponding to unstalling of the early stage group. The combined characteristic of both groups is then unique only when operating at and near maximum mass flow. It should be noted that for each mass-flow point in the region where the early group possesses two values of pressure ratio, the succeeding stage group also will present two values of pressure ratio, corresponding to the two different density (and hence velocity) ratios across the early group.

As the speed is reduced, the matching eventually takes the form of Fig. 14(*b*). Here, the choking flow as determined by the succeeding group of stages moves to lower inlet-stage flow coefficients and appears in the region between the stall and unstall points of the early stage group characteristic. This now results in two distinct over-all characteristics, because two different maximum mass flows are now possible. This is because the maximum flow depends not only upon the choking flow coefficient of the succeeding group of stages, but also upon the density at inlet to those rear stages, which in turn depends upon whether the early stage group operates on the stalled or unstalled branch of its characteristic. Fig. 14(*b*) includes the locus of the point corresponding to the choking flow coefficient of the succeeding group characteristic.

Upon further reduction in speed, the choking flow, as determined by the succeeding group of stages, forces the early-stage-group characteristic beyond the stall point and there is consequently only a single over-all characteristic, Fig. 14(*c*).

Fig. 14(*d*) shows the possible over-all characteristics as they would appear on a compressor map. Which of the dual characteristics would be obtained when testing a compressor on the rig depends on the test schedule followed. Points on the upper pressure-ratio curves would be obtained if these points were approached while the early stages were unstalled, and vice versa. For example, approaching the dual characteristic speeds along the throttle line *A* from, say, design speed, would give points on the higher-pressure curves (early stages unstalled) since the early stages were in this case unstalled initially. Conversely, approaching from the lower speeds, again along throttle line *A*, means that the early stages are initially stalled and hence would remain stalled, thus giving points on the lower-pressure curves. However, if, having run up along line *A* to the highest of these speeds (which has a unique maximum mass flow), the throttle was then opened to allow operation below the point corresponding to unstalling of the early stages, closing the throttle again would then give points on the higher-pressure branch of the characteristic.

Stage-Performance Analysis and Compressor Aerodynamic Development

The analysis of stage performance and relative matching is an important aid toward the development of an axial compressor.

The stage characteristics preferably are obtained from interstage total-pressure readings, but good results can be obtained from outer-wall static pressure taps if the hub/tip ratio is not less than about 0.6. Stage performance so obtained is considered to represent the average for the stage. Interstage data should be read at each point taken on the over-all compressor map. Since it is usually impossible to obtain interstage data at the surge point, it is necessary to take readings at an operating point as close as possible to the surge to facilitate eventual analysis.

It is generally found that the plotted results are quite consistent and show little scatter, except for certain displacements between the sections of stage characteristic corresponding to the Mach-number effect at various speeds.

Before specifying modifications aimed at compressor improvement in a certain performance region, it is necessary to estimate the possible effects such modifications might have on other re-

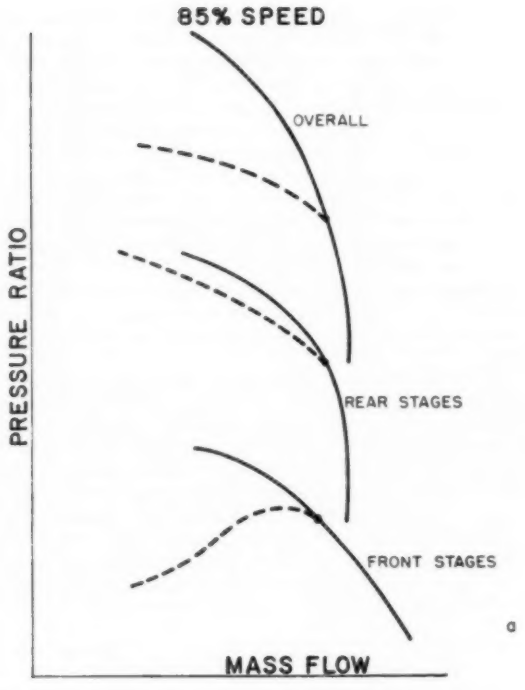

(*a*) Approximately 85 per cent of design speed

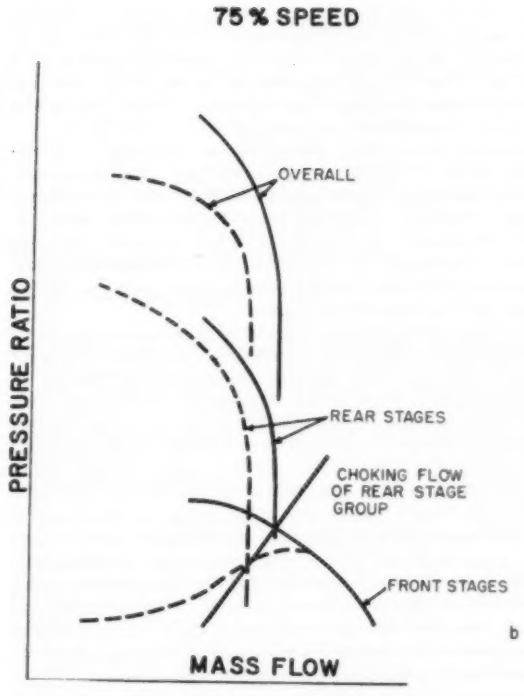

(*b*) Approximately 75 per cent of design speed

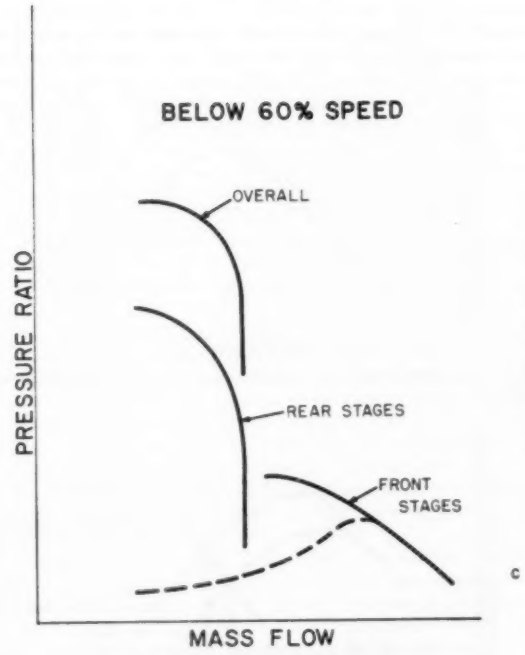

(*c*) Below 60 per cent of design speed

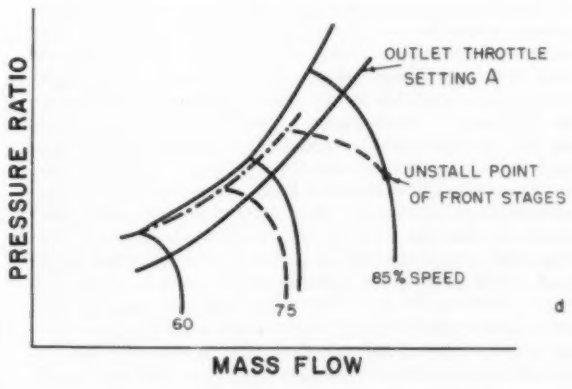

(*d*) Over-all map

Fig. 14 Double-valued performance characteristics

gions. For example, a modification which improves a part-speed surge line may bring a surge-line deterioration at higher speeds. This implies the necessity of analyzing the stage characteristics and relative matching to determine as far as possible how they combine to form the over-all characteristics. Some of the factors that should be considered are presented in the following:

Increasing Mass Flow. Increasing the mass flow to uprate engine power is usually an important part of a compressor-development program. At each speed, the over-all characteristic reaches a maximum mass flow when choking occurs somewhere in the compressor. The choking mass flow at a particular speed is then a function of the maximum flow coefficient of the stage responsible for choke, its annulus area, and the density reached by the gas up to the inlet of that stage.

In general, as described previously, choking somewhere among the later stages is responsible for fixing the maximum flows at low speeds, while some early stage is responsible at high speeds.

Determination of the actual stage which chokes first as the mass flow is increased by opening the outlet throttle at constant speed is facilitated by the fact that when it chokes, all stages upstream of that stage are constrained to operate at fixed points on their characteristics, regardless of further throttle opening.

Normally, the maximum flow is limited by the final stage at low and intermediate speeds. At approximately design speed, it is generally found that several early stages simultaneously operate toward the choking ends of their characteristics and it becomes more difficult to determine exactly which of these stages chokes first, although such information is of rather academic value as regards compressor development, so long as each of the stages which are near choking is known. Eventually, a speed is reached at and above which it is obvious that the first stage chokes first. This speed is generally of at least design value, as discussed previously.

It should be recognized that although at all speeds the last stage will choke eventually if the outlet throttle is opened sufficiently, it is not responsible for fixing the maximum mass flow if some earlier stage chokes first.

An increase in maximum flow at a given compressor speed can be accomplished by increasing the flow area at the choking plane and/or increasing the density into that plane by adjusting the previous stages to provide greater work. For example, if the third-stage choke was limiting the maximum mass flow, a local increase in annulus area at that stage would yield a larger flow. However, the increase probably would be very slight before some other early stage choked instead. One way to obtain a larger increase in maximum flow is to increase the annulus area through the whole group of early stages. Alternatively, the density into the choking stages could be increased by increasing the loading of the first stage, at the same time ensuring that the first stage itself could pass the desired increased flow. A convenient way of accomplishing this is to reduce the stagger of the inlet guide vanes and/or the first rotor blades. Either change uprates the first-stage loading by increasing the change in whirl imparted by the rotor. Both methods also increase the flow capacity of the first stage. Reducing the guide-vane stagger increases the incidences and velocity vectors relative to the first rotor, which results in a higher total pressure relative to the first rotor, thus enabling it to pass a higher flow per unit of throat area. Reducing rotor stagger increases the rotor throat area.

Fig. 15 shows the typical effects on first-stage performance of varying the inlet guide-vane stagger. It may be noted how the stage characteristic moves bodily to higher flow coefficients as the inlet guide-vane stagger is reduced, and also that its stalling slope tends to follow along a common line on the map. At first sight, it may appear that the increased stalling flow coefficient due to a reduction in guide-vane stagger follows from the reduction of prewhirl, causing the stalling incidences along the whole rotor-blade span to occur at a higher average flow coefficient. However, the change in axial-velocity profile as set up at the inlet to the rotor to satisfy radial equilibrium shows that reducing inlet guide-vane stagger increases the ratio of tip/root axial velocities so that, at a given mean flow coefficient, the increase in tip axial velocity tends to compensate for the reduction in prewhirl so that there is, in fact, little change in rotor-tip incidence. However, incidence itself is not a sufficient criterion of stall; blade-element loading also must be considered, and it may be shown that this parameter does, in fact, increase along the whole rotor-blade span as the inlet guide-vane turning is reduced.

Reducing rotor stagger has a similar effect on the stage characteristic as a reduction in inlet guide-vane stagger. In this case, obviously, the incidences onto the rotor increase along the whole span.

Fig. 16 illustrates how uprating the first stage as described affects the maximum mass flow obtained at a given speed. Superimposed on the performance map for stage 1 is a line, any point on which corresponds to the flow coefficient reached by the second stage when it or any succeeding stage reaches choke. This flow coefficient is essentially unchanged by the modifications to stage 1. The increase in maximum mass flow, corresponding to the increase in flow coefficient into the first stage, is seen to depend upon the increase in pressure level of the first stage and also upon the slope of the line corresponding to constant second-stage flow coefficient. This line derives from the continuity equation

$$V_{a1} = \frac{\rho_2}{\rho_1} \frac{A_2}{A_1} V_{a2}$$

or, for a particular blade speed

$$\text{inlet flow coefficient} \qquad \phi_1 = \frac{\rho_2}{\rho_1} \frac{A_2}{A_1} \phi_2$$

where ρ_2/ρ_1 = density ratio across first stage and A_1 and A_2 are inlet annulus areas to first and second stage, respectively. Since

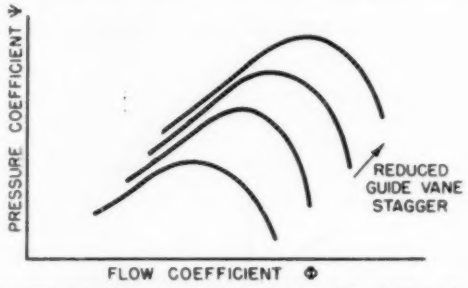

Fig. 15 Effect on first-stage performance of varying inlet guide-vane stagger

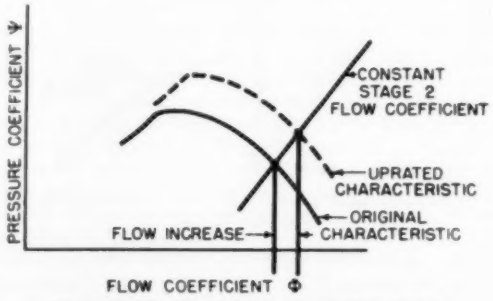

Fig. 16 Mass flow increase by uprating stage 1

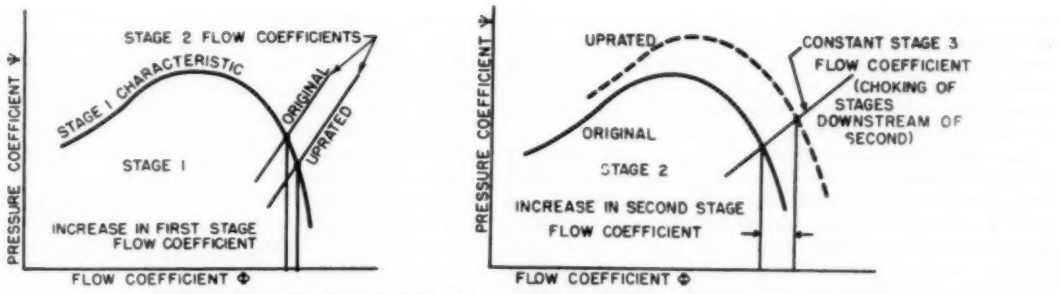

Fig. 17 Effect on stages 1 and 2 of a mass flow increase by uprating stage 2

the density ratio is a function of both pressure and temperature coefficients, it is affected by any change in first-stage efficiency which the modification may bring. For example, if increasing the first-stage pressure coefficient causes a large drop in first-stage efficiency, the new value of inlet flow coefficient corresponding to the constant second-stage flow coefficient may show little increase. This situation is often met when attempting to increase mass flow by uprating an already highly loaded stage.

Increasing compressor mass flow by uprating the first stage is very simple mechanically and is utilized quite often when flow increases of up to 10 per cent are required without increasing annulus area or adding a new inlet stage. Other early stages also can be uprated by reducing rotor stagger and/or the stagger of the previous stator. However, uprating the first stage provides the major contribution to the mass-flow increase. Uprating a later stage yields a smaller mass-flow increase because any increase in flow drawn through the previous stages causes the latter to yield a lower pressure rise and hence reduces the density into the uprated stage. As an example, the effect of uprating a second stage is illustrated in Fig. 17. It may be seen how the slope of the first-stage characteristic affects the increase in inlet flow coefficient. If the first stage were actually choking, its characteristic would be vertical, in which case uprating any following stage would produce no flow increase whatsoever.

It should be noted that any scheme designed to increase the maximum mass flow at design speed, involving as it does, increases in annulus area and/or blade loading in the early stages, is bound to endanger the surge line at part speed. This points to the use of variable-stagger inlet guide vanes and perhaps variable early stators, which may be arranged to adjust automatically for the required mass flow at design speed and vary to maintain a more favorable part-speed surge line for engine acceleration.

Surge Line Improvement

General Considerations. Compressor surge is generally caused by the stalling of one or more stages. The position of the surge point on the characteristic map at a given speed is determined by the point at which stage stalling occurs, and by the pressure ratios reached by all the stages at that point. Thus, in order to improve a surge line, it is first necessary to analyze the stage characteristics systematically to determine as accurately as possible which stage or stages reach stall or are already stalled at the surge points, and also how the other stages are then matched.

At low speeds several early stages are forced to operate well into stall. Thus a large operating range of each of these stages, from high flow coefficients toward the choke (obtained at the higher speeds) to the very low flow coefficients well over stall, is obtained from the data points. The stalling flow coefficients of the early stages are consequently apparent, and it is therefore usually possible to see at which speeds these are associated with surge.

However, it is usually more difficult to determine the stalling flow coefficients of the rear stages. Although there have been some compressors whose rear stages are able to operate some way over stall before surge occurs, these cases are exceptions. Surge is associated with the rear stages only at high speeds where surge tends to occur as soon as a stage reaches its stalling point and before its characteristic can exhibit any stalling slope, which otherwise would define its peak. Among the possible reasons for this are:

(*a*) The disturbances set up when a stage reaches stall are stronger at the higher speeds.

(*b*) Such disturbances may induce adjacent stages to stall prematurely.

(*c*) Stalling of the relatively short-span rear stages may be of the total-span type, giving a sharp discontinuity in stage performance rather than the more gradual drop generally associated with the stalling of longer blades.

When the stalling points of the stages are not apparent from their characteristics, other evidence may be employed to determine which stages reach stall.

A given stage may be triggering surge over a certain range of speed if along the surge line over that range it shows little change in flow coefficient; i.e., that flow coefficient could refer to the stall point of the stage. This possibility still exists even if the flow coefficient shows a certain increase with speed, since a stage stalling point can move to higher flow coefficients as incident Mach number increases.

Conversely, a given stage is unlikely to trigger surge at a particular speed, if at a higher speed it can reach a lower flow coefficient.

Adding to the difficulties in finding stages responsible for surge is the fact that interstage data cannot be taken exactly at the surge point. However, if these data are observed very close to surge, it is possible to obtain a good idea of where the stages match at the surge point by extrapolating the flow coefficients on a mass flow and/or over-all pressure-ratio basis.

Fig. 12 shows the variation in compressor surge-point flow coefficient with speed for each stage of the hypothetical compressor considered earlier. This presents an idealized picture of the plot necessary to facilitate determination of the stages which reach stall, in the manner described.

As development proceeds and various modifications to the original design are tested, further evidence is obtained and conclusions derived from earlier tests can be re-evaluated. The use of interstage bleed to investigate the operating range of the back stages is often very revealing, but the possible changes in velocity profile must be borne in mind.

A surge line may be improved by moving the surge points to higher pressure ratios and/or lower mass flows.

The ideal way of achieving an improvement in a particular region of speed would be to reduce the stalling mass flow of the

stage or stages responsible for surge, without loss in stage pressure ratio at stall or higher flows. This would allow the rest of the stages to attain lower flow and hence higher pressure coefficients, resulting in an extension of the over-all characteristic to both higher pressure ratio and lower mass flow before surge occurred. The maximum mass flows would then remain unchanged.

Such a process may be possible if the stage or stages responsible for surge were initially severely overloaded and inefficient, and consequently possessed narrow ranges. Increasing blade stagger up to a certain amount may then give little change in pressure and maximum flow coefficient while reducing stalling flow coefficient. Similarly, with a stage originally radially mismatched, local twisting also might reduce the stalling flow coefficient with little change over the remainder of its characteristic.

In general, however, it is found that a reduction in stage stalling-point mass flow can be achieved only at the expense of lowering stage performance. The more effective methods of reducing the stalling mass flow of a stage are either to increase blade stagger or to reduce its annulus area. In the first case it is generally found (but for the exceptions mentioned previously) that the whole stage characteristic moves to both lower flow coefficients and pressure coefficients, as shown in Fig. 15. This does two things:

(*a*) The improvement in over-all surge pressure ratio is minimized both by the reduction in stall-point pressure ratio of the restaggered stage, and by the fact that its reduced stall-point density rise does not allow the flow coefficient into the succeeding stages to fall by the same proportion as the stall flow coefficient of the modified stage thus limiting the increase in pressure ratio attained by these later stages. If sufficient stages were restaggered, there may, in fact, be a deterioration in the surge line, with the reduction in surge mass flow being more than counterbalanced by a reduction in surge pressure ratio.

(*b*) If the early stages were restaggered in an attempt to improve the surge line at intermediate speeds, the maximum flows at all speeds would be reduced. Since it is usually the first stage which plays the more important part in causing surge at intermediate speeds and also has the largest effect on high-speed mass flow, it is generally difficult to effect a worth-while surge-line improvement at intermediate speeds without compromising mass flow at high speeds.

Increasing the stagger of later stages generally does not affect mass flow at the higher speeds, but reduces it at lower speeds where those stages are usually the first to reach choke.

Reducing the local annulus area, however, leaves the stage characteristic essentially unchanged. Such a modification will therefore theoretically yield the same surge-point pressure ratio and surge-point mass flow as that which would be given if the stall-point flow coefficient could be reduced without compromising stage pressure coefficient. Again, however, if the annulus area in the early half of the compressor were reduced to improve the part-speed surge line, the maximum mass flow at all speeds would be decreased.

Rather than reducing the stalling mass flow of the stages responsible for surge, the pressure ratio of succeeding stages may be increased to give a larger over-all surge-point pressure ratio.

The implications of the modifications outlined are described more fully in the following.

Surge-Line Improvement at Intermediate Speeds. Fig. 18 illustrates the matching involved when the stalling flow coefficient of the early stage group is lowered by increasing blade stagger. As described earlier, reducing the density ratios over the early stage group has a similar effect to that of lowering speed in that it causes the group characteristic of the succeeding stages to appear at lower compressor mass flows. This minimizes the reduction in flow coefficient into the succeeding stages corresponding to the reduction in stall-point flow coefficient (mass flow) of the early stages. However, at speeds where surge occurs while the rear stages are operating near choke on steep portions of their characteristics, such as at a surge-line knee, Fig. 18(*a*), even a small reduction in flow coefficient into those stages can mean a relatively large increase in their pressure coefficients, resulting in a notable surge-line improvement. However, at a higher speed, Fig. 18(*b*), when compressor surge occurs while the rear stages are operating on flatter portions of their characteristics, the change in their inlet flow coefficient now means little increase in pressure coefficient. The reduction in stall-point pressure coefficient of the early stages then means that the drop in surge-point mass flow is largely counterbalanced by a drop in pressure ratio, resulting in little or no surge-line improvement.

Fig. 18(*c*) shows a typical change in the over-all characteristics resulting from increasing the stagger of early stages. It should be noted how the surge-line knee is moved to a lower speed. As described previously, a knee is characterized by a very narrow mass-flow range between surge and maximum flow, caused by early stage stall and rear-stage choke, respectively. Reducing the stalling flow of the early stages widens this range at the speed which exhibited the original knee, but as speed is reduced, the mass-flow range narrows until eventually a new surge-line knee is formed. The new knee is generally less pronounced and usually does not appear below the original surge line.

It should be noticed from Fig. 18(*c*) that the low-speed surge line remains practically unchanged. Experience shows that the surge line in this region is very difficult to change appreciably, except by adding stages. Increases of surge-point pressure ratio are usually counterbalanced by increases in surge mass flow, and vice versa. At these speeds surge occurs at mass flows below those corresponding to the early stages stall points, which points can thus no longer trigger surge. It may then be that at these low speeds surge occurs at mass flows where the slope of the over-all characteristic becomes sufficiently flat to form an unstable system when matched to the outlet throttle—or engine working line. In other words, surge occurs when the slope of the compressor characteristic approaches that of the effective throttle line. The latter slope diminishes as the throttle becomes unchoked at low pressure ratios, which suggests that at low speed surge may occur when the over-all characteristic has zero or even slightly negative slope. On the other hand, surge at low speed may be triggered by some middle stage reaching stall.

It also may be seen from Fig. 18(*c*) that at high speeds the surge points move to both lower mass flows and lower pressure ratios, resulting in practically no change of the surge line in this region.

Reducing the stall-point mass flow of the early stages by decreasing the early annulus area will have a similar effect on matching as increasing the early blade stagger, except that it generally proves more effective. There are two reasons why this should be so:

(*a*) The stall-point pressure ratio across the early stages is not reduced. Besides contributing to a higher surge-point pressure ratio, this also means that:

(*b*) The flow coefficient into the succeeding stages corresponding to surge falls by the same proportion as that into the early stages. This means that the succeeding stages operate at lower flow coefficients and hence give higher pressure ratios than would result from the alternative method of increasing the early blade staggers.

Wherever surge is triggered by the early stages reaching stall and is independent of the slope (i.e., stabilizing influence) of the characteristics of succeeding stages, the surge line can be improved by loading these succeeding stages. The surge-point over-all pressure ratio will then increase while the surge mass flow remains unchanged. Such a method is therefore usually effective

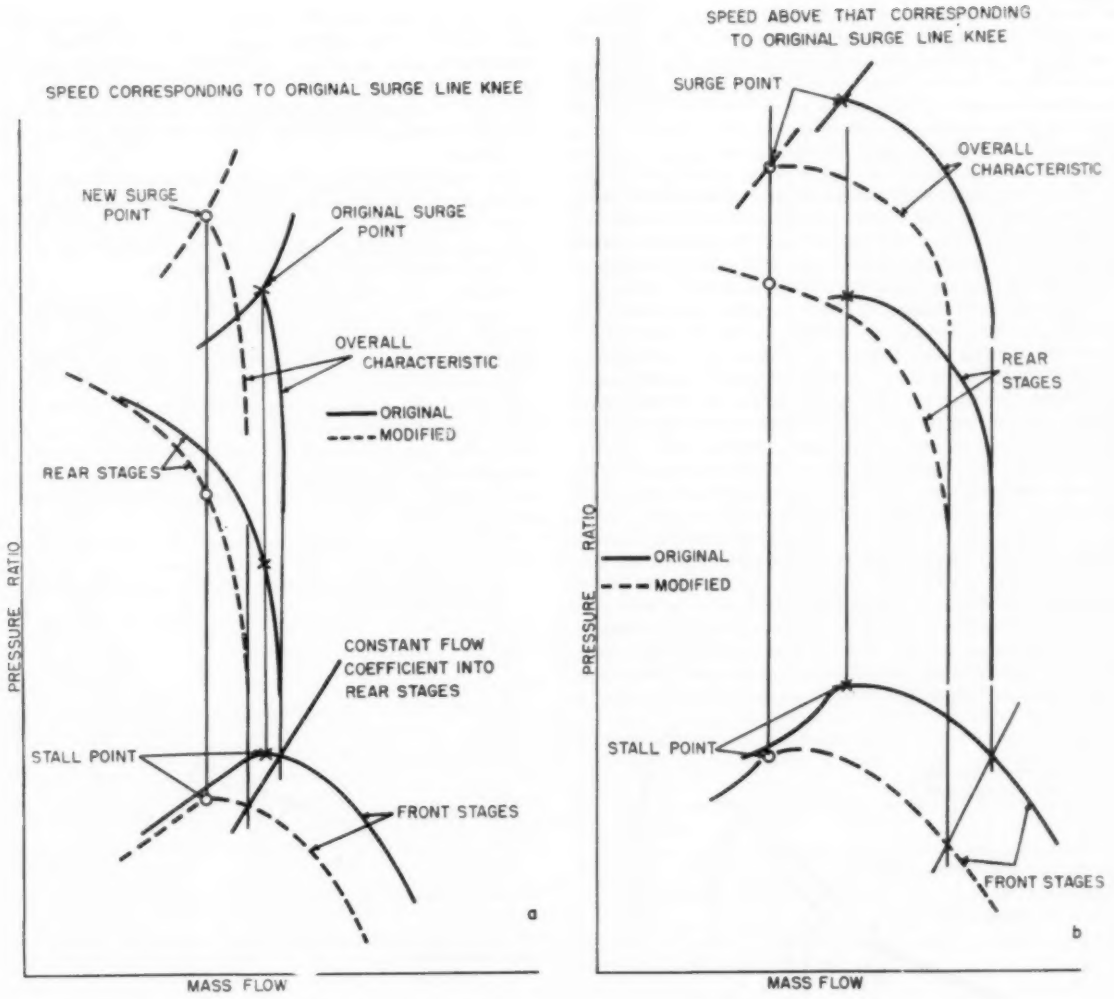

Fig. 18 Surge-line improvement at intermediate speeds by modification to unload front stages

in improving a surge line in the vicinity of a knee. However, when the later stages are able to force the early stages smoothly over stall to produce a relatively smooth surge line, increasing the loading of the later stages usually affords no surge-line improvement because in such a case the surge mass flow is a function not only of the early-stage stall points, but also of the stabilizing influence of the later stages. Increasing the loading of these stages by, say, reducing blade stagger, moves their characteristics to higher flow coefficients as described earlier, thus reducing their stabilizing influence for a given compressor-inlet mass flow. It is then generally found that the increase in surge-point over-all pressure ratio is counterbalanced by an increased surge-point mass flow so that the surge line remains essentially unchanged.

Increasing the loading of the later stages at mass flows corresponding to the early-stage-group stall point can be accomplished either by reducing their stagger or by increasing their annulus areas. (The latter reduces the flow coefficient into the later stages, and hence increases the pressure coefficient, for a given mass flow.) Care should be taken that a stage which might be contributing to surge at intermediate speeds is not uprated.

Since at the higher speeds surge is usually a function of stalling of some rear stage or stages, there is a danger that uprating any of the later stages will cause a surge-line deterioration in this region. Attempts should be made, as described earlier, to ascertain those stages responsible for surge at the higher speeds, so that they can be left unmodified if such deterioration in surge line cannot be tolerated. However, if the engine surge margin at the higher speeds is sufficiently wide to allow some surge-line deterioration, all the rear stages may be uprated by some degree, with consequently a more pronounced surge-line improvement at the intermediate speeds. High-speed surge is discussed in the next section.

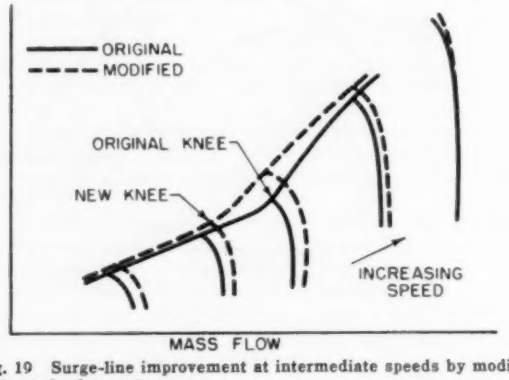

Fig. 19 Surge-line improvement at intermediate speeds by modification to load rear stages

Fig. 19 illustrates the effect on the over-all characteristics of uprating the later stages. There is usually again negligible change in the surge line at low speeds, as similarly shown by unloading the early stages. Also, as is generally the case when unloading the early stages, and for basically the same reason, loading the later stages as a rule causes the surge-line knee to appear at a lower speed; i.e., the loaded rear stages operate farther from choke at a given mass flow, so that the speed at which their stabilizing influence becomes sufficient to enable the early stages to operate over stall without causing surge is lowered.

The change in surge performance which might be expected at high speeds is not shown in Fig. 19, since this depends on the particular stages modified, as described in the next section.

Surge-Line Improvement at High Speeds. Stalling of some later stage or stages is usually the cause of surge at the higher speeds. When such stages possess very small ranges between choke and stall (due perhaps to radial mismatching or to the existence of poor velocity profiles at these stages) or where the relative stage matching is poor, surge can occur while the early stages still operate at high flow coefficients and hence low pressure coefficients. For example, at design speed this can lead to the over-all characteristic reaching surge even before design pressure ratio is attained.

The first step in attempting a surge-line improvement at the higher speeds is to ascertain which stage or stages are responsible, in the manner described earlier. (It may even be possible to note some stage characteristic actually showing a stall at high speeds, but this, as stated previously, is fairly unusual.)

Reducing the stalling flow coefficient of the stages responsible for surge allows the preceding stages to operate at lower flow coefficients and hence higher pressure coefficients at surge. Again, any loss in stall pressure coefficient of the modified stages detracts from the new surge-point over-all pressure ratio, and also tends to prevent the flow coefficient into the succeeding stages from falling. However, the latter means little loss in potential surge pressure ratio, since at these high speeds, any succeeding stage is generally operating on relatively flat portions of characteristics where little pressure coefficient is gained by reducing flow coefficient.

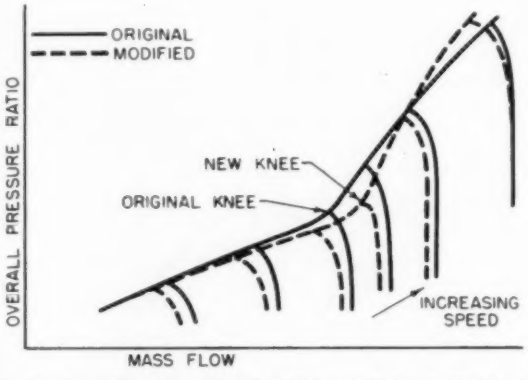

Fig. 20 Surge-line improvement at high speeds by modification to unload rear stages

Typical effects of increasing stagger of those later blade rows responsible for surge at the higher speeds is shown in Fig. 20. At higher speeds, where the earlier stages are generally the first to reach choke, the maximum mass flows are unaffected, but the reduced flow capacity of the later stages cuts down the maximum flows at lower speed. It has been described already how uprating the later stages can improve the surge line at intermediate speeds where surge is triggered by the early-stage stall points. By the same token, unloading the later stages can worsen the surge line in this region. Any knee is generally moved to a higher speed and becomes more acute. When several of the rear stages are suspected of causing surge, restaggering the whole group may more than counterbalance the increased pressure ratio given by the preceding stages, giving a surge point lower in pressure ratio as well as mass flow, with consequently no improvement in the surge line. A more effective method of surge-line improvement in such a case is to reduce the local annulus areas.

Using the continuity equation, and assuming a polytropic efficiency of 0.88 and a ratio of specific heats of 1.4, we may write for any plane in the compressor the approximate relationship

$$M \propto \left(\frac{P}{P_1}\right)^{0.678} A\phi N \quad \ldots\ldots\ldots\ldots\ldots\ldots [5]$$

where

M = mass flow
P_1 = compressor inlet pressure
P = pressure at plane considered
A = annulus area
ϕ = flow coefficient at plane considered
N = compressor rpm

When we consider surge-point conditions for the plane at entry to the stage causing surge, we may write

$$M_s \propto \left(\frac{P}{P_1}\right)^{0.675} A_s \phi_s N \quad \ldots\ldots\ldots\ldots\ldots [6]$$

where s refers to surge-point conditions.

If all the stages succeeding that which causes surge were left unaltered, then the pressure ratio generated by these stages at surge remains constant, and we may then write

$$M_s \propto \left(\frac{P_2}{P_1}\right)_s^{0.675} A_s \phi_s N \quad \ldots\ldots\ldots\ldots\ldots [7]$$

where $(P_2/P_1)_s$ is now compressor over-all pressure ratio at surge.

Thus, if the over-all pressure ratio at a given speed were varied by modifying only stages or annulus areas prior to the stage which causes surge, the surge point always would be constrained to appear approximately on a line corresponding to the stalling flow coefficient of the stalling stage defined by

$$M_s \propto \left(\frac{P_2}{P_1}\right)_s^{0.675}$$

In passing, it may be noted that this is why modifying the early stages to improve the part-speed surge line, as described earlier, has little effect on the high-speed surge line.

If the annulus areas through the stage responsible for surge and any succeeding stages were reduced by a given percentage, the line corresponding to ϕ_s = const on the over-all map thus moves to lower mass flows by the same percentage. This is shown in Fig. 21. The new surge point given by the annulus reduction must lie on this new line.

It is also known that the new over-all pressure ratio at the mass flow corresponding to the original surge point must be somewhat lower than the original because the rear stages now operate at higher flow coefficients. In addition, the new surge pressure ratio will be higher than the original since the earlier stages now operate at lower flow coefficients and hence higher pressure coefficients. Thus the over-all characteristic at high speed will change as shown in Fig. 21. At intermediate speeds, the changes will be similar to those given by increasing the stagger of the later stages as shown in Fig. 20.

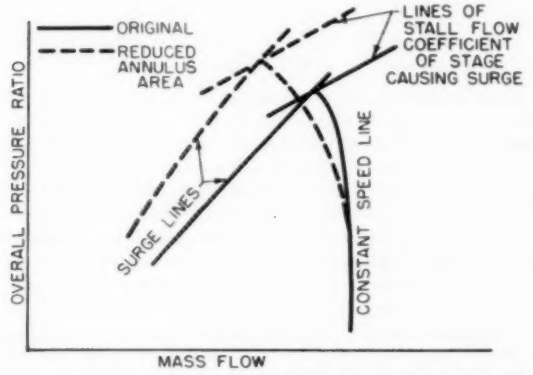

Fig. 21 Effect on surge line at high speeds of a modification to reduce annulus area in rear stages

We may examine Equation [7] to show the relationship between the maximum flows and the surge line at high speed.

Rewriting Expression [7]

$$\left(\frac{P_2}{P_1}\right)_s \propto \left(\frac{M_s}{A_s \phi_s N}\right)^{1.48} \quad \ldots\ldots\ldots\ldots\ldots [8]$$

As described earlier, the rate of increase of maximum mass flow falls off at high speeds when the early stages commence to choke, while surge occurs when the over-all characteristic is still almost vertical (i.e., little difference between maximum and surge-point mass flow). The value of the ratio M_s/N therefore tends to fall with increasing speed. If surge was caused by stages very near the rear end of the compressor, the rate of increase of $(P_2/P_1)_s$ with speed would diminish and, according to Expression [8], the surge-line slope eventually would become zero and then assume a negative value if M_s/N became sufficiently low. The equation, however, takes no account of the falling efficiency with speed, which, in fact, increases the exponent, and also disregards the increase in pressure ratio of the stalling stage itself and any succeeding stages, as speed increases. However, Expression [8] does afford a broad explanation as to why a surge-line slope may diminish at the higher speed.

It has been shown that the surge line is little affected by varying the pressure ratios of stages before that which causes surge. The surge point is constrained to appear on a line such that any change in surge-point pressure ratio tends to be counterbalanced by a change in surge-point mass flow.

However, increasing the loading of stages behind that which triggers surge will raise the surge points to higher pressure ratios without affecting the surge-point mass flows. (This modification is, in fact, the same as described earlier in connection with raising the surge line at intermediate speeds when an early stage triggered surge.) The earlier the stage causing surge, the more stages there are which can be uprated, and the larger the possible surge-line improvement.

When the final stage causes surge, this scheme then cannot be employed. For example, it may be that at design speed the last two stages can be uprated to improve the surge line, but at some overspeed condition, one of these stages may initially have been responsible for surge, so that its uprating consequently could worsen the overspeed surge line.

Efficiency Improvement

The over-all efficiency given at any particular operating point is a function both of the efficiency characteristic of each individual stage and of the stage matching which exists at that point.

At low speeds, the over-all efficiency is poor because several early stages operate stalled while the rear stages operate near choke. The fall-off in efficiency can thus be delayed to lower speeds by either reducing the stalling flow coefficients of the early stages or by increasing the choking mass flow of the later stages. Such schemes are generally employed with the main object of improving the surge line at intermediate speeds.

It is usually more important, however, to increase over-all efficiency in the region of design speed. Here it is unusual to find any stages stalled, but inefficiencies sometimes can be traced to early stages operating near choke even up to the surge point. When there does not appear to be any particular mismatching of the stages, the reason for a poor over-all efficiency must be sought in the detailed flow conditions of the individual stages.

Acknowledgment

The work reported in this paper was performed at Solar Aircraft Company and Orenda Engines Limited.

Discussion

W. A. Benser.[2] The paper presents a very interesting discussion of off-design operating problems of multistage axial-flow compressors. Stage-matching techniques, such as used by the author, are extremely helpful in obtaining and understanding stall and surge problems and in evaluating various design philosophies and modifications to improve part-speed performance. As he points out, publications on this subject have been limited. Several unclassified papers based on stage-stacking techniques have been published and are considered pertinent.

Stage-stacking studies done at the NACA in general verify the conclusions drawn in the subject paper. Messrs. H. B. Finger and J. F. Dugan examined the effect of the shape of the stage-characteristic curves on off-design performance and obtained results similar to those predicted by Mr. Stone. Messrs. Finger and Dugan also examined the effects of stage rematching by means of area change as well as stator-blade resetting. Area change gave a marked improvement in part-speed efficiency; but when scaled to the same design weight flow, indicated no gain in regard to the surge limits. Improvements in low-speed efficiency, however, are beneficial in avoiding low-speed stall in gas-turbine-type engines. These results are presented in detail elsewhere.[3]

Studies also were made on the effects of stage interactions on part-speed compressor operation. In this analysis, a depreciation of performance of several stages was assumed to result from stall of the inlet stages. This study also indicated the double-valued performance characteristics and potential surge-line knee discussed by the author. They also indicated the necessity of careful component test procedures to insure obtaining all possible potential operating conditions for any given compressor. These results have been reported by the writer.[4]

The low-speed operating region where stall exists in the front stages of a multistage matching is of extreme importance from the standpoint of blade vibration. In this region of compressor operation, rotating stall may exist which, if in resonance with the blades, can cause severe blade vibrations even though the resulting flow fluctuations are not sufficiently large to cause severe penalties in compressor efficiency. This problem was discussed by M. C. Huppert and W. A. Benser.[5] In this paper it was assumed that rotating stall occurred at the point of inlet-stage stall. However, E. L. Costilow and M. C. Huppert[6] point out that the occurrence of rotating stall is affected by stability and that adjacent blade rows influence the initial point for rotating stall. Stalling of the inlet stages is a necessary condition for the occurrence of rotating stall at low compressor speeds and, therefore, analysis of first-stage stall limits are valuable in regard to determination of the region of potential blade vibrations resulting from this unsteady-flow phenomenon.

The author points out the potential use of stage stacking in compressor development. He states that changes in stage characteristics as well as blade-incident Mach number must be considered. Wall boundary-layer blockage also may influence the results obtained from such an approach. The stacking analysis determines the blade operating condition from continuity. The stage performance, however, is determined primarily by the conditions over the major portion of the blade span. Large variations in boundary-layer blockage, therefore, will tend to shift the stage characteristic along the flow-coefficient axis and may influence the results obtained experimentally. The general approach, however, is good and, if good stage data are available, the effects of rematching can be evaluated moderately well up to the point where stall occurs in some stage. Beyond this point, variations in stage-interaction effects can be of major significance.

Another approach in regard to development of a compressor is proposed by J. T. Sinnette, Jr., and W. J. Voss.[7] In this report, pitch-radius conditions are calculated by means of one-dimensional-flow equations using an estimated polytropic exponent. This method is applicable to both rotor and stator-blade-angle resetting. The report presents calculated as well as experimental results for an 8-stage compressor for three different stator-angle settings.

Analyses, such as discussed by the author and in the reports mentioned, aid materially in understanding the flow processes in multistage axial-flow compressors. They also furnish the development engineer with tools to simplify development of a given compressor. Development, however, requires a complete performance evaluation of the initial model of the machine.

J. F. Klapproth.[8] This is an interesting presentation of some of the results that can be obtained through a stage-stacking study. As demonstrated, the stage-stacking technique provides a simple means of obtaining an insight into the operation of a multistage compressor at conditions other than the design point. It also provides a powerful tool for evaluating the effect on the compressor over-all performance caused by small changes in the geometry.

The discussion concerning the problem of improving the compressor surge line is a graphical illustration of the dilemma confronting the designer. If a reasonable matching of the stages and proper selection of the blading have been made for the design condition, then a given surge-line characteristic is almost inherent to that design. Significant changes generally can only be made by sacrificing the performance at some other condition, use of bleed, by variable geometry, or split-spool arrangements.

Further useful applications of the stage-stacking technique which were implied by the author are as follows:

1 Evaluation of bleed to determine the best location of the bleed position or positions, as well as an estimate of the amount of bleed required.

2 Evaluation of the axial distribution of stage loading through the compressor or the effect of stage match-point selection on the over-all performance.

3 Determination of the effect on the over-all performance of adding a stage either at the inlet or discharge.

Some additional comments might be made concerning the effect of variation in stage geometry on the stage performance characteristic. Fig. 15 illustrates the general changes that can be expected with a reduction in inlet guide-vane stagger. If the performance is known for a given geometry, then the characteristic for a different vane-setting angle can be obtained as follows:

1 A constant incidence angle on the rotor lies along the line ψ/φ = const if the assumption is made that the stage efficiency, axial-velocity ratio, and rotor-discharge angle are primarily a function of rotor-incidence angle.

---

[2] National Advisory Committee for Aeronautics, Lewis Flight Propulsion Laboratory, Cleveland, Ohio.

[3] "Analysis of Stage Matching and Off-Design Performance of Multistage Axial-Flow Compressors," by H. B. Finger and J. F. Dugan, NACA RM E52D07, June 27, 1952.

[4] "Analysis of Part-Speed Operation for High-Pressure-Ratio Multistage Axial-Flow Compressors," by W. A. Benser, NACA RM E53I15, December, 1953.

[5] "Some Stall and Surge Phenomena in Axial-Flow Compressors," by M. C. Huppert and W. A. Benser, *Journal of the Aeronautical Sciences*, vol. 20, no. 12, 1953, pp. 835–845.

[6] "Some Effects of Guide-Vane Turning and Stators on the Rotating-Stall Characteristics of a High Hub-Tip Ratio Single-Stage Compressor," by E. L. Costilow and M. C. Huppert, NACA TN 3711, April, 1956.

[7] "Extension of Useful Operating Range of Axial-Flow Compressor by Use of Adjustable Stator Blades," by J. T. Sinnette, Jr., and W. J. Voss, NACA Report 915, 1948.

[8] Supervisor, Compressor Development, Flight Propulsion Laboratory Department, General Electric Company, Cincinnati, Ohio.

2 At a constant rotor-inlet angle, the change in flow coefficient associated with a given change in upstream stator-discharge angle is found from

$$d\left(\frac{1}{\varphi}\right) = d\,(\tan \alpha_0)$$

The characteristics obtained from the foregoing procedure should be fairly accurate for the later stages. However, changes in the radial matching might cause the characteristics to deviate for inlet or low-radius-ratio stages.

This procedure is also quite useful in correlating data obtained from tests with variable vane-setting angles. The same approach, suitably modified also can be used to determine the influence of variation in rotor stagger.

One question might be asked concerning the effect of Mach number on the stage characteristic. Fig. 7 indicates that not only the range in flow coefficient is reduced but the maximum pressure coefficient is also reduced over the entire range. This is contrary to what might be expected based on airfoil experience which shows increase in lift coefficient with Mach number at a given angle of attack. In addition, compressibility effects of reduced axial velocity behind the rotor at higher Mach numbers also would tend to increase the pressure coefficient. If a higher pressure coefficient does exist at higher Mach numbers, then caution should be applied when interpreting the point of maximum pressure coefficient as onset of stall. The usual data preferably should be supplemented with information concerning the existence of stall. These data can be obtained from the usual instrumentation such as hot wires, microphones, and so on.

C. B. Wrong.[9] The author has presented a lucid and thorough description of the use of stage characteristics in axial-flow-compressor development. The paper will serve as excellent source material for many people engaged in this type of work.

The writer would like to emphasize the possibilities of stage-stall interaction. Disturbances from a stalled stage can be strong enough to cause premature stalling in downstream stages even when the matching is such that the stall points of these stages are actually well away from that of the upstream stage. In such a case the apparent range of an affected stage can be seriously lower than its true range, thus its potential in development of the compressor cannot be recognized. This situation can be resolved by the use of variable-stagger inlet-guide vanes (IGV). Positive settings of IGV normally affect the inlet stage only. In the case under discussion, however, as the inlet stage is unloaded its stalling flow coefficient will diminish and the true range of downstream stages will be available. This effect is shown in Fig. 22 of this discussion; the solid curves represent the positive-stagger IGV case, the dashed curves the design IGV setting.

Once responsibility for surge at a given speed has been assigned to a particular stage, there still exists the problem of determining the share of responsibility for stall due to each blade row in the stage. If variable-stagger stator blades are incorporated in the test unit, and testing time is available, the performance of each stage for a range of stator-stagger angles can be measured. This can be tedious and uneconomical, however, even if sufficient automatic data handling equipment is used.

Here the calculation of individual blade-row characteristics can be helpful. These may be expressed usefully as the wall static-pressure ratio across a row, plotted against flow coefficient at inlet to the stage, Fig. 23.

The slopes of the blade-row characteristics determine the relative stabilities of the rotor and stator, and thus the blade row needing attention. From basic considerations, the higher speed blade-row characteristics for a rotor exhibit steeper slopes than those for a stator when both are based on outer-wall static pressures. Hence due care must be exercised in the interpretation of these results. Also experience has shown that these characteristics are quite sensitive to the positioning of the wall statics, and generally show slightly pessimistic stator values and correspondingly optimistic rotor values.

Neither the stage characteristic nor the blade-row characteris-

[9] Chief Aerodynamics Engineer, Orenda Engines Limited, Toronto, Canada.

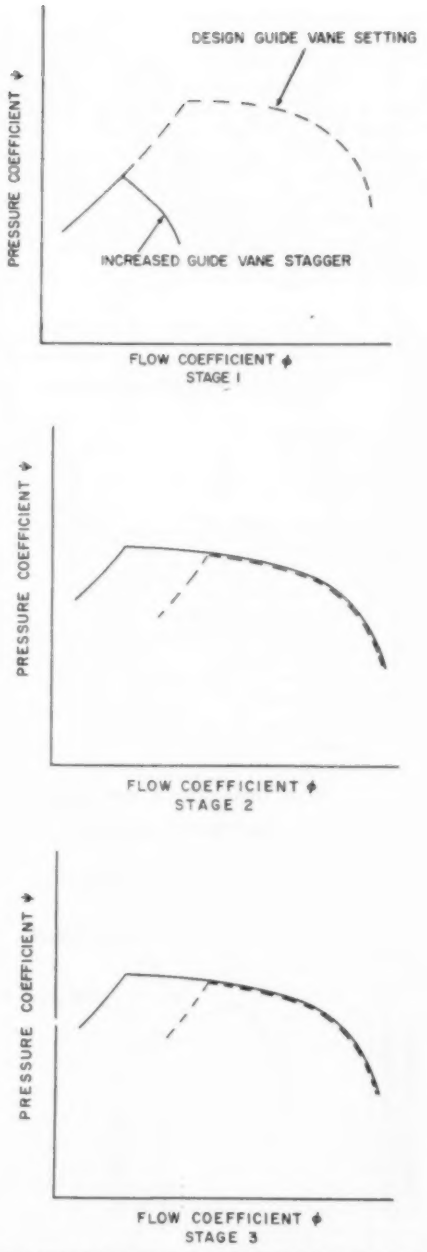

Fig. 22 Differences between actual and apparent operating ranges

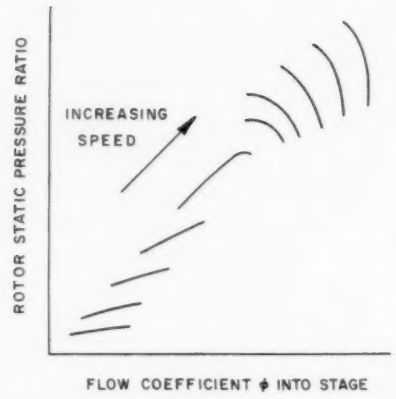

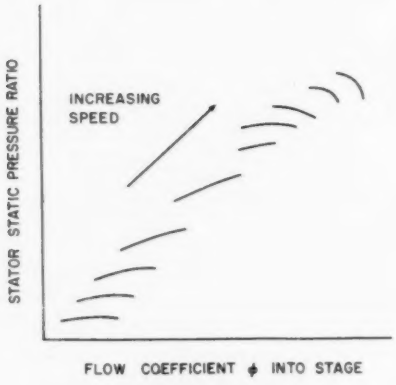

Fig. 23 Blade-flow characteristics

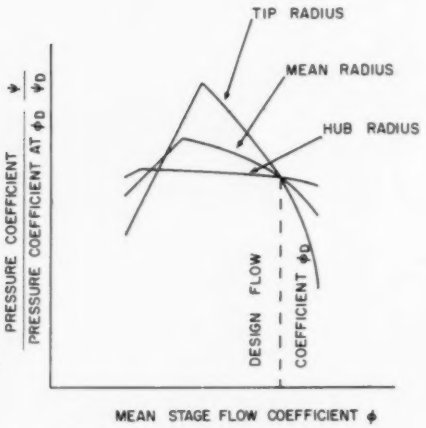

Fig. 24 Local stage characteristics

tic will define how a stage stalls; i.e., which blade section stalls first, if any. Full measurement at inlet to each blade row of pressures, temperature, and yaw angles would determine this, but such measurement is seldom feasible in a multistage axial-flow compressor. If, in addition to wall static pressures, radial readings of total pressure and temperature are available (either from rakes between the stators or suitably instrumented stator blades, the latter causing less blockage), a relatively simple calculation will yield local pressure coefficients. When these are reduced to a common value at the design flow coefficient and plotted together against mean stage-flow coefficient, a relationship such as that shown in Fig. 24 results.

This figure represents a typical stage wherein the tip section triggers stall. The effects of normal low hub stagger and high tip stagger on the rate of change of ΔVw with change in Va are shown clearly here, along with the characteristic sharp and soft stalls of high and low stagger blading, respectively. From such data the critical radial portion of a stage and the extent of corrective action can be determined.

Author's Closure

As Mr. Benser states, prosecution of a logical development program necessitates a complete performance evaluation of the initial model, including conducting test procedures aimed at revealing any potential double-valued performance characteristics. The stage characteristics should then be systematically analyzed to determine as far as possible the reasons underlying the salient features of the over-all performance. This analysis should, for example, attempt to show which stages are responsible for the surge and maximum flow limits at each speed. Some of the conclusions reached will necessarily be tentative and may be disproved by future tests, but at least one has a basis for proposing a logical development program and predicting the effects of modifications.

As Mr. Klapproth suggests, the stage stacking technique is useful not only for theoretical analysis of paper designs, but also as a practical tool to aid compressor development. The simple approximations described by Mr. Klapproth for assessing the effect on stage performance when blade settings are varied generally give quite good results in practice, although it is agreed that the method does tend to lose accuracy when applied to low radius ratio stages.

Regarding the effect of Mach number on the stage characteristic, it is, of course, true that isolated airfoils tend to show an increase of lift coefficient with Mach number at a given angle of attack, but this increase is continuous only up to the critical Mach number of the section. However, both profile drag coefficient and induced drag coefficient increase with Mach number, even before the critical Mach number is reached.

Cascade tests conducted under carefully controlled conditions indicate similar results as regards the change of lift and drag coefficients with Mach number. They also show that the turning angle remains sensibly constant up to the critical Mach number, then falls steeply. As may be seen from the velocity triangle diagram, this implies that the increase of lift coefficient with Mach number is due solely to the reduction in axial velocity ratio resulting from compressibility.

That lift coefficient increases with Mach number until the critical value is reached, implies that stage temperature coefficient behaves similarly. However, the pressure coefficient also depends on stage efficiency, which in turn is a function of profile and induced drag coefficients. The net effect on pressure coefficient for a typical stage is generally that, as Mach number is increased from very low values up to about 0.6, there is a small increase in pressure coefficient, but that there is then little change in pressure coefficient as Mach number is increased up to the critical. Further increase in Mach number usually means a drop in both pressure and temperature coefficient. The critical Mach number depends of course on the type of blade section employed.

Mr. Klapproth's comments concerning finding the stalling point flow coefficient of a particular stage in the compressor are very apt. Generally, only the early stages operate over a suf-

ficiently wide range of flow coefficient to show the peak pressure coefficient followed by the fall-off associated with stall. Even then, the range of flow coefficient which includes this definite evidence of stall generally only occurs at intermediate compressor speeds. At higher speeds the early stages operate over a range of higher flow coefficients and a fall-off in pressure coefficient actually indicating stall may no longer be apparent. But since the stalling point would be expected to occur at higher flow coefficients with increasing speed, it is still possible that stall is again reached, but that compressor surge then occurs, preventing the observation of points at lower flow to show the actual fall-off in pressure coefficient.

In answer to Mr. Wrong, it is agreed that increasing the inlet guide vane stagger can help to determine whether, with standard stagger, stalling of the first stage induces stalling in a succeeding stage. It might be pointed out, however, that due to the reduction of first stage density rise, the reduction of flow coefficient into the succeeding stages is of smaller order than the corresponding reduction of flow coefficient into the first stage. This fact, incidentally, causes difficulties when attempting to rematch a group of inlet stages to obviate simultaneous stalling.

Prediction of Creep in Bending From Tension- and Compression-Creep Data When Creep Coefficients Are Unequal

By W. N. FINDLEY,[1] J. J. POCZATEK,[2] and P. N. MATHUR[3]

The method of predicting creep in bending from data on creep in tension previously described has been extended to the prediction of creep in bending when the creep in tension and compression are unequal, and when the time-dependent and time-independent stress functions are unequal. It was shown that the stress distribution and position of the neutral axis in a beam changed with time when the creep in tension and compression were unequal; and the stress distribution changed with time when the time-dependent and time-independent stress functions were unequal. Computed creep deflections were compared with available data on canvas laminate and polystyrene, with good results for the former and fair results for the latter.

Introduction

In a previous paper [1][4] the existing literature related to this problem was reviewed and a method was derived for predicting creep in bending from the creep data in tension. In that paper, the creep behavior of the material was assumed to be equal in tension and compression, and the coefficients of the time-dependent and time-independent terms of the stress function were considered equal.

The present paper extends the analysis to include bending of materials which have unequal creep in tension and compression, and which exhibit unequal coefficients of the time-dependent and time-independent terms.

Bending With Unequal Creep in Tension and Compression

Derivation:

In previous papers [2, 3, 4] the creep curves obtained from a canvas laminate tested at different constant stresses in tension were found to be closely described by an equation of the form

$$\epsilon = \epsilon_0 + mt^n = (\epsilon_0' + m't^n) \sinh \sigma/\sigma_0 \qquad (1)$$

where ϵ is the strain; t is the time under a constant stress σ; ϵ_0', m', n, and σ_0 are constants whose values depend on the material and temperature; and ϵ_0 and m are functions of stress.

The stress dependence in this relation is of the same form as that in the activation-energy theory of creep as advanced by Kauzmann [5]. It has also been shown [4] that an equation for the stress-strain curve obtained from a constant-strain-rate tension test could be derived from equation (1) and that the resulting equation was in close agreement with the experimental data. It should be noted that the time-independent term $\epsilon_0 = \epsilon_0' \sinh \sigma/\sigma_0$ in equation (1) expresses the instantaneous strain, that is, the strain at time zero, and that it does not represent linear elasticity except when σ_0 is large compared to σ.

Equation (1) accurately represents the creep data of some materials under conditions of constant stress. It may not, however, accurately describe creep under varying stress. Thus if the stress distribution in the beam changes during creep, as described by Popov [6] and Fried [7] some inaccuracy may be introduced by the use of this equation unless the material obeys the time-hardening law [8], which is probably not the case.

Some materials evidently have unequal creep behavior in tension and compression [9].

If the constants in the equation for tension are all different from those for compression, the creep equations may be written

$$\epsilon_T = (\epsilon_{0T}' + m_T't^{n_T}) \sinh \sigma_T/\sigma_{0T} \qquad (2)$$

$$\epsilon_s = (\epsilon_{0s}' + m_s't^{n_s}) \sinh \sigma_s/\sigma_{0s} \qquad (3)$$

where the subscripts T and s denote tension and compression, respectively.

To determine the bending-creep relation, the conditions of equilibrium and geometry must be satisfied. From the observation that plane sections remain plane in a beam subjected to a uniformly or nearly uniformly distributed bending moment the following well-known geometrical relations are obtained

$$\epsilon_s = \frac{y_s}{\rho}; \quad \epsilon_T = \frac{y_T}{\rho} \qquad (4)$$

where y_T and y_s are the normal distances from the neutral axis to any point in the tension or compression side of the beam, respectively, ϵ_T and ϵ_s are the corresponding strains, and ρ is the radius of curvature of the neutral axis. The neutral axis is at some undetermined distance c from the extreme "fiber" on the compression face of the beam.

The fact that plane sections in a beam subjected to pure bending remain plane has been demonstrated for plastically bent beams by Nadai [10] and for creep of lead beams by MacCullough [11]. Also, consideration of compatibility of strains in the different "fibers" of a beam of great length, bent by a constant bending moment into the arc of a circle, suggests that plane sections must remain plane at all points along the beam which are remote from the ends. If this were not so, different fibers would be markedly displaced relative to each other at points at a distance from the mid-span of the beam.

The conditions of equilibrium for a beam are expressed by the following equations when the accelerations involved in the creep are so small as to be negligible—which is usually the case.

$$\int_{c-h}^{c} \sigma \, dA = 0 \qquad (5)$$

$$\int_{c-h}^{c} \sigma y \, dA = M \qquad (6)$$

[1] Professor of Engineering, Brown University, Providence, R. I. Mem. ASME.

[2] Senior Research Engineer, Cook Research Laboratories, Chicago, Ill.

[3] Senior Engineer, Scientific Laboratory, Ford Motor Company, Dearborn, Mich. Assoc. Mem. ASME.

[4] Numbers in brackets designate References at end of paper.

Contributed by the Rubber and Plastics Division and presented at the Annual Meeting, New York, N. Y., December 1–6, 1957, of The American Society of Mechanical Engineers.

Note: Statements and opinions advanced in papers are to be understood as individual expressions of their authors and not those of the Society. Manuscript received at ASME Headquarters, September 24, 1957. Paper No. 57—A-213.

where A is the cross-sectional area of the beam, h is the depth of the beam, and c is the distance from the neutral axis to the compression face of the beam.

Solving for σ_T and σ_s in equations (2) and (3) and substituting equations (4) for ϵ_s and ϵ_T the following equations are obtained

$$\sigma_T = \sigma_{0T} \sinh^{-1} \frac{y_T/\rho}{\epsilon_{0T}' + m_T' t^{n_T}} = \sigma_{0T} \sinh^{-1} \frac{N_T}{\rho} y_T \quad (7)$$

$$\sigma_s = \sigma_{0s} \sinh^{-1} \frac{y_s/\rho}{\epsilon_{0s}' + m_s' t^{n_T}} = \sigma_{0s} \sinh^{-1} \frac{N_s}{\rho} y_s \quad (8)$$

where the symbols

$$N_T = \frac{1}{\epsilon_{0T}' + m_T' t^{n_T}}; \quad \text{and} \quad N_s = \frac{1}{\epsilon_{0s}' + m_s' t^{n_s}}$$

have been introduced.

For a beam of rectangular cross section of width b, $dA = b\,dy$. Making this substitution, equations (5) and (6) become

$$b \int_{-(h-c)}^{0} \sigma_T \, dy + b \int_{0}^{c} \sigma_s \, dy = 0 \quad (9)$$

and

$$M = b \int_{-(h-c)}^{0} \sigma_T y_T \, dy + b \int_{0}^{c} \sigma_s y_s \, dy \quad (10)$$

Substituting for σ_T and σ_s from equations (7) and (8) into equation (9), and integrating, the resulting expression becomes

$$\frac{\sigma_{0T}}{N_T} \left\{ 1 + \frac{N_T}{\rho} (h - c) \sinh^{-1} \frac{N_T}{\rho} (h - c) - \left(1 + \left[\frac{N_T}{\rho} (h - c) \right]^2 \right)^{1/2} \right\} = \frac{\sigma_{0s}}{N_s} \left\{ 1 + \frac{N_s}{\rho} c \sinh^{-1} \frac{N_s}{\rho} c - \left[1 + \left(\frac{N_s}{\rho} c \right)^2 \right]^{1/2} \right\} \quad (11)$$

Substituting for σ_T and σ_s from equations (7) and (8) into equation (10) and integrating

$$M = \frac{b\sigma_{0T}\rho^2}{4(N_T)^2} \left\{ \left[2 \frac{N_T^2}{\rho^2} (h - c)^2 + 1 \right] \sinh^{-1} \frac{N_T}{\rho} (h - c) - \frac{N_T}{\rho} (h - c) \left(1 + \left[\frac{N_T}{\rho} (h - c) \right]^2 \right)^{1/2} \right\} + \frac{b\sigma_{0s}\rho^2}{4(N_s)^2} \left\{ \left[2 \left(\frac{N_s}{\rho} c \right)^2 + 1 \right] \sinh^{-1} \frac{N_s}{\rho} c - \frac{N_s}{\rho} c \left(1 + \left[\frac{N_s}{\rho} c \right]^2 \right)^{1/2} \right\} \quad (12)$$

For a given constant bending moment M applied for a given time t to a given beam, equations (11) and (12) are simultaneous equations in two unknowns, the location of the neutral axis c and the radius of curvature ρ. Values of ρ and c may be obtained by trial.

For a beam of constant bending moment the deflection at mid-span may then be obtained from the well-known geometrical relation

$$z = \frac{l^2}{8\rho} \quad (13)$$

where z is the deflection at the center relative to the ends of a span of a beam of length l subjected to a uniform bending moment.

The stress distribution may be obtained from the value of c and equations (7) and (8).

Since N_s and N_T are functions of time the radius of curvature ρ will change with time. Since N_s and N_T are unequal functions of time it is evident that the ratios N_s/ρ and N_T/ρ cannot both remain constant and independent of time. Hence from equation (11) it follows that c must vary with time.

Since the ratios N_s/ρ and N_T/ρ change with time the stress distribution must change with time. This follows from equations (7) and (8). Not only does the stress distribution change with time because of the time dependence of these ratios but because the position of the neutral axis changes with time and this affects the values of y_T and y_s in equations (7) and (8).

It is easily verified that equations (11) and (12) reduce to equations (16) and (18) in the previous paper [1] when tension and compression creep are equal.

Illustration:

Equations (11) and (12) have been solved for the particular problem of a beam of canvas laminate in which the creep in tension and compression were described by relations of the form of equations (2) and (3). The constants chosen for creep in tension were the same as employed for the canvas laminate analyzed in the previous report [1]; $\epsilon_{0T} = m_T' = 0.001875$ in. per in., $\sigma_{0T} = 4000$ psi, and $n_T = 0.1183$.

The creep behavior of this laminate in compression was not known. So to illustrate the effect of different constants in compression the constants for creep in compression were arbitrarily chosen to be 20 per cent higher than those for tension creep; $\epsilon_{0s} = m_s' = 0.002250$ in. per in., $\sigma_{0s} = 4800$ psi, and $n_s = 0.14196$.

To solve equations (11) and (12) for the purpose of determining the deflection-time relation in bending, the values of N_s and N_T were computed for a particular set of values of time t. Then the constant coefficients in the equations were computed by a numerical procedure in which $N_T(h - c)/\rho$ and $N_s c/\rho$ were used as variables.

From the values of the variables which satisfied equations (11) and (12) the values of ρ and c were computed, and from ρ the deflection was computed by means of equation (13). The deflection-time relation for a bending moment of 679 in-lb determined in this way is shown in Fig. 1 together with the corresponding experimental bending-creep curve and the theoretical creep curve for equal creep in tension and compression. The test selected for inclusion in Fig. 1 was that which was in best agreement with the theory presented in reference [1].

The following observation was of interest: In spite of the fact that the assumed creep in compression varied from 20 per cent greater than in tension at $t = 0$ to 33 per cent greater than in tension at 880 hr for the same stress, the computed creep in bending was nearly the same, over the time interval considered, as that computed for a beam in which the creep in compression was the same as that in tension.

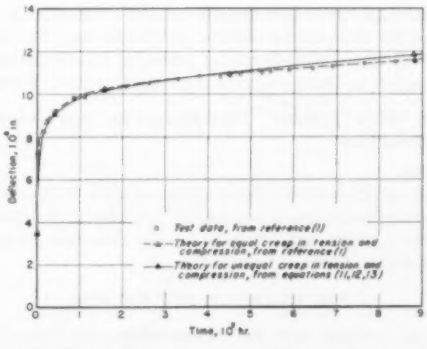

Fig. 1 Deflection-time relation in bending creep from different theories, for canvas laminate at 77 F and bending moment of 679 in-lb

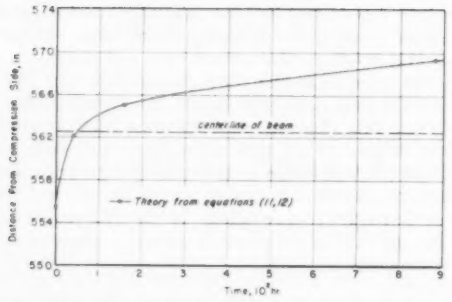

Fig. 2 Location of neutral axis during creep in bending when tension and compression creep are unequal, for canvas laminate at 77 F and bending moment 679 in-lb

stress, the creep in bending can be expressed by equations derived in the following manner:

Equation (14) may be written as follows by dividing by ϵ_0'

$$e = \sinh x + T \sinh ax \tag{15}$$

where

$$e = \epsilon/\epsilon_0'; \quad T = \frac{m't^n}{\epsilon_0'}; \quad a = \sigma_s/\sigma_m \text{ and } x = \sigma/\sigma_s \tag{16}$$

For a straight beam of rectangular cross section in which the creep equations in tension and compression are identical, the neutral axis can be shown to be at half the depth of the beam. Thus from statics the bending moment M in a beam of width b and depth h is related to the stress σ by the following equation

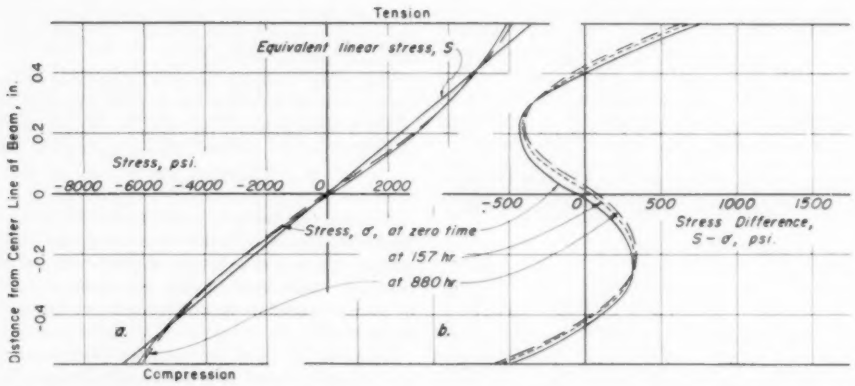

Fig. 3 Creep in bending for canvas laminate at 77 F and a bending moment of 679 in-lb when tension and compression creep are unequal: (*a*) Stress distribution during creep, from equations (7, 8); (*b*) deviation from linear stress distribution during creep

The position of the neutral axis was found to vary with time from one side of the center line to the other as shown in Fig. 2.

The distribution of stress across the beam was computed at two different values of time from equations (7) and (8), and was plotted for a time of zero and of 880 hr in Fig. 3(*a*). It was observed that the change in stress distribution was relatively small—less than 2 per cent in 880 hr at the extreme fiber. This was probably due in part to the fact that the time-dependent and time-independent stress functions were equal.

In order to better illustrate the change which occurred in the stress distribution, the difference between the computed stress distribution and the equivalent linear-stress distribution was determined for three values of time and is shown in Fig. 3(*b*). It was found that a high degree of precision was required in the computations to insure accurate results in the stress distribution.

Bending With Unequal Time-Dependent and Independent Stress Functions

Derivation:

The creep behavior of some materials is accurately represented by a more general form of equation (1) in which the constants in the stress function are different for the time-independent and time-dependent terms as follows

$$\epsilon = \epsilon_0' \sinh \sigma/\sigma_s + m't^n \sinh \sigma/\sigma_m \tag{14}$$

When the tension and the compression-creep behaviors are identical and are single-valued functions of stress and time, as described by equation (14) for constant stresses or small changes in

$$M = \int_{-c}^{c} b\sigma y \, dy = b\int_{-c}^{c} \sigma_s xy \, dy \tag{17}$$

where

c = half the beam depth
y = distance measured from the neutral axis in a direction perpendicular to the neutral axis

From the geometry of strains as expressed by equation (4) and the creep relation, equation (15), the following was obtained

$$y = \rho\epsilon = \rho\epsilon_0' e = \rho\epsilon_0' (\sinh x + T \sinh ax) \tag{18}$$

Differentiating equation (18) at constant ρ and T

$$dy = \rho\epsilon_0' (\cosh x \, dx + aT \cosh ax \, dx) \tag{19}$$

Substituting equations (18) and (19) into equation (17) for any given time t (and corresponding T and ρ) and expanding

$$M = b\sigma_s(\rho\epsilon_0')^2 \left\{ \int_{-x_1}^{x_1} x \sinh x \cosh x \, dx + aT \int_{-x_1}^{x_1} x \sinh x \cosh ax \, dx + T \int_{-x_1}^{x_1} x \sinh ax \cosh x \, dx + aT^2 \int_{-x_1}^{x_1} x \sinh ax \cosh ax \, dx \right\} \tag{20}$$

where the limits of x correspond to the limits of y; that is, x_1 is the stress at $y = c$ and $-x_1$ is the stress at $y = -c$.

Performing the integration as indicated in equation (20), the resulting equation for radius of curvature ρ as a function of

bending moment M and stress at the extreme fiber $\sigma_1 = \sigma_e x_1$ was

$$M = \frac{b\sigma_e(\epsilon_0')^2\rho^2}{2}\left\{[(2\sinh^2 x_1 + 1)x_1 - \sinh x_1 \cosh x_1] + \frac{T^2}{a}[(2\sinh^2 ax_1 + 1)ax_1 - \sinh ax_1 \cosh ax_1] + 4T\left[x_1 \sinh x_1 \sinh ax_1 - \frac{1}{(a^2-1)}(a \sinh x_1 \cosh ax_1 - \cosh x_1 \sinh ax_1)\right]\right\} \quad (21)$$

Solving equation (18) for $1/\rho$ when $y = c$ and $x = x_1$ the following is obtained

$$\frac{1}{\rho} = \frac{\epsilon_0'}{c}(\sinh x_1 + T \sinh ax_1) \quad (22)$$

These two independent relations, (21) and (22), can be solved simultaneously at any given time $t = t_1$ (or $T = T_1$) for the extreme fiber stress function x_1 and the radius of curvature ρ. The deflection for a beam having uniform bending moment may then be obtained from equation (13).

If the ratio $a = \sigma_e/\sigma_m$ is allowed to equal unity, equation (14) reduces to equation (1). Consequently, equation (21) may be shown to reduce to equation (18) of reference [1].

The simultaneous equations (21) and (22) may be solved by substituting equation (22) for ρ in equation (21), expanding and collecting terms in T. The following quadratic equation in T results

$$T^2\{(2M/bc^2\sigma_e)\sinh^2 ax_1 - x_1(1 + 2\sinh^2 ax_1) + (1/a)\cosh ax_1 \sinh ax_1 + T\}\{[4M/bc^2\sigma_e - 4x_1]\sinh ax_1 \sinh x_1 - [4/(a^2-1)]\sinh ax_1 \cosh x_1 + [4a/(a^2-1)]\cosh ax_1 \sinh x_1\} + \{\sinh x_1 \cosh x_1 + (2M/bc^2\sigma_e)\sinh^2 x_1 - x_1(1 + 2\sinh^2 x_1)\} = 0 \quad (23)$$

Equation (23) is then evaluated for the given value of M and several reasonable values of x_1 by using the quadratic formula. The solution of the quadratic formula gives the time function T corresponding to each chosen stress function x_1. From the value of T the time t was determined from equation (16). The curvature $1/\rho$ was determined from equation (22) by substituting T and x_1. Then by utilizing equation (13) the deflection z was determined for the same value of time.

From the values of x_1 at different times the change in extreme fiber stress may be determined as a function of time by use of the last relation in equations (16). Also at any given value of time and corresponding values of T and ρ the stress distribution can be computed from equation (18). Because the creep functions were assumed to be the same in tension and compression the neutral axis does not change position with time.

Illustration:

Creep data were available for tension [12, 13] and bending [12] of polystyrene. The two sets of tension-creep data were both made on polystyrene of the same description from the same manufacturer. One set of tension-creep data did not have enough self-consistency to permit evaluating the constants of the creep equation, but by combining the two sets of data this became possible—though with limited accuracy.

It was found that equation (1) could not adequately describe the data so equation (14) was tried with the results shown in Fig. 4. The corresponding values of the constants in equation (14) were found to be as follows:

$\epsilon_0' = 4.3077 \times 10^{-2}$ in. per in.
$\sigma_e = 20{,}000$ psi
$m' = 4.098 \times 10^{-6}$ in. per in.
$\sigma_m = 700$ psi
$n = 0.475$

These values were obtained largely by trial. The data did not yield readily to rational procedures of evaluating the constants such as used previously [2, 4]. Utilizing these values of the constants and the procedure outlined above, the creep in bending was computed for a beam of the dimensions employed in the tests of reference [12] and a bending moment of 553 in-lb. The results of these computations are shown in Fig. 5 together with test data reported in reference [12].

Also shown in Fig. 5 is the change in the stress at the extreme fiber with time. The computed stress at the extreme fiber decreased 10 per cent in 1000 hr and decreased 12.4 per cent in 3200 hr. Since the bending moment remained constant the stress distribution changed.

The agreement between the theoretical and experimental creep deflections was not as good as would be desired although the shape of the curve was satisfactorily predicted from 100 to 1000 hr. Possible reasons for the lack of better agreement may be among the following: (*a*) Creep of the polystyrene tested in bending and part of the tension tests may not have been accurately described by the constants selected for the creep equation. Some of the tension creep curves for this material showed similar departures from the theory in both tension and bending tests; (*b*) crazing was observed to occur in tension creep and on the tension side of the beams; (*c*) the data in the first 100 hr of

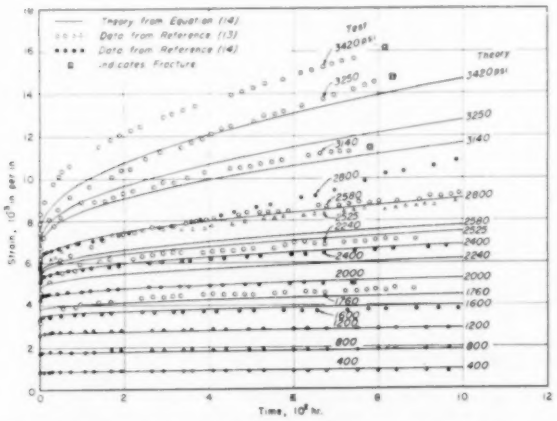

Fig. 4 Creep tests in tension at different stresses for polystyrene at 77 F

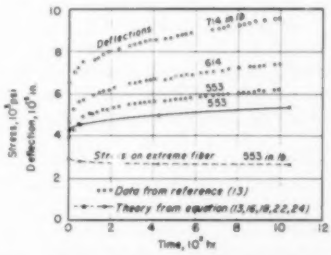

Fig. 5 Creep tests in bending at different bending moments for polystyrene at 77 F

creep in bending appear to be more irregular than subsequent data; (*d*) creep in tension and compression may not have been the same; and (*e*) the change in stress distribution with time caused the stress on a given fiber to change during creep instead of remaining constant as assumed by the use of equation (14).

Conclusions

It has been shown that creep and stress distribution in bending can be predicted from tension and compression-creep data. However, the available test data are inadequate to provide an accurate check of the theory.

The theory showed that the stress distribution and position of the neutral axis in a beam changed with time when the creep in tension and compression were unequal. When the time-dependent and time-independent stress functions were unequal the stress distribution in a beam changed with time.

Acknowledgments

This project was conducted in the Department of Theoretical and Applied Mechanics of the University of Illinois in co-operation with Picatinny Arsenal, Ordnance Corps, Department of the Army.

The authors are grateful to B. K. Ghandi, W. A. Hagemeyer, G. Khosla, and H. G. Russel for assistance in the computations and preparation of illustrations.

References

1 W. N. Findley and J. J. Pocratek, "Prediction of Creep-Deflection and Stress Distribution in Beams From Creep in Tension," *Journal of Applied Mechanics*, vol. 22, TRANS. ASME, vol. 77, 1955, pp. 165–171.

2 W. N. Findley, "Creep Characteristics of Plastics," 1944 Symposium on Plastics, ASTM, 1944, p. 118.

3 W. N. Findley and W. J. Worley, "Mechanical Properties of Five Laminated Plastics," NACA TN 1560, August, 1948.

4 W. N. Findley, "Derivation of a Stress-Strain Equation From Creep Data for Plastics," Proceedings, First U. S. National Congress of Applied Mechanics, June 11–16, 1951, p. 595.

5 W. Kauzmann, "Flow of Solid Metals From the Standpoint of the Chemical Rate Theory," *Trans. AIME*, Institute of Metals Division, vol. 143, 1941, p. 57.

6 E. P. Popov, "Bending of Beams With Creep," *Journal of Applied Physics*, vol. 20, 1949, pp. 251–256.

7 B. Fried, "Some Observations on Photoelastic Materials Stressed Beyond the Elastic Limit," SESA, vol. 8, no. 2, 1951, p. 143.

8 I. Roberts, "Prediction of Relaxation of Metals From Creep Data," *Proceedings ASTM*, vol. 51, 1951, p. 811.

9 J. Marin, Y. H. Pao, and G. E. Cuff, "Creep Properties of Lucite and Plexiglas for Tension, Compression, Bending, and Torsion," TRANS. ASME, vol. 73, 1951, pp. 705–719.

10 A. Nadai, "Plasticity," The McGraw-Hill Book Company, Inc., New York, N. Y., 1935, p. 121.

11 G. H. MacCullough, "An Experimental and Analytical Investigation of Creep in Bending," TRANS. ASME, vol. 55, 1933, p. APM 55-9.

12 J. Marin and G. Cuff, "Creep-Time Relations for Polystyrene Under Tension, Bending, and Torsion," *Proceedings ASTM*, vol. 49, 1949, pp. 1158–1174.

13 W. N. Findley, "Comments on Creep and Damping Properties of Polystyrene," *Journal of Applied Physics*, vol. 21, no. 3, May, 1950, p. 258.

Application of the Analog Computer to Product Dynamic Performance in Typical Hydraulic Circuits

By GERHARD REETHOF,[1] DETROIT, MICH.

The successful use of electronic-analog-computing techniques in the simulation of typical hydraulic systems is demonstrated. As an example, the instabilities of a certain open-center hydraulic-booster system are simulated, and corrective action is indicated and verified. The study involves the analysis of a grossly nonlinear system and methods of function generation are given.

Nomenclature

The following nomenclature is used in this paper:

A_1 = area of orifice opening at valve port 1, in.^{2}
A_2 = area of orifice opening at valve port 2, in.^{2}
A_3 = area of orifice opening at valve port 3, in.^{2}
A_4 = area of orifice opening at valve port 4, in.^{2}
A_{m1} = pressure sensitive area at head end of motor, in.^{2}
A_{m2} = pressure sensitive area at rod end of motor, in.^{2}
B = damping coefficient in wheel system, in-lb-sec/radian
C_O = hydraulic constant for orifice flow $= C_d\left(\frac{2}{\rho}\right)^{1/2}$, (for petroleum base oils $C_O = 96.5$ in.^{2}/sec lb$^{1/2}$)
C_d = orifice discharge coefficient (0.611)
g = acceleration of gravity, 386 in/sec^2 (Note that $\rho g \cong 0.031$ lb/in.^{3} for petroleum-base oils)
J = inertia of load system, in-lb-sec^2/radian
K_a = linkage ratio between load and cylinder, in/radian
K_l = load spring constant, in-lb/radian
k_{es} = coefficient of elasticity of fluid line between pump and valve, in^5/lb
k_{e1} = coefficient of elasticity of fluid line between valve and head end of motor
k_{e2} = coefficient of elasticity of fluid line between valve and rod end of motor
P_1 = pressure drop across valve orifice 1, lb/in.^{2}
P_2 = pressure drop across valve orifice 2, lb/in.^{2}
P_3 = pressure drop across valve orifice 3, lb/in.^{2}
P_4 = pressure drop across valve orifice 4, lb/in.^{2}
P_{m1} = pressure on head side of motor, lb/in.^{2}
P_{m2} = pressure on rod side of motor, lb/in.^{2}
Q_{cs} = compressibility flow in supply system, in^3/sec
Q_{ch} = compressibility flow in head end, in^3/sec
Q_{cc} = compressibility flow in rod end, in^3/sec
Q_s = flow from pump, in^3/sec
Q_1 = flow through restriction 1, in^3/sec
Q_2 = flow through restriction 2, in^3/sec
Q_3 = flow through restriction 3, in^3/sec
Q_4 = flow through restriction 4, in^3/sec
Q_{m1} = flow into head side of motor, in^3/sec
Q_{m2} = flow into rod side of motor, in^3/sec
R = radius of circular port opening, in.
s = absolute spool travel resulting from input signal, in.
t = time, sec
U = underlap of rectangular port, in.
V_s = volume of oil under compression in supply system, in.^{3}
V_1 = volume of oil under compression between valve and head end of motor, in.^{3}
V_2 = volume of oil under compression between valve and rod end of motor, in.^{3}
W = port width of rectangular port, in.
x = relative linear displacement between valve and spool as measured from mid-position of spool, in.
x_0 = height of circular-port segment with valve in mid-position, in.
y = displacement of output, radians
β = bulk modulus of hydraulic oil, lb/in.^{2}
θ_1 = chamfer angle of valve spool at tank side, deg
θ_2 = chamfer angle of valve spool at pressure side, deg
ρ = mass density of fluid, lb sec^2/in.^{4}

Introduction

The development of hydraulic systems has been based primarily on a combination of experience with previous applications and the conducting of well-planned experiments. A great many successful systems have thus been developed. Within recent years the speed-of-response requirements of hydraulic control systems has been raised to the point where the inherent limitations of these well-tried methods have become evident. The experimental procedures, the design by experiment, will at best result in a single solution; a new application will require a new set of experiments to determine the proportions of an acceptable design. Furthermore, since experiments of this sort require extensive hardware modification, an optimum design is seldom determined. There is always a tendency to look for the "quick fix" rather than the establishment of a basic understanding of the system.

The next step in the evolution of design procedures was to attempt a purely analytical approach. The serious nonlinearities inherent in the equations which characterize the hydraulic system indicated the great difficulty of obtaining closed analytical solutions. The most common approach was to linearize the equations by assuming incremental operation about some characteristic value, then applying the well-known control-system synthesis techniques.

Much can be learned about the linearized system by the use of the Routh-Hurwitz test function, which however permits only the determination of conditions of marginal stability (1).[2] The manipulations of the Nyquist criteria (2), Bode diagrams (3), Nichols charts (4), and other graphical techniques become rather cumber-

[1] Chief of Research, Vickers Incorporated, Detroit, Mich. Mem. ASME.

Contributed by the Hydraulic Division and presented at the Annual Meeting, New York, N. Y., December 1–6, 1957, of The American Society of Mechanical Engineers.

Note: Statements and opinions advanced in papers are to be understood as individual expressions of their authors and not those of the Society. Manuscript received at ASME Headquarters, August 2, 1957. Paper No. 57—A-97.

[2] Numbers in parentheses refer to Bibliography at end of paper.

some if several system parameters are permitted to vary. The root-locus plots (5, 6) permit the determination of the degree of stability as well as the essentials of the frequency response and transient response of a system, but still suffer from the same limitations of the previously discussed methods. These methods of systems analysis, it must be emphasized, are limited to linear systems, or the linearizations of mildly nonlinear systems.

The phase-plane methods should be mentioned as they permit the study of nonlinear systems of second order. These methods lend themselves especially to the determination of the transient response. The describing-function method of analyzing nonlinear systems is particularly useful in the study of the response of a nonlinear system to sinusoidal inputs. Zaborszky and Harrington (12, 13, 14) have demonstrated the applicability of the method to hydraulic systems. The accuracy of the describing-function method in the study of fast-response systems has to be carefully evaluated since the neglected harmonics above the fundamental may not be sufficiently well filtered by the system.

In many system studies involving multiple nonlinearities, several system parameters may be permitted to vary. The electronic analog computer offers a far greater flexibility than any of the methods listed, and thus affords an excellent opportunity to experiment analytically.

Any of the system parameters can be changed while the problem is running, or a combination of several parameters may be varied by the mere turning of an accurately calibrated dial. It is thus possible to obtain an unusual understanding of the peculiarities of the effect of nonlinearities on the system performance.

The analog computer has found wider and wider use in recent years as a means of simulating nonlinear and linear systems. The linearized systems were studied with the computer (7) and then these results were compared with the analog simulation of the nonlinear system (8). The introduction of nonlinearities into an analog-computer study do, however, impose far greater demands on the stability and accuracy of the computer than does a linear study. For systems which do not deviate markedly from the linear approximations, excellent results have been found to be obtainable from the far simpler linear simulation (10). The high degree of complexity in certain accurate simulations of nonlinearities is shown in a study by Shearer (11) and to some extent in the present paper.

The validity of the simulation of the physical system depends primarily on our ability to properly describe the behavior of the various elements of the system and their interaccion within the system. We must therefore have a rather complete understanding of the system before we can profitably use an analog computer.

In a recent study, an open-center hydraulic-booster system had been designed by the experimental approach. The system was found to go into sustained oscillations when certain large disturbances were imposed on the system through the input member. For small disturbances and normal steady operation the system behaved acceptably. A purely experimental remedial approach did not give a satisfactory solution. The sustained oscillations resulting from large input disturbances continued to occur. Since experimental procedures did not result in any improvement of the objectionable condition, it must be concluded that there was inadequate understanding of the system dynamics.

A program utilizing electronic-analog-computer simulation was inaugurated. A crucial first step was the attempt to reproduce the behavior of the malfunctioning system. The accuracy of the simulations would thus be established and, most important of all, confidence would be gained in our ability to represent nonlinear systems. The experiments which had not produced any significant improvements would then be simulated in a further attempt to prove the validity of the simulation.

Only after this confidence in our ability to simulate had been established, was a program planned to correct the ills by analytical experimentation on the computer. The interesting concept is thus proposed that a combination of limited experimentation and comprehensive analytical experimentation with the computer would lead to an excellent understanding of system peculiarities, and in the end lead to vastly improved design of nonlinear systems.

Analysis

Description of System. A schematic diagram of the system is shown in Fig. 1. A constant-volume pump supplies flow Q_s to an underlapped 4-way spool-type valve. The sleeve of the 4-way valve is an integral part of the cylinder resulting in a one-to-one follow-up system (unity feedback). The piston rod is fixed to the frame of the unit. The cylinder controls the position of the load through a suitable linkage.

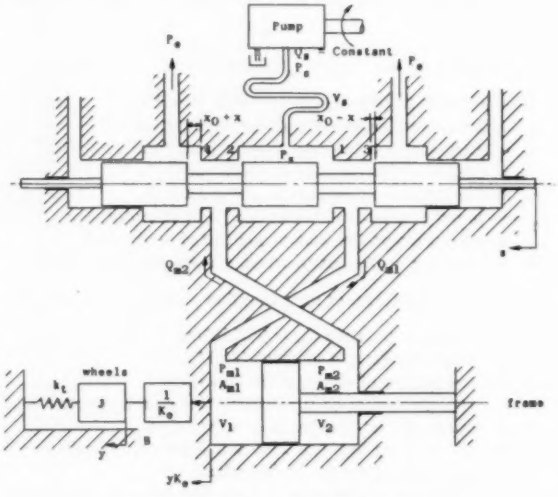

Fig. 1 Schematic diagram of system

Assumptions. The following assumptions were made in order to arrive at a reasonable analytical representation of the system:

1 The load is connected by a linear spring to ground.

2 The circular ports in the sleeve can be approximated by the uncovering of circular holes in flat plates.

3 Since the driving forces on the valve spool are large, all flow-induced forces on the valve spool can be neglected.

4 The effect of valve-spool-centering springs is negligible.

5 There is no leakage across the piston of the motor.

6 The lever arm through which the booster acts is constant.

7 All distributed effects within the system, such as oil-column acoustics, were neglected.

Of interest is the obvious fact that several of these assumptions could not be made without considerable prior knowledge of the system behavior.

The spring to ground was cause for great concern. Only after extensive study of the actual system was it determined that the mounting did not slip on the ground during the oscillations. The system under study has a slow response compared to the acoustic response of the fluid-transmission lines. Therefore acoustic resonances should not be expected to occur. However, in many fast-response systems, such as certain electrohydraulic servomotor systems and pressure-controlled systems using fast-response

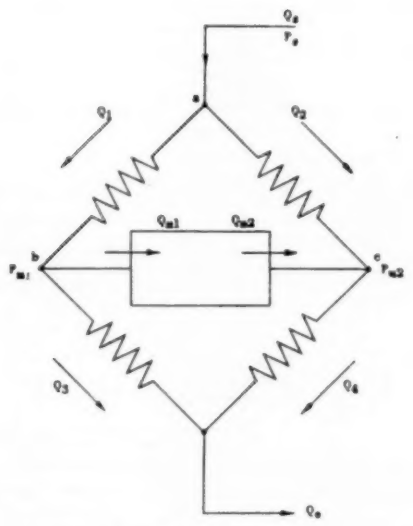

Fig. 2 Schematic diagram of 4-way valve

regulating and relief valves, these distributed phenomena are known to have resulted in the squealing and chattering of valves. In such cases assumption 7 must of course be carefully reviewed.

Basic System Equations. Fig. 1 is a simplified representation of the system which results from the assumptions made in the previous section. The 4-way valve is analyzed by recourse to Fig. 2. The continuity equations for points *a*, *b*, and *c*, Fig. 2, are derived as follows

$$Q_{ca} = Q_s - Q_1 - Q_2 \quad [1]$$

$$Q_{cb} = Q_1 - Q_3 - Q_{m1} \quad [2]$$

$$Q_{cc} = Q_2 - Q_4 + Q_{m2} \quad [3]$$

The compressibility flows are given by

$$Q_{ca} = \left(\frac{V_s}{\beta} + k_{es}\right)\frac{dP_s}{dt} \quad [4]$$

$$Q_{cb} = \left(\frac{V_1}{\beta} + k_{e1}\right)\frac{dP_{m1}}{dt} \quad [5]$$

$$Q_{cc} = \left(\frac{V_2}{\beta} + k_{e2}\right)\frac{dP_{m2}}{dt} \quad [6]$$

The orifice flows are given by

$$Q_1 = C_O A_1 \sqrt{P_1} \quad [7]$$

$$Q_2 = C_O A_2 \sqrt{P_2} \quad [8]$$

$$Q_3 = C_O A_3 \sqrt{P_3} \quad [9]$$

$$Q_4 = C_O A_4 \sqrt{P_4} \quad [10]$$

Also it is assumed that

$$Q_{m1} = A_{m1} K_s \frac{dy}{dt} \quad [11]$$

$$Q_{m2} = A_{m2} K_s \frac{dy}{dt} \quad [12]$$

Similarly the pressures are related as follows

$$P_{m1} = P_s - P_1 \quad [13]$$

$$P_{m2} = P_s - P_2 \quad [14]$$

$$P_3 = P_{m1} - P_o \quad [15]$$

$$P_4 = P_{m2} - P_o \quad [16]$$

Manipulating Equations [1] through [16] results in

$$\left(\frac{V_s}{\beta} + k_{es}\right)\frac{dP_s}{dt} = Q_s - C_O A_1 (P_s - P_{m1})^{1/2} - C_O A_2 (P_s - P_{m2})^{1/2} \quad [17]$$

$$\left(\frac{V_1}{\beta} + k_{e1}\right)\frac{dP_{m1}}{dt} = C_O A_1 (P_s - P_{m1})^{1/2} - C_O A_3 (P_{m1} - P_o)^{1/2} - A_{m1} K_s \frac{dy}{dt} \quad [18]$$

$$\left(\frac{V_2}{\beta} + k_{e2}\right)\frac{dP_{m2}}{dt} = C_O A_2 (P_s - P_{m2})^{1/2} - C_O A_4 (P_{m2} - P_o)^{1/2} + A_{m2} K_s \frac{dy}{dt} \quad [19]$$

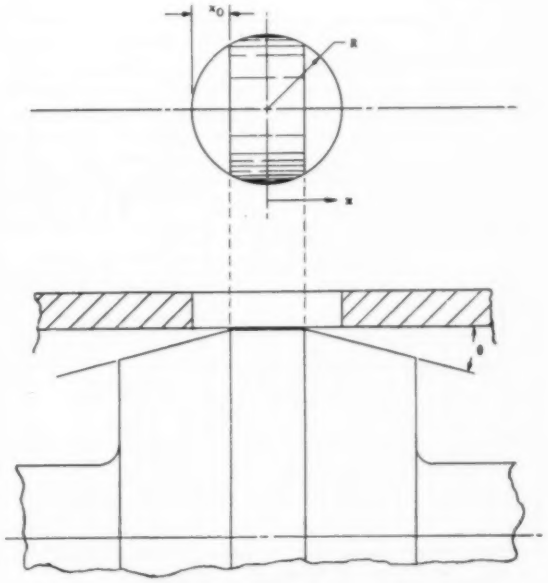

Fig. 3 Diagram of port configuration for circular ports

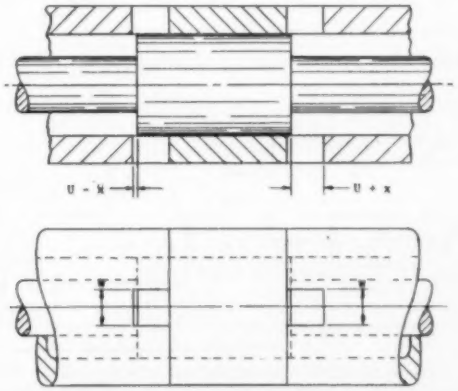

Fig. 4 Diagram of port configuration for rectangular ports

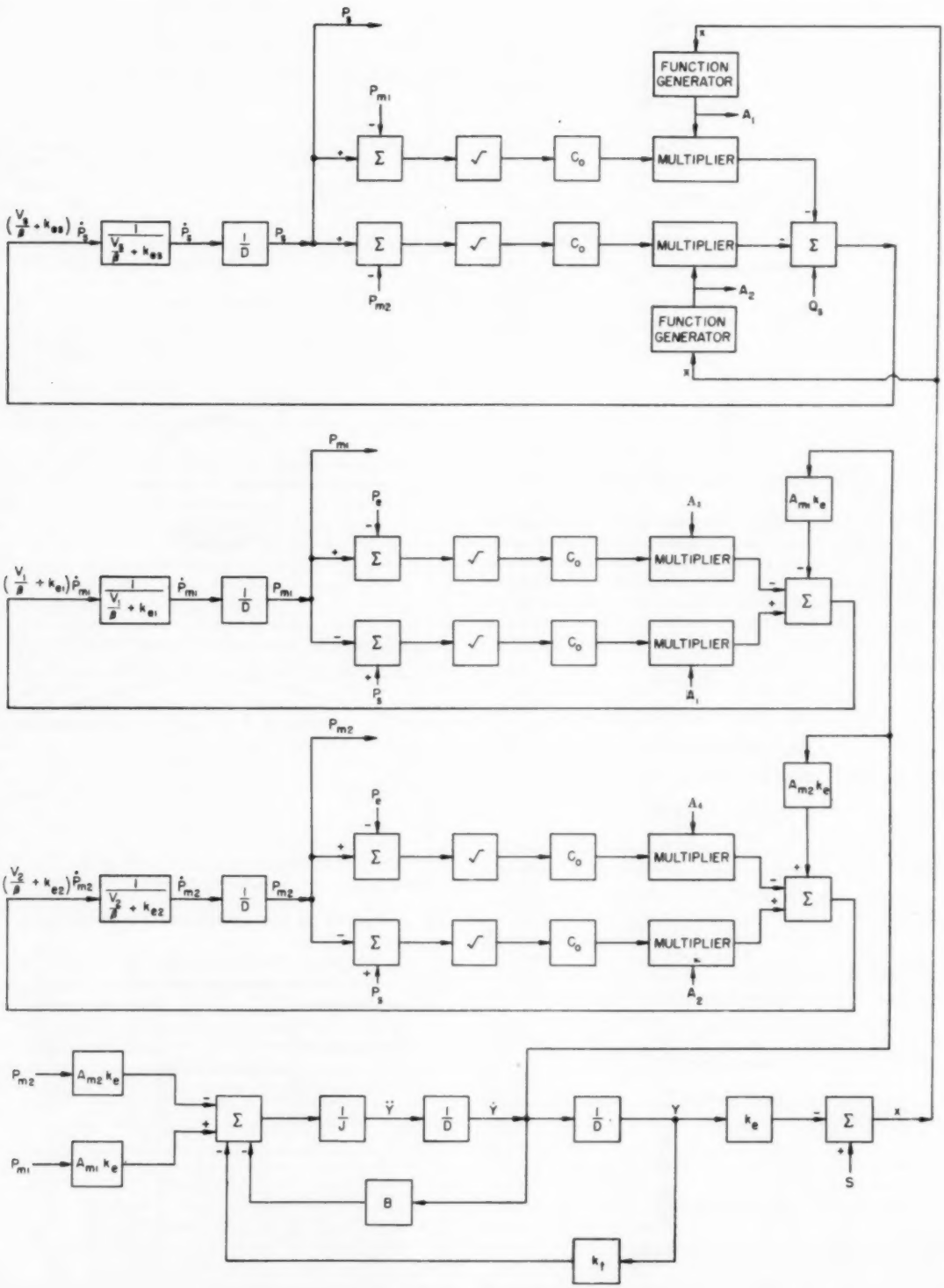

Fig. 5 Block diagram of simulated system

The force equation [20] for the motor-load system is given by

$$A_{m1}K_sP_{m1} - A_{m2}K_sP_{m2} = J\frac{d^2y}{dt^2} + B\frac{dy}{dt} + K_1y \quad [20]$$

The feedback equation between valve sleeve and valve spool is given by

$$x = s - yK_s \quad [21]$$

The equations of the port areas A_1, A_2, A_3, and A_4 must next be derived for a particular case. In the original design a circular-port configuration with a conical-valve-spool land was used as illustrated in Fig. 3. The equation for the area of a segment of a circle can be shown to be

$$A = R^2\left[\cos^{-1}\left(1 - \frac{h}{R}\right) - \left(1 - \frac{h}{R}\right)\sin\cos^{-1}\left(1 - \frac{h}{R}\right)\right] \quad [22]$$

where h is the height of the segment.

Using the conditions of Fig. 3, and assuming that the flat approximation is adequate, results in the following area equations for the 2 ports per land

$$A_1 = 2R^2\sin\theta_1\left[\cos^{-1}\left(1 - \frac{x + x_0}{R}\right) - \left(1 - \frac{x + x_0}{R}\right)\sin\cos^{-1}\left(1 - \frac{x + x_0}{R}\right)\right] \quad [23]$$

$$A_2 = 2R^2\sin\theta_1\left[\cos^{-1}\left(1 + \frac{x - x_0}{R}\right) - \left(1 + \frac{x - x_0}{R}\right)\sin\cos^{-1}\left(1 + \frac{x - x_0}{R}\right)\right] \quad [24]$$

$$A_3 = 2R^2\sin\theta_2\left[\cos^{-1}\left(1 + \frac{x - x_0}{R}\right) - \left(1 + \frac{x - x_0}{R}\right)\sin\cos^{-1}\left(1 + \frac{x - x_0}{R}\right)\right] \quad [25]$$

$$A_4 = 2R^2\sin\theta_2\left[\cos^{-1}\left(1 - \frac{x + x_0}{R}\right) - \left(1 - \frac{x + x_0}{R}\right)\sin\cos^{-1}\left(1 - \frac{x + x_0}{R}\right)\right] \quad [26]$$

For the case of rectangular ports used in subsequent designs (see Fig. 4) the respective areas become

$$A_1 = 2W_1U\left(1 + \frac{x}{U}\right) \quad [27]$$

$$A_2 = 2W_2U\left(1 - \frac{x}{U}\right) \quad [28]$$

$$A_3 = 2W_3U\left(1 - \frac{x}{U}\right) \quad [29]$$

$$A_4 = 2W_4U\left(1 + \frac{x}{U}\right) \quad [30]$$

Equations [17] through [21] with the port-area expressions are the system equations which will be simulated on the analog computer. The block diagram of this system of equations is given in Fig. 5. The top three sections represent the flow equation for the supply system, the rod-end system and the head-end system. The lowest diagram represents the load system and feedback means.

Computer Solution

The problem was solved on a modified Reeves Electronic Analog Computer. The problem was then scaled to fit the limited capabilities of the computer. The limited space allowable does not permit a complete discussion of the methods which were devised to generate the various nonlinear functions. In the Appendix the generation of the port-area function is shown to indicate a possible procedure. There are analog computers available, however, such as the Philbrick Researches, Inc., equipment and others which offer diode "Function Fitters" permitting the direct fitting of an arbitrary function of a variable. Since a rather elaborate computer setup is required to simulate the system, it is imperative that each of the computer loops be checked for stability over the operating range of the variables. The initial conditions of this type of problem can be either set into the computer by adding the appropriate values or the computer may be permitted to find its own quiescent level. Since the values of the initial conditions for the present problem were low compared to the operating values of the variables, the latter method was used.

Discussion of Results

With the problem set up and properly scaled, the first check solutions were run. The attempt was to simulate the conditions existing in the actual steering booster installation and to compare the simulator predictions with the actual performance of the test vehicle. Fig. 6 is the predicted response to a ramp signal with the pressure on the rod side of the piston. The pressure trace indicates a rapid rise from the quiescent supply pressure of 40 psi. This initial pressure is required to accelerate the moving parts to the

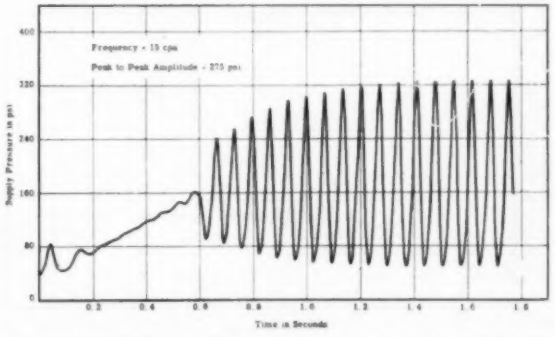

Fig. 6(*a*) Simulated supply-pressure response of steering booster to a ramp input as a function of time; circular ports; pressure on rod side of piston

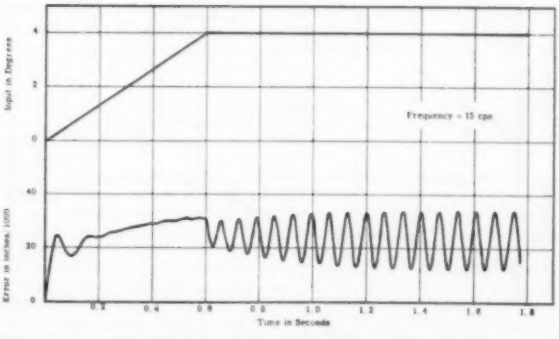

Fig. 6(*b*) *Upper curve*, steering-wheel motion (input signal); *lower curve*, relative position of valve spool to valve sleeve as a function of time; circular ports; pressure on rod side of piston

terminal velocity. The supply pressure and the error signal increase as the turn continues, since the spring loading calls for an increasing force from the ram. As the ramp signal is suddenly stopped, the system assumes a limit cycle and oscillates with a frequency of 15 cps and at a peak-to-peak pressure amplitude of 275 psi. The test-vehicle solution, Fig. 7, is similar in nature. The frequency of the oscillation is 13.5 cps and the peak-to-peak amplitude is 320 psi. A discussion of errors will be presented later.

In Figs. 6 and 7 response data are presented for the pressure existing on the rod side of the piston. In Fig. 8 the computer solution is shown for the case of the high pressure existing on the head end of the piston. The motion in Fig. 8 is thus reversed from that of Fig. 6. The predicted behavior for this case is considera-

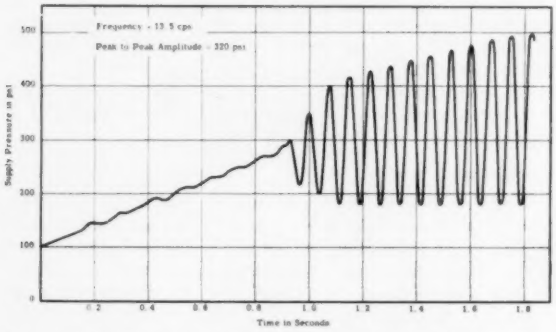

Fig. 7 Test-vehicle response with pressure on rod side of piston; circular ports

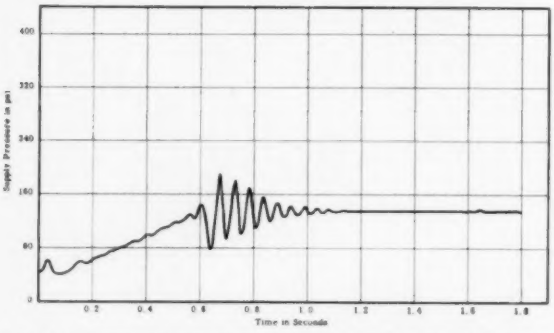

Fig. 8(*a*) Simulated supply-pressure response of steering booster to a ramp input as a function of time; circular ports; pressure on head side of piston

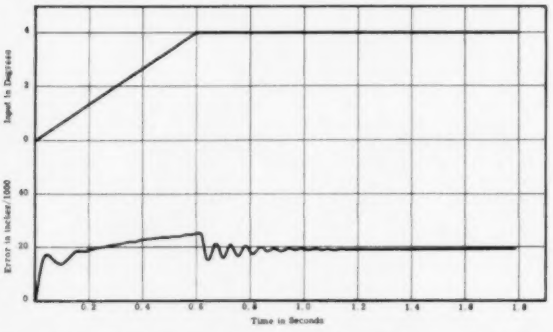

Fig. 8(*b*) *Upper curve,* steering-wheel motion (input signal); *lower curve,* relative position of valve spool to valve sleeve as a function of time; circular ports; pressure on head side of piston

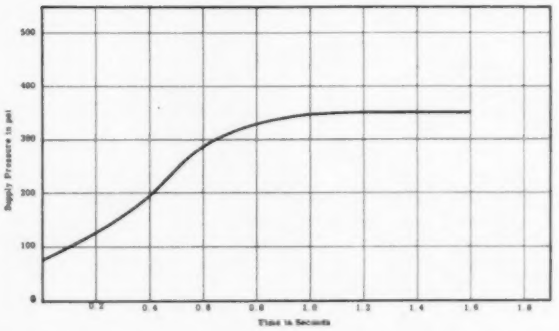

Fig. 9 Test-vehicle response with pressure on head side of piston; circular ports

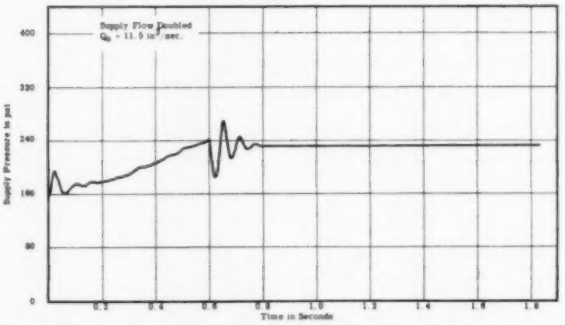

Fig. 10 Simulated supply-pressure response of steering booster to a ramp input as a function of time; circular ports, increased pump flow; pressure on rod end

bly more stable than for the previous case. The test vehicle behavior is shown in Fig. 9. The trends shown by the computer solution are verified by the behavior of the test vehicle. Further tests showed consistent agreement between computer predictions and actual behavior. Thus, increasing the flow from the pump resulted in a more stable system in both computer and test vehicle. The computer solution is shown in Fig. 10.

The next step was to modify the design to assure a stable operation under all operating conditions. The primary cause of the instability of the system was the marked increase in flow-valve gain resulting from the rapidly increasing port areas of the circular ports with increasing valve opening, and the increases in pressure drop across the ports as the load spring is loaded. A rectangular-shaped port to replace the circular port was designed with the computer. Fig. 11(*a*) gives the supply-pressure curve as a function of time as derived from the computer. Fig. 11(*b*) gives again the input-signal and error-signal curves versus time. The simulated system although slightly underdamped is stable. Since the simulation does not include the damping existing in the actual system, the test-vehicle performance should be expected to be more stable. This was proven to be correct from subsequent tests. The computer was also used to design a dashpot for the valve spool in order to stabilize the system. Any of the other system parameters could be varied with ease in attempts to arrive at a stable system.

Various uncertainties existed in the accuracy of the simulation which are worthy of discussion:

(*a*) The inertia of the complex-load system was calculated and is subject to considerable errors.

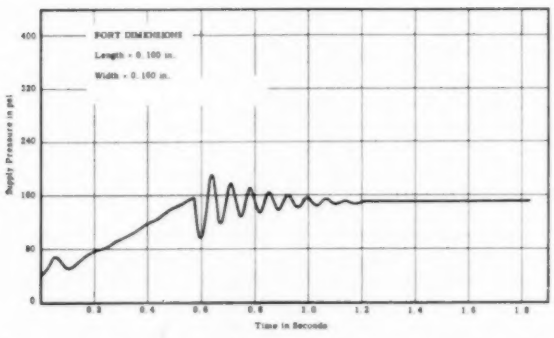

Fig. 11(*a*) Simulated supply-pressure response of steering booster to a ramp input; rectangular ports; pressure on rod side of piston

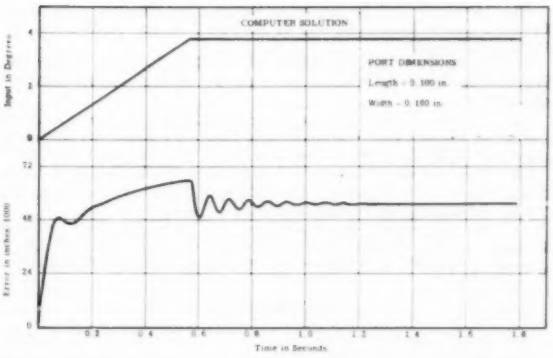

Fig. 11(*b*) *Upper curve*, steering-wheel motion (input signal); *lower curve*, relative position of valve spool to valve sleeve as a function of time; rectangular ports; pressure on rod side of piston

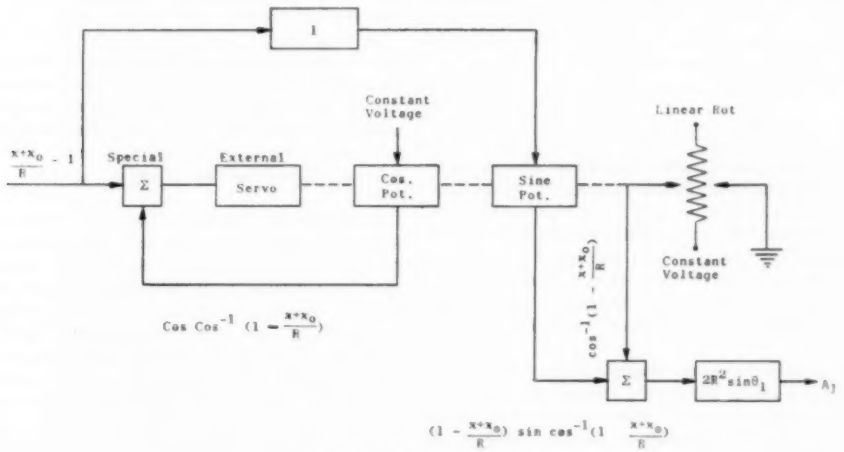

Fig. 12 Circuit diagram

(*b*) Since no load damping was assumed, the computer solutions are actually conservative with regard to stability.

(*c*) The stiffness of the load spring is not linear as was assumed.

In the light of these uncertainties and the assumptions previously discussed, the agreement between simulated and actual results is considered good.

Conclusions

The example has shown that the electronic analog computer can be programmed to realistically simulate nonlinear hydraulic circuits. The validity of the simulation depends entirely on the ability of the analyst to realistically describe the behavior of the elements of the system by analytical means. Thus the analog computer will only solve the engineers' analytical interpretation of the system. If certain important distributed or lumped effects are neglected, the answers from a computer may be embarrassingly misleading. If, however, a reasonably accurate simulation is studied by the analog approach, an excellent physical understanding of the nonlinear system is obtained. As a result of this understanding, the time devoted to developmental experimentation will be greatly reduced.

Acknowledgments

The work reported was carried out with the assistance of Messrs. Anthony Gregory and A. A. Seleno. Mr. Gregory in particular developed the computer circuitry for this problem and programmed the problem on the University of Michigan Reeves Computer. Mr. Leonard Dreisbach provided the information on the performance of the test vehicle.

Bibliography

1 "On the Dynamics of Pressure-Controlled Hydraulic Systems," by G. Reethof, ASME Paper Number 54—SA-7.

2 "Regeneration Theory," H. Nyquist, *Bell-System Technical Journal*, vol. 2, 1932, pp. 125–147.

3 "Network Analysis and Feedback Amplifier Design," by H. W. Bode, D. Van Nostrand Company, Inc., New York, N. Y., 1945.

4 "Theory of Servomechanism," by H. M. James, N. B. Nichols, and R. S. Phillips, McGraw-Hill Book Company, Inc., New York, N. Y., 1947.

5 "Control System Synthesis by Root-Locus Method," by W. R. Evans, *Trans. AIEE*, vol. 69, part 1, 1950, pp. 66–69.

6 "Quick Methods for Evaluating the Closed-Loop Poles of Feed-Back Control Systems," by G. Biernson, AIEE Technical Paper No. 53–42.

7 "The Analog Computer as a Design Tool in the Study of a Velocity Control Hydraulic System," by G. Reethof, Proceedings of the National Conference on Industrial Hydraulics, October, 1955.

8 "Dynamic Characteristics of Valve-Controlled Hydraulic Servo Motors," by J. L. Shearer, ASME Paper No. 53—A-147.

9 "Electrohydraulic Servomechanism With an Ultrahigh-Frequency Response," by D. P. Eckman, C. K. Taft, and R. H. Schuman, TRANS. ASME, vol. 79, 1957, pp. 455–463.

10 "Analysis and Design of a Servomotor Operating on High-Pressure Compressed Gas," by G. Reethof, TRANS. ASME, vol. 79, 1957, pp. 875–885.

11 "Nonlinear Analog Study of a High-Pressure Pneumatic Servomechanism," by J. L. Shearer, TRANS. ASME, vol. 79, 1957, pp. 465–472.

12 "A Describing Function Representation for the Multiple Nonlinearities Present in Electrohydraulic Control Valves," by J. Zaborszky and H. J. Harrington, *Trans. AIEE*, Paper No. 57-107, 1957.

13 "Generalized Charts of the Effects of Nonlinearities in Electrohydraulic Control Valves," by J. Zaborszky and H. J. Harrington, *Trans. AIEE*, Paper No. 57-108, 1957.

14 "A Describing Function for the Multiple Nonlinearities Present in Two Stage Electrohydraulic Control Valves," by J. Zaborszky and H. J. Harrington, AIEE Paper No. 57-779, 1957.

APPENDIX

A circuit diagram is shown in Fig. 12. The amplifier marked "special" has its feedback resistor disconnected and therefore has a very high gain. The "external" above the servo indicates that the linear follow-up potentiometer has been disconnected. The feedback path is therefore through the servo and cosine potentiometer. The servomotor therefore assumes a position, an angular position proportional to $\cos^{-1}\left(1 - \frac{x + x_0}{R}\right)$. The remainder of the circuit is self-explanatory.

Discussion

C. P. Moore.[3] The author illustrates very well the power of combined analog simulation and limited testing. The fact that an analog computer can be used to give rapid results when one is faced with a problem involving multiple nonlinearities permits system investigations that could not be attempted by analytic means. The real disadvantage of the method appears to be the difficulty of performing a systematic examination of the analog and reporting the results in a generalized or nondimensional fashion.

It is interesting to note that in the example used by the author both of the changes made in the system reduced the degree of nonlinear operation in the servovalve. For this reason it may now be of value to re-examine the problem to see if existing linear methods may be used as a basis for design.

The change to rectangular ports, of course, gives a linear relation between valve flow area and stroke. The effect of increase in pump flow may best be examined by reference to a valve-performance curve, Fig. 13, derived from Blackburn's work.[4] In this case the pressure difference across the servomotor, P_m, is nondimensionalized by the quiescent supply pressure, P_{sq}.

It can be seen that, if the pump flow is increased, P_{sq} is also increased and for a given maximum external load the maximum value required for P_m/P_{sq} is thereby reduced. This in effect limits the amount of valve travel necessary and results in the valve operating in a more linear region.

From the author's work it appears that a value of P_m/P_{sq} of 4 would be ample to meet his static load requirements. This could be obtained if the valve had physical stops limiting its travel to $X/U = \pm 0.65$. The flow characteristics then avoid large changes in gain and have a high slope which indicates good servomotor damping. Then if this restriction to valve travel is acceptable, conventional linear methods should be adequate for design.

The writer would like to inquire if the use of an asymmetrical valve was considered in view of the difference between head and rod-end ram areas. It appears that, if the width of the rectangular valve ports supplying the rod end of the actuator could have been reduced by the ratio A_{m2}/A_{m1}, the servomotor rate as a function of valve displacement and load would then be the same for both directions of valve travel. This would further linearize servomotor operation and perhaps avoid the difference in performance shown by Figs. 7 and 9.

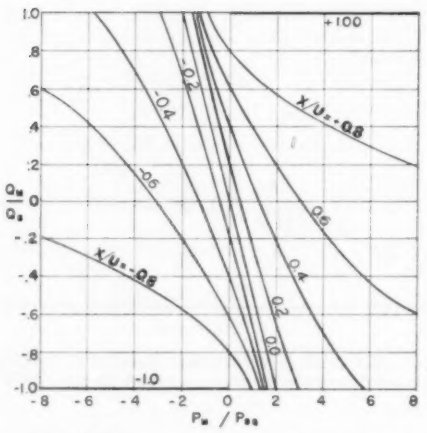

Fig. 13 Characteristics of underlapped valve operated from a constant-flow source

H. Saunders.[5] The author presents a most interesting and informative paper on practical analog-computer application. Many times, a block diagram is arranged without much thought given as to the physical interpretation behind the problem. This leads to erroneous results since the physical aspects of the problem have not been correctly expressed mathematically.

The hydraulic servo problems are very good examples of this misapplication. The hydraulic servo is essentially a nonlinear problem but owing to the application of perturbation principles, a restricted linear solution is obtained within a small finite region. With the further introduction of other nonlinearities, namely stiction, O-ring friction, and so on, the analytical version of the problem becomes extremely unwieldy. The proper application of the analog computer greatly aids in the solution of these problems. As the author states and the writer iterates, a good physical interpretation of the problem must be represented mathematically in order that one may arrive at a correct solution. From the writer's experience this has been brought out. What seems to be of a trivial nature may actually become important in nonlinear problems.

For a problem of the great amount of complexity as clearly shown by the author, the analog solution may be the only logical procedure. Although there are analytical and graphical solutions to the problem, great care must be taken to arrive at a correct solution and even then a tremendous amount of work is usually necessary. The writer appreciates the painstaking efforts of the author and would like to commend him for bringing these aspects to the attention of engineers concerned with this problem.

J. L. Shearer.[6] The author and his company are to be complimented on carrying out the kind of work reported in this paper and making its results available to fellow engineers. The system analysis carried out here with the aid of an analog computer is a

[3] Research Group Engineer, Controls and Autopilot Group, Lockheed Aircraft Corp., Marietta, Ga. Mem. ASME.

[4] "Contributions to Hydraulic Control 3, Pressure-Flow Relationships for 4-way Valves," by J. F. Blackburn, TRANS. ASME, vol. 75, 1953, pp. 1163–1170.

[5] Engineer, Stress Analysis Engineering Operation, General Electric Company, Philadelphia, Pa. Assoc. Mem. ASME.

[6] Associate Professor of Mechanical Engineering, Massachusetts Institute of Technology, Cambridge, Mass. Mem. ASME.

good example of how a thorough understanding of a problem can lead to new and better ways of solving the problem. In addition to the virtues claimed of making an analog-computer study of such a problem, the writer would like to add one more. This sort of work also leads to better communication between engineers and puts on the permanent record for all to see the results of accumulated experience which otherwise would be stored in "the experts'" heads and eventually become inaccessible because of changing interests, old age, and so on.

R. Tyler.[7] This paper illustrates the value as well as the limitations of the computer approach to stability problems. When a problem can be set up intelligently, the results interpreted with precision, and modifications of the parameters set in with imagination, then the computer solution is, without doubt, the finest way to obtain the optimum design.

The computer can best be used in the design of systems which will be applied in identical form for many units or for single systems forming an essential element of a larger system of great value. Thus considerable use has been made of this type of analysis for designing ordnance equipment, aircraft and missile systems, and for systems associated with large, costly projects such as atomic power stations. It is therefore of great value to hear of an application to a problem of general commercial interest. No doubt there will be a considerable number of other problems which will be most conveniently handled on analog computers.

[7] The Oilgear Company, Milwaukee, Wis.

However, the typical hydraulic circuits used in industrial applications are those which are designed for one or a few units. These sometimes fall into a class which, although each application may vary greatly from another, is sufficiently similar that a computer setup will provide advance understanding, allowing a confident approach on the intuitive basis with little actual experience. Such a setup was valuable in the early studies of the hydraulic feedback system described in a paper by R. E. Davis and N. Nitka.[8]

It is quite surprising that the author's analysis required no provision for such discontinuous effects as Coulomb friction and backlash in the mechanical linkages. Our experience has been that even the very slight "stick-slip" effect to be found in well-made valves and linkages often is a major factor in affecting system performance. While computer elements are available for the simulation of these effects, it is very difficult to evaluate the quantities in the actual setup and thus to relate the computer solution to the actual equipment. The close correspondence between the results of the computer solution and the vehicle performance in the example seems to be proof of the excellent fitting of the components. However, backlash is a factor which increases with use and consideration of its effect should be included.

It is to be hoped that this paper will stimulate reports of other applications of the analog computer to problems in the use of fluid power on industrial equipment.

[8] "Methods for Measuring the Performance of Precision Hydraulic Drives," by R. E. Davis and N. Nitka, *Proceedings of the National Conference on Industrial Hydraulics*, vol. 9, 1955, pp. 74–82.

An Index of Cavitation Erosion by Means of Radioisotopes

By S. L. KERR[1] and KJELL ROSENBERG[2]

Introduction

While much has been written about cavitation and its effect on the performance of hydraulic turbines and pumps, the damage caused by it—cavitation erosion—is usually the manifestation that gives the most concern to the operating staff.

The relative resistance of materials of construction has been explored in a number of research investigations both in the United States and elsewhere.

The magnetostriction method (1–4),[3] used initially on a large scale in 1935, sometimes called the vibratory method, has now become a standardized means (5) for evaluating various metals.

The correlation of experimental work with field experience, however, is the subject of much speculation. The areas where cavitation erosion is experienced in the field can often be identified from laboratory tests.

Protective means, such as prewelding critical areas in the shop with wear-resistant materials, has been employed with great success in a number of cases. The repairing of previously unprotected areas using highly resistant metals has also been effective in reducing subsequent cavitation erosion.

To relate laboratory tests to the actual operation of hydraulic turbines in the field, many factors must be considered:

1 Plant-cavitation factor or sigma (σ).
2 Loading of the units.
3 Accuracy of step up of the main unit from the laboratory model.
4 Variation in conditions between original design of the plant including changes in headwater and tailwater levels.

Few of these factors are under the control of the turbine manufacturer, although he is expected to produce an erosion-free unit in any case.

Economic Studies

While the manufacturer has presumably delivered a unit that, within the design limits for cavitation, fulfills its guarantees as to capacity and efficiency, there can be no assurance that the unit will be operated in this range exclusively.

Additional kilowatthours of energy at times of excess flow, more kilowatts of capacity for short-term peak loads or long periods of excess demand are attractive to the operating organizations.

To gain thousands of dollars of revenue by overloading a hydroelectric unit may show an economic advantage, even though expensive repairs and service outages may result.

The balance between operation at points beyond the rated or optimum point on a given turbine and the added maintenance cost is difficult to resolve when the rates of cavitation erosion for increasing overloads or unfavorable draft-head conditions cannot be established.

There is usually some load on most units below which little or no cavitation erosion takes place. Cavitation may cause extensive damage at or below the best efficiency point, or at the rated output of the turbine.

The amount of damage to the runners usually increases rapidly beyond the best efficiency point. The wicket gates, throat rings, and draft-tube liners of propeller and Kaplan turbines, may also show severe erosion from cavitation.

Field Evaluations

In the absence of some quantitative means of evaluating cavitation erosion rapidly, the loss of metal over fixed periods of time, such as six months, one year, or even longer, has been used as a criterion.

The length of time to accumulate such information, and the difficulties of accurate measurements of amount of material eroded has made such a procedure undesirable for economic studies.

A correlation between laboratory and field measurements was reported recently by Knapp (6), where aluminum test plates were attached to the critical areas of a turbine runner.

By running the turbine for periods of 5 to 20 min at a fixed gate opening, shutting down and removing the test plates, examining them, an index of intensity of "pits per second per square inch" was obtained.

Comparison with laboratory experiments under controlled conditions provided a basis of correlation.

Vamma Plant Experiments

A problem concerning an economic balance between output and cavitation erosion existed at the Vamma Hydroelectric Plant in Norway. A summary of the experiments was reported by one of the authors (7).

A more detailed report on this field test is now available and is described in this paper.

Description of Plant and Units. The Vamma plant in Southeast Norway on the Glomma River is connected to the East Norway Transmission Grid System. The plant now has ten units installed totaling 104,000 kw.

All units are of the horizontal-shaft double-runner type, with a central draft chest, Fig. 1. The eight older units installed from 1915 onward have shown considerable loss of metal on the runners, reaching as much as 55 lb (25 kg) per runner per year, Fig. 2. The static draft head on these original units is 18 ft (5.5 m), while the two newer units have only 14.1 ft (4.3 m). On these later units practically no erosion has been experienced in operation at full load after 11 years.

All runner blades are of normal carbon-content plate steel. The water is clear, free from silt and sand, and neutral in character. There is no evidence of chemical action on the runners or other parts of the turbines.

The characteristics of unit No. 4, on which tests were made, are given in Tables 1 and 2.

Unit No. 4 had been rewelded about $2^1/_2$ years previously, and

[1] Consulting Engineer, Flourtown, Pa. Fellow ASME.
[2] Technical Secretary, A/S Hafslund, Sarpsborg, Norway.
[3] Numbers in parentheses refer to the Bibliography at the end of the paper.

Contributed by the Hydraulic Division and presented at the Annual Meeting, New York, N. Y., December 1–6, 1957, of The American Society of Mechanical Engineers.
Note: Statements and opinions advanced in papers are to be understood as individual expressions of their authors and not those of the Society. Manuscript received at ASME Headquarters, July 17, 1957. Paper No. 57—A-64.

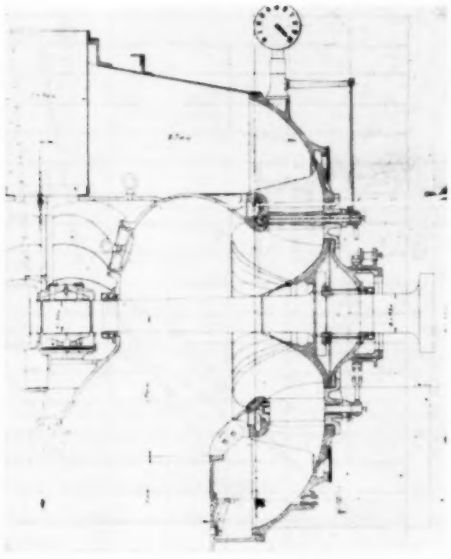

Fig. 1 Cross section of Unit No. 4

Table 1

	Design	Test
Head	85.3 ft (26 m)	88.6 ft (27 m)
Speed, rpm	214	214
Rated capacity, hp	12000	12700
Capacity per runner, hp	6000	6350
Quantity total	.....	1440 cfs (40.8 cu m/sec)
Quantity per runner	.....	720 cfs (20.4 cu m/sec)
Draft head to center-line of runner	18.1 ft (5.5 m)	17.1 ft (5.2 m)
Plant sigma	0.184	0.188
Diameter of runner	5.83 ft (1.78 m)	.....
Specific speed per runner	64.5 (287 metric)	.....
Barometer (mercury)	.....	30.0 in. (760 mm)
Water temperature	.....	39.2 F (+4 C)

Table 2 Characteristics of Unit No. 4 at 88.6 ft (27.0 m) existing during erosion-loss tests

Gate opening, mm	Generator output, kw	Quantity, cfs	Estimated combined efficiency, per cent	Axial velocity, fps
46	3950	...	...	...
62	5600	957	78.3	17.9
78[a]	7450	1192	83.5	22.3
94	8350	1304	85.5	24.4
110	8950	1421	84.0	26.6
123	9300	1510	82.3	28.3

[a] Calibrating and reference output.

the runner blades showed substantial loss of material in the usual location on the outflow side.

Cavitation-Erosion Tests. A novel test using radioisotopes was planned in co-operation with the Isotope Department of the Joint Establishment for Nuclear Energy Research. A brief description has been published of the preliminary tests (8) March 18, 1955. The more complete tests described in this paper were made December 8, 1955.

By means of radioisotopes, it is possible to detect and trace exceedingly small amounts of materials.

Fig. 2 Runner of Unit No. 4 showing cavitation erosion and location of radioactive coating (dark spots)

If a runner or part of a runner itself could be made radioactive, a direct measure of the material loss could be secured. This proposal was not feasible due to the large dimensions of the runners at Vamma.

It was decided to use an insoluble radioactive coating on the areas of the runner blades showing erosion from cavitation, Fig. 2.

Two methods of measuring the loss in radioactivity were studied:

1 Measuring the radioactivity of the water discharged by the unit. This would require large amounts of material and complicated procedures.

2 Measuring the radioactivity of the runner itself at periodic intervals.

The latter method was used, as the radioactivity could be measured between each test run from outside the turbine draft chest, the difference between two successive measurements giving the loss for the run.

Radioactive Coating. The radioactive paint was prepared using 5 grams of radioactive arsenic (As 76) with a total activity of 750 mC added to 200 grams of specially prepared coating material. This was a cement of Manila copal dissolved in alcohol and turpentine. A red toluidine pigment plus chrome yellow was added, with powdered dolomite and talcum as an extender, plus about 5 per cent of resinous oil.

To reduce the risk of harmful radiation to the personnel, the paint was applied to the runner by means of a brush attached to a handle 5 ft long. The painter stood outside the turbine draft chest and worked through the manhole, Fig. 1.

The paint was applied in small spots in the center of the eroded areas of about one half of the blades. Two coats were used, the first coat drying in 4 hr and the second in 12 hr. About 40 per cent of the paint mixture was used giving a calculated total activity of 300 mC.

All work with radioactive paint was under the control of the Norwegian "Radiologisk-Fysiske Laboratorium" to safeguard the health of the workmen. Film-dosimeters showed the tolerances for this type of work were not exceeded.

Test Procedure. The tests were carried out the day following the painting of the runner. A scintillation counter (Super Scintillator, Model 115B, Precision Radiation Instruments, Inc.) was placed outside the draft chest on the manhole cover.

Before and after each run, measurements of radiation were taken. During the readings, the turbine-guide vanes were tightly closed, the draft chest vented so the runner was rotating in air,

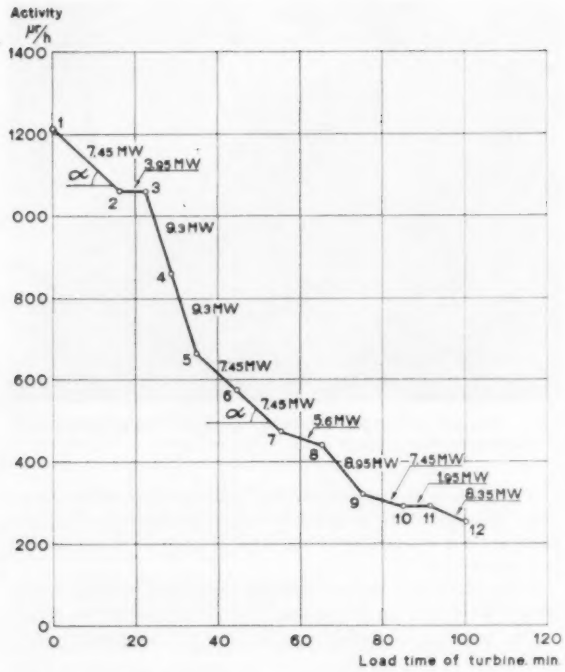

Fig. 3 Residual radiation versus turbine operating time

Table 3 Radioactivity results versus time of operation

Run	Operating time, min Incremental	Operating time, min Summation	Corrected activity; μr/h
1	0	0	1212
2	16.2	16.2	1060
3	6.4	22.6	1059
4	6.0	28.6	857
5	6.3	34.9	664
6	9.8	44.7	573
7	10.5	55.2	471
8	10.5	65.7	438
9	9.5	75.2	320
10	9.8	85.0	291
11	6.5	91.5	291
12	8.8	100.3	252

driven by the generator acting as a synchronous motor. In this way, the errors due to absorption of radiation by the flowing water were eliminated while taking the readings of radioactivity.

Readings of head, generator output, speed, gate opening, and duration of runs were made at various loads. The gate opening was held at a fixed position for each run.

Calibrating and reference runs at a given gate opening were used at the beginning of the test, as well as at several intervals during the test.

Results. Table 3 gives the results of the corrected readings of radioactivity for each measurement. The half-life of the isotope (As 76) is 26.8 hr and was used in correcting the actual readings. Fig. 3 gives the plotting of this information with respect to operating time on load. The corresponding unit output in megawatts is also shown.

It will be noted that the slope of radioactivity versus time is an index of the rate of erosion.

The calibrating load of 7450 kw (78 mm gate opening) showed a constant slope for runs 1–2, 5–6, and 6–7, while run 9–10 showed

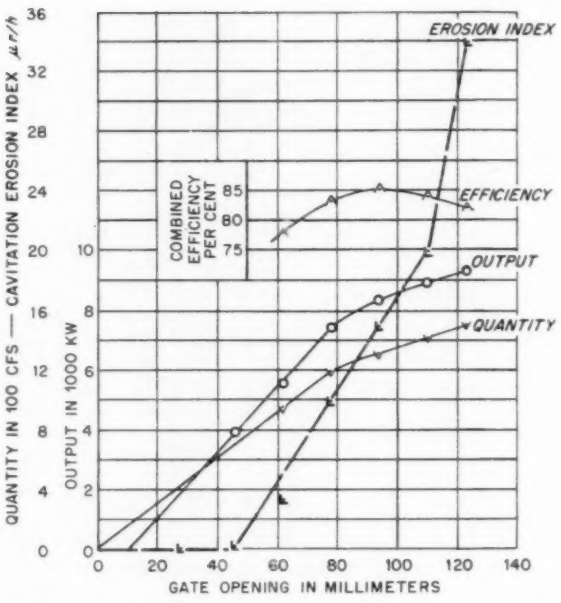

Fig. 4 Turbine characteristics and radiation losses versus gate opening

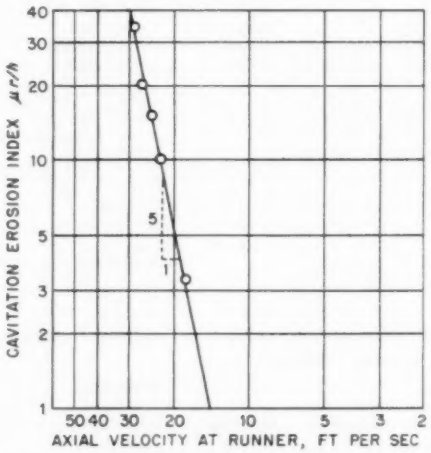

Fig. 5 Erosion index versus axial velocity through runner throat

a lesser slope. Corrections were made to the previous run 8–9 and subsequent runs as noted.

Interpretation of Tests. While the tests were not as extensive as might be desired, they did show the variation in erosion index with respect to turbine output. Fig. 4 superimposes this index on the turbine characteristics.

Computing the axial velocities of flow as well as estimating the relative velocities, the erosion index can be plotted to show the rate at which erosion varies. Fig. 5 shows this relationship computed as the slope of the loss versus velocity curve or the exponent of the velocity of flow.

Taking the five highest rates of erosion, the slope of the line closely approximates Loss $= f(V)^8$. The incremental computation for the two highest points shows a greater slope and the exponent can be increased to some extent with 8 as a limiting

Table 4 Erosion index results

Turbine operating run	Unit output, kw	Effective radioactive factor, tan α	Observed loss of activity per min, $\mu r/h$	Corrected loss of material, $\mu r/h$	Per cent of maximum rate
1–2[a]	7450	0.94	9.4	10.0	29.3
2–3	3950	0.94	0.2	0.2	0.6
3–4	9300	0.94	32.1	34.1	100.0
4–5	9300	0.94	32.1	34.1	100.0
5–6[a]	7450	0.94	9.4	10.0	29.3
6–7[a]	7450	0.94	9.4	10.0	29.3
7–8	5600	0.94	3.1	3.3	9.7
8–9	8950	0.62	12.4	20.0	58.7
9–10[a]	7450	0.30	3.0	10.0	29.3
10–11	1950	0.30	0.0	0.0	0.0
11–12	8350	0.30	4.5	15.0	44.0

[a] Calibrating and reference output.

value. It is interesting to observe that little or no loss of radiation occurs at loads below 4000 kw, or a computed axial velocity of about 13 fps.

This may have two separate interpretations:

1 The magnitude of cavitation is not sufficiently large to cause damage.

2 The "incubation" level or initial resistance of runner material has not been reached. This is evident in many vibratory tests (1).

It is probable that both these factors are present. The first seems to have greater influence in this investigation as the radioactive cement does not have any initial resistance to erosion as would metals.

Conclusions

It is possible to convert the experimental results into a relative scale as shown in Fig. 6. The wear is plotted against unit output in megawatts, but the scale for wear is set up as a percentage of the rate of radiation loss at full-gate output.

Limiting the output to the nominal rating of approximately 9000 kw should result in only 60 per cent of the damage. Thus a $3^1/_2$ per cent reduction in power decreases the cavitation erosion by 40 per cent.

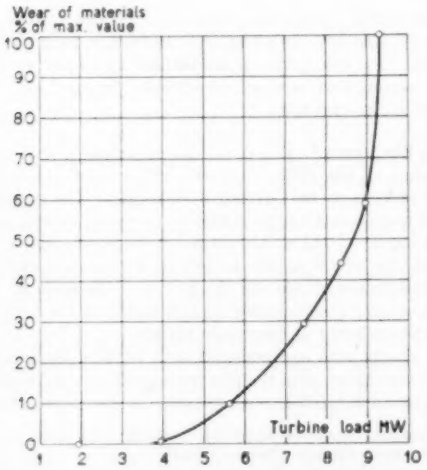

Fig. 6 Erosion index versus turbine output

By limiting the output to the point of maximum efficiency, approximately 8300 kw, the erosion should be about 40 per cent of that at full gate.

Where units have been operating at full output for a sufficient period of time to establish actual weight-loss information, then cost studies can be made from diagrams like Fig. 6.

Each plant will have its own relationship of cavitation erosion versus load and the size, method of operation, and value of power will determine the economics.

The ease with which the experiments can be carried out makes this radioactive-isotope method applicable to many installations, even in the initial operating stages.

Additional determinations can provide a more reliable basis for evaluating erosion losses due to cavitation.

The use of the method in cavitation laboratory tests of model turbines, correlated to field tests of the same runner, may provide a means of predicting the potential damage to runners in advance of construction.

Acknowledgments

Through the co-operation of the ASME Committee on Cavitation, and the willingness of Mr. Rosenberg to make available the information on the experiments at Vamma, it has been possible to present this most interesting investigation to the Society.

Bibliography

1 "Determination of the Relative Resistance to Cavitation Erosion by the Vibratory Method," by S. L. Kerr, TRANS. ASME, vol. 59, 1937, pp. 373–397.

2 "Resistance to Cavitation Erosion," by R. Beeching, *Journal of the Institution of Engineers and Shipbuilders in Scotland*, vol. 85, 1942, pp. 210–276. "The Resistance to Cavitation Erosion of Propeller Alloys," ibid., 1946.

3 "Werkstoffzerstorung durch Kavitation," by H. Nowotny, VDI-Verlag GMBH, Berlin, Germany, 1942, republished from original plates by J. W. Edwards, Ann Arbor, Mich., 1946.

4 "Accelerated-Cavitation Research," by W. J. Rheingans, TRANS. ASME, vol. 72, 1950, pp. 705–724.

5 "Progress Report on Standardization of the Vibratory-Cavitation Test," by L. E. Robinson, B. A. Holmes, and W. C. Leith, TRANS. ASME, vol. 80, 1958, pp. 103–107.

6 "Accelerated Field Tests of Cavitation Intensity," by R. T. Knapp, TRANS. ASME, vol. 80, 1958, pp. 91–102.

7 "Wear of Francis Turbines Due to Cavitation Effects During Operation by Means of Radioisotopes," by Kjell Rosenberg, Fifth World Power Conference, Vienna, Austria, 1956, Paper 192H/44.

8 "Some Industrial Uses of Radio Isotopes in Norway," by U. Been and E. Saeland, U. N. International Conference on the Peaceful Uses of Atomic Energy, Geneva, Switzerland, 1955.

Discussion

J. Desbaillets.[4] A clear understanding of the laws of cause and effect which rule cavitation and pitting will only be achieved by quantitative measurement, sufficiently accurate, of field erosion under controlled operating conditions (load, plant sigma, specific speed, temperature, and so on).

The radioactive method described in this excellent paper has the attractive merit of making possible an accelerated measure of the rate of erosion in the field with relatively simple equipment, and the results obtained at Vamma are extremely encouraging. It is interesting to note that the rate of erosion measured appears as an exponential function of the velocity whose exponent is practically the same as found by Robert Knapp with entirely different methods of investigation.

The characteristics of the runner metal and the isotope used introduce many variables such as relative incubation level, and resistance to pitting, to corrosion, and to kinetic erosion. These variables permit only comparative results to be obtained.

Calibration in the field of the radioactivity counter to read directly in units of mass of metal removed by cavitation is far from practical. Absolute figures converted into dollars and cents would be the only way to determine the most economical mode of operation for a given turbine. However, operators are not Sunday drivers and we are inclined to believe that there will be few cases where they will find it desirable to cut back the power of the turbine rather than incur the expense of repairing cavitation damage.

For comparative analysis, the radioactive method has a large field of application. One use which suggests itself is to test local changes on individual blades of a runner which start to give trouble in the field, so that a rapid evaluation of the necessary correction may be made. Obviously, the radioactive method also can be applied to model tests in the laboratory where control of hydraulic characteristics and modification of blade shape are more widely and readily achieved.

Finally, this method can be used advantageously to analyze the fundamental principle of the pitting of metals and the relative influence of such factors as velocity, corrosion, temperature, and so forth, especially if the isotope coating can be replaced by making radioactive the base metal itself.

In spite of the complications involved in handling harmful isotopes, the radioactive method used at Vamma is undoubtedly a most valuable instrument for cavitation research.

R. G. Folsom.[5] Engineering developments in research frequently require a correlation of laboratory experimental work with field experience. This approach is a very important problem in the hydraulic-engineering field and it is all too frequent that we find tests on full-scale field equipment are not complete enough to provide a correlation and understanding of results with laboratory-obtained values. The authors are to be congratulated on providing more information on this important subject and particularly for their use of radioisotopes to aid in obtaining the information sought.

It is recognized that this is the first approach to the problem of cavitation-erosion studies through the use of radioisotopes. On the other hand, it should be pointed out that there is a basic assumption that the cavitation erosion of paint is the same as the cavitation erosion of propeller-blade metal. The paper assumes that the cavitation erosion of paint provides results which may be applied for prediction of cavitation erosion in the field condition. It would be of help for an evaluation of the results presented here, as well as the basis of future research, if the authors were to provide a brief explanation and any data that might be available to support this assumption.

The paper presents an excellent step forward in the development of the study of cavitation erosion. The writer would be interested in the authors' evaluation of the desirability and the practicability of using welding materials normally applied for cavitation-damage repair, containing appropriate isotopes for direct full-scale measurement of cavitation erosion.

W. C. Leith.[6] The application of radioisotopes to determine an index of cavitation erosion appears very desirable, especially if periodic measurement of the radioactivity of a turbine runner could be correlated to an estimated metal loss per year. Perhaps the maximum depth of pits and the total eroded area could be established by a mapping procedure, so that the operating staff could forecast a shutdown for welding repair based either on the complete perforation of a small critical area or on the total estimated weight loss for the runner.

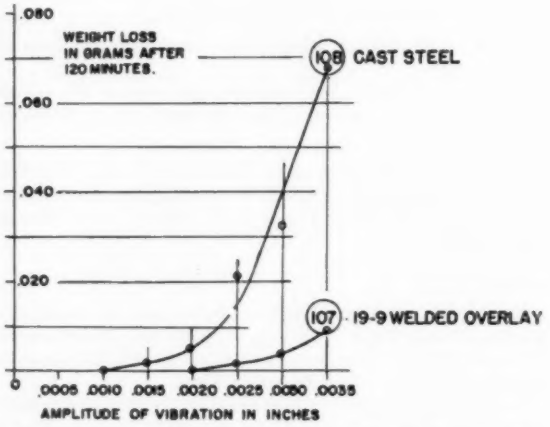

Fig. 7 Accelerated cavitation damage—the effect of amplitude

Fig. 6, which relates the erosion index to the turbine output, can be compared to the effect of amplitude in magnetostriction tests Fig. 7, in which there is an incubation period with no apparent erosion, and then an asymptotic increase in the erosion intensity of the cast steel.

W. J. Rheingans.[7] This paper is very timely in that it follows the theme of the 1957 Cavitation Symposium; namely, the "Effect of Velocity on Cavitation Damage." The authors show that the erosion loss due to cavitation increases approximately as the 5th power of the axial velocity through the runner throat. This velocity varies nearly directly as the relative velocity between the runner blades and the flow, and therefore we can say that the erosion loss increases approximately as the 5th power of the relative velocity at the runner blades.

This checks with experimental data by Robert Knapp. He reports[8] how he counted the pits per second per square inch on a test specimen subjected to a constant size cavitation zone under

[4] Research Engineer, Product and Market Planning, Hydraulic Division, Dominion Engineering Company, Ltd., Montreal, Canada.

[5] President, Rensselaer Polytechnic Institute, Troy, N. Y.; formerly, Director, Engineering Research Institute, The University of Michigan, Ann Arbor, Mich. Fellow ASME.

[6] Mechanical Research Engineer, Dominion Engineering Works, Ltd., Montreal, Canada. Mem. ASME.

[7] Manager, Hydraulic Department, Allis-Chalmers Manufacturing Company, Milwaukee, Wis. Mem. ASME.

[8] R. T. Knapp, "Recent Investigations of the Mechanics of Cavitation and Cavitation Damage," TRANS. ASME, vol. 77, 1955, pp. 1045–1054.

various flow velocities. He found that the number of pits per second per square inch increased as the 6th power of the velocity.

The importance of such a relation between velocity and rate of erosion due to cavitation cannot be overemphasized. As the authors show in Fig. 6, a small change in output can mean an extremely large change in the erosion rate. This should be of considerable interest to the operators of hydraulic turbines.

The authors are to be complimented upon having shown us that the determination of the rate of erosion is not a difficult or costly procedure. It is hoped that operating companies will be interested enough in facts of this nature to conduct similar tests on some of their own installations.

Authors' Closure

The authors appreciate greatly the favorable comments of the discussers and their suggestions that this radioisotope index procedure be used for laboratory tests and for full-scale plants in the United States and Canada.

Since several discussers deal with the same questions, the principal items will be reviewed as follows:

1 Dr. Folsom, Mr. Desbaillets, and Mr. Leith have all suggested the use of radioactive parent metal or radioactive metallic overlays. This procedure, however, would introduce a severe safety hazard in transporting the radioactive metal, applying it, and having to live with it over a long period of time.

With substantial amounts of radioactive metal present, the effect of "background radiation" would tend to introduce errors of measurement. The method described in the paper uses *differences* in radioactivity. These differences must be substantial to permit accurate determinations of "rate of loss" of radioactivity.

By selecting an isotope such as Arsenic 76 with a relatively short "half-life" (about 27 hours), the hazard to health of station operating personnel is reduced to a minimum. On the other hand, if the parent metal or overlay is made radioactive, the half-life must be extended to a matter of weeks or months.

The index requires sufficiently large incremental reductions in total radioactivity to secure accurate rates of loss. This can be obtained by a lacquer applied to the affected areas alone. The radioisotope As 76 becomes harmless in a short period, removing in a few days any residual hazard.

2 Mr. Desbaillets and Mr. Leith both suggest "controlled operation" of generating units. This is interpreted to mean that outputs, head, plant sigma, etc., would be held constant to secure a fixed condition under which to measure the loss of metal due to cavitation erosion. In the case of the Vamma turbines this is essentially the way they are operated, namely, at full load. The amount of welding metal has been established from actual experience, both with ordinary carbon steel and with stainless steel. The index at Vamma is therefore just such a relationship as suggested.

If existing plants in the United States and Canada, having extended statistical records of operating data with repair costs and outage times, could now be tested by the authors' procedure, a number of additional points on an experience curve could be obtained.

It might be noted that the cost of repairs alone will not be the important factor. Outage time during repair periods and the consequent loss of output may far outweigh all other considerations.

3 Mr. Leith's reference to "incubation time" should possibly refer only to extended exposure at a constant amplitude of vibration with the magnetostriction technique and not to variable amplitudes.

His comparison in Fig. 7 of damage versus amplitude as compared with the radioisotope index seems valid however. If the cavitation intensity is negligible, there would be no erosion. As the intensity of cavitation increases, damage increases.

Within the cavitation zone, if the unit is held at a fixed gate opening, "incubation" will develop into active erosion, the rate of which is affected by the intensity of cavitation and the relative resistance of the material itself.

By comparing information such as found in Fig. 7 with data from index determinations on operating units, perhaps the long sought correlation between laboratory and field can be secured.

4 Mr. Desbaillets and Mr. Rheingans comment on the effect of velocity on cavitation erosion rates. Fig. 8 in this closure has been prepared by plotting on logarithmic scales the data in Fig. 5 of this paper on the same sheet with data (Fig. 11) from Dr. Knapp's paper (footnote 8 in the discussion). The pits per sq in. per sec index of Dr. Knapp has been used.

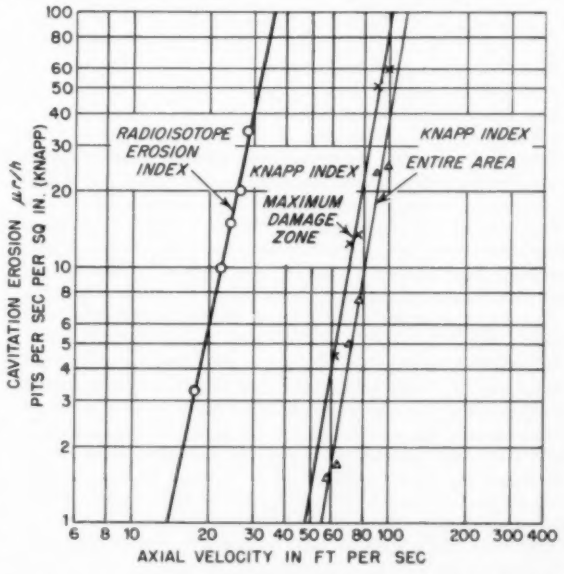

Fig. 8 Comparison of radioisotope cavitation erosion index with R. T. Knapp index

The slope of the radioisotope index is generally 5. If the upper four points only are used, a slope of 5.8 can be obtained. If only the upper two points are used, the slope reaches 8.

The Knapp index points have more scatter than do the foregoing. Slopes ranging from 5.6 to 6.3 can be secured, depending on how the line is drawn and the points evaluated.

The agreement between the two techniques is thus even closer than previously stated.

5 The question as to whether the rapid erosion of a radioactive lacquer is comparable to the erosion of the runner material itself can always be debated.

It should be pointed out, however, that the radioisotope index is a rate of loss and so is not dependent on actual loss. A very short time of exposure of a low resistant material like the radioactive lacquer probably has somewhat the same relative value as compared to a long term exposure of a highly resistant material.

In the magnetostriction apparatus, "relative resistance" scales have been established with exposures of one or two hours which compare favorably with exposures of 16 to 100 hours in a Venturi apparatus and with months of exposure of full scale turbines.

A similar situation would appear to exist between the minutes required to establish the radioisotope index and the months and years needed to produce erosion of the turbine runners themselves.

The matter is further commented on by Mr. Rosenberg as follows:

"There are, however, good reasons to assume that the curve arrived at in Fig. 6 gives a correct picture of the relative loss of steel from the runner. Experimental tests and practical experience seem to show that all materials, irrespective of the quality, are attacked when exposed to cavitation. This must be interpreted so that the forces which appear when the bubbles implode are powerful enough to wear away even the most resistant material sooner or later. The process may be hastened by simultaneous chemical reaction, but the mechanical causes must always be present and start the process of erosion.

"By means of experimental investigations it has also been possible to establish that material loss as a function of the time for various test objects usually shows the same course of process in cavitation apparatus of quite different construction. This result is very interesting, as the intensity of cavitation probably varies from one apparatus to another. Practical experience at Vamma Power Plant also indicates that the intensity of cavitation for the major part is strong enough to wear away normal carbon steel as well as stainless steel, which for repair is welded on the runner blades as a protective overlay. The cavitation zone seems to be the same, independent of the steel quality; only the rate of damage is influenced by the relative resistance of materials.

"Even if there is an intensity threshold of cavitation, below which steel is not exposed to damage, it seems in our case as if most of the cavitation spectrum lies above this threshold value."

Cavitation and Nuclei

By ROBERT T. KNAPP,[1] PASADENA, CALIF.

Contrary to the general impression, water and other common liquids, when pure, have high tensile strength. Cavitation would be impossible at the highest velocities currently encountered. In practice all liquids appear to cavitate as soon as the pressure tends to drop below the vapor pressure, thus implying that liquids have no tensile strength. This discrepancy is explained by the presence of "weak spots" whose characteristics have as yet only been inferred.

This paper presents the results of an experimental investigation of the weak spots present in ordinary water. The results are consistent with the model of the nucleus proposed by Harvey, but are apparently inconsistent with other models currently found in the literature.

After summarizing the results of the experimental program, the paper concludes with a series of implications concerning the engineering significance of the nuclei in industrial liquids.

An experimental knowledge of the property of liquids is universal. From the day of our birth we bathe in liquids, drink liquids, see uncounted numbers of liquid droplets fall as rain, even our own bodies consist largely of liquids. Hence every young scientist or engineer starts his education with a good empirical knowledge of the properties of liquids. Since this knowledge is built up of so many unrelated experiences, it is apt to be present more often as an intuitive feeling rather than as an explicit collection of facts. This intuition generally colors our approach to technical problems related to liquids, and the problem of cavitation is certainly no exception.

The formation of a cavity in a liquid obviously involves a rupture of the liquid, but intuition says that a liquid has no rupture strength as it is always spilling, splashing and bouncing around, dividing and recombining, with little or no apparent application of force. Thus obviously a liquid will rupture and form a cavity at any place within the liquid at which an infinitesimal tension develops. Unfortunately, there are occasional natural examples which cast a shadow on this intuitive feeling that liquids cannot withstand any tensile stress. Trees draw sap up from the ground to far greater heights than can be explained unless the sap can withstand a tension. Technical individuals who work intimately with the cavitation process sooner or later encounter cases which can be understood only on the basis that the liquid is able to withstand a tension, at least for a short time.

It is of practical importance to designers and users of hydraulic equipment to have a clear knowledge of all physical properties of liquids that may affect the cavitation process. Obviously the cavitation-free zones of operation could be greatly extended if liquids could be made to stand appreciable tensions. Unfortunately, our present experience indicates that it is not feasible to do this, at least for aqueous liquids. On the other hand, there is some indirect evidence to show that even natural waters may vary significantly in their ability to withstand momentary tensions. These variations may occur between water derived from different sources, or the same water supply may have different properties at different times of the year. Another field in which knowledge of these physical characteristics of the liquid is important is in model testing of the cavitation characteristics of hydraulic equipment, such as pumps and turbines. These are some of the motivating facts for the investigations which will be discussed.

To understand the nature of these investigations, it is necessary to review some of the known physical facts about the effective tensile strength of liquids. Based on their physical structure, liquids should have very high tensile strengths—of the order of tens or hundreds of thousands of pounds per square inch. If real liquids actually exhibited such strengths, cavitation would be unknown. However, it is common experience that ordinary liquids usually cavitate whenever the local pressure reaches the vapor pressure. Since this is the point at which there is no longer an external force to hold the liquid together, it shows that these liquids have no effective tensile strength. The obvious explanation of this great discrepancy is that ordinary liquids always contain impurities which produce weak spots that rupture or tear at vanishingly small tensions, thus producing cavities. Liquids may contain many types of impurities, only a few of which could be expected to produce weak spots. Since the weak spots are physical in nature, it would appear that the physical characteristics of the impurities would be of prime importance.

The physical state of dissolved impurity is quite different from the undissolved one. The theory of solutions indicates that a dissolved impurity should have very little effect on the tensile strength of the base liquid and thus this class of impurities can be eliminated from consideration. This leaves undissolved solids, immiscible liquids, and free gas as the possible sources of weak spots in ordinary liquids. With undissolved solids and immiscible liquids, the interface between the impurity and the base liquid is a potential source of the weak spot since the tensile strength of the impurities is of a higher order of magnitude. Immiscible liquids do not appear to be a primary source of weak spots. In the first place, they are not universally present in common liquids. In the second place, experiments performed by Weyl and Marboe (12)[2] demonstrated that the interface between immiscible liquids is not weak enough to explain the observed lack of effective tensile strength of normal liquids.

The tensile strength of the interface between a solid impurity and the liquid depends upon the degree of wetting of the solid by the liquid. There is ample experimental evidence to show that with a high degree of wetting the adhesive force across the interface is very high, and even for a low degree of wetting it is probably higher than the effective tensile strengths observed in normal liquids. This reasoning reduces the range of impurities responsible for the weak spots in liquids to undissolved gases, and unwetted, that is, hydrophobic solids.

In considering the probability that either of these two types of impurities is responsible for the weak spots in ordinary liquids, another experimental fact must be considered. Clear water, or even commercial distilled water, cavitates with very little, if any, sign of tensile strength. This means that any undissolved impurities must exist in very tiny units. Otherwise, the liquid would appear cloudy. The effect of a tiny hydrophobic solid particle on the tensile strength of a liquid is not too clear. Among other things, it would depend upon the size and shape of the particle.

[1] Professor of Hydraulic Engineering, California Institute of Technology. Mem. ASME.

Contributed by the Hydraulic Division and presented at the Annual Meeting, New York, N. Y., December 1–6, 1957, of The American Society of Mechanical Engineers.

Note: Statements and opinions advanced in papers are to be understood as individual expressions of their authors and not those of the Society. Manuscript received at ASME Headquarters, July 29, 1957. Paper No. 57—A-80.

[2] Numbers in parentheses refer to the Bibliography at the end of the paper.

Certainly the interfacial tension of the liquid would have to be taken into account. However, the resistance to opening a cavity at the interface would certainly be less than that in the pure liquid. Obviously, the tiny gas bubbles constitute weak spots in the liquid. For the common liquids, and especially for water, the only readily available source of gas is the atmosphere, and the atmospheric gases are relatively soluble. Thus it is difficult to explain the continuing existence of a very small free bubble in a body of liquid, since the surface tension forces should be great enough to increase the pressure within the bubble sufficiently to cause it to dissolve completely.

All of this discussion can be summed up very tersely by saying that liquids should not cavitate, but they do. Furthermore, the only acceptable explanation for the weak spots that are necessary to permit cavitation is that based on the presence of impurities. In recognition of this, these weak spots are commonly called nuclei, although their existence is still wholly inferential. One of the few tenable concepts of the construction of a nucleus is due to Harvey (8). His model of a nucleus is that it consists of a host which is a solid hydrophobic particle which has a re-entrant crack in its surface that is filled with undissolved gas. This gas is the active part of the nucleus, that is, the weak spot in the liquid. Since the particle surface is hydrophobic, the surface of the liquid will be convex toward the gas. Hence the surface tension will tend to keep the gas pressure low rather than high. Consequently, the gas will not dissolve. Harvey made some experiments which showed that this concept is consistent with the physical facts. He reasoned that such nuclei could be destroyed by applying hydrostatic pressures which, if high enough, would force the liquid up into the crack against the force of surface tension and cause the gas to dissolve, thus eliminating the weak spot. The experiments carried out by the author are elaborations of Harvey's original tests. Their objective was not only to obtain a more quantitative check upon the tenability of such a hypothetical nucleus, but also to explore in detail the characteristics of water before and after a wide variety of pressure treatments. It was hoped in this manner some light would be shed on some of the observed inconsistencies in the cavitation performance of hydraulic equipment.

The general plan of all experiments is the same: To compare the physical characteristics of unpressurized water with that of similar samples which have been pressurized. These experiments cover relatively wide ranges of intensity and duration of the pressurizing treatment. The physical characteristic investigated is the development of cavities within the body of the sample. Both static and dynamic tests were made. The static tests were of two kinds: The first was the determination of the boiling point at atmospheric pressure of a previously pressurized sample of water as compared to that of an unpressurized sample. A boiling point in excess of the equilibrium temperature at atmospheric pressure indicates that the liquid has an effective tensile strength. This tensile strength is the difference between the vapor pressure at the boiling temperature and the vapor pressure corresponding to the local atmospheric pressure. During the making of the boiling-point measurements, observations were also taken of the type of boiling and the location of the initial cavities within the body of the liquid.

In the second type of static test the previously pressurized sample was heated in a water-vapor-filled pressure-release chamber until a predetermined pressure and temperature was reached. The chamber pressure was then released at a predetermined rate until cavities appeared in the body of the sample. The effective tension required to produce the first cavity in this test was the difference between the chamber pressure at the beginning of the test and that at the appearance of the first cavity.

The dynamic test was completely different. A glass venturi tube having a large upstream reservoir section was cleaned and filled with water to be tested, and the entire assembly was then pressurized. After this treatment, the venturi was placed in special apparatus and flow was induced by sudden application of air pressure. By suitably adjusting this pressure, the pressure in the throat of the venturi could be controlled. In this manner tensions of several atmospheres could be obtained with relatively low drive pressures. In this test the cavity develops under conditions comparable to that in hydraulic equipment in general. Variations in pressure are produced by changes in the velocity of the flow.

Description of Equipment

The pressurizing chamber and auxiliary equipment is shown in Fig. 1. The pressurizing chamber is $2^1/_8$ in. ID and has a usable length of approximately 30 in. The pressure is produced by a ram in the lower end of the chamber which is driven by a low-pressure hydraulic cylinder that forms the base of the chamber. This low pressure cylinder is a part of a closed hydraulic system that includes a standard gear pump with associated control valves and reservoir. The area ratio of the low-to-high pressure piston is about 33 to 1. Thus working pressures up to 30,000 psi are obtained in the chamber from a maximum operating pressure of 1000 psi in the auxiliary system. A dial gage which measures the change in length of the high pressure cylinder is used to indicate the level of pressurization. Access to the chamber is provided by a plug with an unsupported-area seal. This plug and its holding pin can be seen on the left side of Fig. 1, sitting on top of the pressurization chamber.

Static Test Equipment. For the boiling point and pressure release tests, the water samples were contained in glass test tubes. To avoid contamination from the atmosphere between pressurizing and testing, it was found necessary to seal a glass dome to the

Fig. 1 Complete pressurizing system

top of each tube. This dome was vented to atmosphere by a short length of large-bore glass capillary tubing. The test tubes were approximately 6 in. long and $^3/_4$ in. in diam. Two versions are seen in Fig. 2. The open capillary insures that the pressure within the test tube is in equilibrium with the surrounding pressure while maintaining a small convectionless passage through which dust particles cannot pass into the body of the tube in the short time that it is exposed to the atmosphere. Fig. 3 shows the simple heating equipment used for measuring the boiling point of the liquid in these tubes. It was impossible to measure the temperature directly because any measuring instrument for such use must be chemically clean and inserted in the tube before pressurization. Only a metal thermocouple would withstand these pressures but this would be unsatisfactory because, even after vigorous cleaning, cavities form on metallic surfaces at very low liquid tensions. The temperature for the first cavities to appear is therefore estimated from the heating time. The apparatus is shielded from all air currents. Calibrations were run with thermocouples immersed in standard test tubes filled with unpressurized water. The rate of heating was determined from room temperature to boiling temperature. Similar calibrations were made with high-boiling-point liquids, thus carrying the temperature range up to the limits to be covered by the experiments. The equivalent heating times for water were calculated using the known specific heats of the calibrating liquids. Temperature measurements obtained in this manner are estimated to be accurate within less than 5 F. This is much smaller than the observed scatter between identical tests.

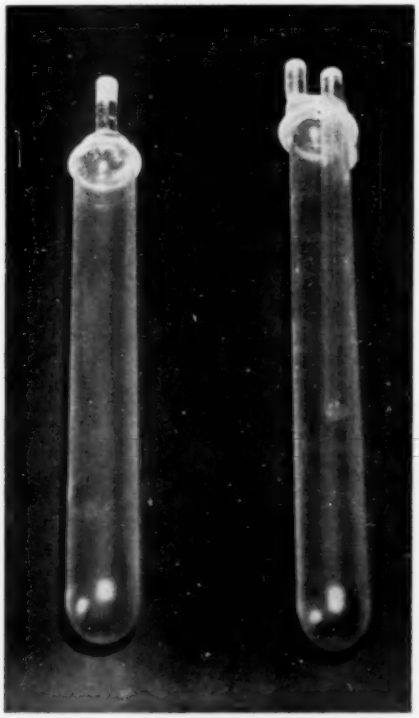

Fig. 2 Single and double capillary closed-top test tubes

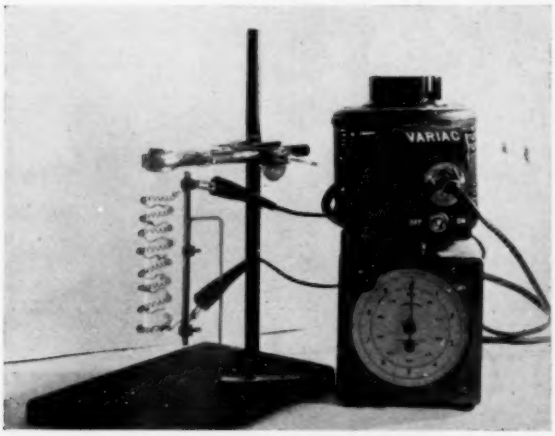

Fig. 3 Heating equipment for boiling-point test

The pressure-release chamber used in the second type of static test is seen in Fig. 4. This is a small rectangular stainless-steel chamber having heavy glass windows in two opposite faces. The chamber is heated electrically on all of the metallic faces. The operating technique was as follows: A pressurized sample in a standard test tube was suspended in the center of the chamber. A small amount of water was then added and the chamber closed. The effective tensile strength of the sample was tested by opening the control valve, thus releasing the pressure of the surrounding vapor. Observations were made of the chamber pressure at the instant at which the first bubble formed in the test tube. It was assumed that during this pressure release the temperature of the sample remained constant. Since it was in its thermoequilibrium with the heated chamber walls, the effective strength of the

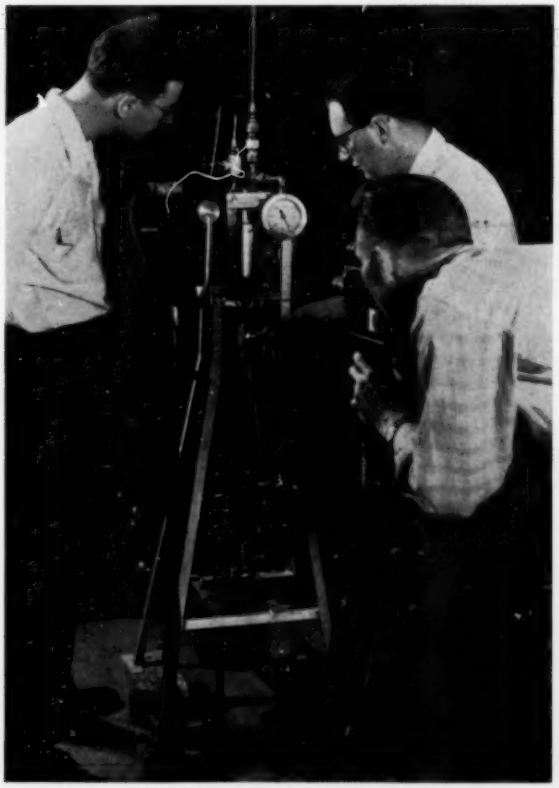

Fig. 4 Pressure-release chamber

liquid was therefore assumed to be the decrease in chamber pressure from the initial value at the instant of first-bubble formation. Two rates of pressure release were used. The fast rate was approximately 30 psi per sec. In these tests the observations were made with a motion picture camera whose field of view included both the sample and the pressure gage. In the slow release, the rate of pressure drop varied from 1 to 5 psi per sec. Here the camera was not needed since sufficient accuracy could be obtained by two observers, one watching the sample and the other the pressure gage.

Equipment for Dynamic Test. Fig. 5 shows the glass venturi tube used for this test. This tube serves as the water container, the nozzle, working section, and diffuser. Its dimensions were limited by the size of the pressurizing chamber. These tubes are of precision construction. They were made by shrinking the glass onto a stainless-steel mandrel.[3] The nozzle profile is geometrically similar to that of the High Speed Water Tunnel in the Hydrodynamics Laboratory. This insures "monotonic" pressure variations during the acceleration, with the lowest pressure occurring in the working section. A uniform velocity distribution is also obtained in the test area.

Fig. 6 shows the tube installed in the test apparatus. With it in position, the system becomes a small transient-flow water tunnel in which both the maximum velocity and the minimum pressure in the working section can be predetermined by the proper choice of the upstream drive pressure and the downstream reservoir pressure. Heating was then commenced with the control valve open. After the free water in the chamber had boiled a sufficient time to flush out all of the air with steam, the valve was closed. Continued heating caused the pressure in the chamber to rise at a relatively slow rate because of the large mass of the steel walls. During this heating cycle, the temperature of the pressurized water in the test tube lagged behind that of the surrounding stream. After the desired chamber pressure had been reached, the heat input was decreased to maintain a constant pressure for a sufficient time to insure that the temperature of the sample had reached equilibrium with that of the surrounding vapor, by the proper choice of the upstream drive pressure and the downstream reservoir pressure.

The test is started by opening a quick-acting valve between the air reservoir and the apparatus. The drive pressure builds up very rapidly, forces out the closure at the lower end of the venturi diffuser, and drives the entire pressurized sample down through the working section in the throat. The flow velocity is computed from the rate of fall of the meniscus in the constant diameter reservoir section, which forms the upper portion of the venturi tube. The pressure in the working section is determined from the calculated velocity at this point and the drive and reservoir pressures. Since both of these pressures are measured quantities, two independent calculations of working velocity can be made. They were found to agree very well. Since the length of runs was normally 1 sec or less, observations were made photographically with a high-speed motion-picture camera and Edgerton-type flash-lamp illumination. The picture-taking rate commonly used was 2000 frames per sec. This photographic record was used to de-

[3] The construction of these precision glass tubes was made possible through the interest and co-operation of Schutte and Koerting Company, and their Chief Engineer, Mr. F. Boehm.

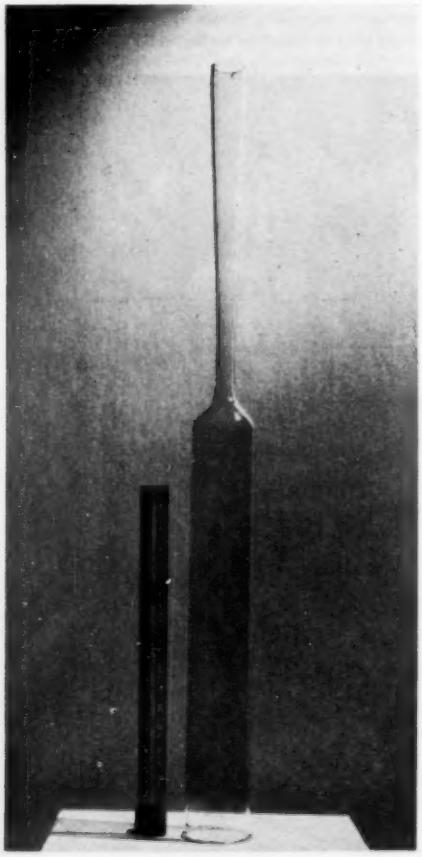

Fig. 5 Glass venturi tube

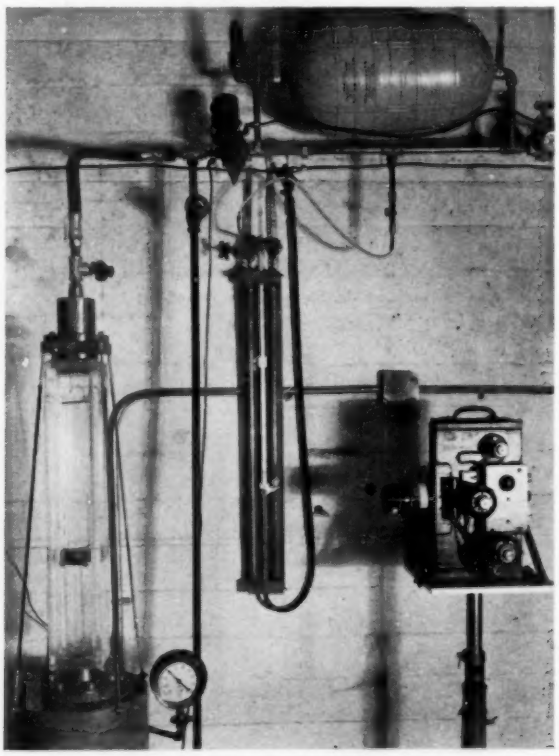

Fig. 6 Venturi-tube test system

termine both the rate of fall of the meniscus in the reservoir section and the time at which the first cavity was observed to form in the working section. Time measurements were determined very accurately by counting the number of frames on the motion pictures since the interval between frames was very precisely controlled.

Cleaning Technique. In tests of this kind if cavities originate on the surface of the container, it implies that the adhesive force between the liquid and the container surface is lower than the tensile strength of the liquid and that the latter is not being measured by the experiment. Therefore considerable time was spent in perfecting cleaning techniques which would permit the development of adhesive forces greater than the tensile stresses applied to the liquid during the tests. The techniques finally perfected proved satisfactory in that only an occasional sample was found to cavitate first at the glass-water interface. Briefly, this technique consisted in thoroughly cleaning the containers in hot chromic acid, followed by removal of the acid by copious washing with water from the same source as that to be used for the test. The significant feature of the technique appears to be that from beginning to end of the cleaning and washing process, the container surface should never be allowed to come in direct contact with the atmosphere. Whenever possible, the entire process was carried on below the surface of the liquid. Some test tubes were rejected because observation showed that in consecutive tests cavities always formed at a given spot on the surface, thus implying a fused-in impurity which could not be removed by the cleaning process.

Experimental Results

Boiling-Point Tests. In order to establish a basis of comparison of the effects of pressurization, preliminary measurements were made of the boiling point of unpressurized water using the closed top test tubes. The results were that first bubbles always appeared within a degree or two of saturation temperature for the existing barometric pressure. It was noted that these bubbles usually formed on the surface of the glass tube. Additional tests were made to try to eliminate the effect of the glass-water interface. In these tests the tubes were carefully cleaned and pressurized. They were then submerged in a bath of unpressurized water. A piece of plastic hypodermic tubing was inserted in the capillary and the pressurized water was flushed out with unpressurized tap water. Boiling-point tests with these refilled tubes gave the same results as that of the first group. The first bubbles appeared within a degree or two of the saturation temperature, but they were now observed to originate in the body of the liquid. In fact, small air bubbles were observed to appear in the body of the liquid at even lower temperatures.

The results of the boiling-point tests of pressurized water are shown in Figs. 7, 8, and 9. One general conclusion stands out immediately. Even with carefully controlled conditions, there is a very wide scatter in the test results. Some of the groups show a range of as much as 5 to 1 in the effective tensions measured under apparently identical conditions. Only a few sets of experiments show less than a 2 to 1 range. Due to the tedious nature of the experimental technique, the number of samples in each group is relatively small. It is very probable that if all of the groups had been very large, the scatter in the results would also have been uniformly large.

Fig. 7 shows the variation in the effective tensile strength of the pressurized samples as a function of the level of pressurization.

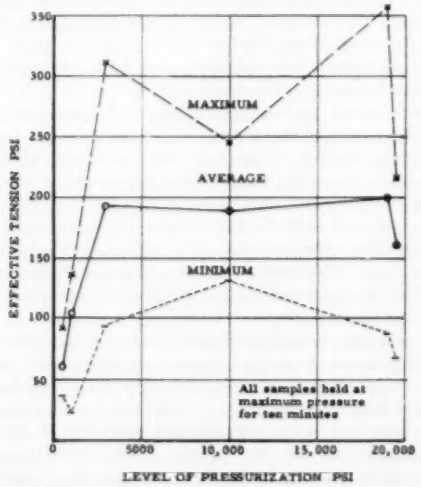

Fig. 7 Effect of level of pressurization on boiling-point tests

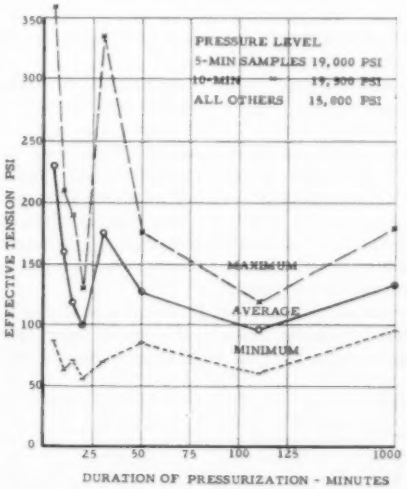

Fig. 8 Effect of duration of pressurization on boiling-point tests

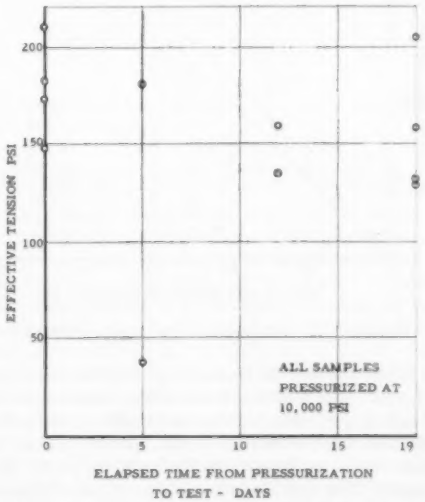

Fig. 9 Effect of time interval between pressurization and test on boiling-point tests

The time of pressurization was 10 min. Two significant conclusions can be drawn from these data. First, even the low-level pressurization of 500 psi produces a significant increase in the effective tensile strength of the water and second, pressurization above 3000 psi appears to produce no significant additional increase in effective tensile strength. Fig. 8 shows the effect of duration of pressurization on the effective tensile strength of the samples. Here the pressurization level was uniformly high, that is, near the top of the range covered by Fig. 7. The results show no significant correlation between duration of pressurization and the effective tension of the liquid. The shortest period of pressurization actually showed the highest maximum and average values, but this is quite surely a chance result due to the small number of samples in each group. The minimum duration of 5 min was controlled only by convenience in operation of the equipment. A few tests were made at a lower pressure, speeding up the entire operation as much as possible. This gave a treatment time of approximately 1 min. There appeared to be no decrease in the effectiveness of the pressure treatment. There is some indirect evidence that pressurization for only a fraction of a second may be effective, although here the intensity of the pressurization might become an important factor.

One question of considerable interest is the permanency of the pressurization effect. Fig. 9 presents some rather conclusive evidence in this regard. Twelve identical samples were prepared and pressurized simultaneously. Four were tested immediately; the others at the intervals shown. The last four, tested at 19 days after the original pressurization, show no significant decay in the effect of pressurization. The only precautions taken during these 19 days was to keep the samples sealed at atmospheric pressure so that there could be no contamination by dust particles from the air.

Pressure Release Tests. Fig 10 is a plot of all the results obtained from previously pressurized samples tested in the pressure-release apparatus. The level of pressurization varied from

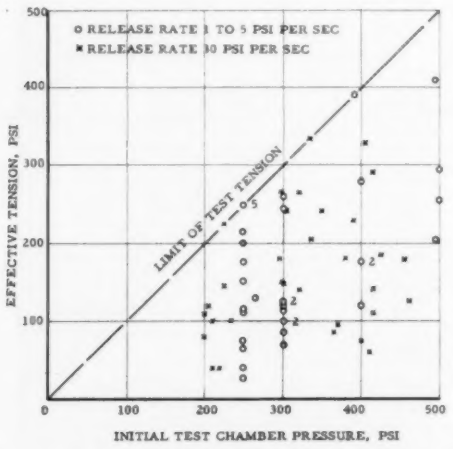

Fig. 10 Summary of test results from pressure-release chamber

5000 to 15,000 psi, and the time of pressurization from 15 min to several hours. The results of the boiling point tests, as shown in Figs. 7 and 8, demonstrated that these differences in the pressurization treatment are not significant. It will be noted that the two release rates previously described are designated by different symbols. The numbers adjacent to several of the points indicate the number of individual tests which gave the same test results. Several conclusions may be based on these results: (*a*) There seem to be no significant differences between the results obtained at the different pressure-release rates. This is rather surprising since it was assumed that the slow release rate would be a more severe test. (*b*) Although it was hoped that this apparatus would yield more consistent test results, it is seen that the scatter ratio is at least as large as it was in the boiling-point tests. (*c*) The average effective tension shown by the test seems to increase with increase of the initial test-chamber pressure.

The significance of this last result is more apparent after an examination of some auxiliary tests made in the pressure-release chamber. Two groups of samples were tested without the pressure treatment. These groups are quite similar to those used in the unpressurized tests in the boiling-point experiments. In one group the tubes were cleaned, filled, and tested without pressurization. In the second group the tubes were cleaned, filled, and pressurized, and then flushed out with unpressurized tap water. In contrast to the results from the parallel groups tested by the boiling point method, these two groups showed relatively high values of effective tensile strength. The highest result obtained with the cleaned, unpressurized tubes was 230 psi, whereas one of the tubes that had been pressurized and flushed with unpressurized water showed an effective tensile strength of 275 psi. Both of these values are higher than the average tension of the pressurized samples although, as seen from Fig. 10, many of the individual tests of the pressurized samples showed much higher values. The average tension found with 19 samples tested in clean, unpressurized tubes was 113 psi. This is in striking contrast to the 1 or 2 psi obtained in the boiling point tests. Examination showed that these 19 tests could be divided into three groups according to the pressure p_e in the test chamber at the beginning of the pressure release. Three samples have been tested at a p_e of 120 psi or lower. The average tension measured in this group was 22 psi. The 12 samples in the second group had a p_e of between 200 and 250 psi. The average tension of this group was 128 psi. The remaining four tubes had been tested at a p_e between 300 and 400 psi. Here the average tension was 136 psi. It is significant that the average tensile strength increased with p_e. It implies that the pressure-release technique inherently includes a low level pressurization at relatively high temperature, which increases the effective tensile strength of the liquid.

These results might have been anticipated from the boiling-point tests shown in Fig. 7. It will be noted that the average effective tension of the small group pressurized at 500 psi was about 60 psi with a maximum of 90 psi. This is good agreement for this type of experiment, especially considering that the pressurization for the boiling-point test was carried on at atmospheric temperature, whereas the pressurization in the pressure-release tests was at saturation temperature.

These low-level pressure-release tests of untreated samples may explain part of the scatter in the boiling-point tests with unpressurized samples. The mean effective tension of these unpressurized-boiling-point samples was only about 1 to $1^1/_2$ psi. However, one sample went as high as 47-psi tension. This value is quite consistent with the 22-psi average tension shown by the unpressurized samples tested at p_e = 120 psi, in the pressure-release chamber. The implication from this is that even the pressure in the city water mains may be sufficient to increase the tensile strength of the water.

There is no significant difference between the effective tensions shown by pressurized samples tested by the two static methods. The maximum tensions measured are very nearly the same, and the scatter is of the same order. This would be surprising if the tensions measured were actually the property of the liquid. This is clearly shown in Fig. 11 [fig. 1 (4)]. This is an experimental curve. At the lower temperatures the experimental points were obtained by the centrifugal test method. The water

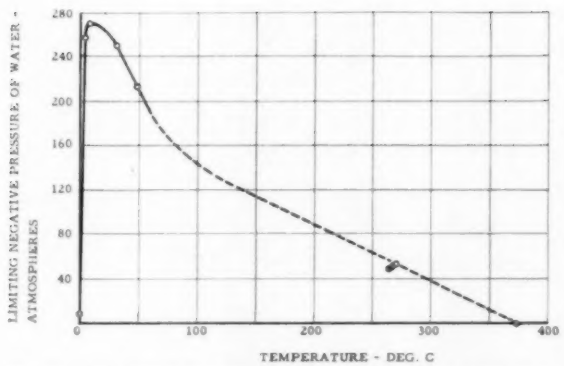

Fig. 11 Variation of limiting negative pressure of water with temperature (fig. 1 of reference 4)

used in these tests was purified by very elaborate methods to eliminate all extraneous weak points. Most of the samples tested by the boiling-point method failed at relatively low temperatures. For this temperature range the limiting tension from Briggs' curve is about 1500 psi. In the pressure-release tests the limiting p_v was 500 lb. The corresponding saturation temperature is approximately 240 C, which, from Briggs' curve, corresponds to a limiting effective tension of about 800 psi. No sample tested by either method in these experiments approached either of these values. This is conclusive evidence that the true tensile strength of the water was not being tested. Instead, the ruptures were due to the impurity weak spots.

Dynamic-Flow Tests. Two series of tests were made with the dynamic-flow apparatus. First, a group of reference runs was made with unpressurized water in the glass venturi tubes. The second group of tests was with pressurized samples. In the discussion of the results it must be remembered that there are several significant differences between these tests and the preceding ones. The basic difference is that these tests are dynamic, or flow tests, whereas the boiling-point and pressure-release tests are static, that is, the liquid is at rest. Another significant difference is that in the dynamic-flow tests each element of the liquid is tested separately as it goes through the throat, or working section, of the venturi tube, whereas in the two static tests all of the liquid elements in the sample are tested simultaneously. The size of the sample in the two types of tests is significantly different. The venturi tubes hold over 50 cu in. of liquid, whereas the test tubes used in the static tests have a volume of less than 2 cu in., thus giving a volume ratio of the two samples of over 25 to 1. One more difference needs to be mentioned. In both static tests the tension applied to the sample could be increased until it failed at the weakest point. In the dynamic test the maximum tension had to be predetermined. If too high a value was chosen, the sample might fail before equilibrium velocity was reached in the working section; if too low a value, the entire sample might flow through it without failure. Table 1 lists the results of the reference runs made with unpressurized samples. Table 2 shows the results obtained with nine runs using pressurized samples. It will be noted that in this group the drive pressures are about the same. The third and fourth columns of both tables give the pressure and the velocity in the working section at the appearance of the first cavitation bubble. The last column gives the per cent of the sample that passed through the working section before cavitation occurred. The average water temperature for both series of tests was 75 F, which corresponds to a vapor pressure of 0.43 psi. The significance of the last column needs clarification which can best be accomplished by examining in more detail the record

Table 1 Dynamic tests of unpressurized samples

Run no.	Drive pressure, psig	Throat velocity, fps	Cavitation pressure, psia	Through-flow at inception, per cent
14	4.71	51	1.33	21
15	4.22	51	1.43	25
16	3.55	50	1.20	30
17	2.98	49	0.99	50
22	4.27	51	1.24	30
23	3.83	52	0.24	35
24	3.69	52	−0.19	40

Table 2 Dynamic tests of pressurized samples

Run no.	Drive pressure, psig	Throat velocity, fps	Cavitation pressure, psia	Through-flow at inception, per cent
33	7.93	90	−32	60
34	9.05	81	−20	54
35	8.99	93	−35	72
37	9.0	64	−4	16
38	9.21	82	−21	45
39	9.15	76	−15	21
40	9.10	79	−18	28
41	9.15	95	−41	65
42	8.54	92	−34	39

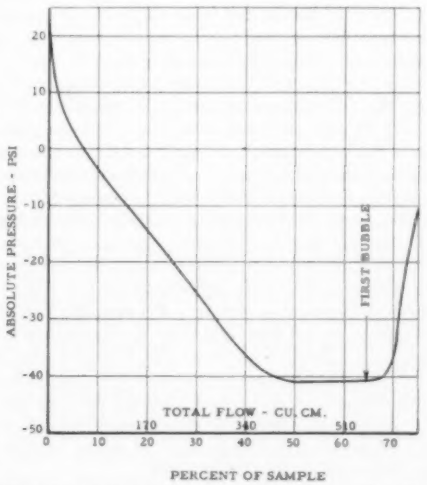

Fig. 12 Variation of absolute pressure in working section during run (Test no. 41)

of a single typical run. Fig. 12 is the pressure history of run No. 41 and is typical of all the runs in Table 2. It will be noted that the flow accelerated during the passage of the first 22 cu in. of the sample through the working section. Of this, the first 3 cu in. passed through before the working-section pressure had dropped to vapor pressure. The remaining 19 cu in. were subjected to tensions varying from 0 to about 40 psi. During the passage of the next 11 cu in. the working-section tension remained nearly constant, decreasing slowly from 41 to about 40 psi. The working-section velocity under these conditions was about 94.5 fps. The first cavitation bubble appeared when there were still 14 cu in. of the sample remaining in the reservoir section. Flow conditions during the passage of this portion of the sample through the working section were indeterminate since, with the beginning of cavitation, both the velocity and pressure fluctuated. However, the photographic records indicated that the average tension during this period was about 25 to 30 psi. After the first cavity

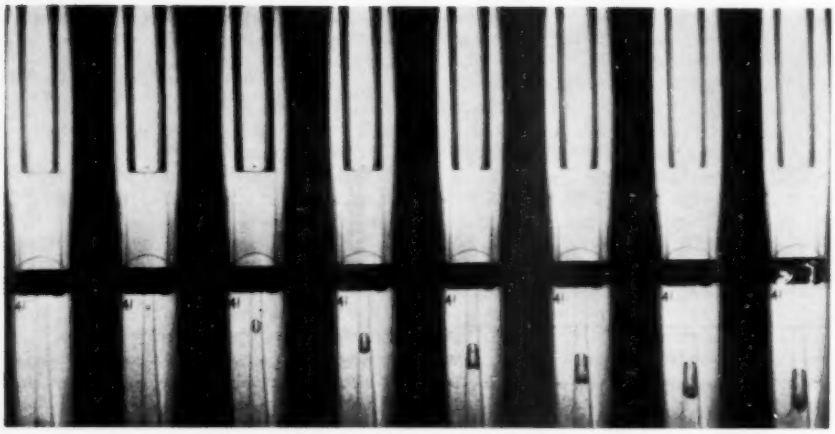

Fig. 13 Formation of first bubble during run No. 41

formed there was undoubtedly a series of relatively high pressure surges. In spite of this, only two or three new cavities formed in the working section. During the period of maximum velocity an element of water passes through the working section in about 0.0007 sec. During this time it is exposed to the maximum tension. The tension decreases rapidly as the flow is decelerated in the diffuser so that the total time of exposure to any tension is at most a few thousandths of a second. This is in sharp contrast to the test procedure of the static tests. There the sample is subjected to a gradually increasing tension until failure occurs, the total time of tension varying from about 5 sec to several minutes. The short duration of the tension in the dynamic tests applies to the main flow. An element of liquid in the boundary layer would be subjected to tension for a much longer time. The photographic records of the runs show that in nearly all cases failure occurred in the main flow, the velocity of the opening cavity corresponding closely to the average velocity determined by the rate of fall of the meniscus in the reservoir section. For example, Fig. 13 shows the development of the first bubble at the point shown by the arrow in Fig. 12. When first observable in the working section, its velocity, as determined by the distance traveled between two consecutive frames of record, was 94 fps, the average velocity of the flow. Records of a few runs showed cavities developing on the wall. These were fixed-type cavities which usually disappeared at the end of the first filling cycle.

This contrast between the results of the static and dynamic tests clarifies one characteristic of nuclei found in normal water; that is, there do not seem to be any nuclei which can resist tension for a short time before failure under the same tension if applied over a relatively long period. In other words, the growth time from nucleus to finite cavity is of the order of milliseconds or less, even for nuclei small enough to resist very appreciable tensions.

The glass venturi tubes used in these dynamic tests were very strong, and withstood for many runs the shock pressures caused by the collapse of the cavities. Fortunately, a good photographic record was obtained of one of the rare runs which terminated in a tube breakage. This record showed clearly that the time of the break coincided with that of the collapse of a large cavity.

Comparison of Results of Static and Dynamic Tests. The maximum tensions observed in the dynamic tests are about one order of magnitude lower than those obtained in the static tests. Thus it might be concluded that the tensile strength of the liquid under flow conditions was much lower than under static conditions. Such a conclusion seems premature. Both the static and the dynamic tests measure the strength of the weakest element of the liquid in the sample. In the static tests the entire volume of the sample is subjected to the maximum tension. In the dynamic test only a part of the total volume passes through the working section under tension before failure occurs. The dynamic test records show that approximately four to six times the volume of a static test passes through the working section under the maximum tension before the first bubble appears. Thus the results of one dynamic test should be compared to the minimum tension failure observed in a group of four to six static tests. It was common laboratory practice to prepare, pressurize, and test static samples in groups of six. Thirteen such groups, all of which were pressurized at relatively high levels, were re-evaluated on the basis of the minimum tension observed within each group. The average of these minimum tensions was 45 psi. The average tension of the nine dynamic tests shown in Table 2 is 26 psi. This is good agreement considering the inherently wide scatter of all of these tests. Thus it must be concluded that these experiments show no significant effect of flow on the tensile strength of water.

One limitation of these conclusions must be recognized. The flow in the working section of the dynamic test apparatus has, in all probability, an extremely low turbulence level. The monotonic design of the nozzle which is required to obviate any possibility of cavitation upstream from the throat insures smooth acceleration with no random-pressure disturbances. At the beginning of the test the liquid is at rest, and the elements that travel furthest before they reach the working section move only about eight tube diameters. Thus there is little energy available for the development of turbulence. It would be desirable to make a similar series of tests with a known turbulence level in the working section. However, this would add serious complications to the test procedure.

Summary of Results of the Effects of Pressurization and Conclusions Regarding the Properties of Natural Waters

1 The effective tensile strength of water is increased by pressurization. The amount of this increase varies with the level of pressurization, but seems to reach an upper limit at about 2000 to 3000 psi.

2 Pressures of the order of 300 or 400 psi produce definite increases in the effective tensile strength and there is some evidence that even lower pressures have a measurable effect. The most probable reason for the effects of low-level pressurization not having been commonly observed is that the solid surfaces in

contact with the liquid usually contain a plentiful supply of nuclei, so that boiling or cavitation readily takes place as soon as vapor pressure is reached, thus masking the fact that within the body of the liquid no cavities are initiated.

3 The duration of the pressurization treatment seems to have little effect on the increase in tensile strength. The treatment time varied from approximately one minute, the minimum practical with the equipment available, to several days. It is quite possible that there is a time effect for very short treatment times.

4 The pressurization effect lasts at least for weeks if the liquid is shielded from contamination with foreign nuclei during the period between pressurization and test.

5 The initial purity of the water does not seem to be a significant factor in the effective tensile strength produced by pressurization. No difference was found between the behavior of multiple-distilled water and air-saturated tap water containing relatively high concentrations of dissolved and suspended material.

6 The duration of the applied test tension in the different types of experiments varied from a few milliseconds to more than one minute. Within this range no correlation could be found between the duration of the applied stress and the tensile strength of the liquid.

7 These experiments show that normal liquids rupture or cavitate at a much lower tension than the true tensile strength of the pure liquid. These ruptures appear to occur at weak spots in the liquid caused by the presence of real nuclei which have continuing existence and specific physical properties.

8 The physical concept or "model" of the nucleus which is most consistent with the results of this series of investigations is that of Harvey; that is, a nucleus is a pocket of undissolved gas in the re-entrant crack in the surface of a solid particle of impurity which is hydrophobic to the liquid.

9 The effectiveness of nuclei as weak spots may be reduced or destroyed by pressurization. Their resistance to pressure varies greatly and is probably related both to the sharpness of the bottom of the re-entrant crack, and to the relative resistance to wetting by the surrounding liquid. The concentration of highly pressure-resistant nuclei in natural water seems to be relatively low. For example, the static test results imply that there is about one nucleus to every 2 cu in. of water whose effective tensile strength is approximately 450 psi and whose resistance to pressurization exceeds 15,000 psi, and one nucleus in each 12 cu in. whose effective tensile strength is only 15 psi but which has an equally high resistance to pressurization.

10 Weak spots which can initiate cavitation usually occur on all solid surfaces in contact with liquids. They can normally be removed from glass surfaces by rigorous cleaning methods. This implies that the weak spots are caused by hydrophobic contamination. Experiments by other investigators have shown that normal cleaning methods are inadequate to remove weak spots from metal surfaces. This is probably due to the presence of innumerable cracks or pockets which serve as hosts for free gas nuclei.

Engineering Significance of Nuclei

At this point the average engineer might well ask, "What is the significance of this information with respect to mechanical engineering?" This is a difficult question to answer at the present state of knowledge. However, it seems probable that the general properties of nuclei in liquids will be the basis for the explanation of many cases of abnormal performance of liquid-handling equipment.

Certainly the results of these experiments raise many practical questions. The following are a few examples:

1 In the operation of steam boilers is there any evidence of low-level pressurization effects which reduce the release rate of steam in the body of the liquid?

2 For the same relative velocities in cavitation areas, are low-head turbines more susceptible to cavitation than high-head turbines, both as regards its effect on performance and on degree of damage? The penstock of a high-head turbine should be an effective means of pressurization. This might not change the degree of fixed cavitation; thus the effect of the cavitation on the performance would remain unaltered. However, due to a decrease in the number of available nuclei, it might lessen the number of traveling cavities and thus decrease the relative amount of damage (10).

3 For machines handling cold water at comparable velocities, are centrifugal pumps more susceptible to cavitation troubles than high-head turbines? Here the viewpoint is the same as in the previous question. Natural waters are exposed to a continuing rain of the dust particles which serve as hosts for gas nuclei. The maximum pressurization before entering the impeller eye is measured by the submergence of the inlet pipe, which is very small compared to that in the penstock of a high-head turbine.

4 Stepanoff has pointed out that a high-pressure boiler feed pump handling hot water is less susceptible to the effects of cavitation than is the same pump handling cold water under otherwise identical conditions. He explains this by the difference in the thermodynamic properties of the liquids. However, modern boilers operate on a closed cycle with deaerated distilled water, which is highly pressurized each time it passes through the boiler. Therefore, might not at least a portion of the improved performance of the pumps be explained by a scarcity of nuclei?

5 There is a general impression that in the petroleum industry there is much less trouble from cavitation in hydraulic equipment than there is in comparable installations using water. Is it not possible that a major reason for the difference is the higher wetting ability of most petroleum derivatives, since this would tend to greatly decrease the concentration of effective nuclei?

There are a host of other questions of this general type that could be raised. In many cases detailed consideration will show that the properties of nuclei do not play a major role in the phenomenon involved. However, it seems clear that, due to variations in their properties, the effective tensile strength of liquids may vary from nothing to quite high values, and that the cavitation performance of equipment operating with such liquids will vary accordingly. Hence nuclei, and the related effective strength of liquids, form one more facet of the cavitation phenomenon which must be considered in the design and operation of hydraulic equipment.

Acknowledgments

The support for these investigations came from research contracts with the Bureau of Ordnance and with the Mechanics Branch of the Office of Naval Research. The experiments were performed by two research assistants, Nathan Gainsboro and Frank Bonamassa. They contributed much to the development of satisfactory techniques and the analysis of the results, in addition to the tedious work of the tests themselves.

Bibliography

1 "The Tensile Strength of Liquids: A Review of the Literature," by F. G. Blake, Jr., Harvard University, Acoustics Research Laboratory, T. M. no. 9, June 11, 1949.

2 "Apparatus and Techniques for a Study of Cavitation," by F. G. Blake, Jr., Harvard University, Acoustics Research Laboratory, T. M. no. 11, June 28, 1949.

3 "The Onset of Cavitation in Liquids I," by F. G. Blake, Jr., Harvard University, Acoustics Research Laboratory, T. M. no. 12, Sept. 2, 1949.

4 "The Maximum Superheating of Water as a Measure of Nega-

tive Pressure," by J. Lyman Briggs, *Journal of Applied Physics*, vol. 26, 1955, pp. 1001–1003.

5 "Gas Bubbles With Organic Skin as Cavitation Nuclei," by Frances E. Fox and Karl F. Herzfeld, *Journal of the Acoustical Society of America*, vol. 26, 1954, pp. 984–989.

6 "Bubble Formation in Animals," by E. Newton Harvey, D. K. Barnes, W. D. McElroy, A. H. Whiteley, D. C. Pease, and K. W. Cooper, *Journal of Cellular and Comparative Physiology*, vol. 24, 1944, pp. 23–44.

7 "Removal of Gas Nuclei From Liquids and Surfaces," by E. Newton Harvey, D. K. Barnes, W. D. McElroy, A. H. Whiteley, and D. C. Pease, *Journal of the American Chemical Society*, vol. 67, 1945, p. 156.

8 "On Cavity Formation in Water," by E. Newton Harvey, W. D. McElroy, and A. H. Whiteley, *Journal of Applied Physics*, vol. 18, 1947, pp. 162–172.

9 "Cavitation Mechanics and Its Relation to the Design of Hydraulic Equipment," by Robert T. Knapp, Clayton Lecture, *Proceedings of The Institution of Mechanical Engineers*, vol. 166, series A, 1952, pp. 150–163.

10 "Recent Investigations of the Mechanics of Cavitation and Cavitation Damage," by Robert T. Knapp, TRANS. ASME, vol. 77, 1955, pp. 1045–1054.

11 "Further Studies of the Mechanics and Damage Potential of Fixed Type Cavities," by Robert T. Knapp, *Proceedings of the Symposium on Cavitation in Hydrodydamics*, held at the National Physical Laboratory, Teddington, England, Sept. 14–17, 1955.

12 "Some Mechano-Chemical Properties of Water," by W. A. Weyl and E. C. Marboe, *Research*, vol. 2, 1949.

13 "Ultrasonically Induced Cavitation in Water: A Step-by-Step Process," by C. W. Willard, *Journal of the Acoustical Society of America*, vol. 25, 1953, pp. 669–686.

Discussion

L. J. Briggs.[4] In the writer's opinion, cosmic radiation may be responsible in part for the low and widely scattered values obtained in cavitation measurements. Glaser[5] has shown that, when a highly energized cosmic ray passes through a superheated liquid, bubbles are formed and the liquid explodes. The probability of such an event is proportional to the product of the maximum cross section of the exposed liquid and the time of exposure.

In the writer's measurements of the maximum negative pressure developed in superheated water (see Fig. 10 of the paper), the maximum exposed area of the liquid was only 0.6 sq cm and the exposure time 5 sec. The probability that an energetic cosmic ray would pass through this area during this time is of the order of only 1 part in 1000. But here the area and time of exposure were kept near a minimum, and in most setups the probability would be much greater.

The most striking feature of the cavitation of water is the remarkable change in cohesive strength which occurs near the freezing point. The highest value observed by the writer for the limiting negative pressure (cohesive strength) of water was about 270 atm (4000 psi) at 8 C, Fig. 10. From here it drops steadily but precipitously to only 7 or 8 atm at its freezing point. Some other liquids which the writer has measured show a slight drop as their freezing points are approached, but nothing compared with this 35-fold change.

[4] Director Emeritus, National Bureau of Standards, Washington, D. C. Mem. ASME.

[5] D. A. Glaser, "Some Effects of Ionizing Radiation on the Formation of Bubbles in Liquids," *Physical Review*, vol. 87, 1952, p. 665; "Bubble Chamber Tracks of Penetrating Cosmic-Ray Particles," *Physical Review*, vol. 91, 1953, pp. 762–763.

The foregoing measurements were made by a centrifugal method.[6] The water was contained in a capillary glass tube, open at both ends, the tips being bent back to form a nearly closed Z. When the capillary was mounted symmetrically on its spinner and filled so that both short legs contained water, the system was dynamically stable at any speed. The open ends of the tube made it easy to clean and fill. The greatest difficulty the writer has experienced is the breaking of the capillary tube when the water column, under high stress, suddenly ruptures at its center and impacts against the curved ends of the tube.

K. F. Herzfeld.[7] In the problem of cavitation, many contradictory experimental results appear in the literature and therefore reliable experiments are very valuable. The necessity for the presence of "nuclei" as weak spots is now generally recognized, but there is no agreement as to their nature. The experimental methods fall into three goups: Pressure release, start of boiling, use of ultrasonic waves. The increase in tensile strength of the liquid due to previous pressurizing found by the author occurs also in ultrasonic tests, but much lower pressures (15–100 psi) are effective there.[8,9] The interesting comparison of tensile strength in flow tests and static tests—comparing application times of milliseconds and of minutes without apparent effect on strength—agrees with the ultrasonic experience according to which cavitation pressure is independent[10] of frequency up to 10 kc.

E. G. Richardson[9] has also discussed the persistence of the nuclei.

One of the most valuable results of the paper, at least for the writer, is the estimate of the number of nuclei.

Some recent experiments of Liebermann[11] on the nature of nuclei should be mentioned.

Author's Closure[12]

In connection with Dr. Briggs' discussion, it is interesting to note that in discussing the effect of pressurization of water in a recent report,[13] Professor Knapp considered the effect of cosmic rays. His conclusion in this regard is as follows:

"No correlation was found between the average tensile strength at failure and the duration of the tension even though this duration varied over several orders of magnitude between the different tests. This result implies that cavity formation in liquids under tension cannot be explained by nucleation resulting from cosmic rays or other high energy radiation received by the liquid while under tension."

[6] *Journal of Applied Physics*, vol. 21, 1950, p. 721.

[7] Department of Physics, The Catholic University of America, Washington, D. C.

[8] M. Strassberg, Catholic University Dissertation, 1956.

[9] K. S. Iyengar and E. G. Richardson, "The Role of Cavitation Nuclei, Department of Science and Independent Research, East Kilbride, Glasgow, Fluids Report No. 57.

[10] R. Esche, *Akustische Beihefte*, 1952, p. 208.

[11] L. Liebermann, "Air Bubbles in Water," *Journal of Applied Physics*, vol. 28, 1957, p. 205.

[12] Written by Dr. Vito A. Vanoni, Professor of Hydraulics, California Institute of Technology, due to the sudden death of Professor Knapp on November 7, 1957.

[13] "Investigation of the Mechanics of Cavitation and Cavitation Damage," Final Report, ONR Contract Nonr-220(08), dated June, 1957. Conclusion 6, p. 35.

Study of Corrosion and Cavitation-Erosion Damage

By J. Z. LICHTMAN,[1] D. H. KALLAS,[2] C. K. CHATTEN,[3] and E. P. COCHRAN, JR.,[4] BROOKLYN, N. Y.[5]

The effects of fluid cavitation and cavitation bubble collapse on a guiding surface have been investigated using two water tunnels, a magnetostrictive-transducer apparatus, a piezoelectric transducer apparatus, and a rotating-disk apparatus. Studies of the mechanism of damage to a surface and its relationship to change in fluid pressure and stream velocity were made. These studies and examination of numerous ships in service showed that although fluid cavitation may occur adjacent to underwater appendages of vessels at normal operating speeds, the areas in which cavity collapse is the primary cause of damage are restricted to propellers. Damage to ships' struts, rudders, and other appendages is shown to be primarily corrosive in nature, aggravated by mechanical scouring action.

Introduction

The damage of certain hydraulic machinery and ships' propellers as a result of cavitation erosion, as well as the phenomenon of cavitation itself, have been reviewed comprehensively by the Admiralty Corrosion Committee [1][6] in England and by Eisenberg [2] in the United States.

It has been the practice of the Department of the Navy to apply elastomeric coatings to struts, sonar domes, sea chests, rudders, and other appendages in order to diminish damage to them from cavitation erosion as well as corrosion. The Bureau of Ships had authorized the Material Laboratory at the New York Naval Shipyard to develop testing techniques for determining the cavitation-erosion resistance of elastomeric coatings. Coatings, intended primarily for protection of underwater appendages against corrosion damage, could then also be evaluated to determine their resistance against cavitation erosion.

Literature Survey

A literature survey indicated that there were two major hypotheses regarding the basic mechanism of damage. One viewpoint, supported by references [3–13], was that the mechanism is primarily mechanical in nature, a material undergoing plastic deformation under the impact of cavity collapse, depending on its hardness and yield properties, resulting in eventual mechanical fatigue and erosion. The belief that the mechanism is primarily electrochemical in nature, damage being caused by galvanic corrosion as a result of nonuniform stresses in the metal, oxygen-concentration cells, or ion-concentration cells was supported by references [14–17].

The evidence presented shows a preponderance of damage by one mechanism or the other depending on the specific conditions of exposure. These conditions include the corrosive nature of the liquid, electrical potentials existing on the material, the resistance of the material to corrosion, the physical properties of the material, and so forth. It is likely that both mechanisms influence the damage of a material simultaneously, the degree of influence of each mechanism depending on the individual conditions of exposure, such as specimen material, fluid characteristics, temperature, and fluid velocity. This viewpoint is shared by Eisenberg [2] and other investigators. The present investigations were made without adopting either viewpoint to the exclusion of the other.

Examination of Naval Vessels

Seventeen combatant vessels, two of which operated in the Great Lakes, the balance largely operated in the Atlantic, were examined for operational damage to underwater structures.

The members examined included propeller shafts, strut barrels, struts, rudders, rudder skegs, and propellers. Damage ratings were assigned to the members based on the degree of removal of protective coatings and the condition of the bared metal, Table 1. Vessels operating in fresh water showed practically no erosion damage to the underwater structures. Zincs attached to these structures were intact and required no replacement after years of service. Fig. 1 shows typical damage to the rudders and skegs of ships operating in the Atlantic. The rudders of the DD 853 were made of special-treatment steel, STS, and exhibited a lower degree of damage, and of a more uniform nature, than the other rudders constructed of mild steel. Fig. 2 shows typical damage to struts and barrels of vessels operating in the Atlantic. Removal of the coatings occurred at many random locations on the struts; the bared areas were relatively large and irregular in shape.

Coatings on propeller shafts were damaged or removed the least, those on strut barrels the most. Erosion occurred in all bared-metal areas, the skegs showing a greater degree of metallic damage in such areas than other structures. No other relationship between operating conditions and resistance of coatings to removal could be determined. Fig. 3 shows typical examples of erosion of propeller blades. Such damage occurred only in small areas of the entire propeller-blade surface and only on individual propellers. The eroded surfaces of the propellers had a granular appearance whereas those of the rudders, skegs, barrels, and struts had a scored, striated, and pitted appearance. Erosion had occurred simultaneously on both pressure and suction faces on only one propeller. The majority of propellers of ships operating in salt water, as well as all operating in fresh water, did not show any erosion damage.

The following conclusions may be made on the basis of the structural examinations:

1 Cavitation-erosion damage occurred only in particular areas on propellers of a minority of vessels, and in only one case on both pressure and suction faces of the blades.

2 Corrosion damage of rudders, struts, barrels, and shafting

---

[1] Supervisory Rubber Technologist, Elastomer Development Section.

[2] Supervisory Mechanical Engineer, Material Development Branch Head.

[3] Supervisory Rubber Technologist, Elastomer Development Section Head.

[4] Commander, USN, *USS Hector* (AR-7), formerly Program Officer, Mechanics Branch. Assoc. Mem. ASME.

[5] Material Laboratory, New York Naval Shipyard.

[6] Numbers in brackets designate References at end of paper.

Contributed by the Hydraulics Division and presented at the Annual Meeting, New York, N. Y., December 1–6, 1957, of The American Society of Mechanical Engineers.

Note: Statements and opinions advanced in papers are to be understood as individual expressions of their authors and not those of the Society. Manuscript received at ASME Headquarters, August 27, 1957. Paper No. 57—A-156.

Fig 1 Service damage of rudders and skegs of high-speed naval vessels

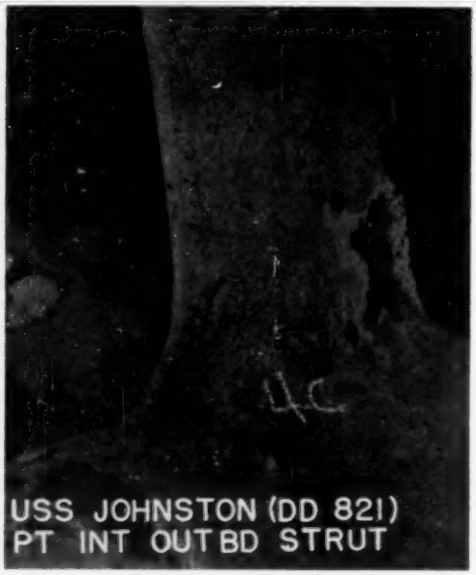

Fig. 2 Service damage on struts of a high-speed naval vessel

Fig. 3 Service damage to the pressure face of the propeller of a high-speed naval vessel

Table 1 Damage ratings of ship's underwater appendages

Vessel	Rating of removal of coating[a] Shafts	Struts	Rudders	Barrels	Skegs	Average Rating	Rating of degree of corrosion of bared metal[a] Shafts	Struts	Rudders	Barrels	Skegs	Average rating
DD 853	1	3	8	4	2	3.6	7	6	2	4	6	5.0
DDR 807	3	5	7	4	4	4.6	4	6	5	6	6	5.4
DDR 830	4	6	7	7	6	6.0	4	5	5	6	6	5.2
DDE 859	1	3	5	2	4	3.0	2.	6	4	3	6	4.2
DDE 860	1	1	8	1	5	3.2	3	1	1	1	7	2.6
DDE 858	1	4	7	6	9	5.4	2	5	2	4	7	4.0
DD 865	2	5	6	6	4	4.6	3	5	4	4	7	4.6
DD 850	4	5	8	10	9	7.2	4	4	3	5	6	4.4
DE 447	1	1	...	9	...	...	3	5	...	3	...	...
DD 821	1	7	6	10	8	6.4	3	5	4	6	7	5.0
DD 844	4	3	9	6	9	6.2	3	5	2	4	8	4.4
CVS 32	1	5	1	8	1	3.2	2	5	2	4	4	3.4
DE 532	1	3	...	9	...	...	1	5	...	6	...	...
CVA 39	1	7	4	9	3	4.8	0	5	3	5	5	3.6
DE 538	...	...	...	...	...	...	7	7	7	5	7	6.6
PCE 880[b]	1	3	3	1	4	2.4	0	1	2	2	2	1.4
PCE 894[b]	1	1	1	0	3	1.2	0	0	1	0	1	0.4
Total	28	62	81	92	71	61.4	49	76	47	68	85	60.6
Average	1.8	3.8	5.8	5.8	5.1	4.4	2.9	4.5	3.1	4.0	5.7	4.0

[a] Rating 10 = maximum, 0 = minimum damage.
[b] Operated in fresh water.

occurred where the metal had been exposed to the corrosive medium as a result of failure of the protective coatings, which occurred generally in random locations.

3 The intensity of corrosion damage appeared to be greater in small areas of coating failures than in large bared-metal areas.

4 The use of special treatment steel, STS, as rudder plating or as strut cladding resulted in a uniform, lower degree of corrosion of the structure when bared than did bare mild-steel structural materials.

5 Service of a vessel in a corrosive environment resulted in considerably greater corrosion damage to bare appendages than service in fresh-water regions, as shown both by greater degree of structural damage, and by larger zinc-anode consumption. The zinc anodes on vessels operating in fresh water were virtually uncorroded after about 18 to 20 months' exposure.

6 Coatings on the strut barrels showed the greatest susceptibility to removal in service.

7 Skegs showed a greater degree of corrosion damage upon removal of the coatings than the other appendages.

Cavitation-Erosion Studies

Assuming that damage to underwater structures may be due primarily to cavitation-impact erosion, various types of equipment designed to produce this type of damage were investigated in the third phase of the project. These included: (*a*) A water tunnel designed by the Bureau of Reclamation [18]; (*b*) a hypersonic transducer apparatus; (*c*) a magnetostrictive apparatus; (*d*) a water tunnel designed by the David W. Taylor Model Basin [19 and 20]; (*e*) a rotating-disk apparatus [21] built in the Material Laboratory on the basis of a Bureau of Reclamation design and work done by Rasmussen [4].

Bureau of Reclamation Water Tunnel

This apparatus provides for the high-velocity recirculation of water past a cylindrical-conical specimen inserted in a $5^3/_4$-in-ID pipe section. The specimen measures 5 in. OD by $13^1/_4$ in. long and is attached to the rear of a hemispherical 5-in-diam nose. A cavitation field develops at the trailing conical surface, collapsing near this surface, about midway downstream. It was designed and built by the Bureau of Reclamation, Denver Federal Center, Denver, Colo., and is installed and operated in the laboratories of that agency.

The water velocity in the throat section during the present tests was 70 fps, providing for a flow of 1380 gpm, the upstream pressure head being 62.4 psi and the downstream pressure head being 16.9 psi.

A number of steel specimens, some coated and some uncoated, were tested in the apparatus, Table 2.

Conclusions. Failure of coatings in adhesion at the leading cylindrical edges and the conical surfaces of the specimens [22] indicated the importance of good adhesive strength of the coating to prevent removal under the hydrodynamic flow stresses not associated with cavitation erosion. Although cavitation-erosion damage was obtained on Thiokol-coated specimens, Fig. 4, no noticeable cavitation-erosion damage of the conical surfaces of the uncoated steel specimens was obtained with this apparatus. The difference in test time for the coated and uncoated specimens may account for the difference in degree of damage, although the test time of the uncoated specimens was believed to be ample for a laboratory evaluation technique. The apparatus required a long test period to achieve erosion damage of the Thiokol-coated specimens. Also it required an excessive amount of floor space and power for a laboratory type of apparatus. Therefore the Bureau of Reclamation apparatus was not believed to be practical for normal laboratory use.

Table 2 Results of test of Bureau of Reclamation water tunnel specimens

Specimen no.	Specimen: Metal pretreatment	Specimen: Coating, thickness	Test time, hr	Results
1	Sandblasted	Flame-sprayed Thiokol, 0.035 in.	10.5	Coating loose, tore at up-stream edge of cylinder
2	Sandblasted	Flame-sprayed Thiokol, 0.035 in.	11.3	Coating removed at cone apex, pitted at cone base
3	Sandblasted	none	40	Slight erosion at conical-cylindrical junction
4	Sandblasted	none	11.3	Slight erosion at conical-cylindrical junction
5	Sandblasted	Formula 84-14 AC(vinyl)	7.5	Separation of coating at cone base, pitting of coating at cone apex, separation at apex
6	Sandblasted	Formula 84-14 AC(vinyl)	4	Removal of coating near apex
7	Sandblasted	Nitrile N351, 0.035 in.[a]	3.5	Removal of coating on cone surface and at cone base
8	Sandblasted	Nitrile N351, 0.035 in.[a]	8.5	Removal of coating on cone surface and at cone base
9	Sandblasted	Neoprene N100-1, N200-1, 0.035 in.[b]	<1	Coating loosened at leading cylindrical edge of specimen, causing downstream pressure drop
10	Sandblasted	Neoprene N100-1, N200-1, 0.035 in.[b]	<1	Coating loosened at leading cylindrical edge of specimen, causing downstream pressure drop
11	Sandblasted	Flame-sprayed Thiokol, 0.035 in.	205	Coating pitted at cone apex, coating removed at cone-cylinder junction
12	Sandblasted	Flame-sprayed Thiokol, 0.035 in.	205	Coating pitted at cone apex, coating removed at cone-cylinder junction Severe adhesion failure of coating on cylindrical surface from leading edge

[a] Supplied by Naugatuck Chemical Division, U. S. Rubber Company (butadiene-acrylonitrile).
[b] Supplied by Gates Engineering Company.

Hypersonic Transducer Apparatus

This apparatus provides for the high-frequency vibration of a piezoelectric ceramic transducer bowl composing part of a fluid container. The high-frequency oscillation of the transducer develops a cavitation field at the focal point in the coupling fluid. A specimen is exposed at the focal point of the bowl in order to determine the extent of damage to the specimen in the cavitating field. The apparatus consisted of the following major assemblies: (*a*) Hypersonic generator (Brush Development Company Model BU204, serial 51B038, input 115 volt, 6.5 amp, 660 watt, 60 cycle, single phase; output 250 watt, 100–1000kc; tuning unit type B,

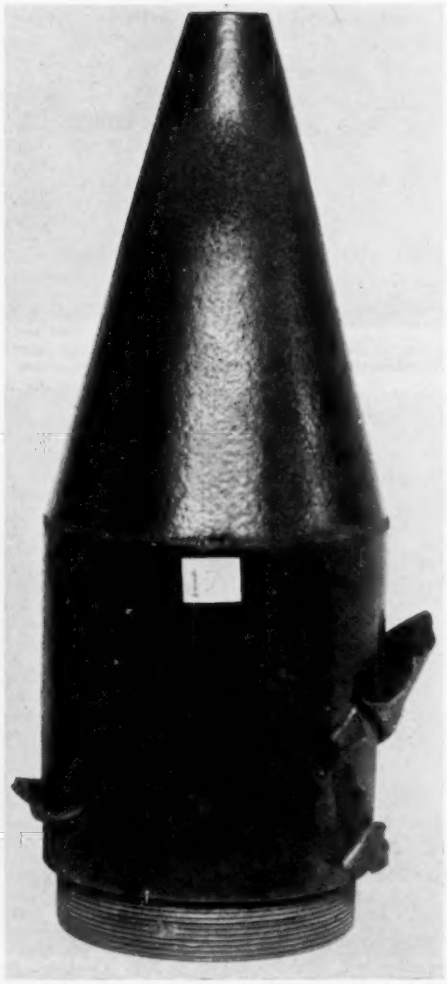

Fig. 4 Coated specimen 12 after test in Bureau of Reclamation water tunnel

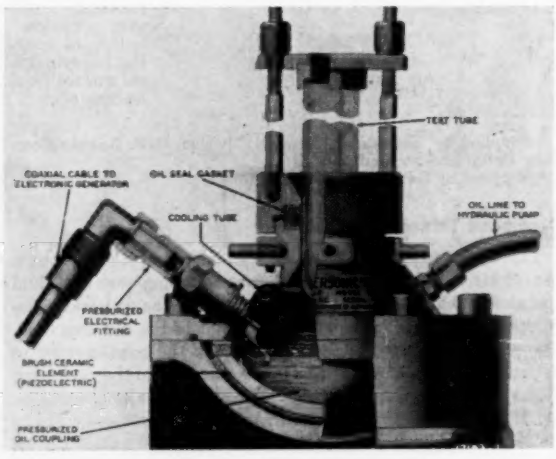

Fig. 5 Piezoelectric transducer assembly

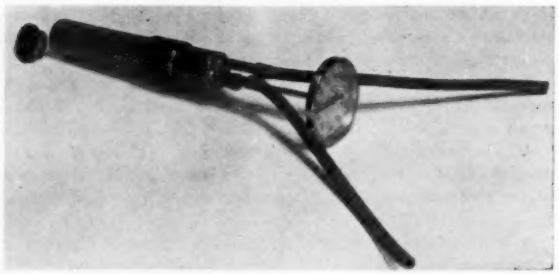

Fig. 6 Coated specimen and water-cooled specimen holder

serial 51B038, frequency range 300–1000 kc); (*b*) bowl-shaped piezoelectric transducer (Brush Development Company Model BU301; transducers of 400 kc, 700 kc, and 1000 kc were available; construction details are shown in Fig. 5); (*c*) pump (Brush Development Company Model BU901); (*d*) thermocouple potentiometer; (*e*) water-cooled specimen holder.

A specimen holder and specimen shown in Fig. 6 replaced the test tube shown in the previous illustration. The $^5/_8$-in-diam × $^1/_2$-in-thick specimen is similar to that used in the magnetostrictive vibratory apparatus described by Rheingans [23], and others [24–28]. The coupling fluid in the bowl remains essentially stationary despite pressure fluctuations in it. As a result, no significant fluid flow parallel to the metallic surface takes place, such as occurs in the service exposure of a ship's underwater structure.

Tests were made at resonance frequencies of 400 or 700 kc at atmospheric pressure and 5 psig using distilled and degassed (boiled) water as the coupling medium. The specimens included bare steel, aluminum, and brass, and eight coatings applied to steel specimens to a thickness of 0.025 in.

The bare aluminum and steel specimens were exposed horizontally, and also vertically, and at 15 deg from the vertical using a modified holder. The coated specimens were exposed in a horizontal position only. The temperature of the coupling medium varied from 104 to 140 F. The results of exposure of the bare and coated specimens are summarized in Tables 3 and 4.

Table 3 Results of tests of uncoated specimens using hypersonic transducer

Specimen material	Fluid pressure in test bowl	Time of exposure, hr	Frequency, kc	Damage
Aluminum	0 psig	$^1/_2$	400	Slight etching
Aluminum	0 psig	$^1/_2$	700	None
Mild steel	5 psig	$^1/_2$	400	Slight etching
Brass	0 psig	6–8	400	None

Table 4 Results of tests on coated specimens using hypersonic transducer operated at 400 kc and atmospheric pressure

Coating on steel specimen	Time of exposure, hr	Damage
Flame-sprayed Thiokol	$^1/_2$	None
Air-sprayed and cured Thiokol T74F1	$^1/_2$	Slight blistering
Nitrile liquid, coating 351	$^1/_2$	None
Nitrile liquid, coating 356	$^1/_2$	None
Neoprene liquid, heat cured	$^1/_2$	Slight blistering
Vinyl coating V-68-A	$^1/_2$	Blistering, plastic flow
Vinyl coating V-68-B	$^1/_2$	Plastic flow
Air-sprayed and cured Thiokol T74F2	$^1/_2$	Slight blistering

Conclusions. Although the hypersonic-transducer apparatus was able to cause slight etching of aluminum and steel specimens, erosion damage of the steel, brass, and coated-steel specimens was not obtained. Undesirable heating effects were shown by plastic flow and blistering of the coatings. In view of these factors and also the negligible fluid velocity relative to the specimen, the evaluation of cavitation-erosion resistance of base materials and coatings with this apparatus was not considered to be feasible. Plesset and Ellis [9] in similar investigations had used a ring-shaped piezoelectric transducer to induce cavitation damage in specimens located on the axis of the ring some distance from it, at 18 and 24 kc. The essential property of a material that determines its resistance to cavitation damage was found to be the fatigue resistance (resistance to plastic deformation or cold work) of the solid. Negligible flow of the water and no pumping action due to motion of the transducer were observed. Damage was determined photomicrographically and by means of x-ray analysis, and showed chemical effects to be at most of secondary significance in influencing cavitation-erosion damage.

Magnetostrictive Transducer Apparatus

This apparatus provides for the high-frequency vibration of a

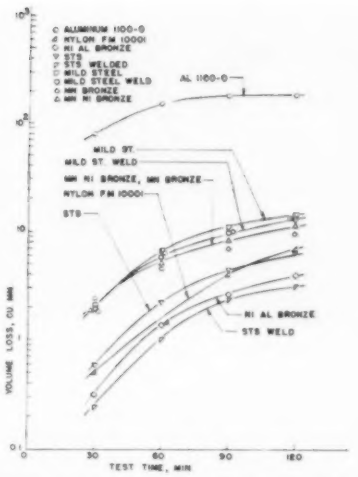

Fig. 7 Volume loss characteristics of magnetostrictive specimens

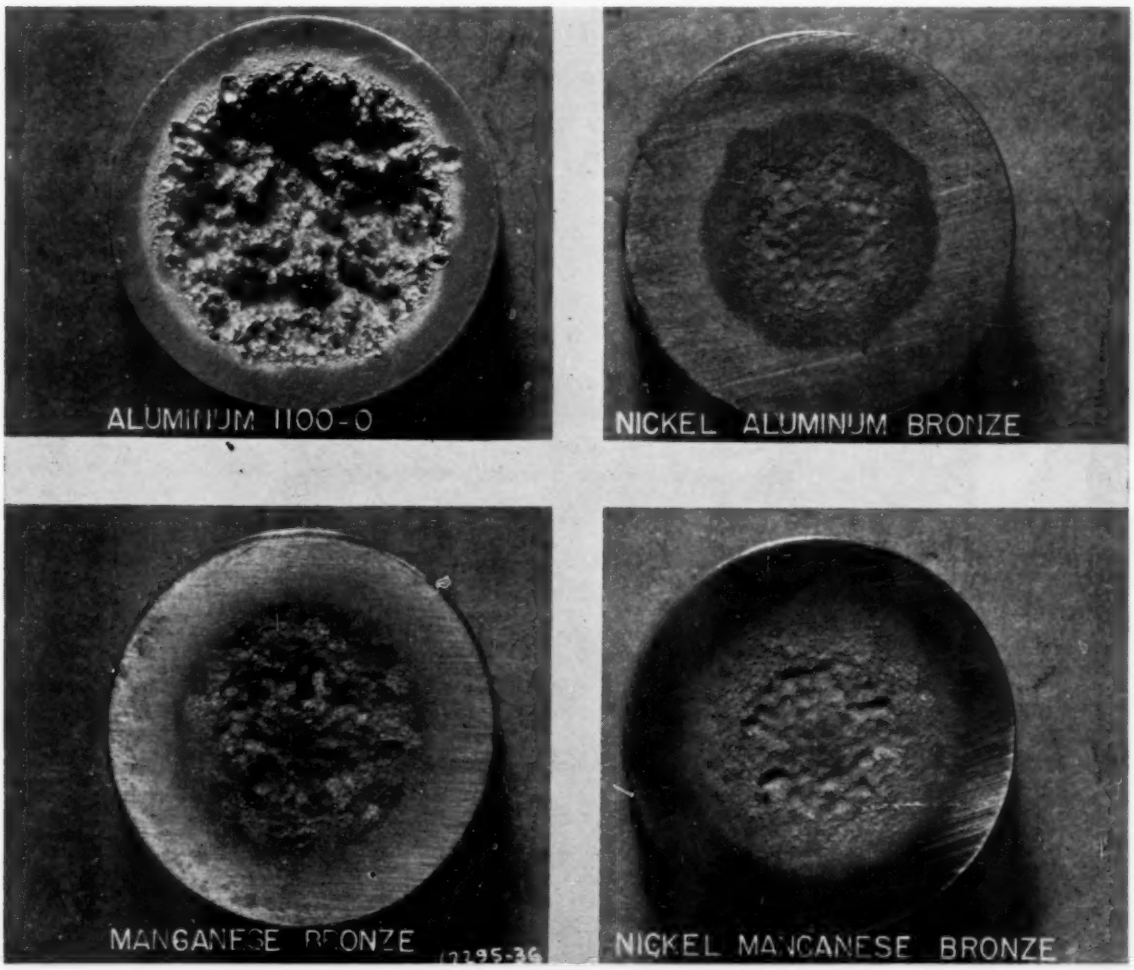

Fig. 8 Aluminum and bronze magnetostrictive specimens

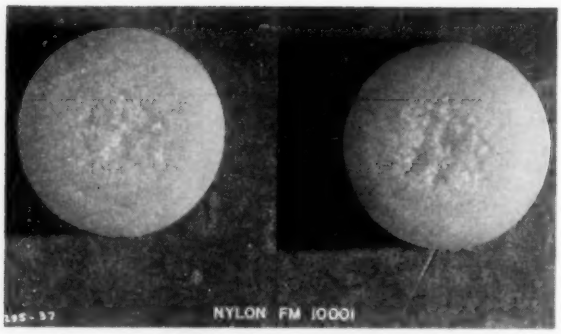

Fig. 9 Nylon FM10001 magnetostrictive specimens

specimen attached to a nickel tube which is caused to oscillate vertically in an oscillating magnetic field, as described by references [23–28]. The specimen is mounted on the lower end of the tube and is immersed in distilled water to a depth of $^1/_8$ in. during a test. The high frequency oscillation of the tube and specimen, similar to the oscillation of the piezoelectric transducer described previously, develops a cavitating field directly below the specimen, the collapse of the cavitating bubbles causing severe impact stresses on the specimen surface.

The apparatus used was located at the Hydraulics Laboratory of the Allis-Chalmers Manufacturing Company, Milwaukee, Wis. The nickel tube was 12 in. long × $^5/_8$ in. OD. The frequency of oscillation of the tube was 6500 cps, and the amplitude of oscillation of the specimen was 0.0034 in. The beaker-water temperature was maintained at 76 F ± 1 F. The specimens were made of STS, mild steel, manganese bronze, manganese-nickel bronze, nickel-aluminum bronze, nylon FM 10001, and aluminum 1100-0.

Several of the special treatment steel (STS) and mild-steel specimens were welded in the surface area to determine the relative resistance of the weld to cavitation-impact damage.

Specimens were tested for a 2-hr period, weight measurements of the specimen being taken after each 30 minutes. Volume-loss characteristics of the various specimens are shown in Fig. 7. These values were calculated from measured-weight values and the specific gravities of the materials. The appearance of the cavitated surfaces of several of the specimens is shown, Figs. 8 and 9.

Conclusions. These tests showed the suitability of the apparatus for use in evaluating the relative resistance of materials to cavitation-erosion damage, as previously indicated by Rheingans [23], Kerr [26], and Schumb, Peters, and Milligan [27]. The resistance of the materials to cavitation erosion is not related directly to hardness; nylon, having the lowest hardness, showed very good resistance to cavitation erosion, following STS weld metal and nickel-aluminum bronze.

The velocity of the fluid relative to the specimen in the apparatus is small, similar to the fluid conditions existing in the piezoelectric-transducer apparatus described previously. Rasmussen [4], Knapp [6, 7], Beeching [13], and deHaller [29] have indicated that the rate of the cavitation erosion of a guiding surface in a cavitating fluid is dependent on the relative fluid velocity.

Since the relative erosion rates of different materials may vary with cavity-collapse intensity, the applicability of the magnetostrictive apparatus in evaluating the resistance of materials to be used under specific service conditions of velocity and pressure would depend on the velocity-erosion rate characteristics of different materials and the velocity range of operation of the magnetostrictive apparatus.

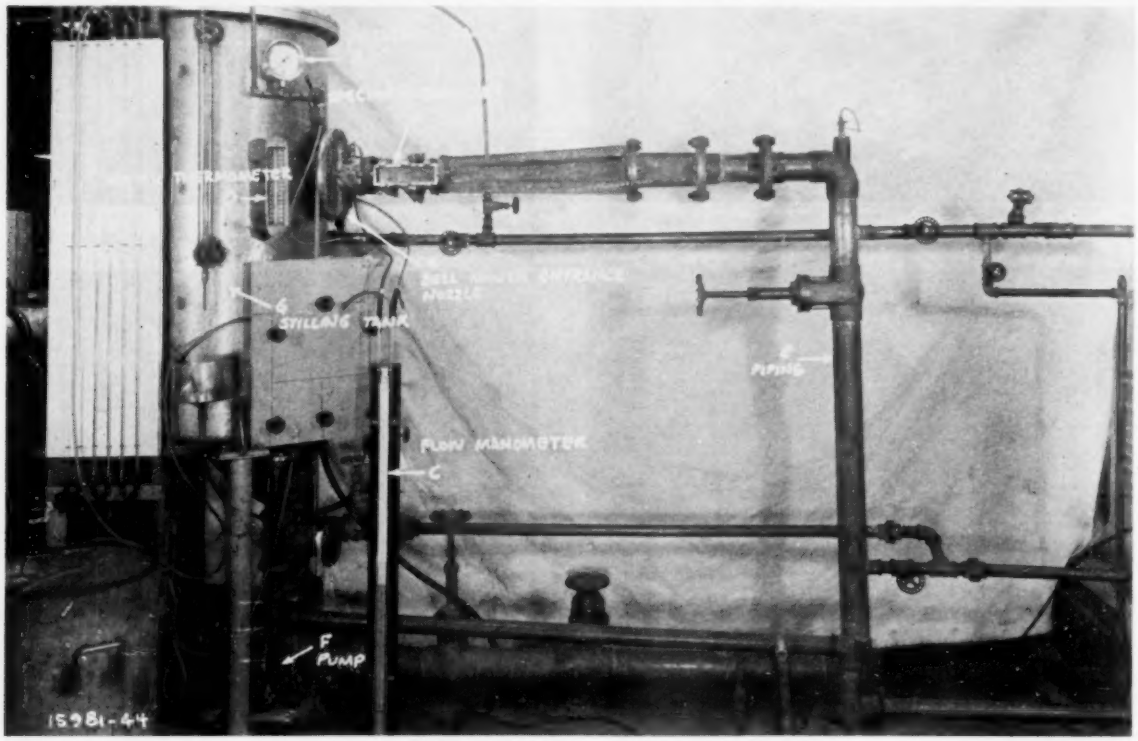

Fig. 10 Taylor Model Basin small size water tunnel

Taylor Model Basin Small Size Water Tunnel

This apparatus, Fig. 10, was designed and constructed by the David Taylor Model Basin (DTMB), Carderock, Md. It provides for flow of a fluid through a specimen chamber containing a stationary specimen, in a closed recirculating system. The apparatus permits control of water pressure up to 15 psig by means of air applied to the fluid system in the 94-gal stilling tank.

The fluid-flow rates in the specimen chamber were determined with a mercury manometer, *C*, attached to taps in the bell-mouth entrance nozzle, *H*. Internally, the specimen chamber *A*, Fig. 10, measured 0.9 in. wide by 1.75 in. high in cross section by 9 in. long. The pump, *F*, was a distiller circulating pump manufactured by the Aldrich Pump Company, Allentown, Pa. It was rated at 100 gpm, 110 volt dc, 25 psi head, 3500 rpm, 2.28 hp.

Cavitation Tests of Bar Specimens. Cavitation tests were made using bar-shaped specimens usually $^1/_2$ in. high by 0.9 in. wide by $5^3/_4$ in. long, mounted in the chamber as shown in Fig. 11, the quarter-rounded end being upstream. This resulted in a throat 1.25 in. × 0.9 in. cross section at the specimen. Cavitation occurred in the throat adjacent to the specimen downstream from

Fig. 11 Bar-shaped specimen mounted in specimen chamber of water tunnel

the rounded nose as shown. Air pressure in the stilling tank was adjusted to cause cavitational collapse in a 1-in. region downstream from the specimen nose, the downstream end of the cavity moving upstream (shortening) with increase in pressure and downstream (lengthening) with decrease in pressure. The time of each run was 72 hr with a few exceptions. The water temperature increased with time during each test from approximately 60

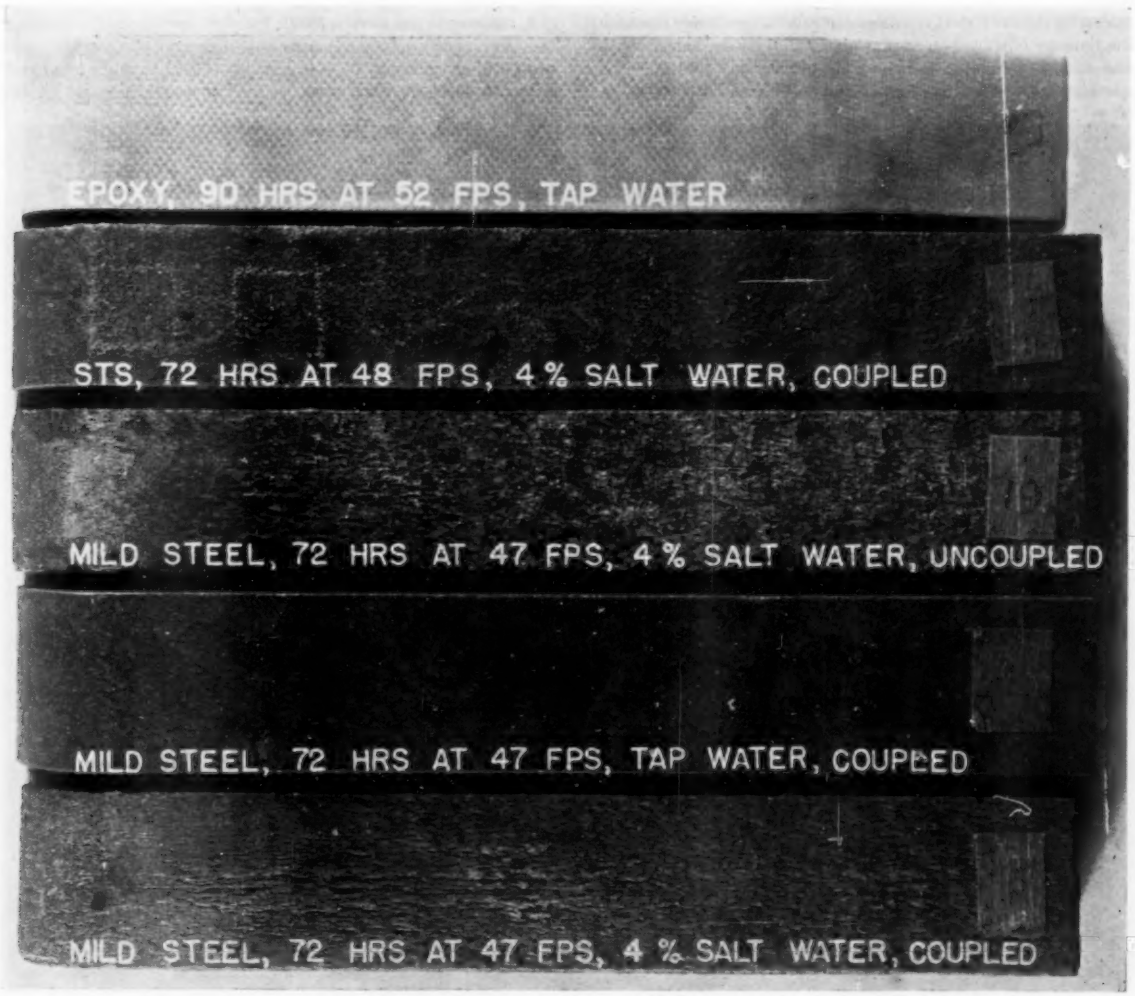

Fig. 12 Typical bar-shaped specimens after test

F initially to 120 F after 72 hr. As the length of the cavitating region tended to increase with increase in temperature (increase in vapor pressure) of the fluid, it was necesary to increase the fluid pressure during a run at a given flow rate to maintain a constant-cavitating-region length.

The specimens included mild-steel, STS, cartridge-brass, commercial-brass, and glass-reinforced-epoxy materials as listed in Table 5. The effects of the following factors on the nature and degree of damage of the specimens were studied: (*a*) Specimen material; (*b*) fluid type and velocity; (*c*) coating of specimen; (*d*) presence or absence of fluid cavitation; (*e*) time of specimen exposure; and (*f*) uncoupling of specimens from the brass walls of the chamber.

The degree and nature of damage to representative specimens after removal of corrosion products obscuring the base material are shown in Fig. 12.

Brass specimens are not illustrated; in the tests they showed over-all tarnishing in fresh water and dezincification in 4 per cent salt water. Suppression of cavitation decreased only slightly the damage of steel and brass specimens. Uncoupling of steel specimens from the brass chamber wall did not materially affect the nature or decrease the extent of corrosion. The corrosion sustained by the bare steel specimens in salt water closely resembled the damage observed on similar material of struts, barrels, skegs, and rudders of ships operating in salt water. Coating of the specimen prevented damage of the mild steel substrate completely. The damage sustained by the brass and steel specimens in salt water was not similar in appearance to the localized erosion damage sustained by propellers as shown in Fig. 3.

Conclusions. The DTMB water-tunnel apparatus is apparently unsuited for use in evaluating the cavitation-erosion resistance of metallic or plastic materials or protective coatings at fluid velocities up to approximately 50 to 60 fps. Damage to the test specimens was primarily dependent on the corrosion-resistance characteristics of the particular materials, galvanic corrosion, and velocity, corrosive nature, and erosion (scrubbing) effects of the cavitating fluid. The cavitating region of the fluid in the water tunnel served only to accelerate the corrosion damage of those specimens basically susceptible to such damage.

Rotating-Disk Apparatus

The last apparatus used in this investigation, shown in Fig.13, provides for the rotation of a 12-in-diam disk within a water-filled chamber under controlled conditions of pressure and disk velocity. By the use of stilling vanes on each side of the disk this apparatus minimizes the tendency of the water within the chamber to rotate with the disk.

A cross-sectional view through the disk test chamber, showing the clearances between a $^1/_8$-in-thick disk and the rear and forward stilling vanes, is given in Fig. 14. Disks 12 in. in diam and either $^1/_4$ or $^1/_2$ in. thick were used. The central position of the

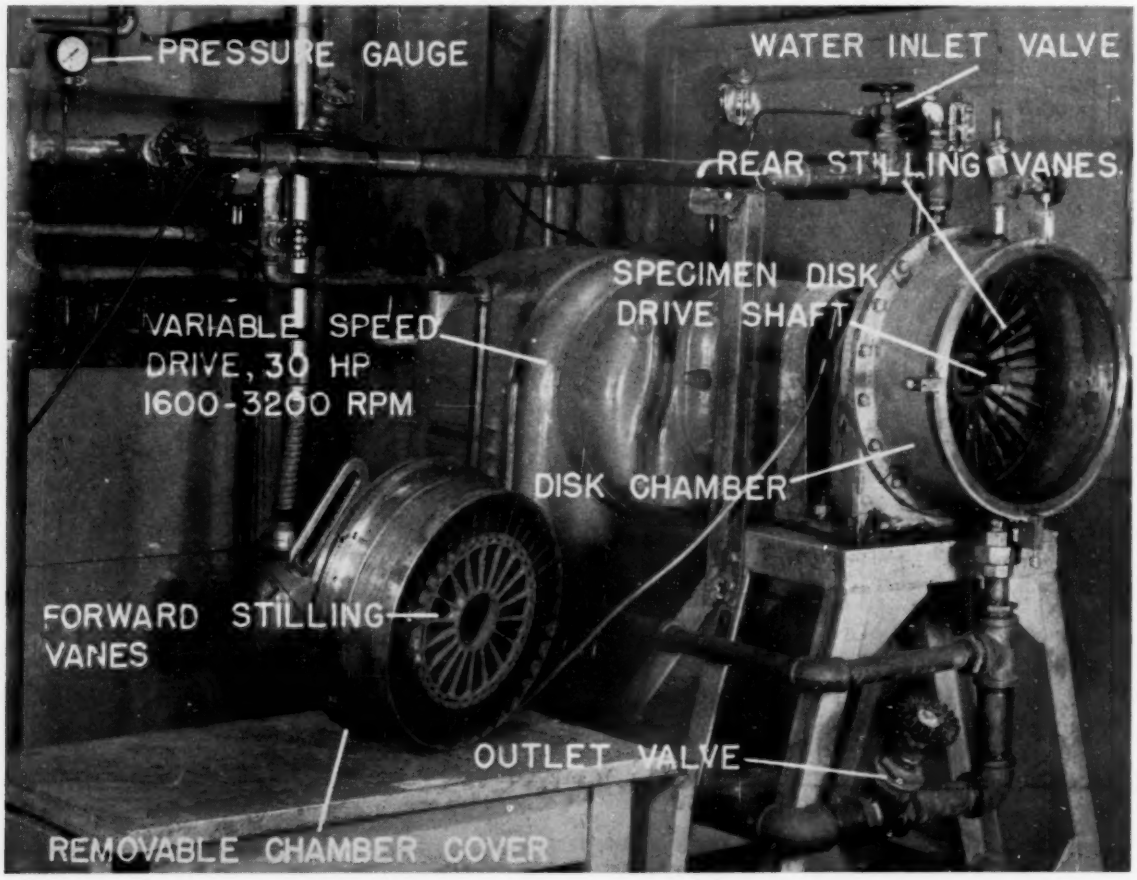

Fig. 13 Rotating-disk apparatus with test chamber opened

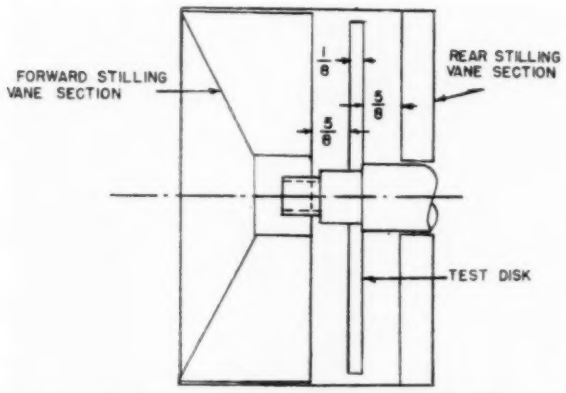

Fig. 14 Clearances between test disk and stilling vanes of rotating-disk apparatus

disk between the stilling vanes is achieved by placing spacer rings between the disk and the shaft shoulder behind it. The disk rotated counterclockwise looking toward the motor in Fig. 13. The water pressure in the chamber was regulated by opening the inlet valve fully and adjusting the outlet valve. Either tap water from building supply or salt water from the DTMB stilling tank was used as desired. Tap water was used in open flow, being dumped to the drain after leaving the chamber; salt water was recirculated through the stilling tank without cooling. A similar rotating-disk apparatus had been used by Rasmussen [4] in evaluating cavitation erosion on the surface of a disk downstream from holes drilled near the periphery of the disk.

Preliminary Tests. A series of preliminary tests using the apparatus and mild-steel disks was made in order to establish standard disk designs necessary to obtain reproducible cavitation-erosion damage and apparatus operating conditions. These studies involved: (*a*) Efficiency of wedges ($^1/_{32}$ to $^1/_8$ in. high) in the disk surfaces, Fig. 15, as surface irregularities to cause cavitation in the fluid; (*b*) different disk thicknesses ($^1/_8$ to $^1/_2$ in.); (*c*) efficiency of holes in the disk as surface irregularities causing cavitation in the fluid ($^1/_4$ to $^5/_8$ in. diam located at radial positions of 2.15 in. to 5.36 in.); (*d*) water pressure, 5 to 15 psig; and (*e*) disk speed, 1600 to 3200 rpm.

Table 5 DTMB water tunnel specimen test conditions

Material	Water	Coupled to wall	Water pressure, psig	Test duration, hr	Water velocity at specimen, fps
Mild steel	Fresh	Yes	7	72	47
Mild steel	4% NaCl	Yes	7	72	47
Mild steel (neoprene coated)	4% NaCl	Yes	7	72	47
Mild steel	4% NaCl	No	7	72	47
Mild steel	4% NaCl	Yes	9	72	45 (No fluid cavitation)
STS	Fresh	Yes	8	72	47
STS	4% NaCl	Yes	9	72	48
STS	4% NaCl	No	7	72	47
Cartridge brass	Fresh	Yes	6	6	48
Cartridge brass	Fresh	Yes	6	72	48
Commercial brass	4% NaCl	Yes	7	72	48
Commercial brass	4% NaCl	Yes	7	72	44 (No fluid cavitation)
Epoxy	Fresh	...	10	90	52
Epoxy	Fresh	...	11.6	72	60

As a result of these studies a disk having a thickness of $^1/_8$ in., a diameter of 12 in., and having $^3/_8$-in-diam holes located as shown in Fig. 16 was adopted as the standard test specimen. Standard test conditions were established as follows:

Disk velocity: 3200 rpm (The cavity region decreases in size with decrease in relative fluid-disk velocity.)
Water pressure: 15 psig (The cavity region decreases in size with increase in pressure.)

The fresh tap-water temperature was not controlled, entering the chamber at approximately 60 F and leaving the chamber (to

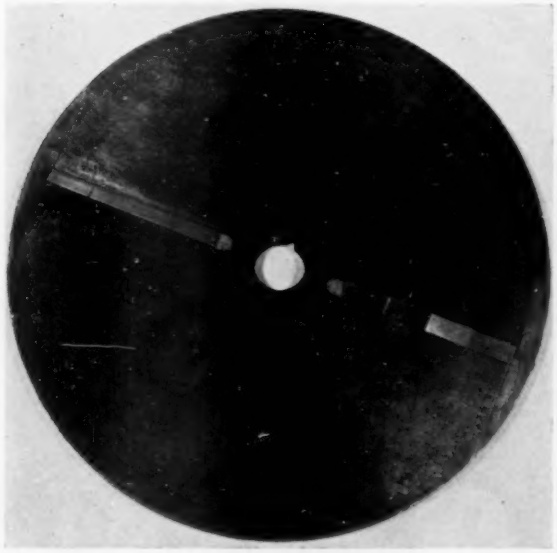

Fig. 15 Disk No. 3 having radially removable wedges

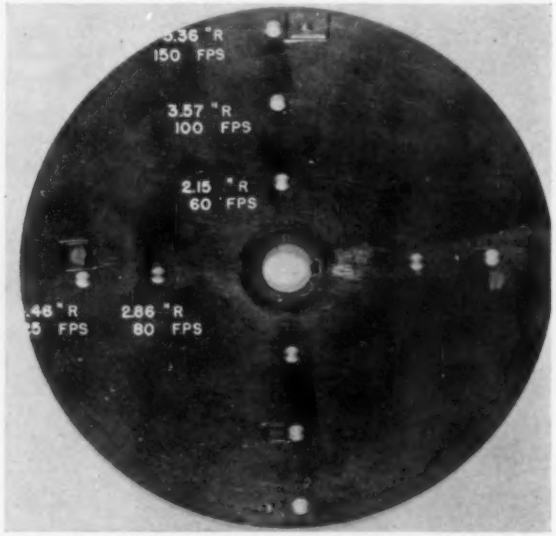

Fig. 16 Typical rotating-disk specimen after test

drain) at 110 to 120 F. The water flow rate was 2.8 gpm. Under these conditions the cavitation region at the 5.36 in. radial location was approximately 1 in. long as observed through recently installed viewing ports, Fig. 17, with the aid of a General Radio Strobatac.

Disks of a number of different materials listed in Table 6 including mild steel, commercial brass, Thiokol-coated mild steel, polyvinyl chloride, stainless steel, polyester-glass laminate, epoxy-glass laminate, styrene-acrylonitrile, aluminum 1100-0, STS, nylon (Zytel 101), Teflon sheeting on mild steel, and three bronzes were tested. The test-duration time was varied from 0.1 hr to 90 hr because of differences in resistance of the individual materials to cavitation-erosion damage. Tests were made in fresh water except for one mild steel disk, *V*, which was tested in 4 per cent salt water.

The nature of the damage sustained by the disks is shown in Figs. 18–21. The damaged areas shown in these enlarged views were located downstream from one of the holes of the respective disks, and occurred at a linear velocity of 150 fps. The damaged areas of the metallic disks are seen to be granular in appearance resembling the erosion observed on some propellers as shown in Fig. 3. Scouring associated with corrosion was absent. The aluminum 1100-0 disk showed numerous small surface depressions at the outer margins of the damaged area, and raising of the metal above the surface at the inner margins of the damaged area, indicative of severe impinging forces.

The loss of disk material downstream from the $^3/_4$-in-diam holes as a result of exposure in the rotating-disk apparatus was measured after the exposure period. The method was a gravimetric one in which a filler material was troweled into an eroded cavity from a weighing bottle until just level with the surface of the disk. The weight of filler material applied, directly related to the eroded volume, was then determined by difference in weight of the bottle and contents. Several filler materials including water (containing surfactants), glycerine, petrolatum, silicone grease

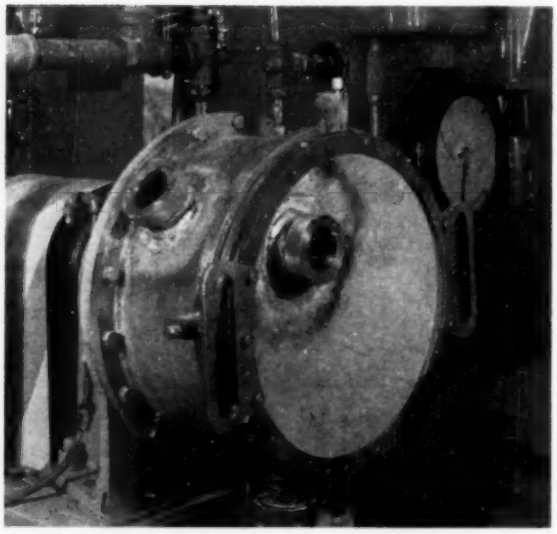

Fig. 17 Viewing ports of rotating-disk chamber

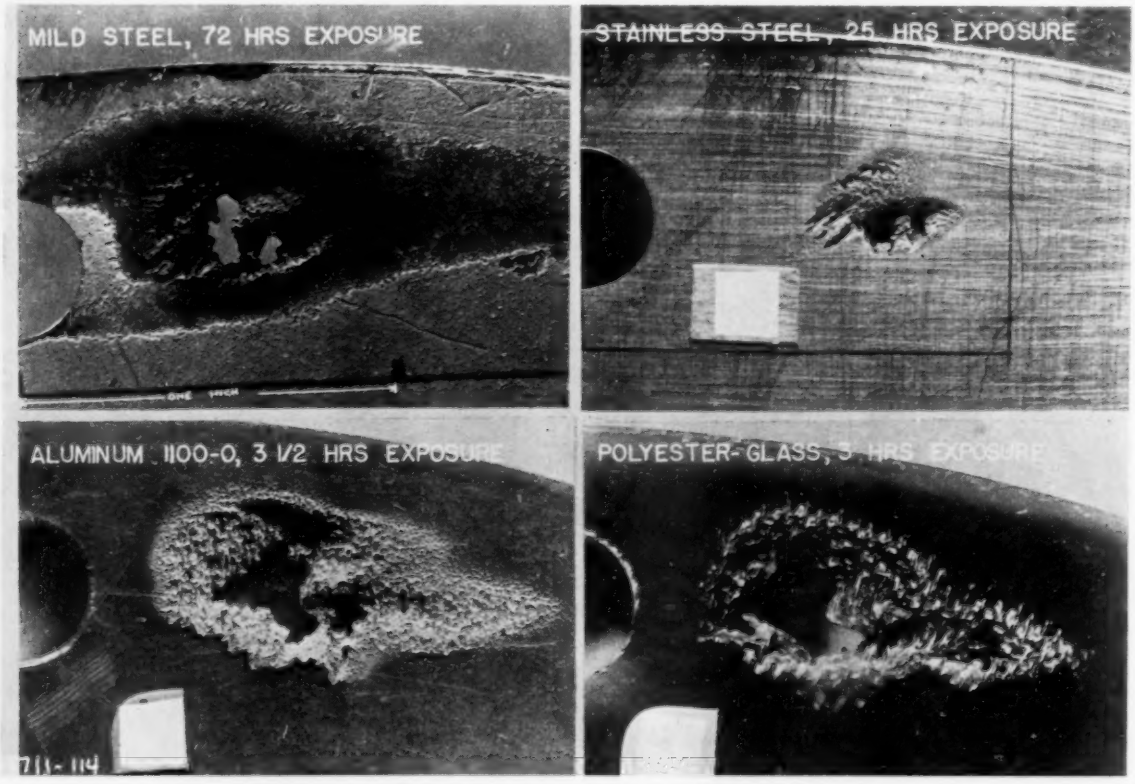

Fig. 18 Damage to mild steel, stainless steel, aluminum 1100-0, and polyester-glass

Table 6 Description of rotating-disk specimens

Disk code	Disk material	Material supplier	Test duration, hr
E	Mild steel, SAE 1016	Navy stock	72
F	Commercial brass, hard	Navy stock	72
J	Mild steel, Thiokol-coated	Navy stock	24
K, L	Polyvinyl chloride (PVC)	Navy stock	8
M	Stainless steel, AISI type 304	Navy stock	25
N	Polyester-glass laminate, 181 style glass cloth	Lunn Laminates, Inc.	3
O	Epoxy-glass laminate, GE Textolite 11546, style 112 cloth	General Electric Co.	3
P	Epoxy-glass laminate, GE Textolite 11546, style 112 cloth	General Electric Co.	51[a]
Q	Epoxy-glass laminate, GE Textolite 11546 style 112 cloth	General Electric Co.	90[b]
R	Styrene - acrylonitrile, Boltron 63	Bolta Corp.	0.4
S	Styrene - acrylonitrile, Boltron 63	Bolta Corp.	1
T	Aluminum 1100-0	Navy stock	3.5
U	Aluminum 1100-0	Navy stock	0.1
V	Mild steel, SAE 1016	Navy stock	3[c]
AT	Special - treatment steel (STS) (Spec MIL-S-890)	Navy stock	72
AS	Nylon (Zytel 101)	du Pont	4.9[d]
AN, AP	Teflon sheet (0.030 in. thick) on mild steel	Garlock Packing	5
AO, AQ	Teflon sheet (0.060 in. thick) on mild steel	Garlock Packing	5
AH, AI	Mn Bronze	Bethlehem Steel	72
AJ, AK	Mn-Ni Bronze	Bethlehem Steel	72
AG	Ni-Al Bronze	Bethlehem Steel	72

[a] Disk velocity 1600 rpm.
[b] Maximum hole centerline radius 3.6 in. No holes at 4.5, 5.4 in. centerline radii. No cavitation erosion.
[c] Salt water (4 per cent NaCl), recirculated. Temperature range 60 F initial, 160 F final.
[d] Test discontinued because of warp of disk. No cavitation erosion.

DC7, and putty compound (specific gravity 2.14) were evaluated before the latter material was adopted for use in this operation. After determining the eroded volume as described, the filler material was removed from the cavity with a probe. The disk was then brushed with methyl isobutyl ketone or warm soapy water to clean the damaged area in those instances where the disk material might be attacked by the solvent.

Volume erosion characteristics of several disk materials are shown in Figs. 22–24. The degree of erosion increases with in-

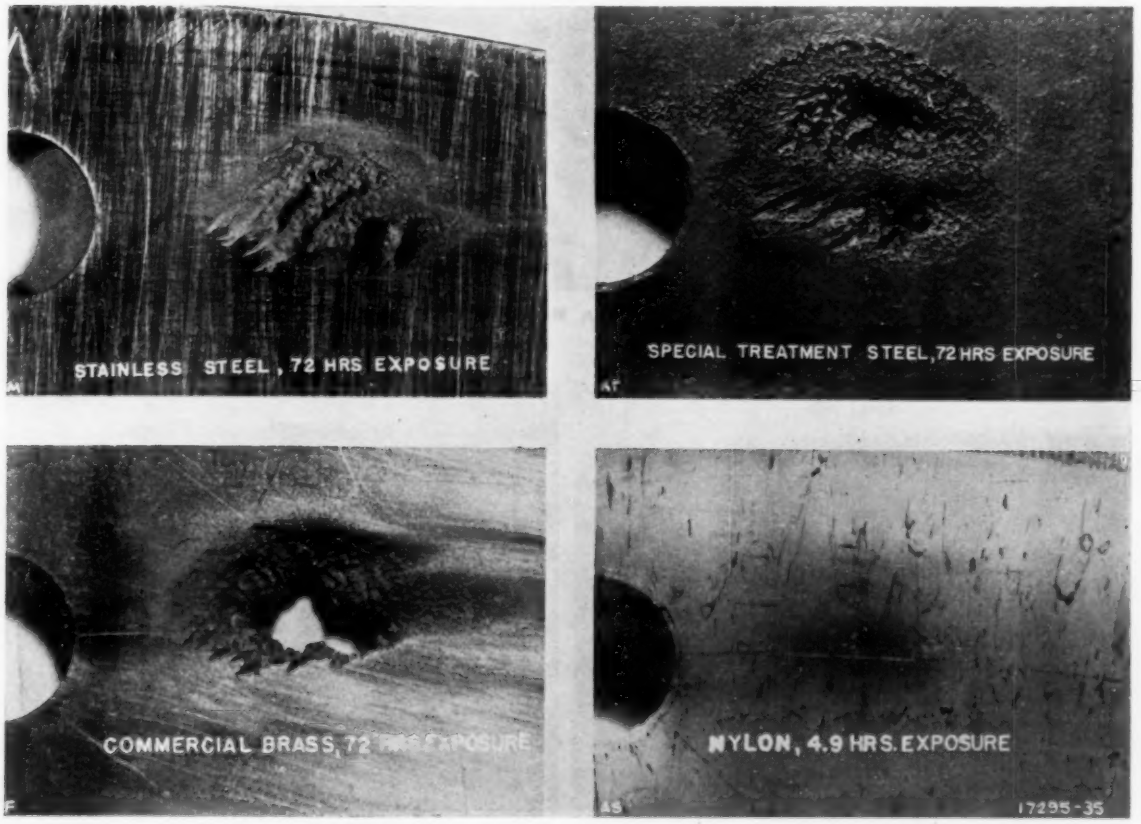

Fig. 19 Damage to stainless steel, STS, commercial brass, and nylon

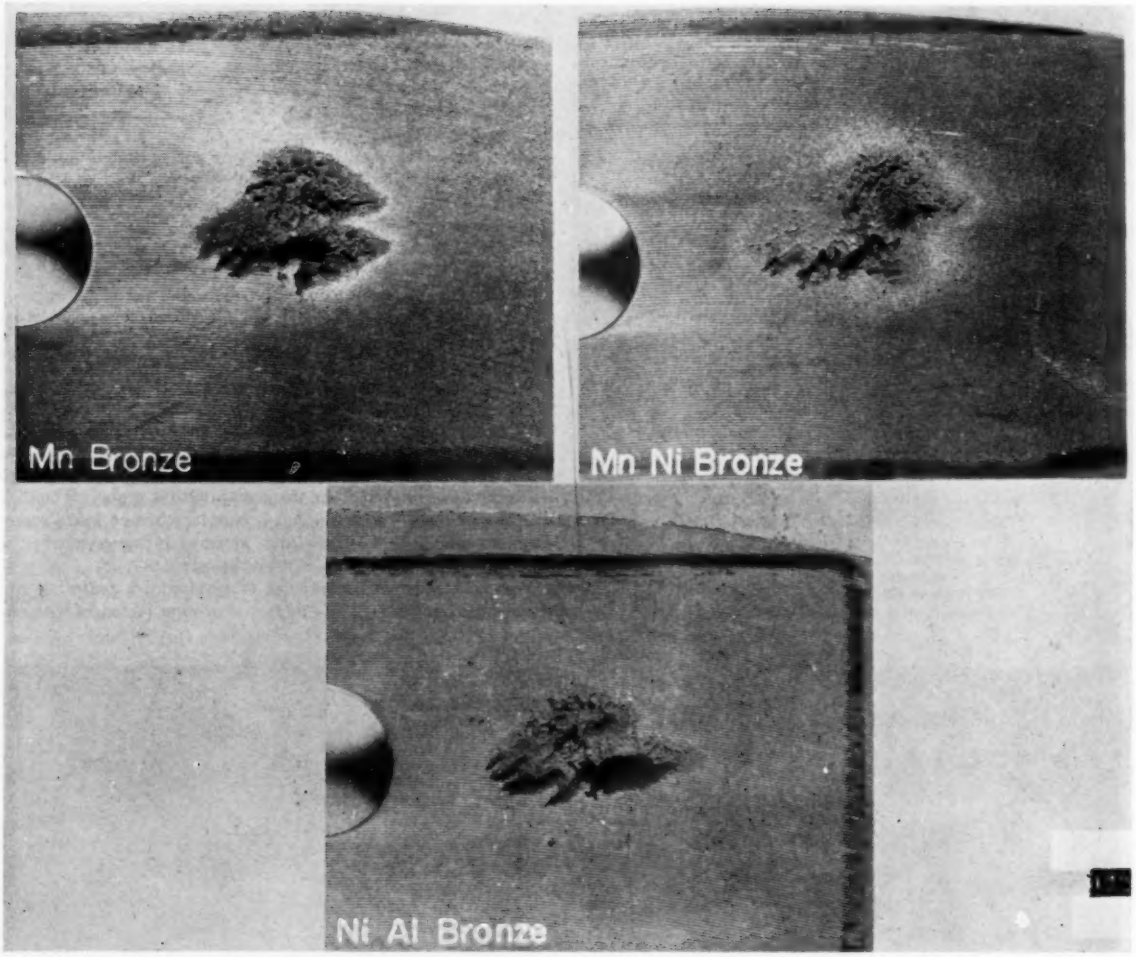

Fig. 20 Damage to Mn, Mn-Ni, and Ni-Al bronzes

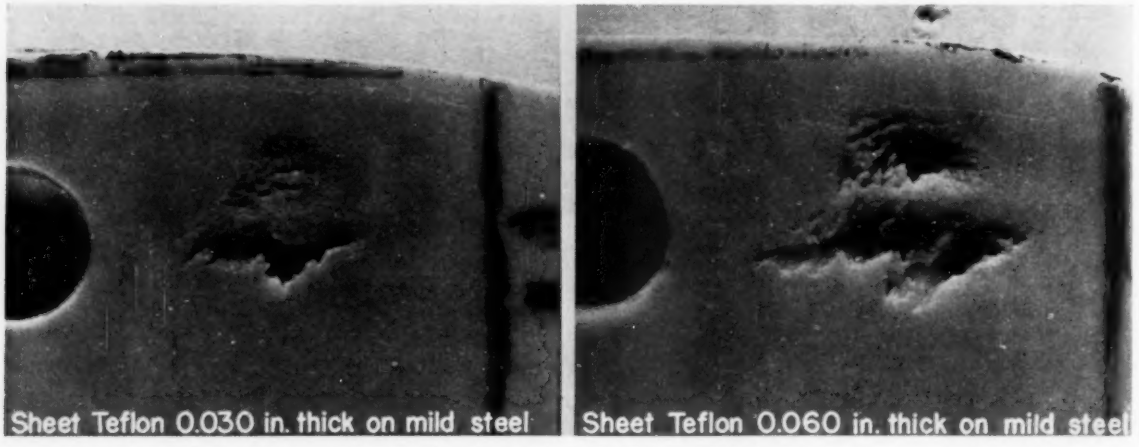

Fig. 21 Damage to Teflon sheeting on mild steel

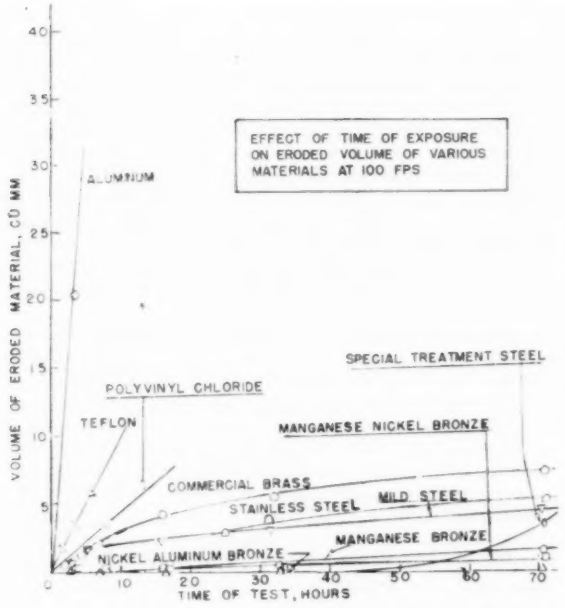

Fig. 22 Volume erosion characteristics at 100 fps

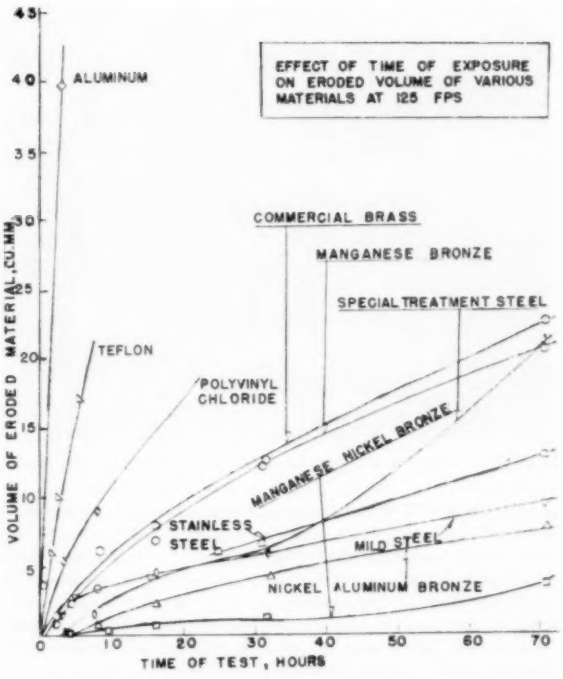

Fig. 23 Volume erosion characteristics at 125 fps

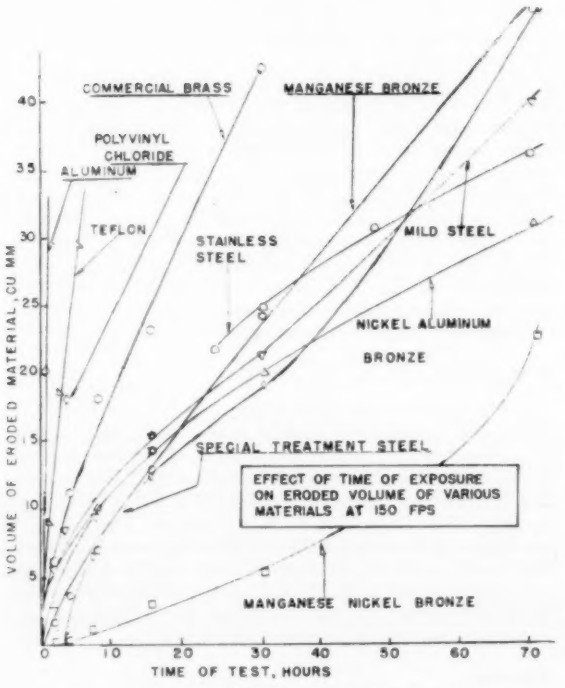

Fig. 24 Volume erosion characteristics at 150 fps

crease in velocity, and is dependent on the nature of the material, although the corrosion (chemical) resistance is considerably less significant than the physical (dynamic fatigue) characteristics. The degree of erosion increases with exposure time at a given velocity while the threshold velocity (velocity below which measurable erosion is not obtained) decreases with increase in exposure time. These factors are also dependent on the material used.

The damage sustained by a mild-steel disk in salt water after 3 hr exposure at 150 fps is shown in Fig. 25. The metal in the entire cavitation region after the exposure period was bare of corrosion products. Corrosion products in areas of the disk outside the cavitation regions were largely undisturbed. Corrosion pitting in the direction of rolling of the material occurred largely in area *B* at the boundary of the cavitation region as well as other areas in the cavitation region. Cavitation erosion occurred in a small area within the cavitation region and to a considerably greater degree than the corrosion attack. Measurements of the erosion volumes of mild steel at 150 fps, showed a slightly higher rate in salt water than in fresh water, probably due to the added effect of corrosion attack. At lower velocities there was no apparent corrosion influence on cavitation-erosion rates, the rates being the same in fresh water and in salt water.

Conclusions. The erosion characteristics of various materials at 125 and 150 fps, Figs. 23 and 24, do not show the same order of erosion resistance as that shown in Fig. 7 in tests with the magnetostrictive apparatus. However, at 100 fps and for periods up to 40 hr, Fig. 22, the erosion rating of materials is more nearly comparable with that found in the magnetostrictive tests. Refinement of the technique of measurement of the erosion volume obtained with the rotating-disk apparatus may permit a more exacting evaluation of this correlation as the erosion volumes are small within this time period. Several alternate techniques are presently being studied.

The lack of correlation at the higher velocities in the rotating-disk apparatus may be related to a variation of dynamic-impact fatigue, rate of crack growth, and other characteristics of the different materials. These factors influence the rate of material erosion and may vary with rate and intensity of impact stresses

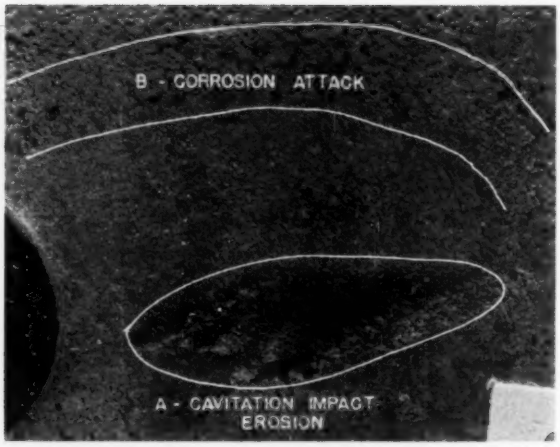

Fig. 25 Damage of mild-steel disk in 4 per cent salt water at 150 fps

associated with different rotational velocities and operating conditions (fluid temperature, pressure, vapor pressure, and so forth). As indicated previously it is important in any simulated test to attempt to duplicate exact conditions existing in service or to know the effect of variation of conditions on performance. Difficulties may arise if service conditions are not known precisely or if the effect of variation of test conditions from service conditions on performance are not known fully.

Summary

Five types of apparatus have been studied to determine their relative merit in evaluating the resistance of coatings and metallic and nonmetallic substrates to fluid-cavitation erosion. Two of these, a magnetostrictive transducer and a rotating-disk device, have been found to be suitable for this purpose although different materials do not show the same order of erosion resistance under all test conditions used.

The relationship between fluid velocity and degree of cavitation erosion discussed by previous investigators [4, 6, 7, 11, 12, 30] has been confirmed by the present studies. This relationship is shown qualitatively in Fig. 26 together with the velocity ranges in which different investigations were made. Cavitational-impact damage to specimens evaluated in the Bureau of Reclamation water tunnel was achieved to a minor degree on the conical surface of coated specimens at stream velocities of 70 fps (42 knots). Cavitation-erosion damage was also obtained in the rotating-disk apparatus using disks of various materials operating at approximate velocities of 80 fps (48 knots) and at 15 psig. Finally, comparable cavitation-erosion damage was not obtained in the DTMB water tunnel on a variety of materials at velocities up to 60 fps (36 knots) either in fresh water or in salt water. On the other hand, considerable corrosion damage of mild-steel and STS specimens was obtained in the DTMB tunnel using salt water at velocities of 48 fps (28 knots).

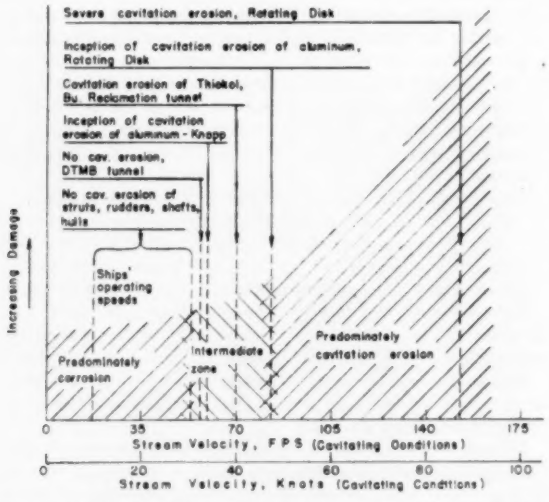

Fig. 26 Relationship between fluid velocity and corrosion and cavitation-damage of guiding surfaces

As the minimum velocities associated with cavitation erosion indicated above exceed the present service velocities of naval vessels it is probable that damage to underwater structures, Figs. 1 and 2, was not caused by cavitation erosion but rather by corrosion of the bared metal accelerated by the turbulence occurring in a cavitating region. Fig. 26 summarizes generally this conclusion and the substantiating experimental sources, showing the velocity regions within which corrosion (accelerated by cavitation turbulence) or cavitation-impact fatigue is a primary cause of damage.

The use of suitable protective coatings is effective in preventing corrosion damage to a metal in a corrosive environment. Deficiencies of these materials in service have been due largely to low adhesive strength of the coating to the substrate, resulting in failures under high hydraulic stresses. Improvement in adhesive strength and other physical properties of coatings by better application procedures, metal preparation, and improved coating materials (body coats and adhesives) would effectively improve their serviceability.

Although it has been shown that damage to the underwater appendages and structures of naval vessels is primarily due to corrosive action, damage to other ships' components such as propellers, high speed pump impellers, and turbine components is due largely to cavitation-impact fatigue and erosion. The magnetostrictive and rotating-disk apparatus are useful in evaluating structural materials such as metals, plastics, spray weld coatings, or elastomeric protective coatings for such service. These types of apparatus will also be suitable for evaluating materials used in construction of ships' underwater structures such as struts and rudders when ship speeds are increased to those at which cavitation-impact damage will become significant.

Acknowledgments

The authors acknowledge the assistance of M. J. Berg of the Material Laboratory and E. A. Bukzin of the Bureau of Ships, Department of the Navy, Washington, D. C., for their technical advice during the progress of the investigation. The assistance of J. P. Craven and S. F. Crump of the David Taylor Model Basin and W. A. Price, J W. Ball, N. R. Spindler, and W. T. Moran of the Bureau of Reclamation, Denver Federal Center in arranging for the use of their water-tunnel apparatus, and W. J. Rheingans, J. F. Roberts, and J. R. Watson of the Allis-Chalmers Manufacturing Company for the use of the magnetostrictive-transducer apparatus is also gratefully acknowledged.

References

1 "Review of Published Information on Cavitation Erosion," Admiralty Corrosion Committee Report ACC/26/54, N151/54, H316/54 (CML Report FBS), October 8, 1954.

2 P. Eisenberg, "On the Mechanism and Prevention of Cavitation," David Taylor Model Basin Report No. 712, July, 1950.

3 E. G. Richardson, "Cavitation in Liquids," *Endeavor*, vol. 9, July, 1950, p. 149.

4 R. E. H. Rasmussen, "Experiments on Flow With Cavitation

in Water Mixed With Air," *Transactions of the Danish Academy of Technical Sciences*, no. 1, 1949.

5 J. M. Mousson, "Pitting Resistance of Metals Under Cavitation Conditions," TRANS. ASME, vol. 59, 1937, pp. 399–408.

6 R. T. Knapp, "Present Status of Cavitation Research," *Mechanical Engineering*, vol. 76, 1954, pp. 731–734.

7 R. T. Knapp, "Recent Investigations of the Mechanics of Cavitation and Cavitation Damage," TRANS. ASME, vol. 77, 1955, pp. 1045–1054.

8 J. C. Hunsaker, "Cavitation Research," *Mechanical Engineering*, vol. 57, 1935, pp. 211–216.

9 M. S. Plesset and A. T. Ellis, "On the Mechanism of Cavitation Damage," TRANS. ASME, vol. 77, 1955, pp. 1055–1064.

10 L. C. Burrill, "Sir Charles Parsons and Cavitation," *Transactions of the Institute of Marine Engineers*, vol. 63, 1951, pp. 149–167.

11 P. deHaller and J. Ackeret, "Über die Zerstörung von Werkstoffen durch Tropfenschlag und Kavitation," *Schweizerische Bautzeitung*, vol. 108, 1936, p. 105.

12 A. J. Stepanoff, "Cavitation in Centrifugal Pumps," TRANS. ASME, vol. 67, 1945, pp. 539–552.

13 R. Beeching, "Selecting Alloys to Resist Cavitation Erosion," *Product Engineering*, vol. 19, 1948, p. 110.

14 W. H. Wheeler, "Mechanism of Cavitation Erosion," Department of Scientific and Industrial Research, Mechanical Engineering Research Laboratory, Fluids Report No. 44, March, 1956.

15 G. Petracchi, "Investigation of Cavitation Erosion," *La Metallurgia Italiana*, vol. 41, 1949, p. 314.

16 E. Galtung, "Study of Causes of Surface Damages of Ships Propellers," *Journal of the American Society of Naval Engineers, Inc.*, 1953, p. 389.

17 S. E. McCrary, "Discussion of Paper on the Effects of Shot Peening on Damage Caused by Cavitation," American Society for Testing Materials, Bulletin no. 186, 46 (TP188) (December, 1952).

18 "Bureau of Reclamation Venturi Type Cavitation Apparatus," Material Laboratory, New York Naval Shipyard Project 4759-14, part 2, Final Report of June 2, 1954.

19 "Taylor Model Basin Small Size Water Tunnel Cavitation Apparatus," Material Laboratory, New York Naval Shipyard Project 4759-14, part 7, Final Report of October 10, 1955.

20 S. F. Crump, "Determination of Critical Pressures for the Inception of Cavitation in Fresh and Sea Water as Influenced by Air Content of the Water," David Taylor Model Basin Report 575, October, 1949.

21 "Rotating Disk Cavitation Apparatus," Material Laboratory, New York Naval Shipyard Project 4759-14, part 1, Progress Report 3, September 8, 1954.

22 "Resistance of Protective Coatings to Cavitation Erosion," Bureau of Reclamation, Denver, Colo., report 293, June 19, 1953.

23 W. J. Rheingans, "Accelerated Cavitation Research," TRANS. ASME, vol. 72, 1950, pp. 705–724.

24 N. Gaines, "A Magnetostriction Oscillator Producing Intense Audible Sound and Some Effects Obtained," *Physics*, vol. 3, 1932, pp. 209–229.

25 J. C. Hunsaker, "Progress Report on Cavitation Research at Massachusetts Institute of Technology," TRANS. ASME, vol. 57, 1935, pp. 423–424.

26 S. L. Kerr, "Determination of the Relative Resistance to Cavitation Erosion by the Vibratory Method," TRANS. ASME, vol. 59, 1937, pp. 373–397.

27 W. C. Schumb, H. Peters, and L. H. Milligan, "A New Method for Studying Cavitation Erosion of Metals," *Metals and Alloys*, vol. 8, 1937, pp. 126–132.

28 L. E. Robinson, B. A. Holmes, and W. C. Leith, "Progress Report on Standardization of the Vibratory-Cavitation Test," TRANS. ASME, vol. 80, 1958, pp. 103–107.

29 P. deHaller, "Erosion and Cavitation Erosion," in "Handbuch der Werkstoffprüfing," vol. 2, "Die Prüfung der Metallischen Werkstoffe," Julius Springer Verlag, Berlin, Germany, 1939, pp. 471–488. (Taylor Model Basin Translation T188, April, 1951.)

30 W. H. Price and G. B. Wallace, "Resistance of Concrete and Protective Coatings to Forces of Cavitation," *Journal of the American Concrete Institute*, 1949, p. 109.

Discussion

L. M. Mosher.[7] The authors are to be commended for their contribution to a subject about which there is a noticeable lack of published information. The reported comparison of the several test methods available for the study of cavitation-erosion damage should be of interest and value to anyone concerned with this particular corrosion mechanism.

The writer, over the years, has had the opportunity of inspecting a sizable number of ship propellers after service on varied types of merchant vessels. His findings with respect to the incidence and extent of cavitation-erosion damage on propellers are in good agreement with those reported by the authors. On not over 20 per cent of the propellers inspected has any evidence of cavitation-erosion damage been observed and in the majority of these cases the damage occurred over relatively small areas at random locations on only one or two blades usually immediately downstream from mechanically damaged (slightly bent) blade edges. On only infrequent occasions has cavitation-erosion damage associated with propeller design been observed; this appeared as localized areas of damage at identical locations on all blades.

The authors' observations as recorded in their Tables 2(*a*) through 2(*g*) indicate that they consider corrosion damage of stern-area appendages other than propellers to be a corrosion mechanism associated with or aggravated by velocity and turbulence effects rather than cavitation-erosion. The writer agrees with this with one possible exception. On a number of occasions, localized attack of spongy or honey-combed appearance typical of cavitation-erosion damage, has been observed on ship structures immediately aft of the propeller tips. Depending on the vessel construction, this attack appears at one or both of the following locations: (*a*) In way of the lower leading edge of the rudder, and (*b*) in way of the upper leading edge of the rudder or alternatively on the rudder horn. This attack appears to be associated with propeller-tip cavitation. Frequently, this damage shows an orientation with respect to the rotation of the propeller. For example, with a right-hand propeller, the localized attack favors both the lower port side of the leading edge of the rudder and the upper starboard side of the leading edge of the rudder or rudder horn. Attention is called to the fact that relatively severe damage of this type is unusual, although these particular areas consistently show some degree of corrosion damage varying from minor pits to fairly widespread general corrosion attack.

W. J. Rheingans.[8] The author has presented some interesting data on the effect of velocity on cavitation damage. The paper states that the Bureau of Reclamation water tunnel would not produce pitting within a reasonable time at velocities up to 70 fps, and that no pitting was obtained on specimens in the Taylor Model Basin water-tunnel apparatus at fluid velocities up to 50–60 fps even though cavitation zones were definitely present in both cases. This indicates that there is a lower limit of velocity or a threshold below which various materials will not be damaged in the presence of cavitation zones.

The tests with the rotating-disk apparatus were especially interesting. They showed that there is a threshold velocity below which various materials had no measurable losses, and that the limiting velocity varied with different materials. This is a confirmation of the findings by Knapp as reported in his papers [6, 7]. However, according to the authors' tests, aluminum, which was equivalent to the type used by Knapp, had a threshold velocity of 80 fps while Knapp indicated that the minimum velocity was about 45 fps. This difference is probably due to the method of measuring the pitting damage. Knapp observed the appearance of indentations in the specimen with a microscope after a few seconds of exposure and counted the number of such pits produced per second of exposure. The authors, on the other hand,

[7] Corrosion Engineer, Development and Research Division of the Central Technical Department, Bethlehem Steel Company, Shipbuilding Division, Quincy, Mass.

[8] Manager, Hydraulic Department, Allis-Chalmers Manufacturing Company, Milwaukee, Wis. Mem. ASME.

determined pitting damage by measuring the volume of material removed. Thus they missed the inception of microscopic damage to the material at the lower velocities.

This would account for the findings of the authors that the longer the test period for a given material the lower the threshold velocity.

Another indication that the authors did not determine the true threshold velocities for the various materials is the shape of their loss curves plotted against velocity. These curves, Figs. 21 and 22 in the preprint, do not approach zero loss asymptotically but at a fairly steep angle, which would seem to demonstrate that microscopic damage occurs at a lower velocity. On the other hand, the curves plotted by Knapp of microscopic damage (pits per second per square inch) show an asymptotic approach to zero number of pits.

If the authors' curves are continued asymptotically below zero loss, then the velocity at which the curve for aluminum becomes tangent is about the same as the velocity where Knapp's curve for the same material becomes tangent.

This has to be taken into account in determining the threshold velocities for various materials which are subject to cavitation damage, not for a few hours as tested by the authors but for a number of years.

It is felt that the pit indentations observed by Knapp at the low velocities eventually would turn into removal of material if subjected at this velocity to the cavitation zone for a sufficient period of time. Also, if the materials tested by the authors were subjected to cavitation in the rotating-disk apparatus for a period, say, of a year instead of a number of hours, the threshold velocities would be lowered considerably and the velocity at which damage would be apparent on the aluminum specimen would approach the threshold velocity shown by Knapp for this material.

It would be very instructive if the authors in a continuation of their research work could make microscopic examination of some of the materials to determine at which minimum velocity microscopic damage occurs.

This is a factor in determining the velocity for a given material below which no cavitation damage occurs in a cavitation zone regardless of the length of time it is exposed.

Another important aspect of the loss curves shown by the authors is that the loss varies approximately as the 7th power of the velocity. This confirms findings by Knapp [7] and by Kerr and Rosenberg.[9]

The tests by the authors as reported in their paper have given us valuable data on the effect of velocity on cavitation damage.

J. C. Schuster.[10] Because of the comparative nature of the text of this paper, additional value may be gained from an experiment performed in the Bureau of Reclamation laboratories approximately 1 year after the water-tunnel tests. This experiment provided information on cavitation-erosion of metal where oil flows under high pressure through control valves of hydraulic machinery.

The tests were made with a 7800-cycle magnetostriction oscillator on two brass specimens from the same stock. These specimens had an exposed face of $^{5}/_{8}$ in. diam. The first specimen was tested in water at 70 F to be compared with the second specimen tested in an SAE 10-viscosity oil at a temperature of 105 F. Although cooling equipment was added to the oil bath, the temperature could not be maintained at the 70-F temperature of the water bath because of the increased power required to drive the specimen.

[9] S. L. Kerr and K. Rosenberg, "An Index of Cavitation Erosion by Means of Radioisotopes," published in this issue, pp. 1308–1314.

[10] United States Bureau of Reclamation, Denver, Colo. Mem. ASME.

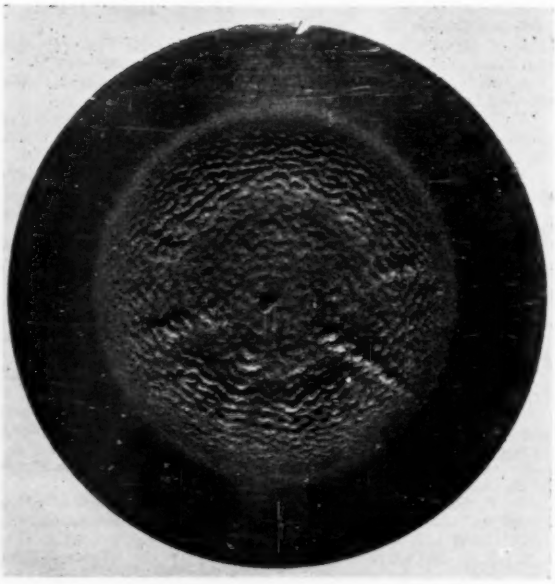

Fig. 27 Specimen after 3-hr test in water. ×6.8

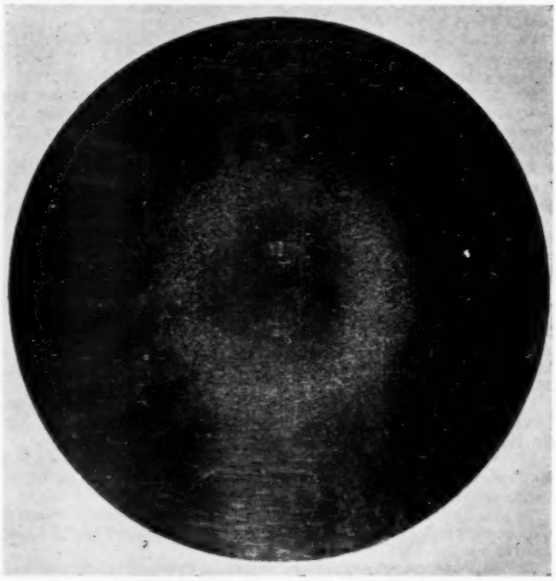

Fig. 28 Specimen after 9-hr test in oil. ×6.8

In a 3-hr test period, the loss of weight of the specimen in oil was approximately 0.5 per cent of the loss of weight for the companion specimen in water. The specimen in oil was tested for a total time of 9 hr and the results indicated a loss of weight at the rate of approximately 0.155 milligram per hr. This compared to a loss of weight at the rate of approximately 30 milligrams per hr for the second and third hours of a 3-hr test of the specimen in water. During the first hour of the water test, only 8.7 milligrams of weight were lost.

Photomicrographs of the eroded surface showed the characteristic pattern of the magnetostriction oscillator, Figs. 27 and 28.

The erosion was considerably more pronounced on the specimen tested in water.

It was concluded from these tests that cavitation-erosion was not a major problem in controlling the flow of oil at high pressures near a temperature of 100 F. Nevertheless, some weight loss occurred which was attributed to cavitation-erosion.

Differences in rate of loss are due primarily to the higher vapor pressure of the oil, but the oil was also a less corrosive and better dielectric liquid than the tap water.

As the authors point out in their conclusions, cavitation-erosion damage occurred only in particular areas on propellers of a minority of the vessels. This damage occurred on 5 out of 17 of the inspected ships. It would be of interest to know what was the relative submergence of the propellers of the five ships that suffered damage to that for the remaining 12 vessels; how many hours of operation did each incur at near maximum speed; and were there any notable differences in the propeller design between the 5 affected and 12 unaffected ships?

Contained in the summary is a comparison of fluid velocity and the inception of cavitation damage. In two cited apparatuses (rotating disks), cavitation damage occurred to some degree at a velocity of 81 fps (48 knots). In the third apparatus (Bureau of Reclamation, water tunnel) cavitation damage occurred at 70 fps (42 knots). In the fourth and fifth apparatus (Knapp, water tunnel and DTMB, water tunnel), a comparable erosion was not obtained at 60 fps (36 knots).

Fixed specimens were used in the third, fourth, and fifth test facilities, but both specimen and water, to some extent, moved in the two rotating-disk facilities. Since damage was obtained in one apparatus at 70 fps and not at 60 fps, it would be interesting to know if the threshold velocity for cavitation damage might be more closely related to a velocity of 70 fps in the rotating-disk apparatus.

This may have been done by measurement of the velocity distribution at the radius of the specimen between the disk and stilling vanes. If this measurement is available, it would be of interest to know what average velocity was affecting the cavities and the region in which they collapsed.

Authors' Closure

Mr. Mosher discusses attack which he has observed in the way of the lower and upper leading edges of the rudder and on the rudder horn, and which he believes to be associated with propeller tip cavitation. Although the authors have no data regarding this type of damage, they are in agreement with Mr. Mosher that this damage is probably cavitation erosion caused by traveling cavities generated at the propeller and collapsing at the indicated localized areas on the rudder and horn.

The authors have been concerned with further studies in the area of lower velocities and increased times of exposure with a view toward determining with greater refinement the threshold velocities below which material may show no measurable damage. Mr. Rheingans' comments along these lines are coincident with the author's views that future tests using the rotating disk or other cavitation erosion equipment should include studies in the regions of lower (threshold) velocities. It is believed that these studies, especially if they include the use of sea water, will shed much additional light on the resistance of materials to cavitation erosion in service.

Microscopic examination referred to by Mr. Rheingans, together with x-ray diffraction techniques for the evaluation of cold working of the test specimens in the eroded areas, are under consideration by the authors as additional tools in our future studies.

Schuster's comment regarding the velocity distribution between the disk and the stilling vanes and the desirability of evaluating this distribution is of great interest and is under our active consideration and study. Technical difficulties in evaluating this profile have so far prevented its accomplishment.

Regarding field observations that the authors have made, Schuster was interested in details of service of the propellers examined. Unfortunately such details are not readily available and cannot be determined with accuracy.

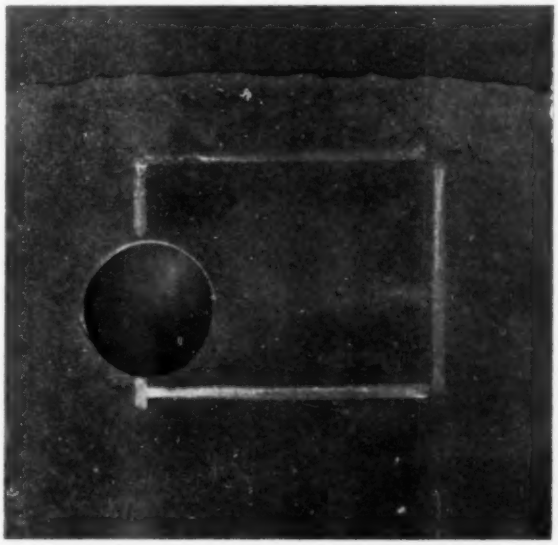

Fig. 29 Neoprene coating, Type II, after test for 72 hours at 150 fps

In respect to the general problem of propeller damage, the authors have recently obtained information using a rubber coated disk in an attempt to develop coatings for possible use on propellers. The disk was tested using the rotating disk apparatus shown in Fig. 13. The coating was a neoprene GN formulation complying with Military Specification MIL-S-15058E, Type II, and was press-cured for 2 hours at 258 F to one side of a $^1/_8$-in. thick mild-steel disk. The coating thickness was 0.082 in. The adhesive strengtn of this coating was 66.3 ppi (avg) and 70.7 ppi (max) when tested as described in Federal Standard 601, Method 8031. This coating after 72 hours of test showed no erosion at 150 fps as indicated in Fig. 29, whereas the mild steel surface showed erosion of the order indicated in Fig. 24. It is likely that the resilient nature of the coating was effective in absorbing the dynamic impact stresses of cavitation collapse at this velocity, and the high adhesive strength prevented stripping of the coating under the high shear stresses. Although the work conducted on this promising rubber coating is only of a preliminary nature at this time, all indications point to the possibility that such coatings on propeller surfaces and on other surfaces subjected to cavitation erosion may provide good protection against damage. In the case of compound surfaces such as propellers, the actual curing of coatings of this type on the surfaces impose considerable technical difficulties which must be overcome.